# ENHANCING SOLUBILITY AND PERMEABILITY OF ACTIVE PHARMACEUTICAL INGREDIENTS (APIs) IN THEIR SALTS, COCRYSTALS AND POLYMORPHS

A Thesis Submitted to the University of Hyderabad in partial fulfillment of the Award of a Ph.D. Degree in Chemistry

By

#### MANISH KUMAR BOMMAKA





School of Chemistry
University of Hyderabad
(P.O.) Central University, Gachibowli
Hyderabad-500046
Telangana State
India
June 2022

## **DEDICATED**

# To MY FAMILY

#### **STATEMENT**

I hereby declare that the matter embodied in the thesis is the result of investigation carried out by me in the School of Chemistry, University of Hyderabad, Hyderabad, India, under the supervision of Prof. Ashwini Kumar Nangia.

In keeping with the general practice of reporting scientific observations, due acknowledgements have been made wherever the work described is based on the findings of other investigators. Any omission, which might have occurred by oversight error is regretted.

Hyderabad

Date: 17-06-2022

Signature: Right 1

Name: Manish Kumar Bommaka

Regd. No. 15CHPH14

#### **DECLARATION**

I, Manish kumara Bommaka, hereby declare that this thesis entitled "Enhancing solubility and permeability of active pharmaceutical ingredients (APIs) in their salts, cocrystals and polymorphs" submitted by me under the guidance and supervision of Professor. Ashwini Kumar Nangia is a bonafide research work which is also free from plagiarism. I also declare that it has not been submitted previously in part or in full to this University or any other University or Institution for the award of any degree or diploma. I hereby agree that my thesis can be deposited in Shodganga/INFLIBNET.

A report on plagiarism statistics from the University Librarian is enclosed.

Hyderabad

Date: 17-06-2022

Signature:

Name: Manish Kumar Bommaka

Regd. No. 15CHPH14



#### **CERTIFICATE**

This is to certify that the thesis entitled Enhancing solubility and permeability of active pharmaceutical ingredients (APIs) in their salts, cocrystals and polymorphs" submitted by Manish Kumar Bommaka bearing Regd. No. 15CHPH14 in partial fulfilment of the requirements for the award of Doctor of Philosophy in Chemistry is a bonafide work carried out by him under my supervision. I hereby agree that this thesis can be deposited in Shodganga/INFLIBNET. The thesis has not been submitted previously in part or in full to this or any other University or Institution for the award of any degree or diploma.

Further the student has passed the following courses towards fulfillment of course work requirement for Ph.D.:

	Course. No	Title	Credits	Pass/Fail
1.	CY-801	Research Proposal	3	Pass
2	CY-805	<b>Chemistry Pedagogy</b>	3	Pass
3	CY-805	Instrumental Methods A	3	Pass
4	CY-501	Spectroscopic Methods for Structure Elucidation	3	Pass

Prof. Ashwini Kumar Nanggaa

Thesis Superivasity of Hyderabad Central University P.O. Hyderabad 500 046

Adwin Mangee Dean

School of Chemistry

School of Chemistry
University of Hyderabad
P.O. Central University
Gathibanii, Hyderabad-500 046.

#### **ACKNOWLEDGEMENTS**

I express my deep sense of gratitude and profound thanks to **Prof. Ashwini Kumar Nangia** for his inspiring guidance and constant encouragement throughout the course of this research work. I have been able to learn a great deal in this fascinating field of research through his inspiring lectures and thought provoking discussions, and I consider my association with him a rewarding experience.

I thank Prof. **Ashwini Kumar Nangia**, Dean, School of Chemistry, former Deans Prof. K. C. Kumara Swamy, Prof. T P Radhakrishna, Prof. Durga Prasad, and faculty for their co-operation in providing facilities in the School. I thank Prof. K. C. Kumara Swamy, Prof. Lalitha Guruprasad, Prof. R. Chandrasekar, and Prof. Samar Kumar Das for their inspiring lectures and motivation in my career. I thank DRC members Prof. Lalitha Guruprasad, Prof. R. Chandrashekar, and Prof. Samar Kumar Das for their constant guidance and suggestions during the course of my Ph.D. research projects.

I am thankful to my teachers Dr. Sayan Datta Gupta, Dr. N.M. Ragavendra, Mr. Madukar, Mr. Jyoganandam, Mr. Godandaraman, and Dr. Karthik all other lecturers who taught me throughout my career for their special classes and encouragement.

I am grateful to RGNF, New Delhi, for providing fellowship support. I thank UGC and DST for providing instrumentation and infrastructure facilities at the School of Chemistry.

I thank each and every non-teaching staff of the School of Chemistry, CIL, and administrative section for their assistance on various occasions. I take this opportunity to thank Mr. Ramana, and Mr. Mahesh for his kind help in acquiring the Single crystal data on various occasions. I thank Turabuddin and Mr. Durgesh for their help in recording solid state and solution NMR spectra. I thank Mr. Mallaya Shetty, Smt. Geeta, Mr. Naik, Mr. David and Mr. Venkat, Smt. Rani and Smt. Radhika for their cooperation. I thank Mr. Durgaprasad and Mr. Pavan for their help in recording SEM and facilities.

It gives me immense pleasure to thank my lab mates Geetha, Suresh, Swapna, Sudhir, Anil, Surya, Sruthi and Madhu for their help, cooperation and maintaining a cheerful atmosphere in the lab. My association with them is unforgettable and cherishable. I appreciate the support of D. Chaitanya, M. Chaitanya, Swarupa and Abhijit on various occasions. I would like to thank Dr. Jagadeesh Babu, Dr. Srinivasulu Bandi, Dr. Abin Sebastian, Dr. Sunil Rai and Dr. Balakrishna Reddy for their help and encouragement.

My stay on this campus has been pleasant with the association of many students, Dr. Suresh, Dr. Anjaneyulu, Dr. Ramesh, Dr. Tanmai, and all others whose names are not mentioned due to lack of space. I would like to thank my friends, Ramesh, Harilal, and Ankit, for their wonderful friendship.

My heart full thanks to grandfather and grandmother for their blessings. I would like to take this opportunity to appreciate the support from my brother's families, Naresh, Sindhuja, Anish, Lavanya, Nirmanyu, Anirvaan rudra, shiva.

The unconditional love of my Amma & Nanna and their blessings made me what I am today and I owe everything to them. The love and support I received from my brothers B. Naresh and B. Anish is invaluable. Thanks to my wife Mounika Devi for her support and encouragement. Thanks to my friends Mr. Vithoba Rao, Mr. Sheshadri, Mr. Kiran, Mr. Ramakrishna, and Mr. Praveen, and dedicating this thesis to my parents is a minor recognition to their boundless love and invaluable support.

Manish kumar Bommaka

#### **SYNOPSIS**

This thesis entitled "Enhancing Solubility and Permeability of Active Pharmaceutical Ingredients (APIs) as Salts, Cocrystals and Polymorphs" consists of Five Chapters.

#### **CHAPTER ONE:**

#### Introduction to Crystal Engineering and Tuning Solid-State Properties of Pharmaceutical Materials

Chemistry is an evolving subject and it is traditionally divided into four categories as organic, inorganic, physical and analytical chemistry. A new classification in the modern era is supramolecular solid-state chemistry which is different from the molecular chemistry of liquids and gases. The subject has now reached a significant maturity at the level of identification, separation and characterization of different crystalline forms of the same molecule or of aggregates of molecules with other molecules to take advantage of the difference in their physical and chemical properties. Physical properties are an intrinsic part of solid-state chemistry since the broad area of structure-property relationship is about the identification of new solid crystalline forms such as polymorphs, solvates/hydrates, salts and cocrystals (Fig. 1) and understand their properties to modulate their activity. The importance of identifying these crystalline materials is to investigate physical and chemical issues of active pharmaceutical ingredients (APIs) and address their solubility, stability and hydration problems using the crystal engineering approach. Crystal engineering of APIs through cocrystallization has gained an immense interest among pharmaceutical scientists and structural chemists to optimize the physicochemical properties and stability of solid dosage forms.

McCrone defined the term polymorphism as "a solid crystalline phase of a given compound resulting from the possibility of at least two different crystalline arrangements of the molecules of that compound in the solid state". ". It can be classified as conformational polymorph (due to flexible rotation of molecule), synthon polymorph (due to difference in hydrogen bonding patterns) and packing polymorph (because of changes in the crystal packing of molecules) in 2D or 3D. The term Cocrystal can be

defined as "cocrystals are solids that are crystalline single phase materials composed of two or more different molecular and/or ionic compounds generally in a stoichiometric ratio". Polymorphism and Cocrystallization have great significance in pharmaceutical industry, dyes and pigments, agrochemicals, explosive materials etc. due to their ability to alter the melting point, color, compressibility, filterability, stability, solubility etc. of important and commercial crystalline materials. Salt formation is an acid base reaction and a compound having an acidic or basic group can crystallize in salt form by cocrystallizations. The conventional approach of salt formulation to improve drug solubility is unsuccessful with molecules that lack of ionisable functional groups, have sensitive moieties that are prone to decomposition/ racemisation and/or are not sufficiently acidic /basic to enable salt formation.

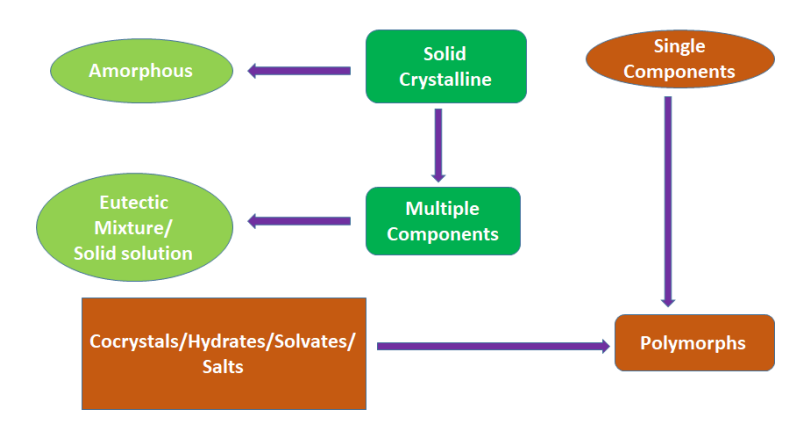


**Figure 1** Various solid-state crystalline and amorphous forms based on structure and composition variations.

Solubility is one of the most important physicochemical properties when evaluating compounds as potential drug candidates. The thermodynamic solubility of a compound in a solvent is the maximum amount of the most stable crystalline form of the compound that can remain in solution under equilibrium conditions. Kinetics is a time-dependent phenomenon, and thermodynamics is, by definition, time independent. Poor aqueous solubility of any drug is likely to result in poor absorption, even if the permeation rate is high, since the flux of a drug across the intestinal membrane is proportional to the concentration gradient between the intestinal lumen and the blood. Again very high concentrations of poorly soluble drugs in organisms may result in crystallization and

overall, poor solubility of drug candidates has been identified as the cause of numerous drug development failures at the final stages of formulations. We have addressed these issues in some of the active compounds by correlating the differences in conformation, changes in functional groups in polymorphs and this study provides a guide in drug delivery for solubility optimization. In this thesis, we have chosen few drugs or biologically active compounds to study their polymorphic behaviour and cocrystal/salt formation using high throughput screening and highlight their solubility and stability improvement with respect to the structure modifications such as cocrystals and salt formation.

The Biopharmaceutical Classification System (BCS) is based on permeability and solubility under prescribed conditions. According to intestinal absorption and oral administration parameters, drugs are classified in to Class-I, Class-II, Class-III and Class-IV which are mentioned below.

uo	Class-I	Class-II
sorpti	High solubility	Low solubility
nal ab	High permeability	High permeability
Permeability-intestinal absorption	Class-III	Class-IV
bility-i	High solubility	Low solubility
rmeal -	Low permeability	Low permeability
ጟ		

Solubility-dissolution across the physiological pH range

#### **CHAPTER TWO:**

# **Entacapone: Improving Aqueous Solubility, Diffusion Permeability and Cocrystal Stability with Theophylline**

Cocrystallization is a well-established technique to improve the solubility, bioavailability and stability of active pharmaceutical ingredients (APIs) but permeability and diffusion rate control via cocrystals is relatively less studied and the exact role of coformers in influencing diffusion rate of drug cocrystals is still not fully understood. The aqueous solubility and permeability diffusion of Entacapone (ETP, a Biopharmaceutical Classification System (BCS) Class IV drug of low solubility and low permeability) cocrystals with Generally Regarded as Safe (GRAS) coformers was studied. Fixed stoichiometry cocrystals of ETP with acetamide (ACT, 1:1), nicotinamide (NAM, 1:1), isonicotinamide (INAM, 1:1), pyrazinamide (PYZ, 1:1), and isoniazid (INZ, 1:1) were prepared by solvent-assisted grinding. Theophylline (THP) coformer resulted in a cocrystal hydrate (ETP-THP-HYD 1:1:1). The cocrystals were structurally characterized by single crystal and powder X-ray diffraction, DSC and TGA thermal measurements, and IR and NMR spectroscopy. Solubility and dissolution rate showed that there is a correlation between cocrystal stability and solubility governed by the heteromeric N-H···O, O–H···N and O–H···O hydrogen bonds and different conformational changes in ETP in the cocrystal structure. ETP-THP-HYD and ETP-PYZ exhibit faster dissolution rate and high solubility and they are also stable in phosphate buffer medium compared to the other cocrystals which dissociate partially during solubility experiments. Diffusion rates in a Franz cell showed surprisingly that the stable and high solubility ETP-THP-HYD cocrystal has good permeability. Given that stability, solubility and permeability are in general inversely correlated, the entacapone-theophylline hydrate cocrystal is a rare example of the thermodynamically stable cocrystal exhibiting high solubility and high permeability.

Six pharmaceutical cocrystals of ETP in a 1:1 stoichiometry were crystallized and structurally characterized. ETP-THP-HYD and ETP-PYZ displayed enhanced solubility and dissolution rate together with good stability due to stronger hydrogen bonds and different ETP conformation changes in the crystal structure. Furthermore, ETP-THP-

HYD cocrystal exhibits high diffusion and flux rate for possible BBB cross over. ETP-THP-HYD scores on high solubility, good stability and high permeability criteria. This case study presents a crystal engineering approach to solve solubility and permeability challenges in BCS class IV drugs.

# ETP-THY-HYD ETP-NAMI Time interval in (min) ETP-ACT

**Figure 2.** Entacapone Co-crystals with Acetamide, Iso-nicotinamide, Theophylline and Pyrazinamide.

#### **CHAPTER THREE:**

## Entacapone Polymorphs: Crystal Structures, Dissolution, Permeability and Stability Analysis

Entacapone (ETP) is a catechol-O-methyltransferase (COMT) drug used to treat Parkinson's disease. ETP is available in the market under the brand name COMTAN since 2010, and ETP form-I was first reported in a patent published in 2001. However, analysis of its X-ray crystal structures and stability relationship of ETP polymorphs and their dissolution, permeability profile is not reported. We observed two new conformational polymorphs of ETP in a study to better understand the structural origin of polymorphism and their phase transformations, stability, equilibrium solubility, dissolution and permeability properties. Both the new forms were obtained by

crystallization from water and acetone. The ETP molecule adopts different conformations in the polymorphic structures with slight changes in carbonyl and nitrile group orientation. Thermal analysis suggests that form-III and form-IV are enantiotropically related to form-I, which is the thermodynamically stable form at ambient conditions. In contrast, form-II is monotropically related to form-I. Based on the equilibrium solubility, dissolution and permeability studies, form II is stable in slurry medium and dissolves faster with high flux rate than the stable form-I in phosphate buffer solution at 37  $\pm$  0.5 °C. Form-II, form-III, and form-IV persist for a limited duration in PBS medium but are subsequently converted to form-I after 48, 24, and 24 h, respectively, and hence ETP form-I is the most stable modification among these polymorphs. From the dissolution and permeability experiments, form-II dissolved and diffused faster than the form-I, as well as form-III and form-IV. Further, the rod-shaped morphology and comparatively smaller size particles of form-II favour a higher solubility and dissolution due to a larger surface contact area. Even though form-IV has a much smaller particle size compared to form-II, the aggregation/agglomeration of such irregular-shaped small particles eventually reduces the dissolution rate of form-IV (as well its transformation during dissolution/solubility to form-I). There is thus an optimal range of particle size for high solubility and a faster dissolution rate, which are realized in ETP form-II.

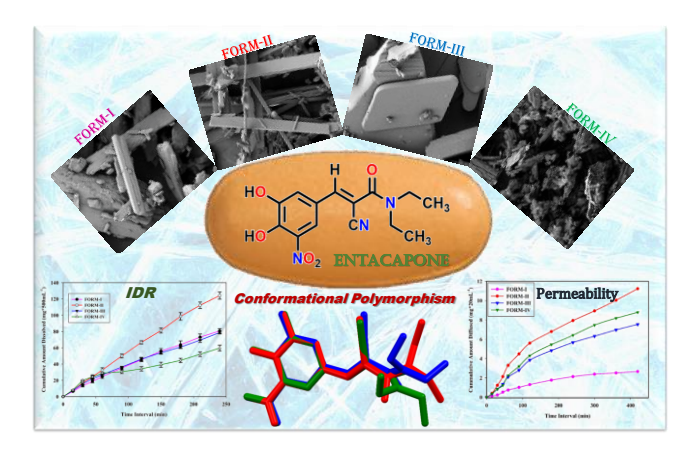


**Figure 3.** Novel polymorphs of entacapone are reported along with stability, solubility and permeability comparison. Form-II exhibits high solubility, high permeability and good stability requirements for a drug formulation

Solubility and permeability are two important parameters for optimal drug adsorption to accomplish high bioavailability. The change in flux across the dialysis membrane gives a measure of drug permeability or log P. Furthermore, a higher dissolution rate and lower enthalpy of fusion of form-II also impart to its highest membrane permeability and flux pass. Compared with the commercial form-I, the above results substantiate that the permeability of novel ETP form-II is superior to that of the marketed form-I.

#### **CHAPTER FOUR:**

# Improvement of Physiochemical Properties of Pimozide through Co-crystalization with Dicarboxylic Acids

Pimozide is regarded as an antipsychotic drug of the diphenyl-butyl piperidine class. This drug is used in schizophrenia and chronic psychosis, Tourette syndrome, and resistant tics and it can be also used to treat Delusional parasitosis. Due to its low solubility and high permeability, it is considered as BCS class II drug. In order to improve physicochemical properties of PMZ, cocrystallization strategy was employed. Cocrystal screening experiments of PMZ resulted in the formation of five binary molecular salts with the coformers oxalic acid (OA), succinic acid (SA), glutaric acid (GA), adipic acid (AA) and fumaric acid (FA). Glutaric-acid salt was found as monohydrate. All these complexes were characterized with IR, DSC, TGA, PXRD and Single Crystal X-ray Diffraction (SCXRD) studies. Crystal structure analyses showed that strong and ionic – N+-H···-OOC- interactions between protonated piperidine moiety of PMZ and carboxylate ion of the coformers are present in all the complexes. Protonated PMZ units act as molecular clips to encapsulate the deprotonated coformers with the abovementioned charge-assisted hydrogen bonds. From the equilibrium solubility and intrinsic dissolution rate studies (pH 1.2), it was observed that PMZ-FA salt exhibited superior performance for both the experiments. In diffusion/permeability (Franz diffusion cell, pH 7.0) experiment also PMZ-FA salt exhibited highest permeability among all the complexes and pure PMZ. So, due to significant improvement in solubility as well as permeability, PMZ-FA salt may be considered as more effective formulation for PMZ.

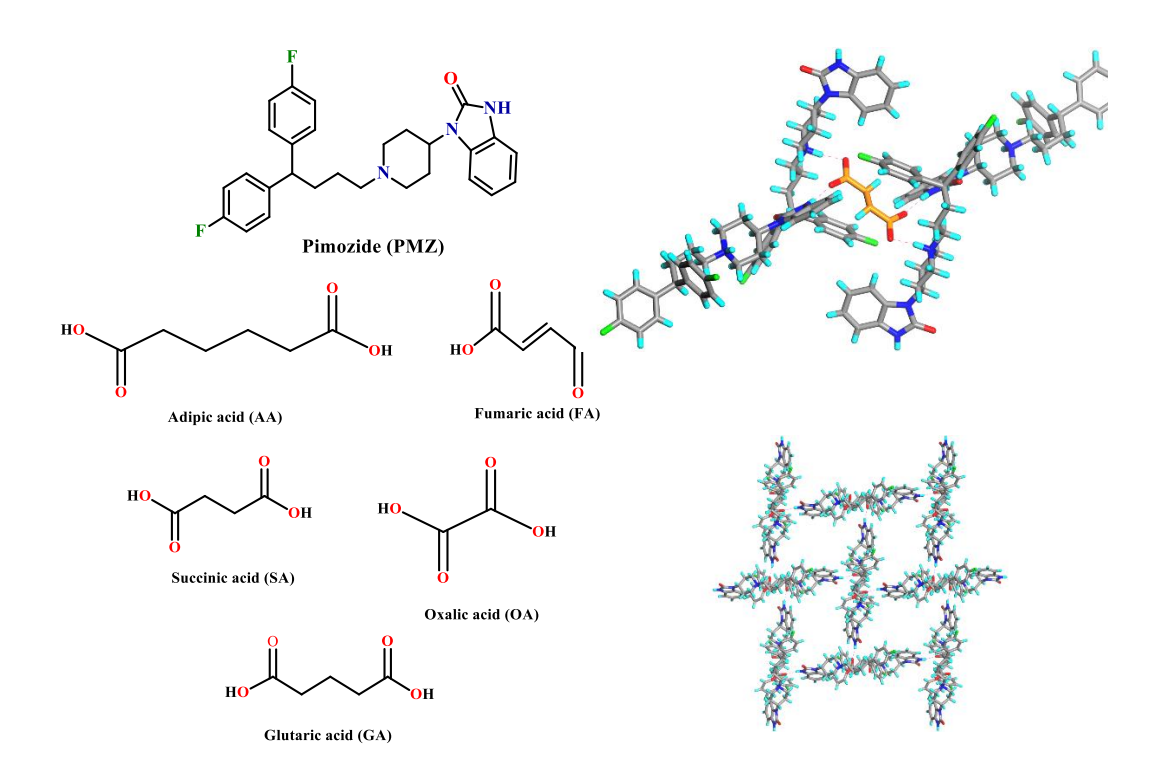


**Figure 4.** Molecular structures and acronyms of Pimozide and coformers. Crystal diagram of hydrogen bond interactions with Fumaric acid

#### **CHAPTER FIVE:**

#### Curcumin-Artemisinin Coamorphous Solid: Xenograft Model Preclinical Study

Curcumin is a natural compound present in Indian spice turmeric. It has diverse pharmacological action but low oral solubility and bioavailability continue to limit its use as a drug. With the aim of improving the bioavailability of CUR, The low solubility and short half-life of curcumin, and hence high dosage administered, have been a limitation to making drug formulations of curcumin. We have overcome the multiple disadvantages of curcumin in the designed CUR-ART coamorphous dispersion we evaluated Curcumin-Pyrogallol (CUR-PYR) cocrystal and Curcumin-Artemisinin (CUR-ART) coamorphous solid. Both these solid forms exhibited superior dissolution and pharmacokinetic behavior compared to pure CUR, This novel binary solid exhibits high solubility and bioavailability, extended half-life and action of bioactive curcumin at normal drug dose regime of 100 mg/kg CUR-ART coamorphous solid showed two

fold higher bioavailability than CUR-PYR cocrystal (at 200 mg/kg oral dose). Moreover, in simulated gastric and intestinal fluids (SGF and SIF), CUR-ART is stable up to 3 and 12 hours, respectively. In addition, CUR-PYR and CUR-ART showed no adverse effects in toxicology studies (10 times higher dose at 2000 mg/kg). CUR-ART showed higher therapeutic effect and inhibited approximately 62% of tumor growth at 100 mg/kg oral dosage of CUR in xenograft models, which is equal to the positive control drug, doxorubicin (2mg/kg) by IV administration. Given the diverse biological action of curcumin and artemisinin, the high quantity of net drug delivered as coamorphous solid could open opportunity for an herbal formulation in cancer, malaria and several other treatments

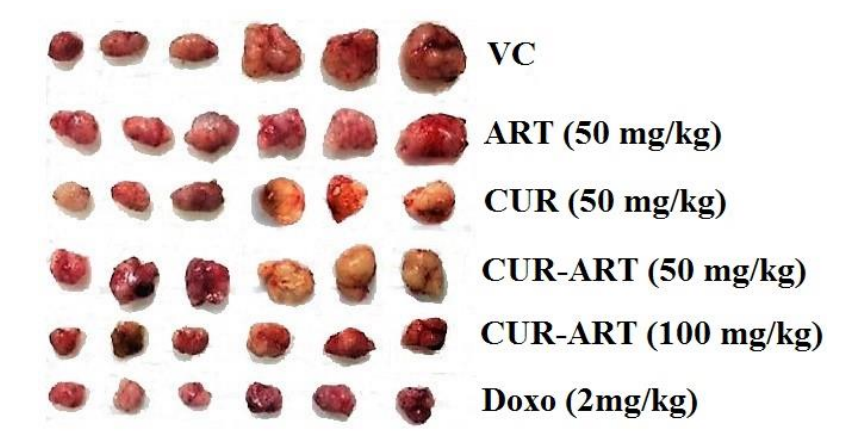


**Figure 5.** Tumor volume of established Panc-1 xenograft model in nude mice during therapy under different treatments.

#### **CHAPTER SIX:**

#### Crystal Structure Analysis of Ribociclib Salts.

Crystal engineering is a fascinating technique for constructing the various multi-component solid-state forms using non-covalent interactions. Ribociclib (**RBC**) named as chemically 7-cyclopentyl-N,N-dimethyl-2-{[5-(piperazine-1-yl)piperidine-2-yl]amino}-7H-pyrrole[2,3-d]pyrimindine-6-formamide belongs to the Biopharmaceutics Classification System (BCS) Class IV drug of poor solubility (0.231 mg/mL) and low permeability (log P 2.38, Chemaxon calculator). Herein, we report the synthesis and crystal structure investigation for pharmaceutical salts of Ribociclib (**RBC**) with acid

based coformers such as benzoic acid (**BA**), 3-methoxybenzoic acid (**3-MBA**), 4-Hydroxybenzoic acid (**4-HBA**) and 345-Tryhydroxy bezoic acid (**345-THBA**). **RBC** containing basic (-NH) group of piperazine is found to show a strong tendency toward subtraction of protons from acid (-COOH) group of the coformers which leads to the formation of binary pharmaceutical salts. The salts of **RBC** were prepared utilizing the solvent-assist grinding method. In addition to the single-crystal X-ray diffraction studies, these solids were characterized by powder X-ray diffraction (PXRD), Infrared spectroscopy (IR) and differential scanning calorimetry (DSC). Single crystals of the binary salts were obtained in various solvents by solution crystallization. It is noteworthy that these binary solids may have the potential to improve the physicochemical properties of this drug. These studies are currently in progress.

**Figure 6.** Chemical structures of Ribociclib (**RBC**) and acid coformers (Benzoic acid, **BA**; 3-Methoxybenzoic aci, **3-MBA**; 4-Hydroxybenzoic acid, **4-HBA** and 345-Tryhoroxybenzoic acid, **345-THBA**).

#### **CHAPTER SEVEN:**

#### **Conclusions and Future Prospects**

From the above four working chapters, the following implications and conclusions can be given. Crystal engineering principles and hydrogen bonding rules were applied to improve the physicochemical properties such as solubility, dissolution rate, melting point and stability of drug substances. In this thesis, extensive studies of different solid forms such as polymorphs, salts, Cocrystals, and their polymorphs and co-amorphous. In chapter 2, we have highlighted that cocrystals represent a viable alternative for an API to improve solubility. Here, six pharmaceutical cocrystals of ETP were crystallized and structurally characterized. ETP-THP-HYD and ETP-PYZ displayed enhanced solubility and dissolution rate together with good stability due to stronger hydrogen bonds and different ETP conformation changes in the crystal structure. Furthermore, ETP-THP-HYD cocrystal exhibits high diffusion and flux rate for possible BBB cross over. This case study presents a crystal engineering approach to solve solubility and permeability challenges in BCS class IV drugs. In Chapter 3, polymorphic screening was carried out and three polymorphs of Entacapone were identified and their phase transformations and stability relationships were established. The thermal behavior of the polymorphs is investigated with DSC to detect the phase transformation from the metastable to the stable polymorph by performing heat-cooled-heat controlled experiments and found that, the form-IV and form-III are enantiotropically related to form-I. Whereas, the form-II is monotrpically realted to form-I. In chapter 4, we have highlighted the importance of solid form screening for the low soluble conventional antipsychotics drug Pimozide. We have prepared pharmaceutical salts of this drug with various GRAS molecules to improve solubility of the drug. Two salts with the coformers fumaric acid and glutaric acid exhibited significant improvement in solubility, IDR and permeability. In chapter 5, we have shown how to overcome the multiple disadvantages of curcumin in the designed CUR-ART co-amorphous dispersion. This novel binary solid exhibits high solubility and bioavailability, extended half-life and action of bioactive curcumin at normal drug dose regime of 100 mg/kg. The therapeutic activity of CUR-ART in Xenograft models of Panc-1 is comparable to commercial drug doxorubicin. Given the diverse biological action of curcumin and artemisinin, the high quantity of net drug delivered as coamorphous solid could open opportunity for an herbal formulation in cancer, malaria and several other treatments. In chapter 6, syntheses and crystal structure analyses of four salts/salt-hydrates of an anti-cancer drug Ribociclib (RBC) with the coformers benzoic acid, 3-methoxy benzoic acid, 4-hydroxy benzoic acid and 3,4,5,-trihydroxy benzoic acid have been delineated. These binary salts of RBC may improve solubility as well as permeability of this BCS class IV drug.

### **CONTENTS**

Statem	ent	V
Declar	ation	vii
Certifi	cate	ix
Ackno	wledgements	xi-xii
Synop	sis	xiii-xxiv
Chapte	r One	
Crystal	<b>Engineering and Pharmaceutical Solids</b>	1-40
1.1	Supramolecular Chemistry	2
1.2	Self-Assembly and Intermolecular Interactions	3
1.3	Hydrogen bonding	4
1.4	The Design of Supramolecular solids Crystal Engineering	5
1.5	Supramolecular Synthons.	7
1.6	Active Pharmaceutical Ingredients	8
1.7	Solid-State Chemistry of Pharmaceutical Drugs and its	9
	classification.	
1.7.1	Polymorphism.	11
1.7.1.1	Classification of Polymorphs.	12
1.7.1.2	Polymorphs generation and transformation	14
1.7.1.3	Importance of Polymorphs in Pharmaceutical Industry	16
1.7.2	Pseudopolymorphism-Solvates and Hydrates	18
1.7.3	Pharmaceutical Salts	19
1.7.4	Cocrystal Definition.	21
1.7.4.1	Importance of Cocrystal in Pharmaceutical Industry	22
1.7.4.2	Spring and Parachute model for solubility enhancement of	23
	cocrystals	
1.7.4.3	Cocrystals in pharmaceutical sciences	24
1.7.5	Amorphous solids	27
1.7.6	Coamorphous solids	28
1.8	Conclusions	30
1.9	References	30

Chapter	Two
---------	-----

Entaca and Co	41-72	
2.1	Today dayadiga	42
2.1	Introduction	42
2.2	Results and Discussion.	43
2.3	Crystal Structure Analysis	45
2.4	FT-IR Spectroscopy	50
2.5	Powder X-ray diffraction	55
2.6	Differential Scanning Calorimetry	56
2.7	Solubility and Dissolution	59
2.8	Diffusion and Permeability Flux	65
2.9	Conclusions.	66
2.10	Experimental Section	67
2.11	References.	69
-	er Three aponePolymorphs: Crystal Structures, Dissolution, Permeability	73-104
3.1	Introduction	74
3.2	Results and Discussion	75
3.3	Crystal Structure Analysis	76
3.4	Hirshfeld surface analysis	82
3.5	FT-IR Spectroscopy	85
3.6	Thermal analysis	86
3.7	Field emission scanning electron microscope analysis	89
3.8	Solubility and Dissolution	90
3.9	Permeability	92
3.10	Conclusions	93
3.11	Experimental Section	94
3.12	References	101

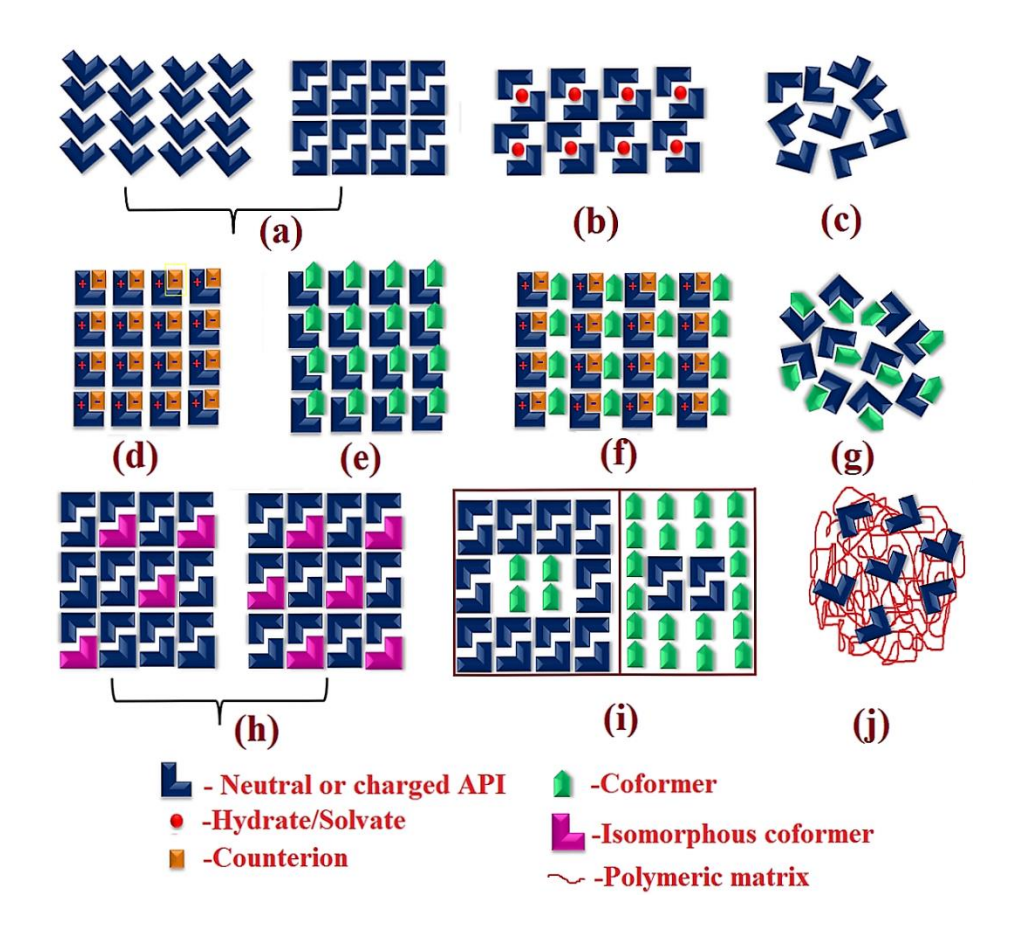
#### **Chapter Four**

-	ovement of Physiochemical Properties of Pimozide through Co- lization with Dicarboxylic Acids	105-130
4.1	Introduction	106
4.2	Results and Discussion	100
4.3	Crystal Structure Analysis	100
4.4	FT-IR Spectroscopy.	114
4.5	Powder X-ray diffraction	117
4.6	Differential Scanning Calorimetry	117
4.0 4.7	Solubility and Dissolution	110
4.7	Diffusion	121
4.0 4.9		121
4.9 4.10	Conclusions.	122
4.10 4.11	Experimental Section	123
7.11	References	120
Chapt	ter Five	
Curcu	ımin-Artemisinin Coamorphous Solid: Xenograft Model	131-156
Precli	nical Study	
5.1	Introduction	132
5.2	Results and Discussion	133
5.3	Bioavailability studies	134
5.4	Phase stability in SGF and SIF media	136
5.5	Acute toxicity study	140
5.6	In vivo antitumor effect of CUR-ART against Panc-1	145
5.0	Xenograft	113
5.7	<b>C</b>	148
	Materials	
5.8	Methods.	148
5.9	In Vivo Study Design and Drug Administration	148
5.10	Preparation of SGF and SIF media.	149
5.11	Acute Toxicity Study	150
5.12	In Vitro Cell culture	150
5.13	In vivo PANC-1 Tumor Growth Xenograft Model	150
5.14	Statistical Analysis	152
5 15	Conclusions	152

5.16	References	153
Chapt	er Six	
Crysta	al Structure Analysis of Ribociclib Salts	157-176
6.1	Introduction	158
6.2	Results and Discussion.	158
6.3	Crystal Structure Analysis.	160
6.4	FT-IR Spectroscopy.	165
6.5	Powder X-ray diffraction.	167
6.6	Differential Scanning Calorimetry	168
6.7	Conclusions.	171
6.8	Experimental Section.	172
6.9	References.	174
Chapt	er Seven	
Concl	usions and Future prospects	177-180
About	the Author.	181
List of	Publications	183
Partici	pation in Symposia, Workshops & Conferences	185

#### **CHAPTER ONE**

#### **Introduction: Crystal Engineering and Pharmaceutical Solids**



Schematic representation of various solid forms, (a) Polymorphs (b) Solvate/hydrate (c) Amorphous (d) Salt (e) Neutral cocrystal (f) Ionic cocrystal (g) Coamorphous (h) Solid solution or alloy (i) Eutectic (j) Polymeric solid dispersion.

#### 1.1 Supramolecular Chemistry

In the first quarter of the 19<sup>th</sup> century, Friedrich Whöler had successfully synthesized urea,<sup>1</sup> and with this important experiment began the subject of molecular chemistry, which represents a broad spectrum of highly powerful sequential methods for constructing synthetic superior complex molecules from covalently linked intramolecular atoms. Ever since the establishment of molecular chemistry over the mastery of covalent bond by producing the molecules of modest size and complexity, it has limitations to produce large complex molecular structures that are required for the development of various efficient materials. Since then, in the late 20<sup>th</sup> century, the introduction of "Supramolecular Chemistry" has evolved as traditional organic synthesis to gain over the intermolecular bond for generating super complex structures using molecular recognition and self-assembly. <sup>2</sup>

"Beyond molecular chemistry based on the covalent bond there lies the field of supramolecular chemistry, whose goal it is to gain control over the intermolecular bond."

#### -Jean-Marie Lehn<sup>3</sup>

The chemistry of the intermolecular bond called as the "Supramolecular Chemistry" is defined by Jean Marie Lehn as "chemistry beyond the molecule" is therefore inherently reliant upon the molecular level understanding, that results from the association of two or more neighboring chemical species held together by non-covalent interactions. It is the study of high-level aggregates ("Übermoleküles" or "supermolecules") which were systematically observed to gain insight into the intermolecular interactions in such conglomerations.<sup>4</sup> In the year 1894, Emil Fischer investigated substrate-receptor binding in the context of biological processes and coined the famous "Lock and Key" analogy to specify enzyme reactions.<sup>5</sup> This "Lock and Key" model further led to the development and explained the fundamental principles of molecular recognition and host-guest chemistry between two different but complementary molecules initially described as the receptor and the substrate. In the early decade of the 20th century with the realization of nature success of noncovalent bonds were understood in greater detail with molecular recognition. The led by Charles J. Pederson to the first deliberate design of complexes founded upon molecular recognition such as crown ethers which has the significance of ligand in supramolecular complexes.<sup>6</sup> Later, Lehn and coworkers, <sup>7</sup> synthesized nitrogen-containing bridged crowns called cryptands and reference to this work other researchers such as Donald J. Cram and Fritz Vogtle became active in synthesizing shape and ion selective receptors or host-guest complexes. Other active researchers Vögtle,8 Atwood,9 and Gokel subsequently took forward this concept into the synthetic receptors by involving hydrogen bonding and other non-covalent interactions. After a long wait, in 2002 Jean-Marie Lehn gave the functional definition<sup>7</sup>: "Supramolecular chemistry aims at developing highly complex chemical systems from components interacting by non-covalent intermolecular forces". Since then, several reviews and books were published on supramolecular chemistry. The development of supramolecular field requires an understanding of molecular chemistry (the chemistry of the covalent bond) together with chemistry of noncovalent bond interactions for molecular self-assembly to tweak the structure, properties and functionalities of the desired products (Figure 1.1).

"Chemistry beyond the molecule', bearing on the organized entities of higher complexity that result from the association of two or more chemical species held together by intermolecular forces"

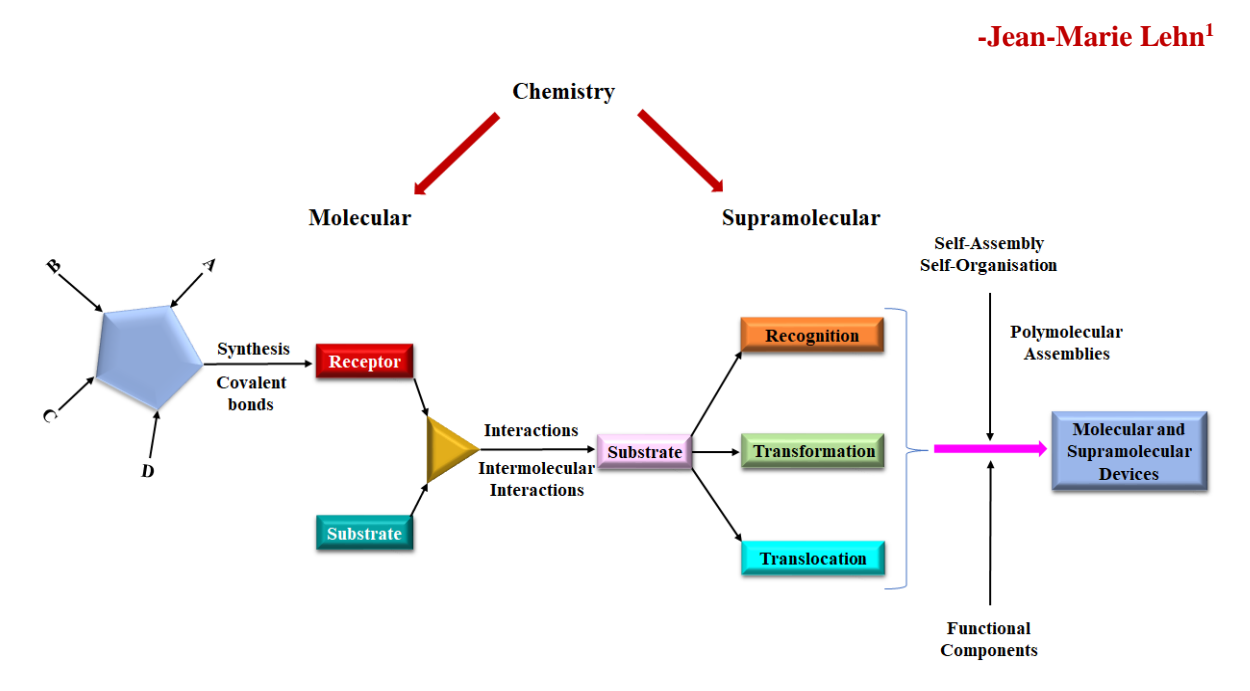


**Figure 1.1:** From the scope of molecular to supramolecular chemistry according to Lehn. (Adapted from ref. 3)

#### 1.2 Self-Assembly and Intermolecular Interactions

In supramolecular chemistry, the effective aggregation of noncovalent interactions such as hydrogen bonds, metal coordination bonds, CH- $\pi$ ,  $\pi$ - $\pi$ , van der Waals forces, and electrostatic interactions occur between molecular building blocks, rely upon molecular recognition and the directed self-assembly of (functional) supramolecular entities. A summary of bond energy range of different set of intermolecular interactions<sup>10</sup> commonly seen in supramolecular chemistry are provided with the covalent bond for comparison and an example is illustrated in Figure 1.2.

The utilization of these intermolecular interactions for directed self-assembly requires an understanding of their strength, distance and directionality to control the supramolecular architecture of a molecule. These intermolecular interactions can be divided into two categories, (a) isotropic or non-directional which are long range dispersion forces and short-range repulsive forces which includes C···C, C···H, H···H interactions that defines the shape, size and close packing and. (b) anisotropic or directional includes hydrogen bonds, charge transfer interactions, halogen interaction, and heteroatom

interactions such as C–H···O, C–H···N, O–H···O, N–H···O O–H··· $\pi$ , halogen···halogen, nitrogen···halogen, sulfur···halogen etc.). Among them hydrogen bonding is the most reliable because of its strength and directionality and there is particular importance in supramolecular chemistry. <sup>11</sup>

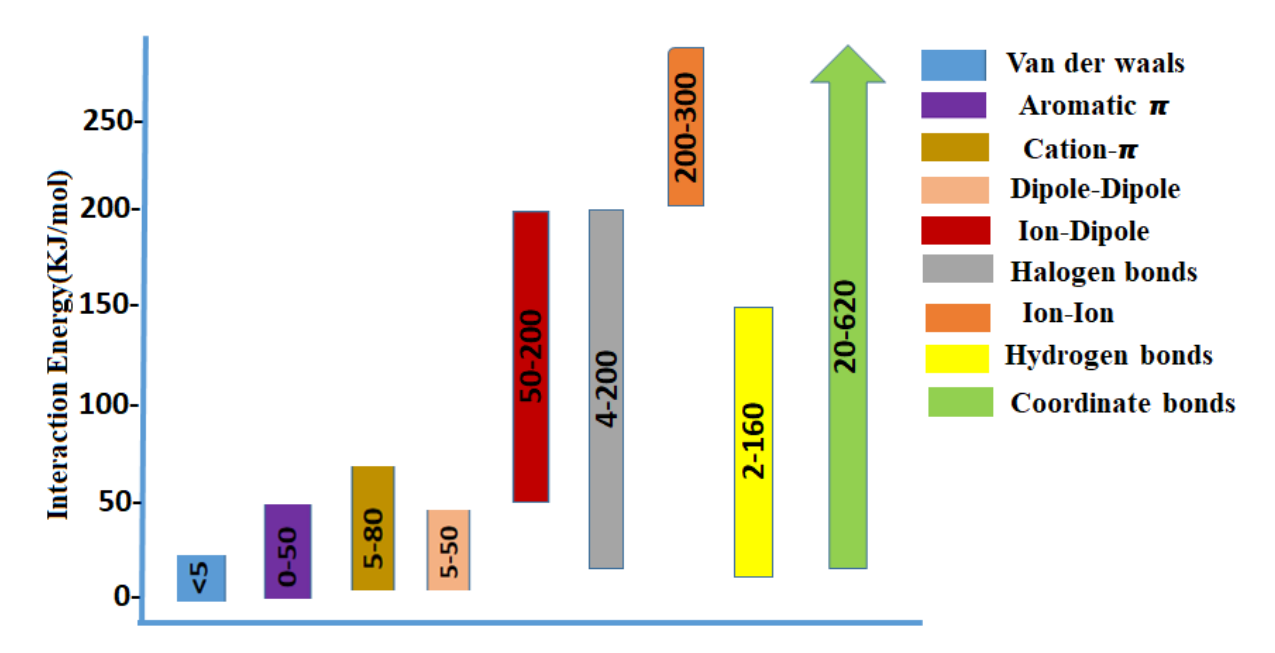


Figure 1.2: Representation of bond energy of covalent and non-covalent interactions with examples.

#### 1.3 Hydrogen bonding

"Under certain conditions an atom of hydrogen is attracted by rather strong forces to two atoms instead of only one, so that it may be considered to be acting as a bond between them"

#### - Linus Pauling

Linus Pauling was the first to define the hydrogen bond in the year  $1939^{12}$ , later it has been described by many authors with the most recent definition, being from IUPAC in the year 2011. The International of Pure and Applied chemistry (IUPAC) definition of a hydrogen bond states that "the hydrogen bond (designated as D-H···A, where acceptor A and donor D are electronegative atoms) is an attractive interaction between a hydrogen atom from a fragment or molecule D-H in which D is more electronegative is than H, and an atom or a group of atoms A, in the same or different molecule where there is evidence of bond formation". The bond energy varies in the range of 0.5 to 40 kCal/mole. The nature of the hydrogen donor (D) drags the electron density away from the hydrogen atom, resulting in a partial positive charge  $(+\delta)$ , subsequently pulls towards the electrostatic interaction to the acceptor (A) with partial negative charge  $(-\delta)$  and is directional in nature. Based on the strength and directionality the hydrogen bond is classified into three categories, see below Table 1.1.<sup>14</sup>

Hydrogen bonding is a key element throughout this thesis, and it will include interactions between two electronegative atoms, typically separated by a distance less than the sum of the van der Waals radii, where one atom can be defined as the hydrogen bond donor and the other atom acts as the acceptor, where hydrogen is located between the two atoms and is directional in nature and it will be the main intermolecular interaction focused upon for crystal structure analysis.

**Table 1.1:** Some properties of very strong, strong and weak H-bonds.

	Very strong	Strong	Weak
Bond Energy (kcal/mol)	15-40	4-15	< 4
Examples	[F–H····F <sup>-</sup> ]	O–H···O=C	C–H···O
IR vs relative shift	>25%	5-25%	< 5%
<b>Bond lengths</b>	$H-A \approx X-H$	$H \cdots A > X - H$	$H \cdots A >> X - H$
Lengthening of X-H (Å)	0.05-0.2	0.01-0.05	≤ 0.01
D (X···A) range (Å)	2.2–2.5	2.5–3.2	3.0-4.0
d (H···A) range (Å)	1.2–1.5	1.5–2.2	2.0-3.0
Bonds shorter than vDW	100%	Almost 100%	30-80%
θ (X–H···A) range (°)	175–180	130–180	90–180
Effect on crystal packing	Strong	Distinctive	Variable
Covalency	Pronounced	Weak	Vanishing
Electrostatics	Significant	dominant	moderate

#### 1.4 The Design of Supramolecular solids-Crystal Engineering

Supramolecular chemistry initially focused on the study of supermolecules in solution. Later, this field broadly split into two categories in a natural way: (I) The study of supramolecular assembly in solution dynamics in host guest complexes for recognition and binding; and (II) The study of noncovalent intermolecular interactions in the solid-state called as "Crystal Engineering". The understanding of structural information from molecular crystal structure began from the roots of crystal engineering. It can be traced back in the year 1921 by W. H. Bragg, 15 who first comprehensively taught the interrelationship between molecules and crystals by comparing the unit cell parameters of naphthalene and anthracene, where the two axial lengths were nearly identical, while the third one differed for the above two molecules. Perhaps this was the first correlation between a crystal structure and a property of molecule on one hand and those of extended assemblies of molecules on the other. Later in the year 1951 Robertson who was a student of Bragg significantly explained the relation between crystal property and molecular property by taking examples from polynuclear aromatic hydrocarbons based on molecular thickness and molecular area. 16,17 Later another student of Braggs corrected the chemical formula of phenanthrene related aromatic hydrocarbons while studying crystal unit cell parameters.

The physicist Pepinsky first introduced the term crystal engineering in the literature at the American Physical Society meeting held at Mexico City in the year 1955. Before that, from 1950-1971 Schmidt was first scientists to practice and conceptualize organic solid-state photochemical

reactions of trans-cinnamic acids derivatives.<sup>20</sup> He noticed that the introduction of a dichlorophenyl group in unsaturated molecules steers crystallization into a unit cell with a short axis of ca. 4 Å, a distance optimal for photodimerization of alkenes. This resulted in  $\alpha/\beta$ -truxillic/ truxinic acid, whereas  $\gamma$ -form intermolecular distance of >4.7 Å was photo stable (Figure 1.3).

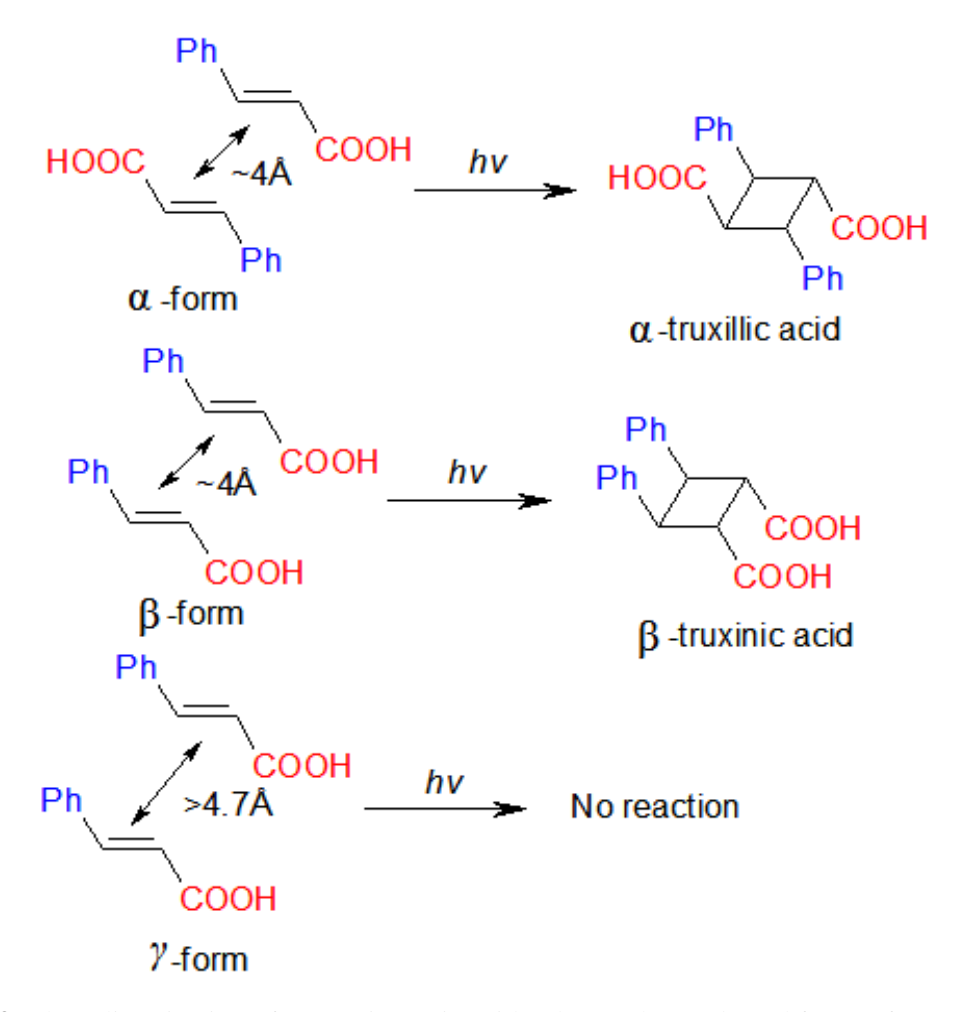


**Figure 1.3:** Photodimerization of *trans*-cinnamic acid polymorphs. (Adapted from ref. 20)

Crystal engineering was later defined by Desiraju and widely accepted as "the understanding of the intermolecular interactions in the context of crystal packing and the utilization of such understanding in the design of new solids with desired physical and chemical properties". Subsequently Desiraju's definition portrays the potential of crystal engineering to result in the development of novel materials. Further exploration of organic supramolecular assemblies via crystal engineering by Etter, Desiraju, Wuest, Aoyama, Whitesides, Stoddart, and many others has since realized this potential, affording a plethora of materials that are sustained by various molecular recognition events, including supramolecular synthons.

#### 1.5 Supramolecular Synthons

In 1995, Desiraju introduced the term supramolecular synthon<sup>21</sup> to design the mixed or multicomponent molecular crystals by reviving the term "synthon" coined by E. J. Corey<sup>22</sup> to simplify organic synthesis into an organized sequence of steps, and subsequently to focus in the chemical thought process, from starting material to the target substance. Corey defined synthons as "structural units within which molecules can be formed and/or assembled by known or conceivable synthetic operations" and the term has been used since its inception to represent key structural units in the target molecules. Desiraju defined the term Supramolecular synthon<sup>21</sup> as "structural units within supermolecules which can be formed and/or assembled by known or conceivable intermolecular interactions". In the regular usage, the supramolecular synthons have been defined as non-covalent bonding between at least two complementary functional groups. The study of supramolecular synthons began with the carboxylic acid dimer formation with acetic acid in solution and has since progressed into two distinct types: the supramolecular homosynthon and the supramolecular heterosynthon.<sup>23</sup> The supramolecular homosynthon is generated by a non-covalent interaction between same two moieties or functional groups. A supramolecular heterosynthon incorporates a non-covalent interaction between two different but complementary moieties such as acid-pyridine, 24 acid-amide, 25 phenol-amine, 26 phenol-pyridine, 27 aminopyridine-acid,<sup>28</sup> amide–pyridine-*N*-oxide<sup>29</sup> and sulfonamide-pyridine-N-oxide. These heterosynthons are well exploited in crystal engineering (Figure 1.4).

Figure 1.4: Common supramolecular synthons observed in CSD.

#### 1.6 Active Pharmaceutical Ingredients

Active Pharmaceutical Ingredient (API) is a chemical substance and it has a biologically active component of a finished drug product currently in the form of tablet, capsule, cream, and injectable that produces the intended effects in the physiological systems to the recipient for prevention, cure/treatment of the disease.<sup>30</sup> APIs which are also called as drug substance (DS) can initiate to formulate the drug product (DP) or medicine that can find application to treat a disease pertaining to oncology, cardiology, CNS and neurology, orthopedic, pulmonology, gastroenterology, nephrology, ophthalmology, and endocrinology etc. APIs can potentially create a sustainable healthcare system by introducing more innovative medicine that can initiate the pharmacological action through the systemic or local administration, only when active forms of the drugs are absorbed properly without change effect in the recipients,<sup>31</sup> Therefore, the active form drug absorption is an important prerequisite step where the fraction of administered dose that gets absorbed. The most assessable and affordable route of administration is the oral route by making solid dosage formulations because of ease of manufacture, storage and compliance to the patients which are in the form of tablet, capsule, or lyophilized powder forms. However, the main factors affecting the oral tablet route absorption are stability, solubility, dissolution rate and permeability are the physicochemical and molecular properties respectively that can influence bioavailability of a drug.

Based on solubility and permeability property of the APIs, Amidon et. al.<sup>32</sup> introduced the term Biopharmaceutics Classification System (BCS) which were categories into four namely BCS Class I, II, III and IV (Figure 1.5).<sup>33-35</sup> Rosenberg et al. redefined the developability classification system (rDCS) based on Amidon's BCS Classification II into two sub-categories, IIa the dissolution is limited, whereas IIb has limited solubility).<sup>36</sup> The management or interplay of these challenges with respect to altering their physical properties and optimizing the APIs without changing their desirable molecular behavior along with enhanced therapeutic efficacy is the main goal for pharmaceutical industry. Solid forms offer a lot of advantages over other forms, but often face the problem of physical and chemical properties such as solubility, melting point, chemical interaction, stability, bioavailability etc.<sup>37</sup>

Possible ways to these issues in the solid formulation space can be found during early and late development through screening studies are polymorphs, cocrystals, salts, amorphous, solvates/ hydrates and amorphous. Owing to their hydrophilic/ hydrophobic nature, drugs exhibit physicochemical behavior which can be controlled with coformers and additives, such as solubility, stability, bioavailability and dissolution rate for improved shelf-life and drug-patient compatibility. As a result, they play a crucial role in developing optimal formulations of drugs for better therapeutic efficacy.

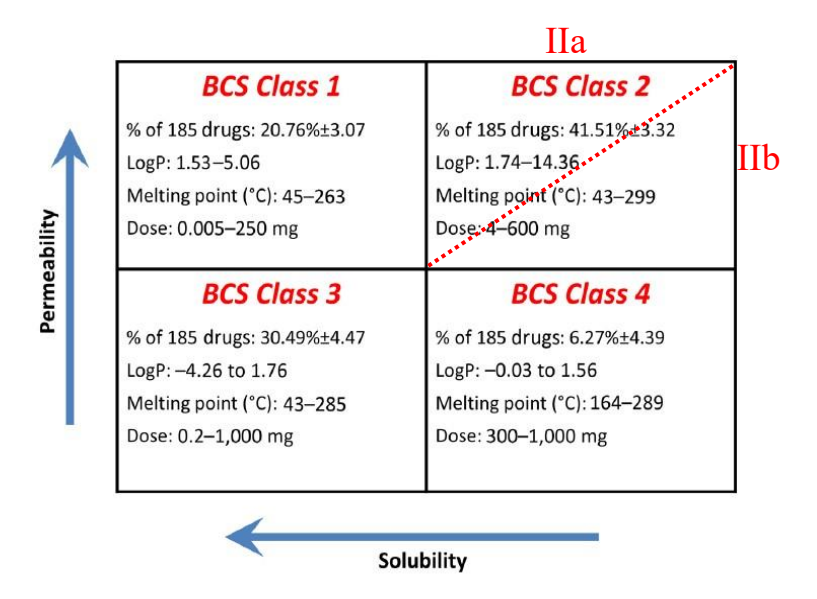
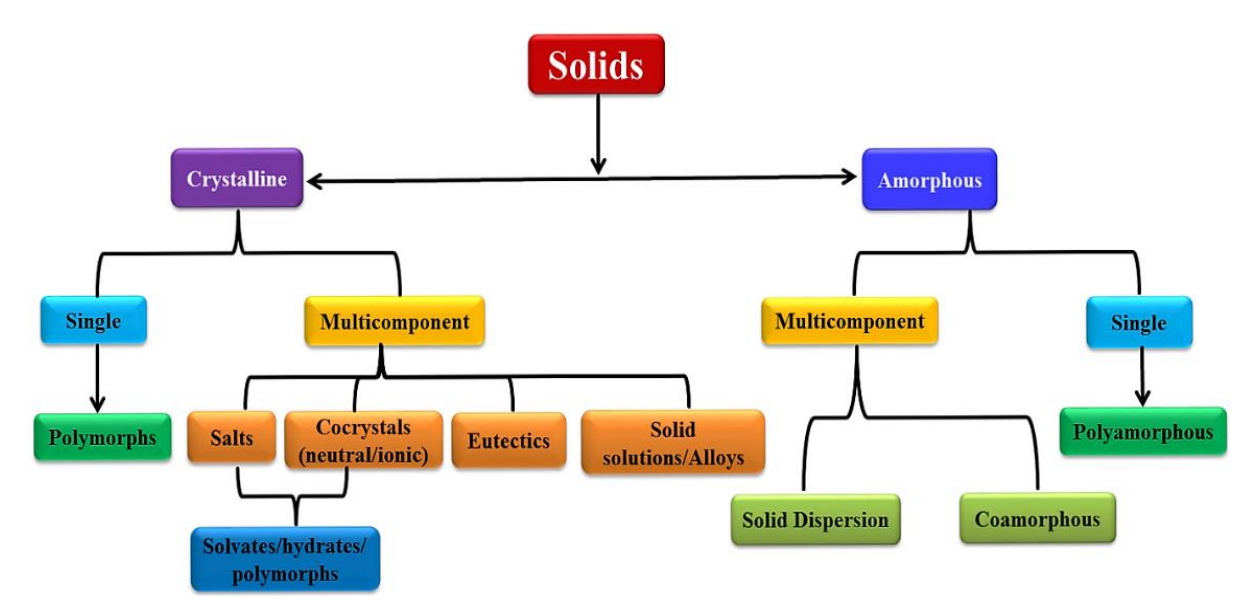


Figure 1.5: Biopharmaceutical Classification System (BCS) of drugs.

#### 1.7 Solid-State Chemistry of Pharmaceutical Drugs and its classification:

The 'Solid State Chemistry of Drugs', 38 which primarily focuses on solid state reactions of active pharmaceutical ingredient and their physical/chemical stability issues, has now widened its scope to 'pre-formulation development' and 'intellectual property management' of drugs to address and achieve the ultimate goal by altering their physicochemical properties and optimizing the APIs without changing their molecular structure and in a desired manner to meet patient.<sup>39</sup> Several strategies and techniques are well pursued and adopted in the area of solid-state chemistry of pharmaceutical drugs. Based on the number of components in the crystal lattice, they are broadly classified as single molecular entities or multi-component molecular entities are shown in Figure 1.6 Different crystalline arrangements of the same chemical substance are "polymorphs" of single component molecules. Multicomponent crystal structure lattice includes such as hydrates/solvates, salts, complexes and, more recently, cocrystals of the molecules with a second component i.e., ion, water, solvent or a coformer. The cocrystal concept has been addressed very recently via systematic approach for the formation of pharmaceutical cocrystal. All these are broadly classified as crystalline. When there is no periodic arrangement of the molecules, i.e., randomly arranged with short range of contacts, they are defined as amorphous substances (Figure 1.8) that includes single component and multicomponent coamorphous solids. The stoichiometric ratios of two or more solids are held together through weak but discrete interactions resulted an aperiodic arrangement. The individual components are crystalline but the resulted adducts are X-ray diffraction amorphous (broad halo peak). For better understanding packing arrangement in crystal lattice of those solids is shown in Figure 1.7. In this chapter further there will be discussion on polymorphs, salts, cocrystals and coamorphous solids.



**Figure 1.6:** Classification of pharmaceutical solids based on the molecular packing in a crystal lattice into various solid-state categories.

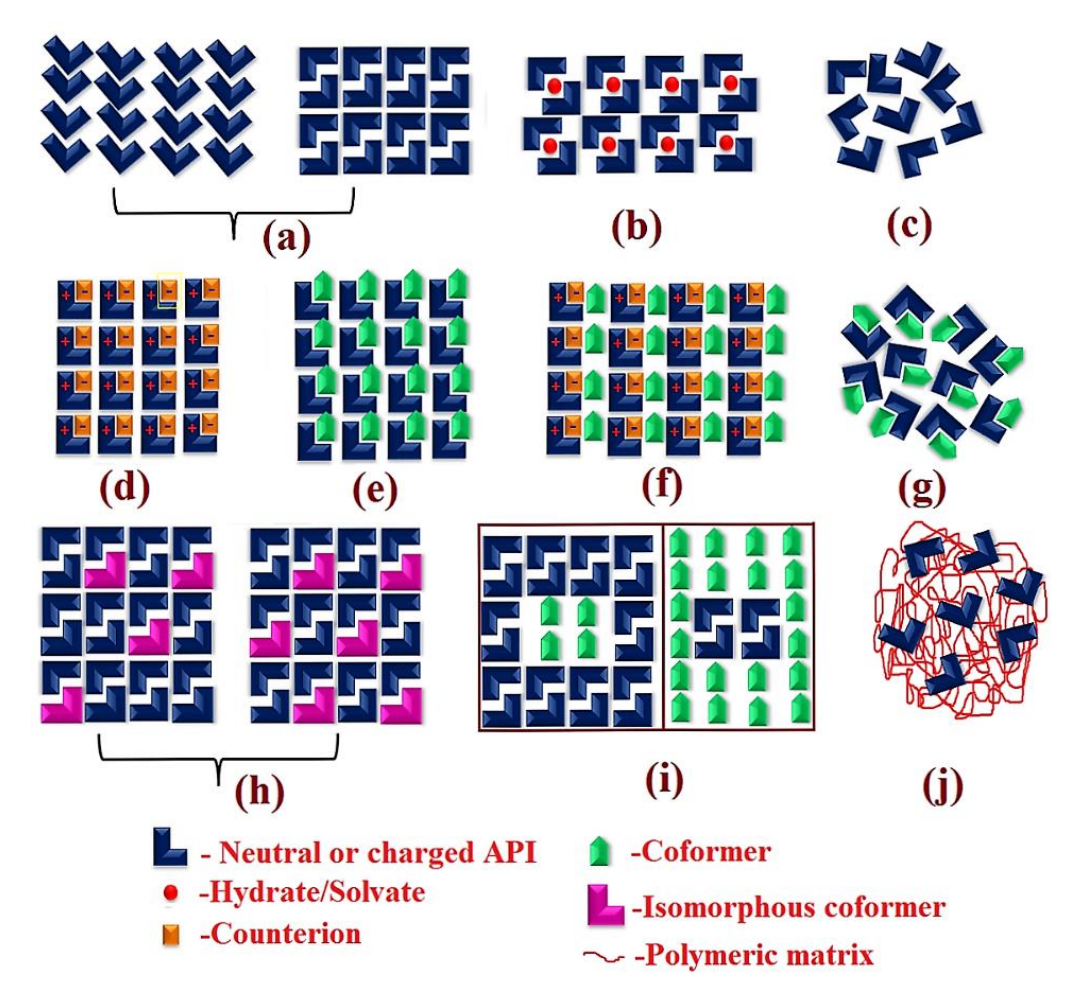


**Figure 1.7:** Schematic representation of various pharmaceutical solid forms possible for a solid when combined with the same solid which can be polymorphic (a) and amorphous (c) or with a different material which can be solid or liquid (b). salt (d), cocrystal (e) and ionic cocrystal, (f) compounds with

similar size and crystal structures can form 'continuous solid solutions' (h) and the ones with mismatch and misfit can give rise to a 'eutectic' (i). A 'eutectic' is a 'conglomerate of solid solutions' wherein the solid solution domains are held by weak interactions. Solid solutions/eutectics resemble crystal structures of their individual components. Binary system existing in aperiodic lattice is called coamorphous (g). A drug is dispersed in polymeric matrix is called solid dispersion (j).

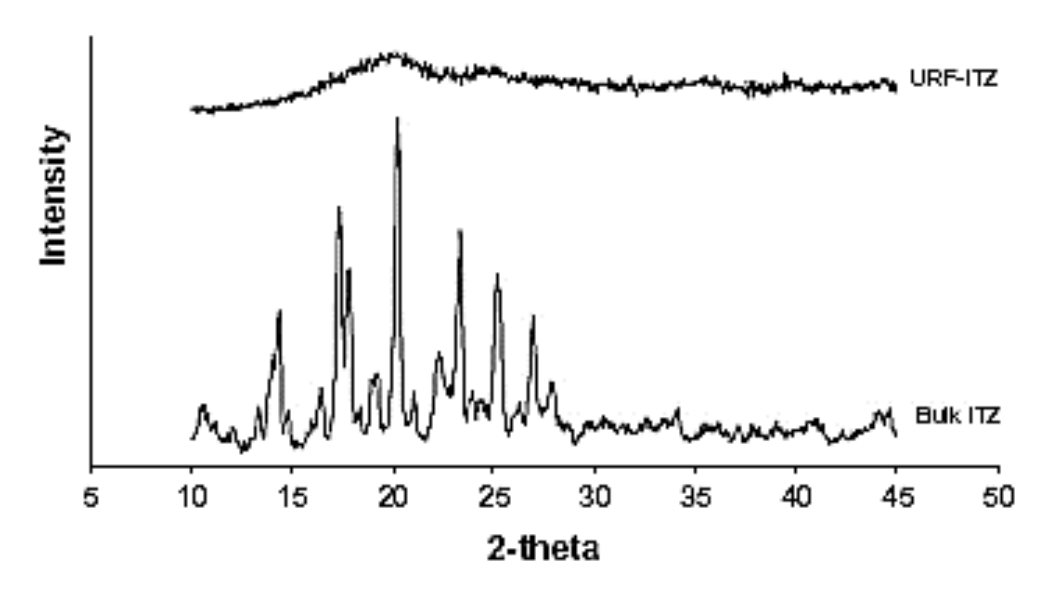


Figure 1.8: Powder X-ray diffraction patterns of amorphous (top) and crystalline (bottom) Itraconazole.

#### 1.7.1 Polymorphism

The word 'Polymorphism'  $^{13,32,33}$  derived from Greek, poly = many + morph = form. 13 the phenomenon of polymorphism pertains to crystalline solid state, it is typically attributed by Mitscherlich<sup>41</sup> (1822, 1823), who recognized different crystal structures of the same compound in a number of arsenate and phosphate salts (NaH<sub>2</sub>AsO<sub>4</sub>,H<sub>2</sub>O and NaH<sub>2</sub>PO<sub>4</sub>,H<sub>2</sub>O). Polymorphism refers to the ability of a compound to exist in more than one crystal form. Berzelius<sup>42</sup> was the first used the term allotropism to describe the occurrence of an element existing in several crystal structures called allotropes. Therefore, in a broad sense, polymorphs and polymorphism to a compound, while allotropes and allotropism is to an element. 40 Even though the history of polymorphism can be traced in nineteenth century and its importance in the field in pharmaceuticals was brought to light by Walter McCrone who gave the widely accepted definition that "a solid crystalline phase of a given compound resulting from possibility of at least two different arrangements of the molecules of the compound in a solid state". 43 As per the Structure-property relationship point of view, the different polymorphs exhibit different properties just as different compounds. 43 In effect, polymorphs of an API by virtue of their difference in structures can display differences in physico-chemical properties, such as melting point, compressibility, stability, solubility, dissolution rate and bioavailability, which form important criterion for the selection of optimal solid form for formulation and usage. 44,45

#### 1.7.1.1. Classification of polymorphs

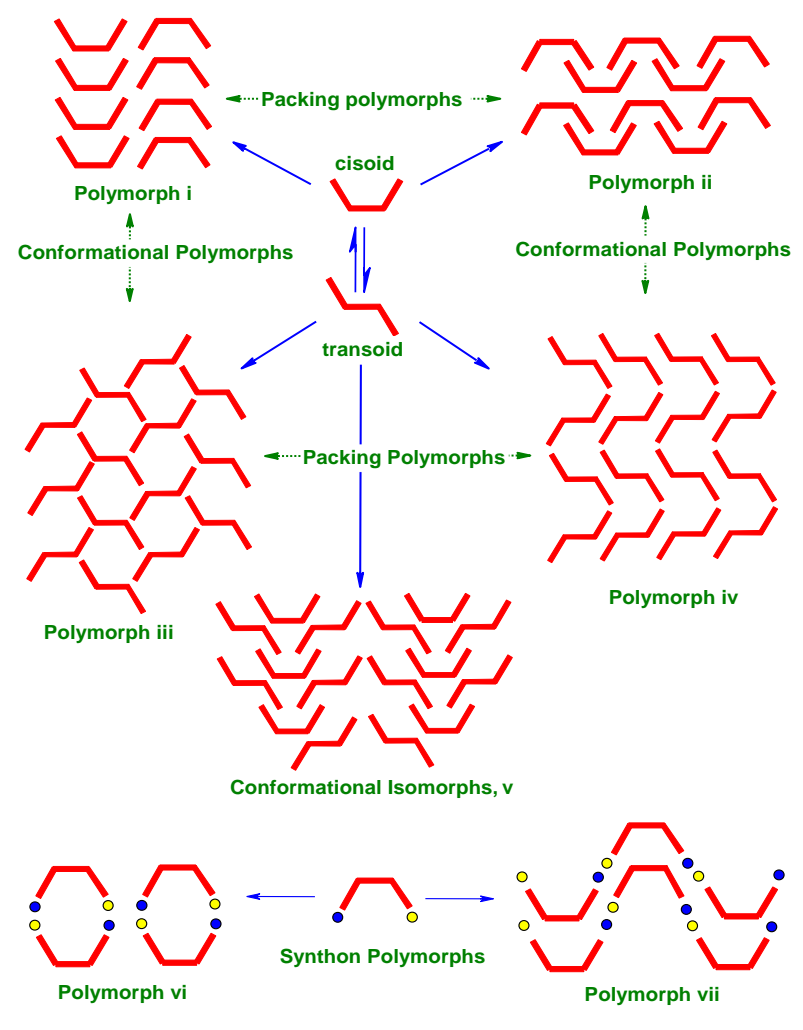


Figure 1.9: Schematic representation of different kinds of polymorphs. (Adapted from Ref. 47)

From a structural point of view, different polymorphs are having different physical, thermodynamic (density, refractive index, thermal and electrical conductivity, hygroscopicity, melting point, solubility and stability), spectroscopic, kinetic (rate of dissolution, stability), surface (surface area, crystal habit), mechanical (hardness, compression, thermal expansion), chemical (chemical reactivity, photochemical reactivity) properties so there is a need of understanding on molecular arrangement and control over polymorphs for rational solid-state design. Polymorphism can be classified as 1. Conformational polymorphism, 2. synthon polymorphs, 3. packing polymorphs<sup>46</sup> (Figure 1.9). The differences in molecular conformations lead to different crystal structures, it is called 'conformational polymorphism'<sup>47,48</sup> e.g., dimorphs of anti-HIV drug Ritonavir.<sup>49</sup> When the supramolecular synthon or non-covalent interactions are different in different crystal structures, it is called 'synthon polymorphism'<sup>46,50</sup> e.g., acid dimer and acid catemer in the dimorphs of Oxalic acid<sup>51</sup> (Figure 1.10). When the arrangement of molecules (whether conformational flexible or rigid) varies in different crystal structures, it is called 'packing polymorphism'.<sup>46,52</sup> In broader sense all polymorphs arise from

differences in molecular packing and so referring them as packing polymorphs is a gross classification which does not give information about structural details. Though these classifications are subjective because of overlap possible between them and more than one can coexist in a given system, for e.g. conformational and synthon polymorphism (in the trimorphs of diuretic drug Furosemide, Figure 1.11)<sup>46</sup> or synthon and packing polymorphism (in the tetramorphs of anti-tuberculosis drug Pyrazinamide, Figure 1.12),<sup>53</sup> the advantage of classifying polymorphs in the above categories is to facilitate understanding of the differences between polymorphs at the molecular level.

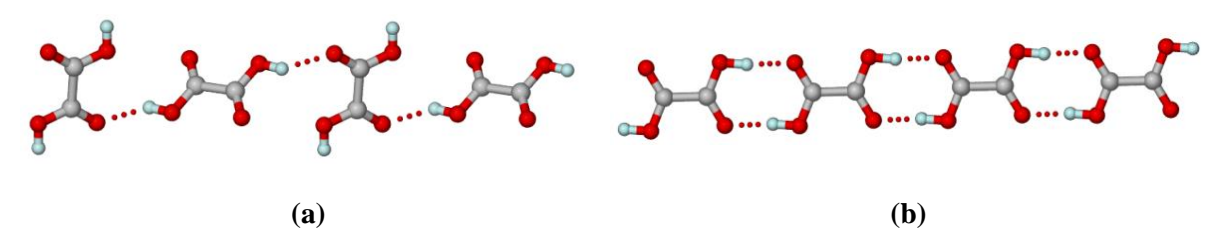
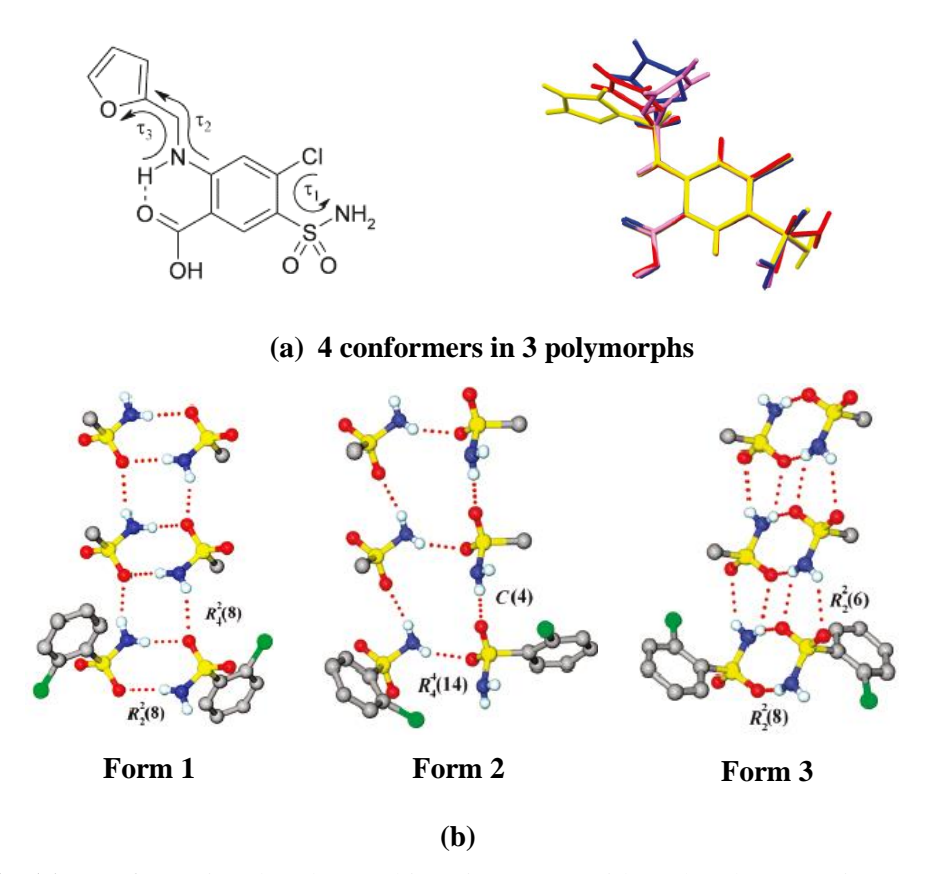
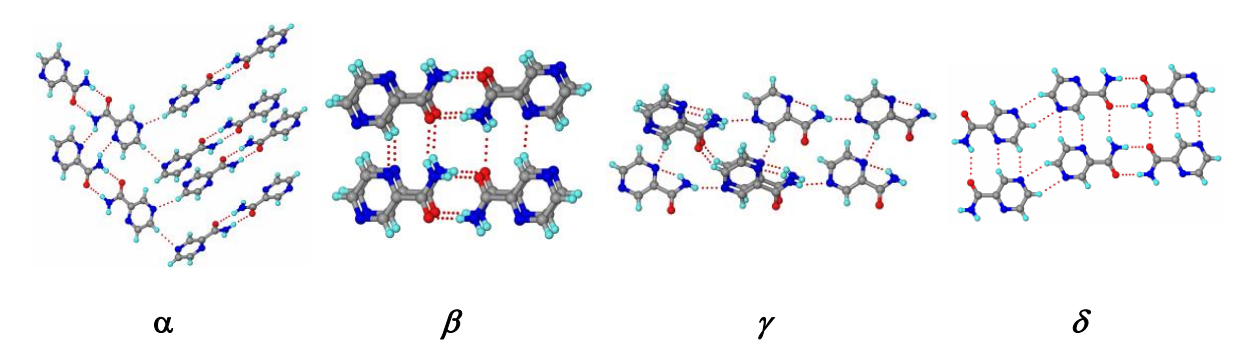


Figure 1.10: Synthon polymorphs of Oxalic acid. (a)  $\alpha$ -form has acid catemer and (b)  $\beta$ -form has acid dimer in their crystal structures. (Adapted from Ref. 51).



**Figure 1.11:** (a) Conformational polymorphism in Furosemide. The three torsion parameters in Furosemide:  $\tau$ 1=C-C-S-N,  $\tau$ 2=C-N-C-C,  $\tau$ 3=N-C-C-O. The anthranilic acid moiety is conformationally locked by intramolecular hydrogen bond but conformational flexibility in the furan and sulfonamide

moieties resulted in four conformers (red, blue, pink and yellow) manifested in three polymorphs. (b) Synthon polymorphism in Furosemide.  $R_2^2(8)$  N–H···O dimer and  $R_4^2(8)$  motif in form 1, C(4) catemer and  $R_4^4(14)$  tetramer motif in form 2,  $R_2^2(8)$  N–H···O motif and  $R_2^2(6)$  rings in skewed dimer of form 3. (Adapted from ref. 46).



**Figure 1.12:** Synthon and packing polymorphism in Pyrazinamide. In α polymorph, zigzag tapes formed by  $R_2^2(8)$  N–H···O and  $R_2^2(10)$  N–H···N hydrogen bonds are connected orthogonally to  $2_1$  screw related tapes through C–H···N interactions in a 3D arrangement. The  $\beta$  polymorph has non-planar  $R_2^2(8)$  N–H···O dimers that make a helix along the b-axis through anti N–H···O and C–H···N interactions. In  $\gamma$  polymorph, 1D tapes assembled via N–H···N hydrogen bonds of C(6) notation are connected through C–H···O and C–H···N interactions. In  $\delta$  polymorph, carboxamide tapes formed by  $R_2^2(8)$  dimer and C(4) catemer N–H···O synthons and  $R_2^2(6)$  C–H···N synthons make 2D sheets. (Adapted from ref. 52)

#### 1.7.1.2. Polymorphs generation and transformation

Screening and generating desired polymorph is an essential component of pharmaceutical research.<sup>54,55,56</sup> The conventional methods are evaporative crystallization in different solvents, varying temperature of crystallization, milling etc., new techniques such as sublimation and melting, <sup>59,60</sup> crystallization with structurally related additives, <sup>59</sup> using polymers as heteronuclei, <sup>61,62</sup> laser induced nucleation, <sup>63</sup> crystallization in capillaries, <sup>64</sup> rotavaporization, <sup>65</sup> controlled desolvation, <sup>66</sup> freeze and spray drying etc. are being employed for the generation of polymorphs. Of late, new polymorphs are being obtained during cocrystallization experiments. <sup>67,68</sup> Once a polymorph with desired properties is obtained, conditions need to be standardized for bulk manufacture and sustenance of the polymorph to prevent potential transformation to a more stable polymorph with time. This can happen because the polymorphs are at different levels on the 'free energy' surface and therefore inter-conversions are quite possible which lead to changes in the properties of bulk drug material finally affecting its efficacy. <sup>43,55</sup> Therefore, it is essential to gain adequate understanding of their properties so as to optimize the conditions to develop a desired polymorph for formulation.

The desired polymorphs can be obtained from the interplay of thermodynamic functions (free energy, enthalpy and entropy) and kinetic factors (activation energy, temperature, supersaturation, rate of evaporation etc.) that govern the crystallization process (Figure 1.13a). 40,55 According to Ostwald's rule of stages, 69-71 a system reaches the low energy state and attains equilibrium from an initial high-energy state through minimal changes in free energy involving different intermediate forms at different stages (Figure 1.13b). Thus, the form that crystallizes first is the one which has the lowest energy barrier (high energy, metastable form) from liquid to solid state. This form then transforms to the next lower energy polymorph on the energy diagram and the process continues until the crystallization of the thermodynamically stable form. 69-71 The transformation of the metastable form to the stable form and number of intermediate forms manifesting during the process is dependent on free energy of activation, nucleation as well as time. On the other hand, as the energy difference between the polymorphs is typically within a 5 kcal mol<sup>-1</sup> window, 47,48 several polymorphs can crystallize simultaneously if their nucleation rates are equal. This phenomenon is called 'concomitant polymorphism' wherein the polymorphs, both stable and metastable, crystallize under the same conditions and the same vessel. Concomitant polymorphs are generally 'near-energetic'. 40

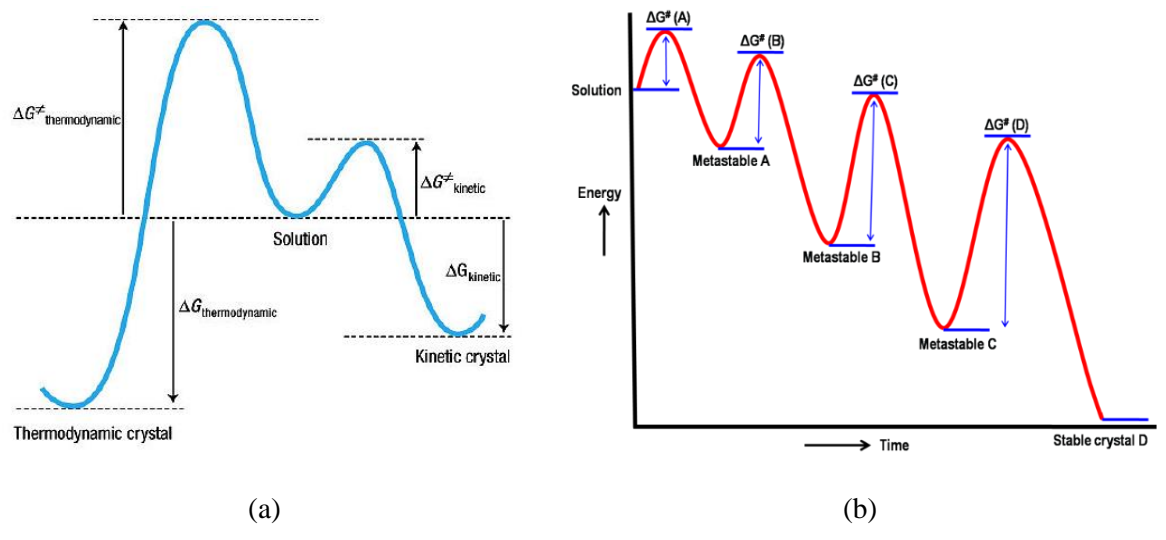


**Figure 1.13:** (a) Kinetic and thermodynamic outcome of crystallization reaction. (b) Ostwald's Rule of Stages. Initial high-energy state (metastable A) through minimal changes in free energy crystallizes first and is the one which has the lowest energy barrier. Metastable A form will then transform to the next lower energy polymorph (metastable B) and so on (metastable C) until thermodynamically stable crystal D. (Adapted from ref. 71)

Polymorphic transformations (solid-solid phase transformations) can happen during crystallization as above i.e. in solution, upon storage and with variation in temperature. The transformation or interconversion from metastable to stable form or even stable to metastable form in a given set of conditions, depends on how the free energy of activation is achieved by the system for the

nucleation of a polymorph and its consequent growth.<sup>72</sup> The manufacturing processes such as granulation, milling, compression etc. can also facilitate transformation.<sup>73-76</sup> Seeding also induces the formation of particular polymorphs since the process bypasses the rate-limiting nucleation step.<sup>72</sup> In all, the transformation is dependent on the inherent thermodynamic functions of the system with respect to temperature, which can also provide the activation energy for nucleation and transformation. The entropy and temperature components influence the free energy of a system and thus are crucial in establishing the relative thermodynamic stability relationships of polymorphs.<sup>40,42,72</sup> They can shift the balance from one polymorph to another polymorph with respect to their stability depending on the conditions prevalent.

Thus, thermodynamically, polymorphs are divided into monotropic and enantiotropic systems. 40,43,78 Monotropism is the phenomenon in which only one polymorph is the stable form at any temperature and all other polymorphs convert to through exothermic phase transition. Enantiotropism is the phenomenon in which one polymorph is stable at one temperature and other at another temperature and the two are related by a reversible phase transition. An endothermic phase transition at some temperature before melting is characteristic of an enantiotropic system. In general the situation of an enantiotropic system is like this: when a polymorph is heated, it transforms to another polymorph, by taking energy, at one particular temperature called 'transition temperature', above which the new polymorph is stable; this high temperature polymorph reversibly converts to the original polymorph, by losing energy, upon cooling beyond the transition temperature. 40,78 Sometimes, if the conditions favor, the high temperature polymorph, though metastable at room temperature, can elude transformation. 46,77 The same is true for near-energetic polymorphs of a concomitant crystallization batch. If the conditions are such that the free energy of activation required for the transformation to the stable polymorph is high and the nucleation of stable polymorph is not favoured, all these metastable polymorphs can sustain from days to many years. 40,77 But, once the conditions favoring the formation of stable form prevail, the metastable forms can convert to it at any time. Nevertheless, the metastable nature of such polymorphs can be translated as solubility advantage over stable polymorphs which have lower solubility, as per the inverse relationship of solubility and stability. 44,76 Thus, this attribute of metastable polymorphs is taken advantage of for pharmaceutical formulation purposes. However, their potential transformation to the stable form is a serious concern and special care should be exercised to avoid the transformation and achieve the desired objective.

### 1.7.1.3. Importance of Polymorphs in Pharmaceutical Industry

Polymorphs received tremendous attention in pharmaceutical industry because of its importance in formulation<sup>76</sup> as the different properties of polymorphs make them commercial and patentable.<sup>79</sup> Once a polymorph with desired properties is obtained, conditions need to be optimized for the bulk manufacturing to prevent potential transformation to a more stable polymorph. This can happen because

the polymorphs are at different levels on the 'free energy' surface and therefore inter-conversions are quite possible which lead to changes in the properties of bulk drug material finally affecting its efficacy. 80-84 Therefore, it is essential to gain adequate understanding of their properties so as to optimize the conditions to develop a desired polymorph for formulation

Polymorphism gained immense interest to understand and control the production and stability of polymorphs in pharmaceuticals. If a generic pharmaceutical company discovers a novel crystal form of an existing marketed drug, it will gain an early access into the marketplace; therefore, the innovator must find out all possible polymorphs of the drug and patent them in order to extend their monopoly in pharmaceutical industry and protect their product. The well-known example is anti-ulcer drug Ranitidine hydrochloride polymorphs to show the importance in the context of polymorphism (Figure 1.15). Glaxo obtained a patent on the two polymorphs (I, followed by II) of Ranitidine hydrochloride. <sup>85</sup> In the mid-1990s, as the patent on the drug form I was approaching expiration and it opened the market for the entry of generic manufacturers to sell a generic version of form I of the drug. But the generic manufacturers were not able to crystallize form I exclusively as it was always crystallizing as a mixture of form I and form II. This kept the generic company's products off the market for several years and during that period Glaxo was making \$10 million in sales each day on this blockbuster drug. Ultimately Novopharm could find a method to prepare form I exclusively with less than 1% amounts of form II, and won the battle. Since then, generic entry was made into the market. This case demonstrated the importance of phase purity and characterization techniques for patentability.

Another example Ritonavir (brand name 'Norvir'), a HIV protease inhibitor, developed by Abbott Laboratories is a popular example which drew a lot of attention both from academia and industry with respect to polymorphic transformations and control and their potential implications. After two years of its launch in the market (1996-98), a new stable but less soluble polymorph II (4 times less soluble than form I) of Ritonavir was detected in the drug formulations which led to inadequate activity/bioavailability. Abbott withdrew the drug from the market and re-entered the market after standardizing the procedures to obtain the original more soluble polymorph I. In this process, the company lost an estimated \$250 million in sales the year the drug was withdrawn. Ritonavir polymorphs represent an example of conformational polymorphs and also polymorphism induced by an impurity. It is hypothesized that a carbamate impurity (hydrolytic product of Ritonavir), having *syn* conformation of amide moiety, in bulk drug, induced the crystallization of form II having amide in *syn* conformation from form I with amide in *anti*-conformation (Figure 1.14).

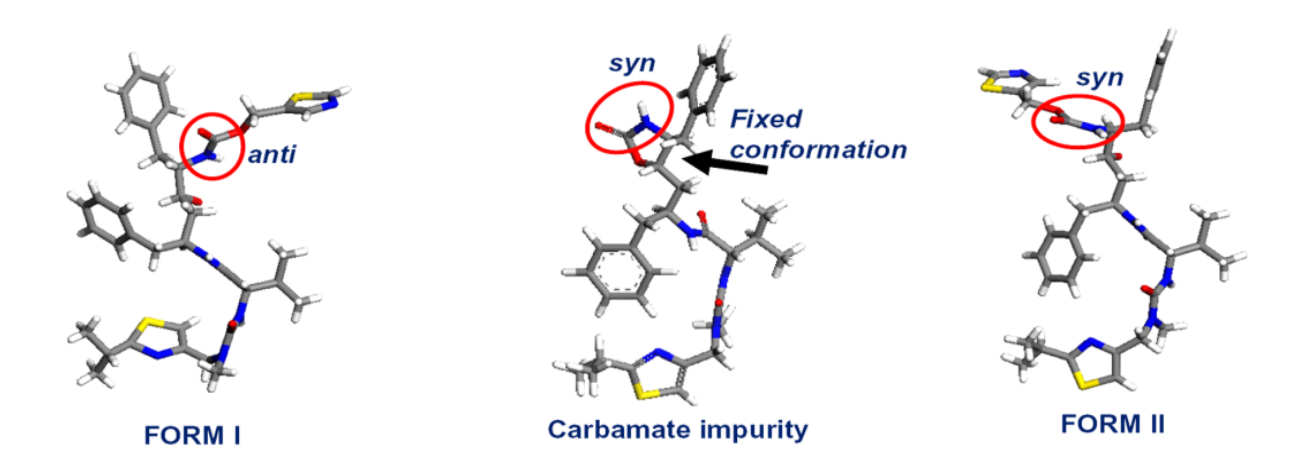
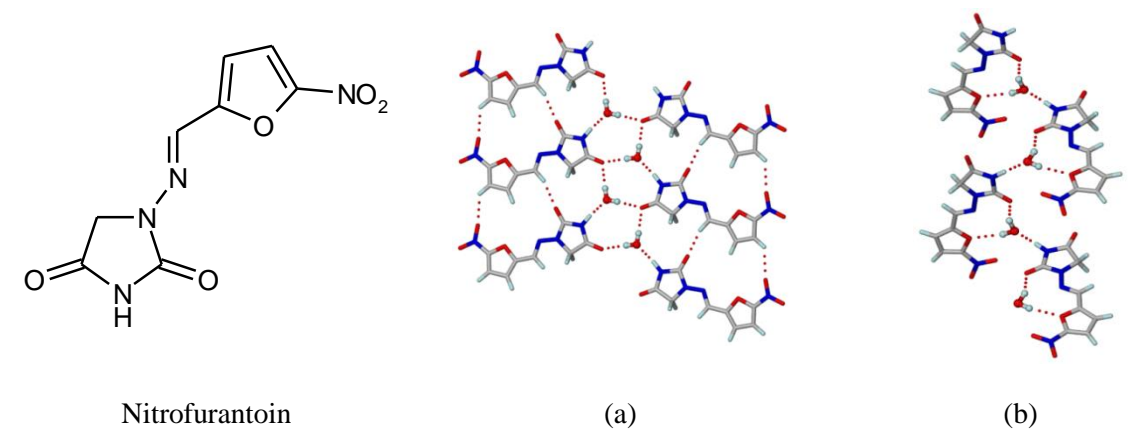


Figure 1.14: The anti and syn amide conformers of Ritonavir form I and II. (Adapted from Ref. 87)

## 1.7.2 Pseudopolymorphism-Solvates and Hydrates

McCrone introduced the term 'pseudopolymorphism'.88 It is defined as the phenomenon wherein a "Compound is obtained in crystalline forms that differ in the nature or stoichiometry of included solvent molecules" and the resulting solid forms are known as pseudopolymorphs.<sup>79</sup> Pseudopolymorphs also termed as solvates or hydrates or solvatomorphs, and this class of compounds exhibit different solubility, dissolution rate, mechanical behavior, stability and bioavailability from their unsolvated counterparts.<sup>39b</sup> The propensity of a compound to form pseudopolymorphs is deemed to be relevant to molecular structures, hydrogen bonding ability and crystal packing.<sup>89</sup> Generally, during crystallization process, strong solute-solvent interactions result in the nucleation of solvated crystals. In particular water molecule, because of its small size, and ability to act as both a hydrogen bond donor and acceptor found to be more capable of linking to drug molecules to form new crystal structures than any other solvent. It is found that approximately one third of active pharmaceutical ingredients (APIs) can form crystalline hydrates.<sup>39d</sup> Sometimes, solid can incorporate different ratios of the same solvent for example, antibiotic drug norfloxacin forms a dihydrate, 1.25 hydrate and 1.125 hydrate. On the other hand different solvents can incorporate in the crystal lattice for example, antibacterial drug nitrofurantoin forms solvates with water, DMF, DMSO, methanol etc. 91 Sometimes polymorphs of solvates also observed example includes nitrofurantoin monohydrate polymorphs I and II (Figure 1.15).91 The choice between solvated or unsolvated forms of a drug will depend on its pharmaceutical properties like stability under different conditions, shelf life etc. Various drug molecules are currently marketed as solvates/hydrates, for example, indinavir sulfate is marketed as its ethanol solvate and paroxetine hydrochloride is marketed as its hemihydrate. 92



**Figure 1.15:** Pseudopolymorphs of nitrofurantoin monohydrate. (a) In form I, tapes of translation related nitrofurantoin molecules are connected by water molecules through O–H···O and N– H···O hydrogen bonds. (b) In form II, discrete nitrofurantoin molecules form a zigzag tape through water molecules. (Adapted from ref. 91)

As a general rule, solvates are not preferred for pharmaceutical development, except for hydrates and occasionally ethanolates, because of the toxicity and undesirability of ingesting most of the solvents. Hence, solvents with low toxicity need to be used for pharmaceutical purpose, and these solvents are classified based on decreasing toxicity, from Class I (such as benzene, carbon tetrachloride etc., should be avoided) to Class II (such as acetonitrile, methanol, pyridine etc., should be limited) to Class 3 (such as ethanol, acetic acid, acetone etc., can be preferred). Some solvents although present in the crystal lattice of the parent solid (in channels/voids) have no or little role on the integrity of the crystal structure and hence can be readily desolvated and resolvated for practical purposes for instance, cephalosporin solvates. But, some solvents upon controlled desolvation can produce new polymorphs of the parent material example of caffeine Form II from its hydrate. Hence, purposive solvation and desolvation experiments are routine during polymorph screening of APIs and important for crystallization of a desired polymorph. In all, pseudopolymorphs are one of the important class of drug solid forms which have several applications in the pharmaceutical industry.

#### 1.7.3 Pharmaceutical Salts

Salt formation has been a traditional way and primary approach to modify the physicochemical properties of an API. A crystalline salt is an ionic solid involving a charge-charge interaction between ions of opposite charge. Salts are formed when a compound that is ionized in solution forms a strong ionic interaction with an oppositely charged counterion. Its success and stability are dependent on the relative strength of the acid or base and the acidity and basicity constant of the components involved. The general rule of thumb for salt formation is that the acid ionization constant, pKa, between the acid and the base should be different by at least two or three units. The limitation of this is that the pKa values are only valid under the solution equilibrium conditions at which they were determined. Salts of

their inherent strong ionic interactions tend to be stable and in general exhibit higher melting points than their parent APIs. Their ability to form electrostatic interactions and charge-assisted hydrogen bonds with water in the biological media confers higher solubility to the API salt formulation. Thus, salts offer dual advantages of solubility and stability.<sup>97</sup>

The bestseller drug Ranitidine hydrochloride (brand name 'Zantac)<sup>98</sup> used in the treatment of gastro-intestinal ulcers is one of the best examples of the case and is also another instance of commercial success through polymorphs as intellectual property. Ranitidine base is low water soluble (25 mg/mL)<sup>99</sup> and becomes unstable when exposed to light.<sup>100</sup> It also gives a sulfurous odor and has a low melting point of 70 °C. But, ranitidine hydrochloride salt has all the desirable attributes of high water solubility (1 g/mL),<sup>101</sup> higher melting point (136 °C), more stability and is almost odorless.<sup>100</sup> With regard to the IP issue of polymorphs, Glaxo patented two polymorphs of Ranitidine hydrochloride because of which it could sustain in the market even after patent expiry of the first polymorph.<sup>44</sup> This is because the generic companies have to make a formulation that should be free of the second polymorph, otherwise it would be infringement of reigning patent on the second polymorph. Thus, ranitidine hydrochloride is the illustrative example of 'pharmaceutical form development' and 'intellectual property management'.

However, salts have their own setbacks. The hygroscopic nature of salts, by virtue of their inherent affinity to water/moisture, is a serious problem in several cases. 98,102 The hygroscopicity of the anti-tuberculosis drug Ethambutol dihydrochloride salt is reported to cause instability of the anti-TB fixed dose combination (FDC) drug formulations, thus leading to poor quality medicines which will not be useful for treatment (Figure 1.16). Moreover, for neutral and weakly ionizable APIs, salts cannot be made. Of late, majority of the new drug candidates coming into the area are hydrophobic and lack ionizable functional groups. These issues warrant the need of novel solid forms that can avoid these problems. Although, prodrugs, solid dispersions, nanoparticles, cyclodextrin inclusion complexes etc. Or-109 were shown to be promising approaches, the ultimate goal of modulation of physico-chemical properties of drugs in a desired way warrants other strategies to achieve the objective.



**Figure 1.16:** Marketed anti-TB FDC products in packed and unpacked state and their behavior when unpacked products are exposed to humidity and photostability chambers after 5 days. (a) Strip pack,

packed control; (b) unpacked control; (c) exposed to 40 °C/75% RH; (d) exposed to 40 °C/75% RH/Light; (e) blister pack, packed control; (f) unpacked control; (g) exposed to 40 °C/75% RH; (h) exposed to 40 °C/75% RH/Light. RH = relative humidity. (Adapted from ref. 110).

### 1.7.4 Cocrystal Definition

The earliest example of a cocrystal between quinine and hydroquinone was reported by Friedrich Wöhler in midst of 19th century, and they were called organic molecular compounds, heteromolecular crystals and molecular complexes.<sup>111</sup> However, the term cocrystal as used today did not come into widespread usage until it was introduced by MC Etter in the 1990s. 112 The definition of cocrystal is a decade old debate when the importance of 'pharmaceutical cocrystals' in the current context began around 2000s. 113-116. This debate was started in 2003 only when Desiraju expressed the unsuitability of the term "co-crystal" and suggested that the previously used terms such as "molecular complexes" should be considered. 117 Dunitz, however, irrevocably established that the term "molecular complex" is too uncertain and while the term "cocrystal" is not perfect. 118 He defined a co-crystal as "a crystal containing two or more components together". Both Dunitz and Desiraju agreed that the term should be "co-crystal" in contrast to "cocrystal" to indicate togetherness of two components. Aakeroy offered a more restrictive definition in that the components of cocrystals must be neutral and exists as a solid at ambient conditions with a well-defined stoichiometry. 119 However, Bond found this definition unsatisfactory due to the restriction that all components must be solid. 120 Again Desiraju proposed at least one of the components is molecular (target molecule) and forms a supramolecular synthon with the remaining component (cocrystal former)." Many definitions of cocrystals have been offered by various scientists and there is no hard and fast definition.

To bring a consensus on the definition of a cocrystal, a bilateral Indo-U.S. workshop on Pharmaceutical Cocrystals and Polymorphs held in India, year 2009 brought the organizers from both sides. A lively debate on nomenclature issues starting from what is a cocrystal, or co-crystal, and definition of terms such as pseudopolymorph, solvate, host-guest compounds, etc. engaged an active discussion among participants. In the year 2012 the widely accepted definition of cocrystal was proposed in another Indo-US Bilateral Meeting as the "cocrystals are solids that are crystalline single-phase materials composed of two or more different molecular and/or ionic compounds generally in a stoichiometric ratio". These workshops sent in a clear message that the timing is right for FDA (food and drug administration, USA) to draft the definition of a solid state cocrystals. And thereafter cocrystals brought in the novelty to existing drugs and have been center to the pharmaceutical patents. The fact that the new drug molecule discovery pipeline has slowed down worldwide is an excellent opportunity for Indian scientists and industry to create novel intellectual property.

The US-FDA in the year 2018 published the guidelines as; "Co-crystals are crystalline materials composed of two or more different molecules, typically active pharmaceutical ingredient (API) and co-crystal formers ("coformers"), in the same crystal lattice that provide opportunities for engineering solid-state forms beyond conventional solid-state forms of an API, such as salts and polymorphs. Only if these cocrystals can be tailored to enhance drug product bioavailability and stability and to enhance the processability of APIs during drug product manufacture. With added advantage of diverse array of solid-state forms for APIs that lack ionizable functional groups, which is a prerequisite for salt formation". <sup>123</sup>

#### 1.7.4.1. Importance of Cocrystals in Pharmaceutical Industry

Pharmaceutical cocrystals approach is unique and generated enormous interest, in that it does not affect the pharmacological properties of the drug, but it improves the drugs' bioavailability by improving the several of its physicochemical characteristics, such as melting point, stability, tabletability, solubility, permeability and bioavailability. The factors play an important role on drug by altering the physicochemical properties are the properties of APIs and coformers, the nature of molecular interaction between them and the employed synthetic procedures. The APIs will benefit in presence of coformer in its crystal lattice which is a property modifying component. The effect on the physicochemical properties of the API is dependent on the available coformer generally from GRAS list (generally regarded as safe). Therefore, cocrystals have unique advantage over the more common salts is that cocrystals can be made for non-ionisable APIs as well as for those complex drugs which have sensitive functional groups that may not survive the harsh reaction conditions of strong acids or bases. 124,125 There are several other main advantages behind the formulating the cocrystals. It has a potential to shorten the drug development timeline equate to less cost, which is appealing to pharmaceutical companies.

Different steps are involved for the pharmaceutical cocrystal design and synthesis. This includes selection of coformer guided by crystal engineering and hydrogen bonding principles followed by screening of cocrystal in different methods where the components are mixed together and subjected to solution crystallization, co-sublimation, co-melting, solid state grinding, liquid assisted grinding, slurry crystallization, reaction crystallization, spray drying etc (Figure.1.17). These solid-state synthesis techniques of cocrystals can be classified as green chemistry as they offer high yield, less solvent use and there are few by-products. Pharmaceutical cocrystals are structurally different to their bulk forms; it is possible to patent cocrystals of existing APIs as a new crystal form. Different formulations of pharmaceutical cocrystals are available in the market such as Viagra (Pfizer) to treat erectile dysfunction and pulmonary arterial hypertension, Entresto (Novartis), for treatment of chronic heart failure. Monosodium Sacubitril and Disodium Valsartan cocrystal forms are in the market. Entresto is the first multidrug cocrystal approved following the cocrystal guidance by US-FDA. Entresto

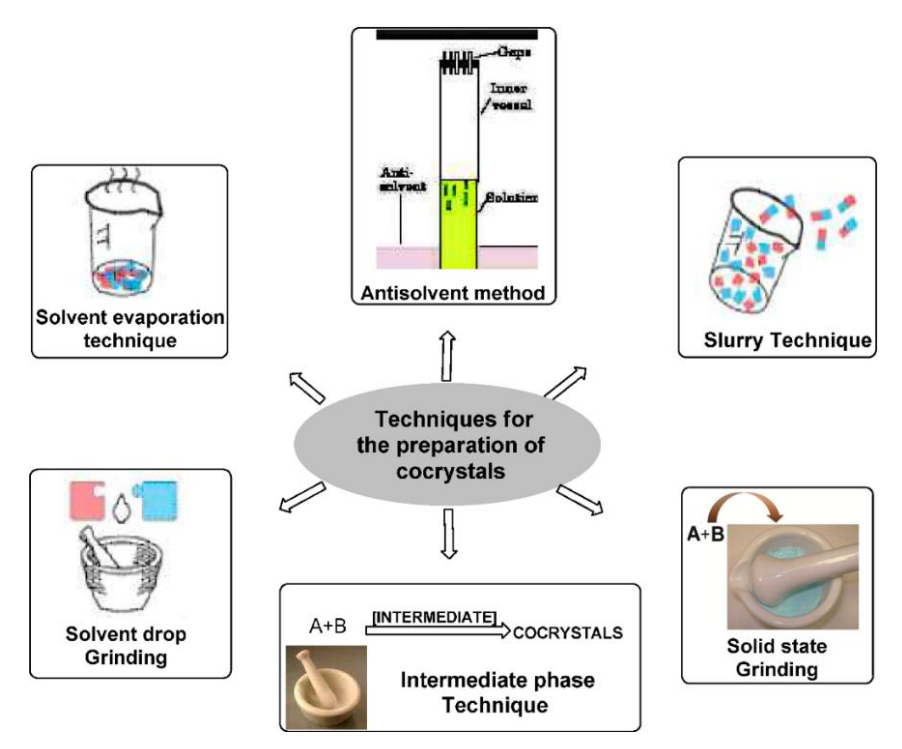
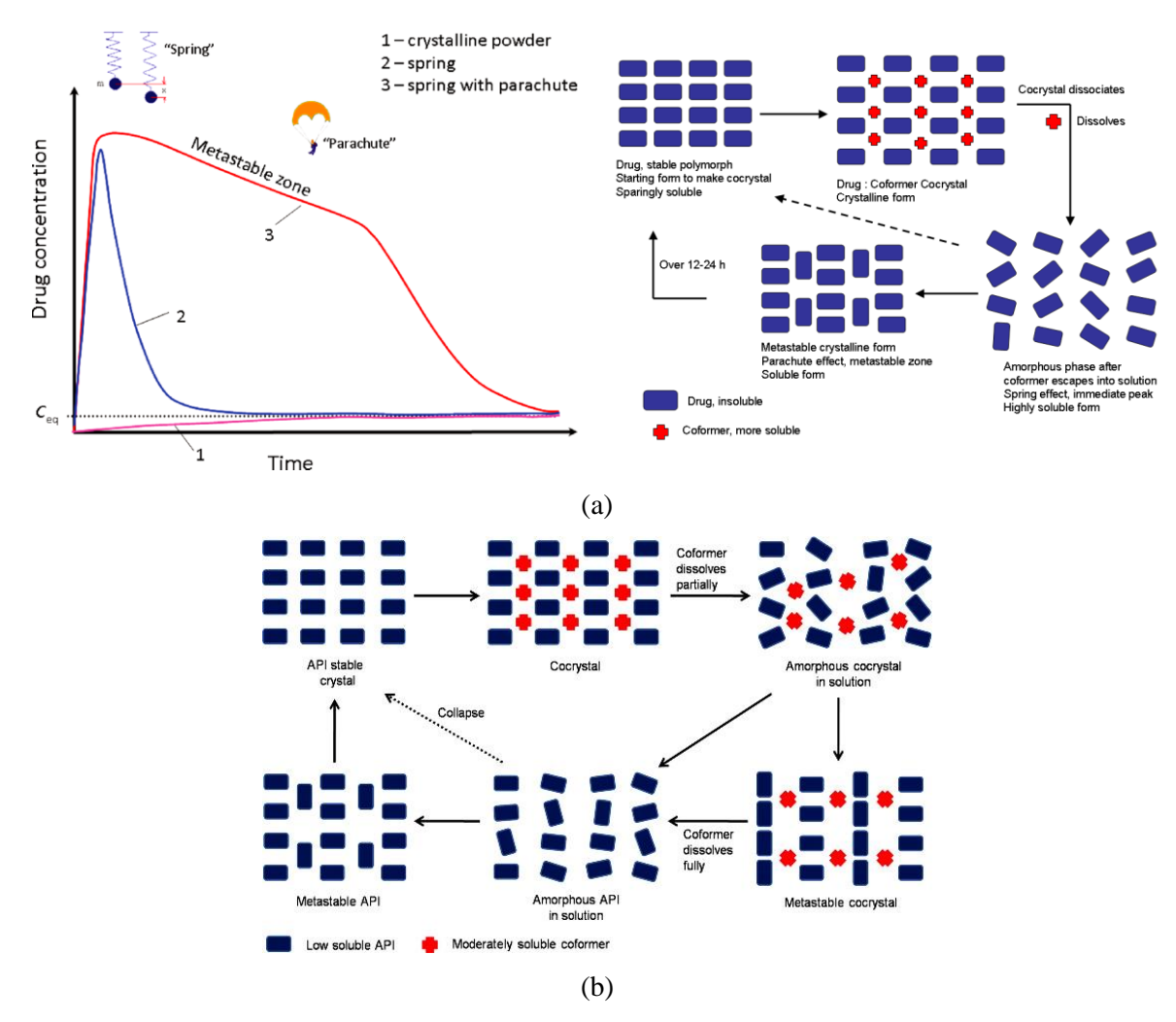


Figure 1.17: General methods used for the preparation of cocrystals.

## 1.7.4.2 Spring and Parachute model for solubility enhancement of cocrystals

In the year 2011, Nangia proposed a model to explain how a coformer can improve the solubility of cocrystals, based on 'spring and parachute' model of amorphous forms. <sup>107</sup> According to the model, a cocrystal containing a high soluble coformer can facilitate faster dissolution of a low soluble component. They explained that fast release of high soluble coformer into aqueous medium (because of its higher affinity to the latter) results in the dissociation of cocrystal, thereby leaving behind the low soluble component in an amorphous/randomized state. This amorphous/randomized state understandably leads to an increase in the free energy of the system, ultimately leading to an improvement of solubility/dissolution of the low soluble component (Figure 1.18 a & b). Later Desiraju extended the model ascribing the retention of high solubility over prolonged duration to the formation of a loosely bound, amorphous cocrystal structure in solution through a supramolecular synthon effect (Figure 1.18 c). <sup>128</sup> This model complies with the 'coformer solubility rule' in that high solubility coformers will give rise to high solubility cocrystals and vice-versa. If the coformer has low water solubility, it does not dissociate from the lattice easily and in effect can control the solubility/dissolution of the drug.



**Figure 1.18:** (a) Nangia's model of solubility enhancement of a drug through a pharmaceutical cocrystal (adapted from ref.107). (b) Extended model of Nangia's by Desiraju et. al. (Adapted from ref.128)

#### 1.7.4.3 Cocrystals in pharmaceutical Sciences

The application of cocrystal in pharmaceuticals used today haven't come into widespread usage until it was popularized by Nangia et al form early 2000 to till date. Nangia et al <sup>130</sup> also reported the hydrolytic stability of anticancer drug temozolomide (TMZ) by forming cocrystals. It is a BCS class I drug with high solubility and permeability but it has poor stability during storage. It is transformed to 5-aminoimidazole-4-carboxamide (AIC) and this makes the drug less effective. This issue was addressed by making cocrystal with succinic acid (SA) and showed that TMZ-SA is stable for over six months in accelerated stability conditions of 40°C and 75%RH and 30°C and 65%RH. Whereas pure TMZ transformed to AIC with two weeks and after six months only 30% of TMZ is left. Further bioavailability study of TMZ-SA cocrystal on sprague dwaley rat's results shown that TMZ-SA is bioequivalent to TMZ (Figure 1.19). <sup>131</sup>

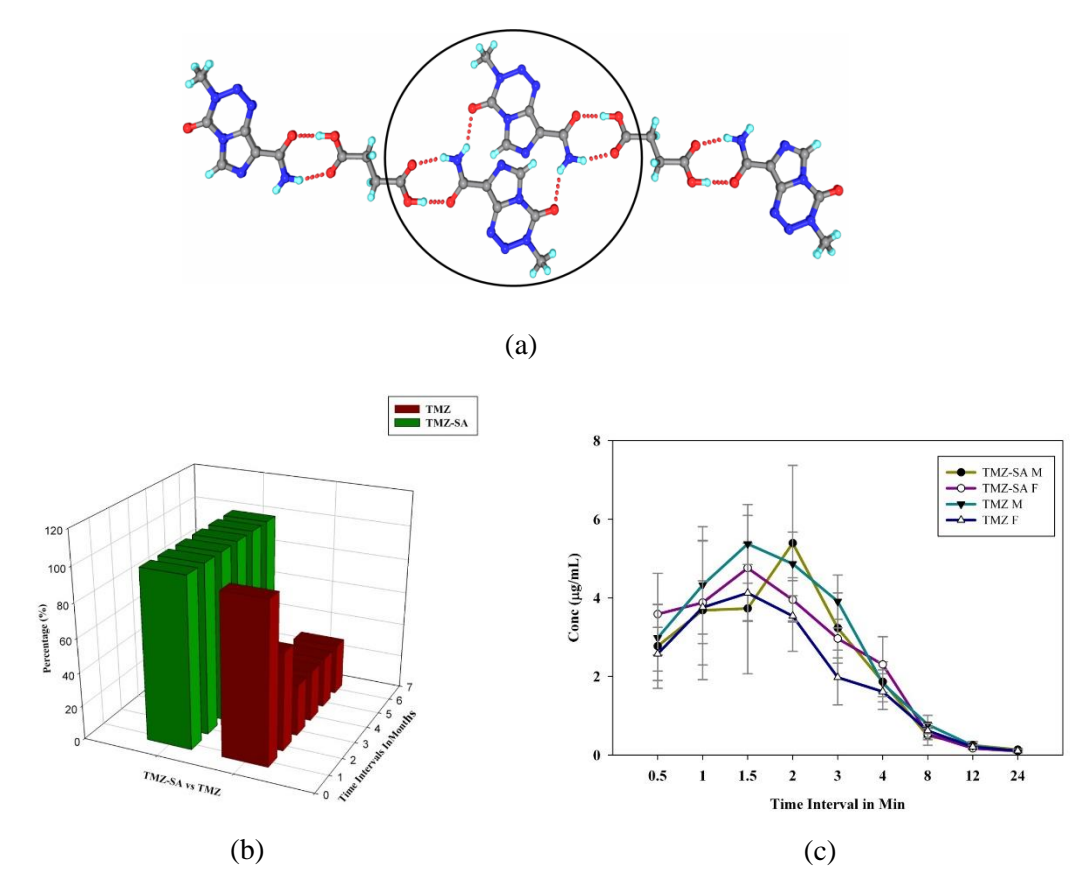


**Figure 1.19:** (a) TMZ–succinic acid cocrystal sustained by acid-amide dimer interaction (b) chemical stability of pure TMZ and TMZ-SA cocrystal (for temozolomide) by HPLC analysis stored at accelerated conditions. TMZ showed degradation to 30% of the original purity in the 6-month period. TMZ-SA test cocrystal remained stable during the entire 6 months of study with final drug concentration of over 99%. (c) mean plasma concentration versus time profile of TMZ reference drug and TMZ-SA test cocrystal. (Adapted from ref. 130 & 131)

In this manner many groups worked extensively worked on pharmaceutical cocrystals and reported that, cocrystals can modulate/tune the properties (stability, tabletability, solubility, dissolution, permeability, and bioavailability) of drug component without altering the chemical composition and biological activity. Itraconazole which is a highly insoluble antifungal drug and marketed in amorphous form (as Sporanox capsule) to achieve good bioavailability. In order to solve the issue, Remenar et al. <sup>132</sup> prepared the cocrystals of Itraconazole by using carboxylic acid coformers such as malic, succinic (Figure 1.20a), tartaric acid. Later they performed the dissolution studies (Figure 1.20b) for all crystalline forms in 0.1N HCl and compared, the cocrystals improved dissolution rate by 4-20 times compared to its crystalline API and the peak values were maintained for about 8h. Among all the cocrystals malic acid cocrystal showed similar dissolution profile as amorphous form but with lesser stability, the succinic acid cocrystal showed better stability, dissolution profile and suitable for drug formulation. Curcumin which is an active ingredient in the traditional herbal remedy, it possesses diverse pharmacological

activities such as anti-inflammatory, antioxidant, anti-proliferative and anticancer etc. but the poor aqueous solubility limits pharmacological activity. The issue was solved by Nangia et al. <sup>133</sup> via cocrystals approach using GRAS coformers (resorcinol and pyrogallol, Figure 1.20c&d). The solubility studies were performed for cocrystals in 40% ethanol/water and observed that cocrystals improved the solubility about 5 and 20 times compared to pure curcumin (Figure 1.20e).

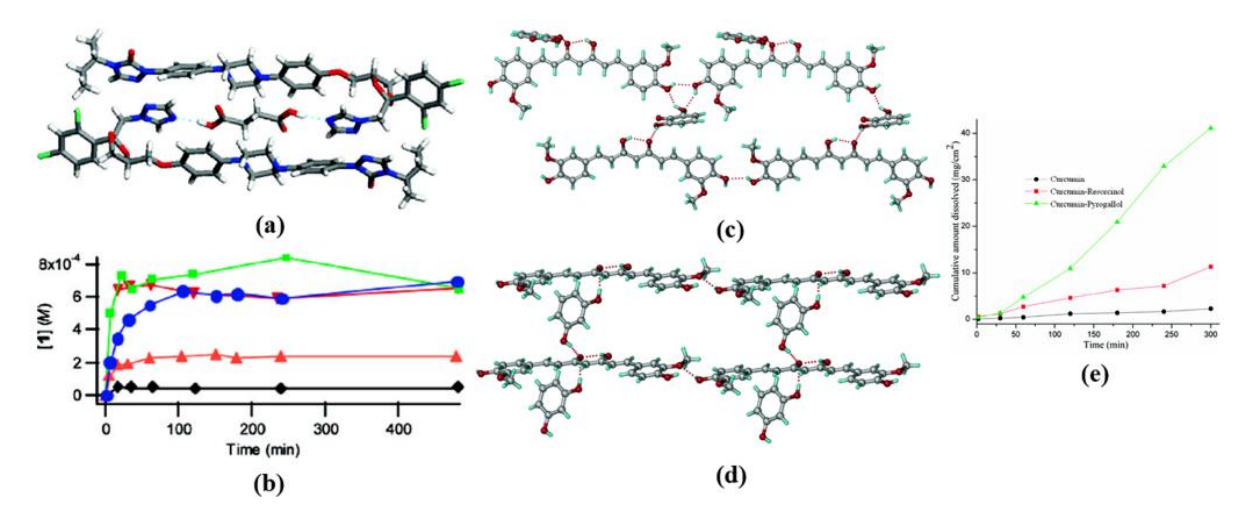


**Figure 1.20:** (a) X-Ray structure of Itraconazole-Succinic acid cocrystal. (b) Comparison of dissolution rate for amorphous and newly prepared cocrystals in 0.1 N HCl. (c), (d) crystal structures of Curcuminresorcinol and pyrogallol cocrystals. (e) Dissolution profile for Curcumin and its cocrystals in 40% ethanol-water medium. (Adapted from ref. 132 & 133)

McKellar and coworkers<sup>134</sup> reported the solid forms of a liquid drug Propofol, which is an intravenous anesthetic drug. They prepared cocrystals of Propofol (Figure 1.21a) with biologically acceptable coformers such as isonicotinamide, nicotinamide, isonicotinic acid and nicotinic acid. These results highlight the cocrystallization is a tool for improving the melting point of API's and which will open the doors for optimizing the properties of a liquid drug in to the solid state. Paracetamol which is an anti-pyretic and analgesic exists in two polymorphic forms such as form 1 and 2. The layered packing of molecules in metastable form 2 results in superior compressibility whereas in thermodynamically stable form 1, molecules were arranged in corrugated layers and exhibited poor tabletability. Later Karki et al.<sup>135</sup> solved the issue by making the cocrystals with planar molecules (theophylline, naphthalene, oxalic acid and phenazine) as cocrystal formers. In the crystal structure of theophylline (Figure 1.21b), layers are formed by a combination of 0D dimer motifs of theophylline and 1D tapes of paracetamol, exhibited good tabletability (Figure 1.21c).

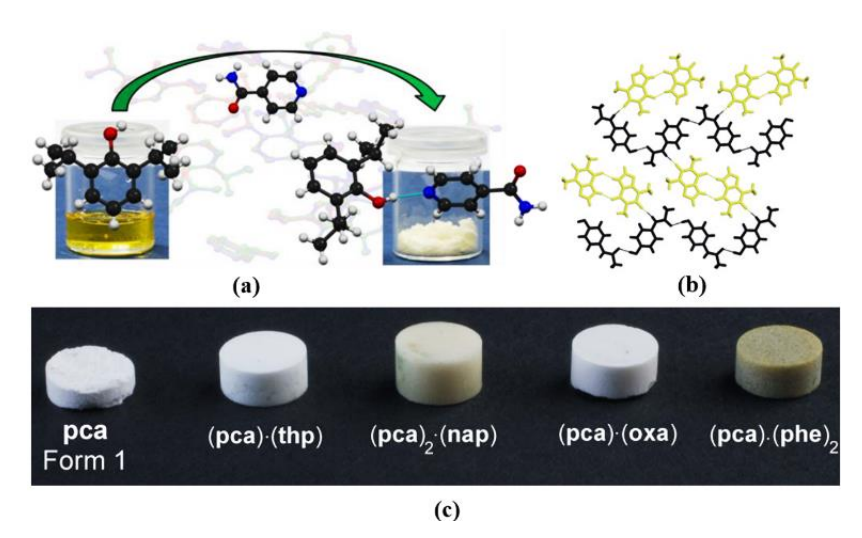


**Figure 1.21:** (a) Proposol before and after cocrystallization. (b) Crystal structure of paracetamol-theophylline cocrystal. (c) Tabletability of paracetamol form 1 and cocrystals prepared.

There are very few reports available on salts/cocrystals ability to modulate the flux rate resulting the enhanced permeability profile of drugs that affects oral absorption and sustains a good pharmacokinetics profile of drug substances. Lu et al. enhanced the permeability of a BCS class-III drug, 5-fluorouracil by cocrystallization with different coformers such as 3-hyroxybenzoic acid, 4-aminobenzoic acid and cinnamic acid. Desiraju and coworkers reported the permeability study of hydrochlorothiazide and its cocrystals with different coformers by using Franz diffusion cells. The amount of drug flux in all cocrystals was higher as compared to pure drug except for succinamide cocrystals. Cocrystals permeability was improved due to formation of heterosynthon between drug and coformer. Nangia et al. reported on Entacapone (BCS class-IV) by theophylline coformer resulted ETP-THP-HYD cocrystal scores on high solubility, good stability and high permeability. These case studies present a crystal engineering approach to solve solubility and permeability challenges mainly depends upon the drug-coformer interactions/weaker heterosynthons, layer crystal structures, lower melting point/crystal density/lattice energy, enhanced solubility/dissolution rate/molecular mobility, and polar/nonpolar interactions of the binary solid.

#### 1.7.5 Amorphous solids

Amorphous solids lack the long-range order in the lattice space characteristic of a crystal. <sup>139-142</sup> It occupies a prominent place in pharmaceuticals with their ability to improve solubility and dissolution rate APIs due to excess thermodynamic functions of amorphous phases. But when compared to crystalline phases, amorphous compounds do not show a regular diffraction pattern. These aperiodic solids can be produced by several techniques such as spray- and freeze-drying, melt quenching, milling, wet granulation<sup>33</sup> etc. and recently manual grinding<sup>141</sup> was shown to result in amorphous salts. They are characterized by thermal techniques with glass transition temperature ( $T_g$ ). It is the temperature at which a glassy material (plastic) is converted to rubbery phase retaining some properties of the liquid. <sup>140</sup>

Similar to their crystalline counterparts, amorphous forms are also known to exhibit polymorphism<sup>143</sup> which is termed as 'polyamorphism'. For example, polyamorphism in H<sub>2</sub>O is extensively studied, <sup>145</sup> but the data interpretation remains controversial since the diffraction pattern does not show any Bragg lines. In another example, the evolution of acetaminophen polyamorphous phases I and II forms corresponding polymorphs I and II in different solvent systems was also studied by radial distribution functions derived from the pair distribution function (PDF). <sup>146</sup> On one hand the excess thermodynamic functions of amorphous phases confer solubility/dissolution advantage of the poorly soluble APIs. Therefore drugs Itraconazole, Lopinavir, Cefuroxime axetil, Quinapril hydrochloride etc., are marketed either as purely amorphous phases or in combination with other solid forms. But on the other hand, the higher entropy and enthalpy can be disadvantageous since they make the amorphous solid forms highly unstable. Several excipients such as methyl cellulose, alginic acid, polyvinyl pyrrolidone (PVP), polyethylene glycol (PEG) etc<sup>33</sup> have been developed to stabilize the amorphous forms.

#### 1.7.6 Coamorphous solids

More recently the concept of "coamorphous" system was introduced by Norman Chieng et al. in the year 2009,  $^{147,148}$  the formulation of binary amorphous mixture of ranitidine hydrochloride and yindomethacin in different stoichiometric (1:1, 1:2, and 2:1) ratios. Later Thomas Rades and his coworkers started to explore the coamorphous system as a formulation. 149,150 Coamorphous system has thus gained considerable interest in the pharmaceutical field because of their potential to improve the solubility and dissolution rate of poorly soluble drugs. It is a single homogenous phase mixture of two or more low molecular weight components or non-polymeric components which lacks periodic arrangement in the lattice and associated by weak and discrete intermolecular interactions between the components in the lattice. They can have short range ordering similar to amorphous solids of single component systems. In contrast to polymeric matrix solid dispersion, where API molecules are dispersed in high molecular weight polymeric matrix in non-stoichiometric ratio, a coamorphous solid in which a molecule of interest and a coformer interact with each other via non-covalent interactions in a fixed stoichiometry ratio and dispersed in lattice.<sup>151</sup> Similarly both polymeric solid dispersion and coamorphous solid can facilitate the high thermodynamic functions such as free energy, enthalpy and entropy, and confer solubility and dissolution advantage similar to amorphous solids. Additional Advantage gained coamorphous solid is stabilize the amorphous form due to non-covalent interaction among them. It contrasts with a cocrystal, salt or eutectic primarily by its amorphous nature in that it exhibits a broad hump ('amorphous halo') when subjected to powder X-ray diffraction. 152-154 The identity and integrity of the components of coamorphous systems can be established by FT-IR and Raman spectroscopic techniques and eventually coamorphous solids exhibit single glass transition temperature. 149 Together with the more well-known counterparts such as salts, eutectics and cocrystals, coamorphous solids are a new entry to pharmaceutical solid form space. However, there is no clear information on the rational coformer selection to make the coamorphous form. There are few reports

representing the amino acids repeatedly forming coamorphous forms during mixing with APIs.<sup>78</sup> Still the microstructure of coamorphous is elusive by pair distribution function. These solids can be produced by several techniques such as spray- and freeze-drying, melt quenching, milling, manual grinding and rotaevaporation.<sup>149-155</sup>

Till date coamorphous solids were extensively studied in pharmaceutics specifically to improve the solubility, stability and bioavailability. Few examples are highlighted here. Recently Zhang et.al<sup>155</sup> has reported the improved solubility and stability of Lurasidone hydrochloride (LH) with saccharin in a 1:1 molar ratio. They stated the LH-SAC coamorphous solid stored at 25 °C/60% RH, is stable up to 60 days and it has higher stability than pure LH amorphous which showed only 7 days stability at same conditions (Figure 1.25a). Laitinen et.al<sup>156</sup> reported the drug-drug coamorphous of simvastatin (SVP) and glipizide (GPZ) in different stoichiometric ratios (1:1, 2:1 and 1:2). Cryo-milled 1:1 and 1:2 of the SVP-GPZ showed two months phase stability at 25 °C/65% RH (Figure 1.25b). Likewise, coamorphous system is gaining considerable attensison in the academic and pharma industry because of their potenial utility to the improve drug dissoultion rate, stability consequently oral bioavailiblity. <sup>157</sup> In chapter 4 we highlit the Curucmin-Artemisinin coamophous solid utility in terms of oral bioavailiblity enhancement and xenograft studies.

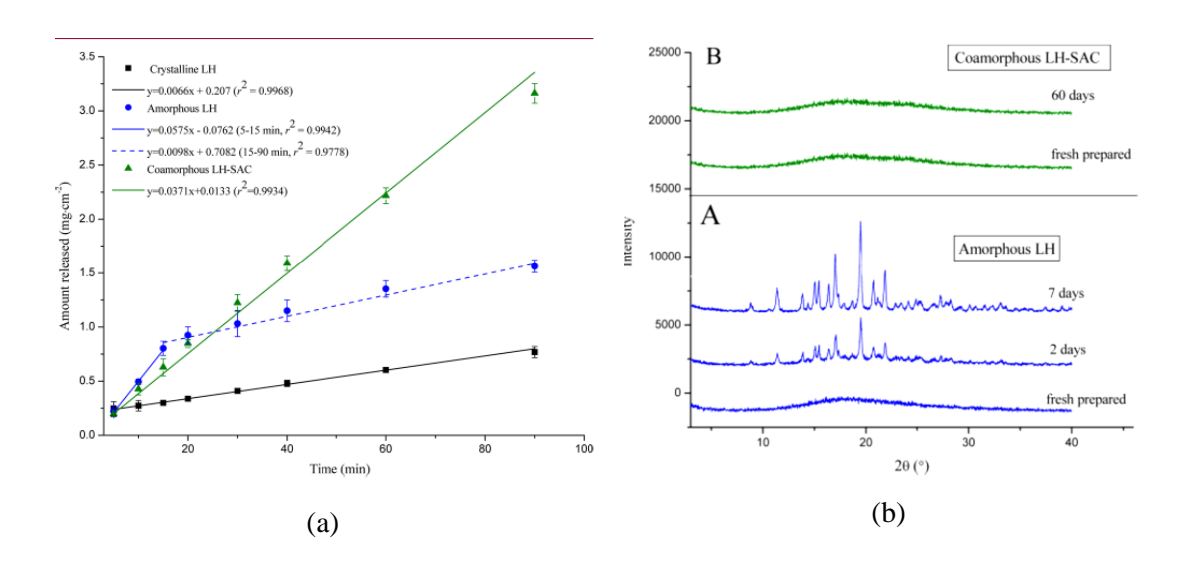


**Figure 1.22:** (a)Intrinsic dissolution rate profiles crystalline LH, amorphous LH, and coamorphous LH-SAC in 0.2M phosphate buffer solution (3.8, n=6). (b) PXRD patterns for amorphous LH (A), coamorphous LH-SAC (B) stored at 25 °C/60% RH over a specified period.

## 1.8 Conclusions

In this chapter, the origin and evolution of crystal engineering as a primary design element in developing pharmaceutical solid forms has been discussed. Alongside, intermolecular interactions and supramolecular synthons were. This understanding would be vibrant in the context of 'pharmaceutical form development' which allows the design of several solid forms with varying strengths of intermolecular interactions such as salts, cocrystals towards better therapeutic efficacy.

An API molecule can give rise to a multitude of crystal forms upon solid form screening. A review of all these solid forms was reviewed in various subdivisions of this chapter, which would focus the inherent differences in the structural aspects among these crystalline forms. By virtue of their uniqueness, these solid forms would result in varied physicochemical properties which are significant for best solid form selection and development. Since there is no single solution to the problems arising from the physicochemical behavior of various drug molecules, it is enormously essential to screen for all the possible solid forms (salts and coamorphs), which via their unique physicochemical properties would provide specific and desirable applications in different systems.

In the following chapters, chapter 2 deals with high solubility of Entacapone by forming cocrystals with amide coformers. Chapter 3 describes the stability, solubility and permeability of Entacapone, Polymorphs. Chapter 4 explores the improvement of the solubility and permeability of Pimozide *via* salt formation. Chapter 5 discusses the Xenograft model preclinical study of Curcumin-Artemisinin Coamorphous solids. Chapter 6 describes the crystal structure analysis of Ribociclib salts and cocrystal. This thesis mainly focuses on the use of crystal engineering principles in the design and synthesis of various solid forms of drug molecules including cocrystals, salts, co-amorphous materials and polymorphs in order to improve poor physicochemical properties of APIs.

#### 1.9 References

- 1. Lehn, J.-M. Supramolecular Chemistry: Concepts and Perspectives; Wiley-VCH Verlag: Weinheim, Germany, 1995.
- 2. Supramolecular Chemistry, eds. J.W. Steed and J.L. Atwood, Wiley, Chichester, 2000.
- 3. Lehn, J. M. Cryptates: Inclusion Complexes of Macropolycyclic Receptor Molecules. *Pure Appl. Chem.* **1978**, 50 (9–10), 871–892.
- 4. Wolf, K. L.; Wolff, R. Übermolekeln. *Angew. Chem. Weinheim Bergstr. Ger.* **1949**, 61 (5), 191–201.
- 5. Fischer, E. Influence of Configuration on the Action of Enzymes. *Journal of the American Chemical Society*. **1894**, 3, 2985-2993.
- 6. Pedersen, C. J. Cyclic Polyethers and Their Complexes with Metal Salts. J. Am. Chem. Soc. 1967, 89 (26), 7017–7036.

- 7. Lehn, J. M.; Sauvage, J. P. Cation and Cavity Selectivities of Alkali and Alkaline-Earth "Cryptates." *J. Chem. Soc. D* **1971**, No. 9, 440–441.
- 8. Steed, J.w. and Atwood, J.I. (2000) supramolecular chemistry. Wiley, Chichester. references scientific research publishing https://www.scirp.org/(S(351jmbntvnsjt1aadkposzje))/reference/ReferencesPapers.aspx?ReferenceID=1433391 (accessed Dec 13, 2021).
- 9. Atwood, J. L. *Comprehensive Supramolecular Chemistry*; Lehn, J.-M., MacNicol, D. D., Vogtle, F., Eds.; Pergamon Press: London, England, 1996.
- 10. Schuster, P. G. C. Maitland, M. Rigby, E. b. Smith, W. a. Wakeham: Intermolecular Forces Their Origin and Determination, Clarendon Press, Oxford 1981. 616 Seiten, Preis \$ 39.50. *Ber. Bunsenges. Phys. Chem.* **1983**, 87 (3), 291–292.
- 11. Steed, J. W.; Atwood, J. L., Supramolecular Chemistry. John Wiley and Sons: West Sussex, United Kingdom, 2009; Vol. 2.
- 12. Pauling, L., The Nature of the Chemical Bond. Cornell University Press: Ithaca, New York, 1939.
- 13. Arunan, E.; Desiraju, G. R.; Klein, R. A.; Sadlej, J.; Scheiner, S.; Alkorta, I.; Clary, D. C.; Crabtree, R. H.; Dannenberg, J. J.; Hobza, P.; Kjaergaard, H. G.; Legon, A. C.; Mennucci, B.; Nesbitt, D. J. Definition of the Hydrogen Bond (IUPAC Recommendations 2011). *Pure Appl. Chem.* **2011**, *83* (8), 1637–1641.
- 14. Perlstein, J. The Weak Hydrogen Bond in Structural Chemistry and Biology (International Union of Crystallography, Monographs on Crystallography, 9) by Gautam R. Desiraju (University of Hyderabad) and Thomas Steiner (Freie Universität Berlin). Oxford University Press: Oxford and New York. 1999. ISBN 0-19-850252-4. *J. Am. Chem. Soc.* **2001**, *123* (1), 191–192.
- 15. Bragg, S. W. H. The Intensity of X-Ray Reflection by Diamond. *Proc. Phys. Soc. Lond.* **1920**, *33* (1), 304–311.
- 16. Robertson, J. M.; White, J. G. 164. The Crystal Structure of Coronene: A Quantitative X-Ray Investigation. *J. Chem. Soc.* **1945**, 607.
- 17. Robertson, J. M.; White, J. G. 72. The Crystal Structure of Pyrene. A Quantitative X-Ray Investigation. *J. Chem. Soc.* **1947**, 358.
- 18. Coulson, C. A.; Daudel, R.; Robertson, J. M. Bond Lengths in Naphthalene and Anthracene. *Proc. R. Soc. Lond.* **1951**, 207 (1090), 306–320.
- 19. Frazer, B. C.; Danner, H. R.; Pepinsky, R. Single-Crystal Neutron Analysis of Tetragonal BaTiO3. *Phys. Rev.* **1955**, *100* (2), 745–746.
- 20. Schmidt, G. M. J. Photodimerization in the Solid State. Pure Appl. Chem. 1971, 27 (4), 647–678.
- 21. Desiraju, G. R. Supramolecular Synthons in Crystal Engineering—A New Organic Synthesis. *Angew. Chem. Int. Ed. Engl.* **1995**, *34* (21), 2311–2327.
- 22. Corey, E. J. General Methods for the Construction of Complex Molecules. *Pure Appl. Chem.* **1967**, *14* (1), 19–38.

- 23. Walsh, R. D. B.; Bradner, M. W.; Fleischman, a. S.; Morales, L. A.; Moulton, a. B.; Rodríguez-Hornedo, N.; Zaworotko, M. J. Crystal Engineering of the Composition of Pharmaceutical Phases. *Chem. Commun. (Camb.)* **2003**, No. 2, 186–187.
- 24. Bhogala, B. R.; Basavoju, S.; Nangia, A. Three-Component Carboxylic Acid-Bipyridine Lattice Inclusion Host. Supramolecular Synthesis of Ternary Cocrystals. *Cryst. Growth Des.* **2005**, *5* (5), 1683–1686.
- 25. Reddy, L. S.; Bhatt, P. M.; Banerjee, R.; Nangia, A.; Kruger, G. J. Variable-Temperature Powder X-Ray Diffraction of Aromatic Carboxylic Acid and Carboxamide Cocrystals. *Chem. Asian J.* **2007**, *2* (4), 505–513.
- 26. Dey, A.; Kirchner, M. T.; Vangala, V. R.; Desiraju, G. R.; Mondal, R.; Howard, J. A. K. Crystal Structure Prediction of Aminols: Advantages of a Supramolecular Synthon Approach with Experimental Structures. *J. Am. Chem. Soc.* **2005**, *127* (30), 10545–10559.
- 27. Bis, J. A.; Zaworotko, M. J. The 2-Aminopyridinium-Carboxylate Supramolecular Heterosynthon: A Robust Motif for Generation of Multiple-Component Crystals. *Cryst. Growth Des.* **2005**, *5* (3), 1169–1179.
- 28. Reddy, L. S.; Babu, N. J.; Nangia, A. Carboxamide-Pyridine N-Oxide Heterosynthon for Crystal Engineering and Pharmaceutical Cocrystals. *Chem. Commun. (Camb.)* **2006**, No. 13, 1369–1371.
- 29. Goud, N. R.; Babu, N. J.; Nangia, A. Sulfonamide-Pyridine-N-Oxide Cocrystals. *Cryst. Growth Des.* 2011, 11 (5), 1930–1939.
- 30. Drug definition US FDA Drug approval process https://www.pharmacistspharmajournal.org/2010/11/definitions-of-drug-radioactive-drug\_11.html (accessed Dec 13, 2021).
- 31. Faragau, T.; Almufti, S. Editors: Title: Lippincott's Illustrated Reviews: Pharmacology, 4th Edition. **2020**.
- 32. Shah, V. P.; Amidon, G. L. G.L. Amidon, H. Lennernas, V.P. Shah, and J.R. Crison. A Theoretical Basis for a Biopharmaceutic Drug Classification: The Correlation of in Vitro Drug Product Dissolution and in Vivo Bioavailability, Pharm Res 12, 413-420, 1995--Backstory of BCS. *AAPS J.* **2014**, *16* (5), 894–898.
- 33. Dahan, A.; Miller, J. M.; Amidon, G. L. Prediction of Solubility and Permeability Class Membership: Provisional BCS Classification of the World's Top Oral Drugs. *AAPS J.* **2009**, *11* (4), 740–746.
- 34. Benet, L. Z.; Amidon, G. L.; Barends, D. M.; Lennernäs, H.; Polli, J. E.; Shah, V. P.; Stavchansky, S. A.; Yu, L. X. The Use of BDDCS in Classifying the Permeability of Marketed Drugs. *Pharm. Res.* **2008**, *25* (3), 483–488.
- 35. Hendriksen, B. A.; Felix, M. V. S.; Bolger, M. B. The Composite Solubility versus PH Profile and Its Role in Intestinal Absorption Prediction. *AAPS PharmSci* **2003**, *5* (1).

- 36. Rosenberger, J.; Butler, J.; Dressman, J. A Refined Developability Classification System. *J. Pharm. Sci.* **2018**, *107* (8), 2020–2032.
- 37. Duggirala, N. K.; Perry, M. L.; Almarsson, Ö.; Zaworotko, M. J. Pharmaceutical Cocrystals: Along the Path to Improved Medicines. *Chem. Commun. (Camb.)* **2016**, *52* (4), 640–655.
- 38. Byrn, S. R. Solid-State Chemistry of Drugs, 2nd ed.; Ssci, 1999
- 39. Thayer, A. M. FINDING SOLUTIONS: Custom Manufacturers Take on DRUG SOLUBILITY ISSUES to Help Pharmaceutical Firms Move Products through Development. *Chem. Eng. News Archive* **2010**, 88 (22), 13–18.
- 40. Davey, R. J. Polymorphism in Molecular Crystals Joel Bernstein. Oxford University Press, New York, 2002. ISBN 0198506058. *Cryst. Growth Des.* **2002**, *2* (6), 675–676.
- 41. Mitscherlich, E. Über Die Körper, Welche in Zwei Verschiedenen Formen Krystallisieren, Abhl. Akad. Berlin 1822, pp 43–48.
- 42. J. Berzelius, Jahresbericht, 1844, 23, 44.
- 43. Haleblian, J.; McCrone, W. Pharmaceutical Applications of Polymorphism. *J. Pharm. Sci.* **1969**, *58* (8), 911–929.
- 44. Polymorphism: In the Pharmaceutical Industry; Hilfiker, R., Ed.; Wiley, 2006.
- 45. Byrn, S. R.; Pfeiffer, R. R.; Stephenson, G.; Grant, D. J. W.; Gleason, W. B. Solid-State Pharmaceutical Chemistry. *Chem. Mater.* **1994**, *6* (8), 1148–1158.
- 46. Babu, N. J.; Cherukuvada, S.; Thakuria, R.; Nangia, A. Conformational and Synthon Polymorphism in Furosemide (Lasix). *Cryst. Growth Des.* **2010**, *10* (4), 1979–1989.
- 47. Nangia, A. Conformational Polymorphism in Organic Crystals. *Acc. Chem. Res.* **2008**, *41* (5), 595–604.
- 48. Aitipamula, S.; Nangia, A. Polymorphism: Fundamentals and Applications. *Supramolecular Chemistry*; John Wiley & Sons, Ltd: Chichester, UK, 2012.
- 49. Bauer, J.; Spanton, S.; Henry, R.; Quick, J.; Dziki, W.; Porter, W.; Morris, J. *Pharm. Res.* **2001**, *18* (6), 859–866.
- 50. Sreekanth, B. R.; Vishweshwar, P.; Vyas, K. Supramolecular Synthon Polymorphism in 2:1 Co-Crystal of 4-Hydroxybenzoic Acid and 2,3,5,6-Tetramethylpyrazine. *Chem. Commun.* (*Camb.*) **2007**, No. 23, 2375–2377.
- 51. Derissen, J. L.; Smith, P. H. Refinement of the Crystal Structures of Anhydrous α- and β-Oxalic Acids. *Acta Crystallogr. B* **1974**, *30* (9), 2240–2242.
- 52. Vippagunta, S. R.; Brittain, H. G.; Grant, D. J. Crystalline Solids. *Adv. Drug Deliv. Rev.* **2001**, *48* (1), 3–26.
- 53. Cherukuvada, S.; Thakuria, R.; Nangia, A. Pyrazinamide Polymorphs: Relative Stability and Vibrational Spectroscopy. *Cryst. Growth Des.* **2010**, *10* (9), 3931–3941.
- 54. Byrn, S. R. Solid-State Chemistry of Drugs, 2nd ed.; Ssci, 1999.
- 55. Polymorphism: In the Pharmaceutical Industry; Hilfiker, R., Ed.; Wiley, 2006.

- 56. *Polymorphism in Pharmaceutical Solids*, 2nd ed.; Brittain, H. G., Ed.; CRC Press: Boca Raton, FL, 2009.
- 57. Sarma, B.; Roy, S.; Nangia, A. Polymorphs of 1,1-Bis(4-Hydroxyphenyl)Cyclohexane and Multiple Z' Crystal Structures by Melt and Sublimation Crystallization. *Chem. Commun.* (*Camb.*) **2006**, No. 47, 4918–4920.
- 58. Sarma, B.; Sanphui, P.; Nangia, A. Polymorphism in Isomeric Dihydroxybenzoic Acids. *Cryst. Growth Des.* **2010**, *10* (5), 2388–2399.
- 59. Thallapally, P. K.; Jetti, R. K. R.; Katz, A. K.; Carrell, H. L.; Singh, K.; Lahiri, K.; Kotha, S.; Boese, R.; Desiraju, G. R. Polymorphism of 1,3,5-Trinitrobenzene Induced by a Trisindane Additive. *Angew. Chem. Int. Ed Engl.* **2004**, *43* (9), 1149–1155.
- 60. Miller, J. M.; Rodríguez-Hornedo, N.; Blackburn, A. C.; Macikenas, D.; Collman, B. M. Solvent Systems for Crystallization and Polymorph Selection. In *Biotechnology: Pharmaceutical Aspects*; Springer New York: New York, NY, 2007; pp 53–109.
- 61. Lang, M.; Grzesiak, A. L.; Matzger, A. J. The Use of Polymer Heteronuclei for Crystalline Polymorph Selection. *J. Am. Chem. Soc.* **2002**, *124* (50), 14834–14835.
- 62. Price, C. P.; Grzesiak, A. L.; Matzger, A. J. Crystalline Polymorph Selection and Discovery with Polymer Heteronuclei. *J. Am. Chem. Soc.* **2005**, *127* (15), 5512–5517.
- 63. Sun, X.; Garetz, B. A.; Myerson, A. S. Supersaturation and Polarization Dependence of Polymorph Control in the Nonphotochemical Laser-Induced Nucleation (NPLIN) of Aqueous Glycine Solutions. *Cryst. Growth Des.* **2006**, *6* (3), 684–689.
- 64. Hilden, J. L.; Reyes, C. E.; Kelm, M. J.; Tan, J. S.; Stowell, J. G.; Morris, K. R. Capillary Precipitation of a Highly Polymorphic Organic Compound. *Cryst. Growth Des.* **2003**, *3* (6), 921–926.
- 65. Nath, N. K.; Nilapwar, S.; Nangia, A. Chiral and Racemic Tetramorphs of 2,6-Di-t-Butylditolylfuchsone. *Cryst. Growth Des.* **2012**, *12* (3), 1613–1625.
- 66. Martins, D.; Sanselme, M.; Houssin, O.; Dupray, V.; Petit, M. N.; Pasquier, D.; Diolez, C.; Coquerel, G. Physical Transformations of the Active Pharmaceutical Ingredient BN83495: Enantiotropic and Monotropic Relationships. Access to Several Polymorphic Forms by Using Various Solvation–Desolvation Processes. *CrystEngComm* **2012**, *14* (7), 2507–2519.
- 67. Karanam, M.; Dev, S.; Choudhury, A. R. New Polymorphs of Fluconazole: Results from Cocrystallization Experiments. *Cryst. Growth Des.* **2012**, *12* (1), 240–252.
- 68. Nath, N. K.; Kumar, S. S.; Nangia, A. Neutral and Zwitterionic Polymorphs of 2-(p-Tolylamino) Nicotinic Acid. *Cryst. Growth Des.* **2011**, *11* (10), 4594–4605.
- 69. Ostwald, W. Studien Über Die Bildung Und Umwandlung Fester Körper: 1. Abhandlung: Übersättigung Und Überkaltung. Z. Phys. Chem. (N F) **1897**, 22U (1), 289–330.
- 70. Nývlt, J. The Ostwald Rule of Stages. Cryst. Res. Technol. 1995, 30 (4), 443–449.

- 71. Threlfall, T. Structural and Thermodynamic Explanations of Ostwald's Rule. *Org. Process Res. Dev.* 2003, 7 (6), 1017–1027.
- 72. Davey, R. J.; Blagden, N.; Righini, S.; Alison, H.; Ferrari, E. S. Nucleation Control in Solution Mediated Polymorphic Phase Transformations: The Case of 2,6-Dihydroxybenzoic Acid. *J. Phys. Chem. B* **2002**, *106* (8), 1954–1959.
- 73. Morissette, S. L.; Almarsson, O.; Peterson, M. L.; Remenar, J. F.; Read, M. J.; Lemmo, A. V.; Ellis, S.; Cima, M. J.; Gardner, C. R. High-Throughput Crystallization: Polymorphs, Salts, Co-Crystals and Solvates of Pharmaceutical Solids. *Adv. Drug Deliv. Rev.* **2004**, *56* (3), 275–300.
- 74. Lu, J.; Rohani, S. Polymorphism and Crystallization of Active Pharmaceutical Ingredients (APIs). *Curr. Med. Chem.* **2009**, *16* (7), 884–905.
- 75. Zhang, G. G. Z.; Law, D.; Schmitt, E. A.; Qiu, Y. Phase Transformation Considerations during Process Development and Manufacture of Solid Oral Dosage Forms. *Adv. Drug Deliv. Rev.* **2004**, *56* (3), 371–390.
- 76. Byrn, S. R. Solid-State Chemistry of Drugs, 2nd ed.; Ssci, 1999.
- 77. Zencirci, N.; Gelbrich, T.; Apperley, D. C.; Harris, R. K.; Kahlenberg, V.; Griesser, U. J. Structural Features, Phase Relationships and Transformation Behavior of the Polymorphs I–VI of Phenobarbital. *Cryst. Growth Des.* **2010**, *10* (1), 302–313.
- 78. Burger, A.; Ramberger, R. On the Polymorphism of Pharmaceuticals and Other Molecular Crystals. II: Applicability of Thermodynamic Rules. *Mikrochim. Acta* **1979**, 72 (3–4), 273–316.
- 79. Nangia, A.; Desiraju, G. R. Pseudopolymorphism: Occurrences of Hydrogen Bonding Organic Solvents in Molecular Crystals. *Chem. Commun. (Camb.)* **1999**, No. 7, 605–606.
- 80. Latimer, W. M.; Rodebush, W. H. Polarity and Ionization from the Standpoint of the Lewis Theory of Valence. *J. Am. Chem. Soc.* **1920**, *42* (7), 1419–1433.
- 81. Burrows, J. A. Pauling, Linus. The Nature of the Chemical Bond and the Structure of Molecules Aid Crystals. Ithaca: The Cornell University Press, 1939. 430 p. \$4.50. *Sci. Educ.* **1941**, 25 (2), 120–120.
- 82. Coulson, C. A. Pauling's Chemical Bond. *Nature* **1961**, *189* (4758), 3–3.
- 83. Bodor, N. Techniques of Solubilization of Drugs. (Drugs and the Pharmaceutical Sciences Series, Vol 12.). *J. Pharm. Sci.* **1984**, *73* (2), 288.
- 84. Porter, W. W., 3rd; Elie, S. C.; Matzger, A. J. Polymorphism in Carbamazepine Cocrystals. *Cryst. Growth Des.* **2008**, 8 (1), 14–16.
- 85. Thakuria, R.; Thakur, T. S. Crystal Polymorphism in Pharmaceutical Science. In *Comprehensive Supramolecular Chemistry II*; Atwood, J. L., Ed.; Elsevier, 2017; pp 283–309.
- 86. Cruz-Cabeza, A. J.; Bernstein, J. Conformational Polymorphism. Chem. Rev. 2014, 114 (4), 2170–2191.
- 87. Bauer, J.; Spanton, S.; Henry, R.; Quick, J.; Dziki, W.; Porter, W.; Morris, J. *Pharm. Res.* **2001**, *18* (6), 859–866.

- 88. Fox, D.; Labes, M. M.; Weissberger, A.; Rice, S. A. Physics and Chemistry of the Organic Solid State. Volume 2. *Phys. Today* **1965**, *18* (8), 59–59.
- 89. Bingham, A. L.; Hughes, D. S.; Hursthouse, M. B.; Lancaster, R. W.; Tavener, S.; Threlfall, T. L. Over One Hundred Solvates of Sulfathiazole. *Chem. Commun. (Camb.)* **2001**, No. 7, 603–604.
- 90. Roy, S.; Goud, N. R.; Babu, N. J.; Iqbal, J.; Kruthiventi, A. K.; Nangia, A. Crystal Structures of Norfloxacin Hydrates. *Cryst. Growth Des.* **2008**, *8* (12), 4343–4346.
- 91. Caira, M. R.; Pienaar, E. W.; Lötter, A. P. Polymorphism and Pseudopolymorphism of the Antibacterial Nitrofurantoin. *Mol. Cryst. Liq. Cryst.* **1996**, 279 (1), 241–264.
- 92. Lin, J. H.; Ostovic, D.; Vacca, J. P. The Integration of Medicinal Chemistry, Drug Metabolism, and Pharmaceutical Research and Development in Drug Discovery and Development. In *Pharmaceutical Biotechnology*; Kluwer Academic Publishers: Boston, 2006; pp 233–255.
- 93. Pfeiffer, R. R.; Yang, K. S.; Tucker, M. A. Crystal Pseudopolymorphism of Cephaloglycin and Cephalexin. *J. Pharm. Sci.* **1970**, *59* (12), 1809–1814.
- 94. Martins, D.; Sanselme, M.; Houssin, O.; Dupray, V.; Petit, M. N.; Pasquier, D.; Diolez, C.; Coquerel, G. Physical Transformations of the Active Pharmaceutical Ingredient BN83495: Enantiotropic and Monotropic Relationships. Access to Several Polymorphic Forms by Using Various Solvation–Desolvation Processes. *CrystEngComm* **2012**, *14* (7), 2507–2519.
- 95. L.D. Bighley, S.M. Berge, and D.C. Monkhouse, "Salt Forms of Drugs and Absorption," in *Encyclopedia of Pharmaceutical Technology*, Swarbrick, J.; Boylan, J.C. Eds. Marcel Dekker, New York, **1996**, 453–499.
- 96. Cruz-Cabeza, A. J. Acid-Base Crystalline Complexes and the PKa Rule. CrystEngComm 2012, 14 (20), 6362–6365.
- 97. Goud, N. R.; Suresh, K.; Nangia, A. Solubility and Stability Advantage of Aceclofenac Salts. *Cryst. Growth Des.* **2013**, *13* (4), 1590–1601.
- 98. Heinrich Stahl (Editor), P.; Wermuth (Editor), C. G. *Pharmaceutical Salts: Properties, Selection, and Use*, 2nd ed.; Stahl, P. H., Wermuth, C. G., Eds.; Helvitica Chimica Acta Verlag, 2011.
- 99. (Z)-Ranitidine http://www.chemspider.com/Chemical-Structure.571454.html accessed Dec 14, 2021).
- 100. Mirmehrabi, M.; Rohani, S.; Murthy, K. S. K.; Radatus, B. Solubility, Dissolution Rate and Phase Transition Studies of Ranitidine Hydrochloride Tautomeric Forms. *Int. J. Pharm.* **2004**, 282 (1–2), 73–85.
- 101. Kasim, N. A.; Whitehouse, M.; Ramachandran, C.; Bermejo, M.; Lennernäs, H.; Hussain, A. S.; Junginger, H. E.; Stavchansky, S. A.; Midha, K. K.; Shah, V. P.; Amidon, G. L. Molecular Properties of WHO Essential Drugs and Provisional Biopharmaceutical Classification. *Mol. Pharm.* 2004, 1 (1), 85–96.
- 102. Gould, P. L. Salt Selection for Basic Drugs. Int. J. Pharm. 1986, 33 (1-3), 201-217.

- 103. Bhutani, H.; Singh, S.; Jindal, K. C.; Chakraborti, A. K. Mechanistic Explanation to the Catalysis by Pyrazinamide and Ethambutol of Reaction between Rifampicin and Isoniazid in Anti-TB FDCs. *J. Pharm. Biomed. Anal.* **2005**, *39* (5), 892–899.
- 104. Lipinski, C. A.; Lombardo, F.; Dominy, B. W.; Feeney, P. J. Experimental and Computational Approaches to Estimate Solubility and Permeability in Drug Discovery and Development Settings. *Adv. Drug Deliv. Rev.* **2001**, *46* (1–3), 3–26.
- 105. Gardner, C. R.; Walsh, C. T.; Almarsson, O. Drugs as Materials: Valuing Physical Form in Drug Discovery. *Nat. Rev. Drug Discov.* **2004**, *3* (11), 926–934.
- 106. Schultheiss, N.; Newman, A. Pharmaceutical Cocrystals and Their Physicochemical Properties. *Cryst. Growth Des.* **2009**, *9* (6), 2950–2967.
- 107. Babu, N. J.; Nangia, A. Solubility Advantage of Amorphous Drugs and Pharmaceutical Cocrystals. *Cryst. Growth Des.* **2011**, *11* (7), 2662–2679.
- 108. Fahr, A.; Liu, X. Drug Delivery Strategies for Poorly Water-Soluble Drugs. *Expert Opin. Drug Deliv.* **2007**, *4* (4), 403–416.
- 109. Stella, V. J.; Nti-Addae, K. W. Prodrug Strategies to Overcome Poor Water Solubility. *Adv. Drug Deliv. Rev.* **2007**, *59* (7), 677–694.
- 110. Singh, S.; Mohan, B. A Pilot Stability Study on Four-Drug Fixed-Dose Combination Anti-Tuberculosis Products. *Int. J. Tuberc. Lung Dis.* **2003**, *7* (3), 298–303.
- 111. Wöhler, F. Untersuchungen Über Das Chinon. Ann. Chem. Pharm. **1844**, 51 (2), 145–163.
- 112. Etter, M. C. Hydrogen Bonds as Design Elements in Organic Chemistry. *J. Phys. Chem.* **1991**, *95* (12), 4601–4610.
- 113. Trask, A. V. An Overview of Pharmaceutical Cocrystals as Intellectual Property. *Mol. Pharm.* **2007**, *4* (3), 301–309.
- 114. Vishweshwar, P.; McMahon, J. A.; Bis, J. A.; Zaworotko, M. J. Pharmaceutical Co-Crystals. *J. Pharm. Sci.* **2006**, *95* (3), 499–516.
- 115. Aakeröy, C. B.; Forbes, S.; Desper, J. Using Cocrystals to Systematically Modulate Aqueous Solubility and Melting Behavior of an Anticancer Drug. *J. Am. Chem. Soc.* **2009**, *131* (47), 17048–17049.
- 116. Alhalaweh, A.; Velaga, S. P. Formation of Cocrystals from Stoichiometric Solutions of Incongruently Saturating Systems by Spray Drying. *Cryst. Growth Des.* **2010**, *10* (8), 3302–3305.
- 117. Desiraju, G. R. Crystal Engineering. From Molecules to Materials. *J. Mol. Struct.* **2003**, *656* (1–3), 5–15.
- 118. Dunitz, J. D. Crystal and Co-Crystal: A Second Opinion. CrystEngComm 2003, 5 (91), 506.
- 119. Aakeröy, C. B.; Salmon, D. J. Building Co-Crystals with Molecular Sense and Supramolecular Sensibility. *CrystEngComm* **2005**, *7* (72), 439–448.
- 120. Bond, A. D. What Is a Co-Crystal? CrystEngComm 2007, 9 (9), 833.

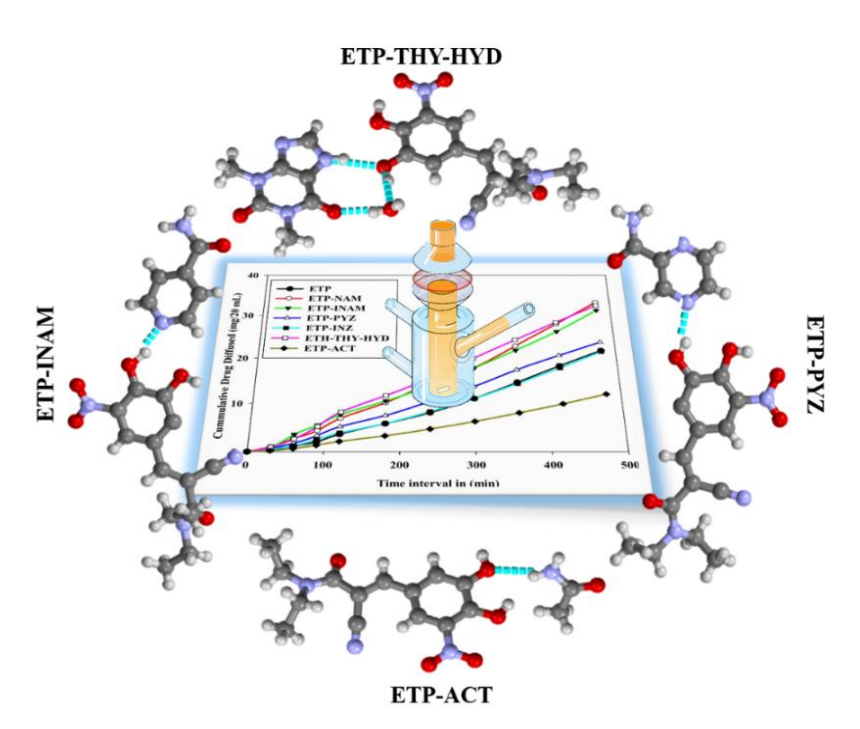
- 121. Nangia, A.; Rodríguez-Hornedo, N. Indo-U.S. Workshop on Pharmaceutical Cocrystals and Polymorphs. *Cryst. Growth Des.* **2009**, *9* (8), 3339–3341.
- 122. Aitipamula, S.; Banerjee, R.; Bansal, A. K.; Biradha, K.; Cheney, M. L.; Choudhury, A. R.; Desiraju, G. R.; Dikundwar, A. G.; Dubey, R.; Duggirala, N.; Ghogale, P. P.; Ghosh, S.; Goswami, P. K.; Goud, N. R.; Jetti, R. R. K. R.; Karpinski, P.; Kaushik, P.; Kumar, D.; Kumar, V.; Moulton, B.; Mukherjee, A.; Mukherjee, G.; Myerson, A. S.; Puri, V.; Ramanan, A.; Rajamannar, T.; Reddy, C. M.; Rodriguez-Hornedo, N.; Rogers, R. D.; Row, T. N. G.; Sanphui, P.; Shan, N.; Shete, G.; Singh, A.; Sun, C. C.; Swift, J. A.; Thaimattam, R.; Thakur, T. S.; Kumar Thaper, R.; Thomas, S. P.; Tothadi, S.; Vangala, V. R.; Variankaval, N.; Vishweshwar, P.; Weyna, D. R.; Zaworotko, M. J. Polymorphs, Salts, and Cocrystals: What's in a Name? Cryst. Growth Des. 2012, 12 (5), 2147–2152.
- 123. Co-Crystals, P. Regulatory Classification of https://www.fda.gov/files/drugs/published/Regulatory-Classification-of-Pharmaceutical-Co-Crystals.pdf (accessed Dec 14, 2021).
- 124. Qiao, N.; Li, M.; Schlindwein, W.; Malek, N.; Davies, A.; Trappitt, G. Pharmaceutical Cocrystals: An Overview. *Int. J. Pharm.* **2011**, *419* (1–2), 1–11.
- 125. Bolla, G.; Nangia, A. Pharmaceutical Cocrystals: Walking the Talk. *Chem. Commun.* (*Camb.*) **2016**, *52* (54), 8342–8360.
- 126. Emami, S.; Siahi-Shadbad, M.; Adibkia, K.; Barzegar-Jalali, M. Recent Advances in Improving Oral Drug Bioavailability by Cocrystals. *BioImpacts* **2018**, *8* (4), 305–320.
- 127. Wang, X.; Du, S.; Zhang, R.; Jia, X.; Yang, T.; Zhang, X. Drug-Drug Cocrystals: Opportunities and Challenges. *Asian J. Pharm. Sci.* **2021**, *16* (3), 307–317.
- 128. Banik, M.; Gopi, S. P.; Ganguly, S.; Desiraju, G. R. Cocrystal and Salt Forms of Furosemide: Solubility and Diffusion Variations. *Cryst. Growth Des.* **2016**, *16* (9), 5418–5428.
- 129. Maheshwari, C.; André, V.; Reddy, S.; Roy, L.; Duarte, T.; Rodríguez-Hornedo, N. Tailoring Aqueous Solubility of a Highly Soluble Compound via Cocrystallization: Effect of Coformer Ionization, PHmax and Solute–Solvent Interactions. *CrystEngComm* **2012**, *14* (14), 4801.
- 130. Babu, N. J.; Sanphui, P.; Nangia, A. Crystal Engineering of Stable Temozolomide Cocrystals. *Chem. Asian J.* **2012**, *7* (10), 2274–2285.
- 131. Sravani, E.; Mannava, M. K. C.; Kaur, D.; Annapurna, B. R.; Khan, R. A.; Suresh, K.; Mittapalli, S.; Nangia, A.; Kumar, B. D. Preclinical Bioavailability–Bioequivalence and Toxico-Kinetic Profile of Stable Succinc Acid Cocrystal of Temozolomide. *Curr. Sci.* 2015, 108 (6), 1097–1106.
- 132. Remenar, J. F.; Morissette, S. L.; Peterson, M. L.; Moulton, B.; MacPhee, J. M.; Guzmán, H. R.; Almarsson, O. Crystal Engineering of Novel Cocrystals of a Triazole Drug with 1,4-Dicarboxylic Acids. *J. Am. Chem. Soc.* **2003**, *125* (28), 8456–8457.
- 133. Sanphui, P.; Goud, N. R.; Khandavilli, U. B. R.; Nangia, A. Fast Dissolving Curcumin Cocrystals. *Cryst. Growth Des.* **2011**, *11* (9), 4135–4145.

- 134. McKellar, S. C.; Kennedy, A. R.; McCloy, N. C.; McBride, E.; Florence, A. J. Formulation of Liquid Propofol as a Cocrystalline Solid. *Cryst. Growth Des.* **2014**, *14* (5), 2422–2430.
- 135. Karki, S.; Friščić, T.; Fabian, L.; Laity, P. R.; Day, G. M.; Jones, W. Improving Mechanical Properties of Crystalline Solids by Cocrystal Formation: New Compressible Forms of Paracetamol. *Adv. Mater.* **2009**, *21*, 3905–3909.
- 136. Dai, X.-L.; Li, S.; Chen, J.-M.; Lu, T.-B. Improving the Membrane Permeability of 5-Fluorouracil via Cocrystallization. *Cryst. Growth Des.* **2016**, *16* (8), 4430–4438.
- 137. Gopi, S. P.; Banik, M.; Desiraju, G. R. New Cocrystals of Hydrochlorothiazide: Optimizing Solubility and Membrane Diffusivity. *Cryst. Growth Des.* **2017**, *17* (1), 308–316.
- 138. Bommaka, M. K.; Mannava, M. K. C.; Suresh, K.; Gunnam, A.; Nangia, A. Entacapone: Improving Aqueous Solubility, Diffusion Permeability, and Cocrystal Stability with Theophylline. *Cryst. Growth Des.* **2018**, *18* (10), 6061–6069.
- 139. Hilden, L. R.; Morris, K. R.; Physics of amorphous solids. *Journal of pharmaceutical sciences*. **2004**, *93*(1), 3-12.
- 140. Yu,L.; Amorphous pharmaceutical solids: preparation, characterization and stabilization. *Advanced drug delivery reviews*. **2001**, *48*(1), 27-42.
- 141. Thakuria, R.; Nangia, A. Highly soluble olanzapinium maleate crystalline salts. *CrystEngComm*, **2011**, *13*(6), 1759-1764.
- 142. Willart, J. F.; Descamps, M. Solid state amorphization of pharmaceuticals. *Molecular Pharmaceutics*. **2008**, *5*(6), 905-920.
- 143. Poole, P. H.; Grande, T.; Angell, C. A.; McMillan, P. F. Polymorphic phase transitions in liquids and glasses. *Science*. **1997**, *275*(5298), 322-323.
- 144. Kieffer, J. Structural transitions and glass formation. *The Journal of Physical Chemistry B.* **1999**, *103*(20), 4153-4158.
- 145. Mishima, O.; Calvert, L. D.; Whalley, E. 'Melting ice'I at 77 K and 10 kbar: A new method of making amorphous solids. *Nature*. **1984**, *310*(5976), 393-395.
- 146. Johari, G. P.; Hallbrucker, A.; Mayer, E. The glass-liquid transition of hyperquenched water. *Nature*. **1987**, *330*(6148), 552-553.
- 147. Chieng, N.; Aaltonen, J.; Saville, D.; Rades, T. Physical characterization and stability of amorphous indomethacin and ranitidine hydrochloride binary systems prepared by mechanical activation. *European Journal of Pharmaceutics and Biopharmaceutics*, **2009**, 71(1), 47-54...
- 148. Allesø, M.; Chieng, N.; Rehder, S.; Rantanen, J.; Rades, T.; Aaltonen, J. Enhanced dissolution rate and synchronized release of drugs in binary systems through formulation: Amorphous naproxencimetidine mixtures prepared by mechanical activation. *Journal of Controlled Release*. **2009**, *136*(1), 45-53.

- 149. Löbmann, K.; Laitinen, R.; Grohganz, H.; Gordon, K. C.; Strachan, C.; Rades, T. Coamorphous drug systems: enhanced physical stability and dissolution rate of indomethacin and naproxen. *Molecular pharmaceutics*. **2011**, *8*(5), 1919-1928.
- 150. Laitinen, R.; Löbmann, K.; Grohganz, H.; Priemel, P.; Strachan, C. J.; Rades, T. Supersaturating drug delivery systems: the potential of co-amorphous drug formulations. *International Journal of Pharmaceutics*. **2017**, *532*(1), 1-12...
- 151. Hilden, L. R.; Morris, K. R. Physics of amorphous solids. *Journal of pharmaceutical sciences*. **2004**, *93*(1), 3-12..
- 152. Löbmann, K.; Grohganz, H.; Laitinen, R.; Strachan, C.; Rades, T. Amino acids as co-amorphous stabilizers for poorly water soluble drugs—Part 1: Preparation, stability and dissolution enhancement. *European journal of pharmaceutics and biopharmaceutics*. **2013**, 85(3), 873-881.
- 153. Laitinen, R.; Lobmann, K.; Grohganz, H.; Strachan, C.; Rades, T. Amino acids as co-amorphous excipients for simvastatin and glibenclamide: physical properties and stability. *Molecular pharmaceutics*. **2014**, *11*(7), 2381-2389.
- 154. Jensen, K. T.; Larsen, F. H.; Cornett, C.; Löbmann, K.; Grohganz, H.; Rades, T. Formation mechanism of coamorphous drug-amino acid mixtures. *Molecular pharmaceutics*. **2015**, *12*(7), 2484-2492.
- 155. Qian, S.; Heng, W.; Wei, Y.; Zhang, J.; Gao, Y. Coamorphous lurasidone hydrochloride–saccharin with charge-assisted hydrogen bonding interaction shows improved physical stability and enhanced dissolution with pH-independent solubility behavior. *Crystal Growth & Design.* **2015**, *15*(6), 2920-2928.
- 156. Löbmann, K.; Strachan, C.; Grohganz, H.; Rades, T.; Korhonen, O.; Laitinen, R. Co-amorphous simvastatin and glipizide combinations show improved physical stability without evidence of intermolecular interactions. *European Journal of Pharmaceutics and Biopharmaceutics*. **2012**, 81(1), 159-169..
- 157. Dengale, S. J.; Grohganz, H.; Rades, T.; Löbmann, K. Recent advances in co-amorphous drug formulations. *Advanced drug delivery reviews*. **2016**, *100*, 116-125.

## CHAPTER TWO

# **Entacapone: Improving Aqueous Solubility, Diffusion Permeability and Cocrystal Stability with Theophylline**



Entacapone, ETP, a BCS Class IV drug of low solubility and low permeability. Cocrystalization of ETP with acetamide (ACT, 1:1), nicotinamide (NAM, 1:1), isonicotinamide (INAM, 1:1), pyrazinamide (PYZ, 1:1), and isoniazid (INZ), 1:1) were prepared by solvent-assisted grinding. Theophylline (THP) resulted in a cocrystal hydrate (ETP-THP-HYD 1:1:1). The were characterized by SC-XRD and PXRD, DSC, TGA, IR and NMR spectroscopy. Solubility and dissolution rate showed that there is a correlation between cocrystal stability and solubility governed by the heteromeric N-H···O, O-H···N and O-H···O hydrogen bonds and conformational changes of ETP in cocrystal structures. ETP-THP-HYD and ETP-PYZ exhibit faster dissolution rate and high solubility compared to the other cocrystals which dissociate partially during solubility experiments. Diffusion rates showed that the stable and high solubility ETP-THP-HYD cocrystal has good permeability. Given that stability, solubility and permeability are in general inversely correlated, the entacapone-theophylline hydrate cocrystal is a unique example of the thermodynamically stable cocrystal exhibiting high solubility and high permeability.

#### 2.1 Introduction

Parkinson disease is a chronic and degenerative disorder of the central nervous system which leads to progressive deterioration in motor system function control due to loss of dopamine function as a neurotransmitter. Dopamine cannot be taken as a medicine to lift the brain depleted levels because it cannot cross the blood-brain-barrier (BBB). <sup>1-3</sup> A chemical precursor of dopamine which can pass to the brain where it is readily converted into dopamine<sup>2-5</sup> is levodopa (L-Dopa). It is widely used in Parkinson's disease treatment for over 40 years. However, only 5-10% of levodopa crosses the BBB and much of the drug dose is metabolized to dopamine elsewhere in the body.<sup>6</sup> With the intention of avoiding the metabolism outside the brain and to improve the availability of levodopa inside the brain, another medication carbidopa (dopa decarboxylase inhibitor) and entacapone (catechol-omethyltransferase enzyme, COMT) are often combined.<sup>7-9</sup> Among these two drugs, carbidopa across the BBB but inhibits the conversion of levodopa to dopamine outside the brain tissue. <sup>10</sup> Entacapone (ETP) is a potent and specific reversible inhibitor of catechol-o-methyltransferase enzyme (COMT) enzyme, which crosses BBB and stops the metabolism of dopamine by COMT activity inside the brain. 11,12 Currently, a fixed dose combination of levodopa, carbidopa and entacapone is marketed by Novartis.<sup>13</sup> However, ETP is a Biopharmaceutics Classification System (BCS) Class IV drug and exhibits erratic oral bioavailability. 14 This problem is attributed to poor aqueous solubility, low membrane permeability, and first pass metabolism. The aqueous solubility of ETP is less than 80 µg/mL at pH \le 5.0 but rises with increasing pH. 15 The apparent permeability of ETP is logP<sub>app</sub> 0.18±0.02 cm/s at pH 7.4.<sup>16</sup> In order to improve the solubility and oral bioavailability, ETP-hydroxypropyl-βcyclodextrin (HP-β-CD) complex formulations were developed, which showed improved solubility and intravenous bioavailability compared to pure ETP. 15 Solid/liquid self-micro emulsifying drug delivery system (SMEDDS) of ETP exhibit high drug release rate and enhanced shelf-life in the treatment of acute parkinsonism.<sup>17</sup> Crystal forms of entacapone are eliminate in the Cambridge Structural Database (CSD), 18 with no report on polymorphs, solvates/hydrates, or cocrystals, except one guest free form Xray crystal structure.<sup>19</sup> However, ETP polymorphic forms have been characterized by powder X-ray diffraction and on a surface template.<sup>20-22</sup> Crystal engineering<sup>23</sup> of multi-component solids to improve the solubility and permeability of entacapone are reported in this paper. Cocrystals are solids which are crystalline single phase materials composed of two or more different molecular and/or ionic compounds generally in a stoichiometric ratio which are neither solvates nor simple salts.<sup>24</sup> If at least one of the molecules is an active pharmaceutical ingredient (API) and other is generally recognized as safe (GRAS)<sup>25</sup> substance then it is called as a pharmaceutical cocrystal.<sup>26-30</sup> The development of pharmaceutical cocrystals has become a well Known strategy to improve the biopharmaceutical properties of an API. Cocrystallization is a viable platform suited for drugs for which salt formation is not an option due to the absence of ionizable (acid/base) functional groups in the molecule, e.g., as in ETP. Cocrystals provide new opportunities for intellectual property, patent protection and novel pharmaceuticals.31-32

Scheme 2.1: Molecular structures and acronyms of Entacapone and coformers.

#### 2.2 Results and Discussion

Entacapone ((E)-2-cyano-3-(3,4-dihydroxy-5-nitrophenyl)-N,N-diethylacrylamide, ETP, Scheme 2.1) is a conformationally flexible and functionally diverse (phenolic and nitro functional groups) molecule of neutral character (no acid, amine groups which are ionizable at physiological pH). The phenolic OH and nitro O have a tendency to form multiple supramolecular synthons, such as O-H···N, N-H···O and O-H···O in cocrystals with amine, amide, pyridine, acid, and hydroxyl functional group of the coformers.<sup>26,30-35</sup> The nitro group with two O acceptors has propensity to form cocrystals with urea derivatives through N-H···O heterosynthon. <sup>36</sup> In this background, GRAS coformers and drugs with amide functional groups (pyrazinamide and isoniazid) were selected for cocrystallization with entacapone (full list of coformers in Table 2.1). The amide and pyridine coformers such as acetamide (ACT), nicotinamide (NAM), isonicotinamide (INAM), theophylline (THP), pyrazinamide (PYZ) and isoniazid (INZ) afforded cocrystals (Scheme 2.1). Several coformers were unsuccessful in our hands, e.g. 2,6 dihydroxybenzoic acid, 3,4 dihydroxybenzoic acid, benzoic acid, maleic acid, ethyl vanillin, vanillin, guaiacol, caffeine, etc. (Table 2.1). The formed cocrystals were characterized by PXRD, DSC, TGA, IR and NMR. The molecular packing and hydrogen bonding in four cocrystals namely ETP-ACT, ETP-INAM, ETP-PYZ and ETP-THP-HYD was confirmed by single crystal X-ray diffraction (Table 2.2 and Table 2.3). Attempts to obtain single crystals of ETP-NAM and ETP-INZ were unsuccessful due to incongruent solubility in organic solvents (such as ethanol, chloroform, acetonitrile, isobutanol, ethyl methyl ketone, acetone, methanol, diethyl ether, ethyl acetate, etc.) and / or cocrystal phase instability in that solvent system. Nevertheless, these cocrystals were characterized by their unique powder X-ray diffraction pattern and intermolecular interactions by FT-IR spectroscopy. Their stoichiometry was determined by <sup>1</sup>H NMR integration. Solubility, dissolution rate, and diffusion permeability were measured to compare the cocrystal properties with that of pure ETP.

**Table 2.1:** List of coformers attempted for cocrystallization with ETP in this study. The successful molecules which gave crystalline products are shown in bold font.

molecules which gave crystamine products are shown in bold font.						
List of Coformers selected in this chapter						
2,6-Dihydroxybenzoic acid	Vanillic acid	Resorcinol				
3,4-Dihydroxybenzoic acid	L-Arginine	Phloroglucinol				
4-Aminobenzoic acid	Hydroquinone	Hydroquinone				
Benzoic acid	Apocyanin	Theophylline				
Maleic acid	Catechol	Thymine				
Fumaric acid	3-Hydroxybenzaldehyde	3-Methoxyoxy benzoic acid				
Oxalic acid	L-Lysine	4-Methoxy benzoic acid				
Salicylic acid	Histidine	Saccharin				
Ferulic acid	Isonicotinamide	Isoniazid				
Adipic acid	Acetamide	Caffeine				
Succinic acid	Urea	Adenine				
2,5-Dihydroxy benzoic acid	Cytosine	2,4-Dihydroxy benzoic acid				
p-Hydroxy benzoic acid	Nicotinamide	2-Methoxy benzoic acid				
L-Tartaric acid	Piperazine	D-Glucose				
Ethyl vanillin	Adenine	Vanillyl alcohol				
Vanillin	Guaiacol	Pyrazinamide				

**Table 2.2:** Crystallographic parameters of ETP cocrystals.

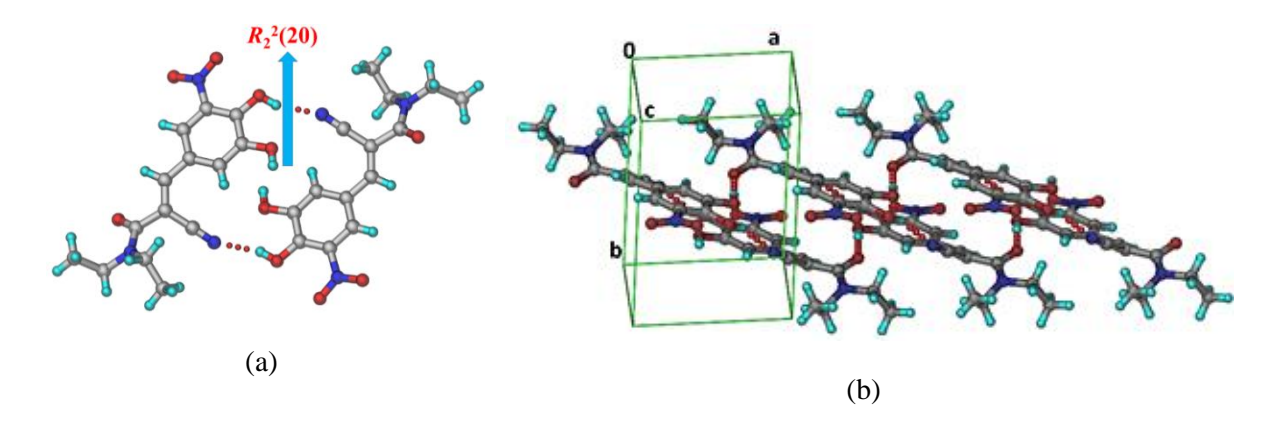
	ETP-ACT (1:1) ETP-INAM (1:1)		ETP-THP-HYD	ETP-PYZ
	EIP-ACI (1:1)	E1P-INAM (1:1)	(1:1:1)	(1:1)
Emp. form.	$C_{14}H_{15}N_3O_5$	$C_{14}H_{14}N_3O_5$	$C_{12}H_{10}N_3O_5$ ,	$C_{14}H_{14}N_3O_5$ ,
	$(C_2H_5NO)$	$(C_6H_6N_2O)$	$(C_9H_{13}N_4O_2)(H_2O)$	$(C_5 H_5 N_3 O)$
Form. wt.	364.36	427.42	503.48	428.41
Cryst. system	Monoclinic	Monoclinic	Triclinic	Monoclinic
Space group	<i>I</i> 2/a	$P2_{1}/n$	P-1	Pn
T(K)	298(2)	298(2)	298(2)	298(2)
a (Å)	15.934(13) Å	13.901(13)	7.1018(2)	4.88(2)
<b>b</b> (Å )	7.000(6) Å	7.426(7)	7.3346(2)	16.55(7)
c (Å )	32.06(02) Å	20.12(2)	22.7120(7)	12.49(5)
a (°)	90	90	95.075(2)	90
β (°)	95.18(5)	100.30(4)	90.438(2)	96.4(2)
γ (°)	90	90	101.915(2)	90
Z	8	4	2	2
$V(\mathring{A}^3)$	3561(5)	2044(3)	1152.61(6)	1003(7)
Rflns. collect	3657	3493	3793	2996
Unique rflns.	3538	3481	3793	2732
Obsd. rflns.	2511	2965	2390	1644
<b>Parameters</b>	240	298	345	290
$R_1$	0.0810	0.0554	0.0703	0.0867
$\mathbf{w}\mathbf{R}_2$	0.2151	0.1577	0.1804	0.2897
GOF	1.320	1.091	1.013	1.072
Diffractometer	Bruker APEX-II CCD detector	Bruker APEX-II CCD detector	Bruker APEX-II CCD detector	Bruker APEX- II CCD detector

**Table 2.3:** Selected geometric parameters of hydrogen bonds in ETP cocrystals.

D-H···A	D···A (Å)	H···A (Å)	D–H···A (°)	symmetry code			
		ETP-ACT (1:1)	<u> </u>				
O1-H1···O5	2.669(4)	1.85	178	1/2-x,3/2-y,1/2-z			
O2-H2···O3	2.635(2)	1.96	140	1/2-x,3/2-y,1-z			
O2-H2···N1	2.962(3)	2.56	112	Intra			
O2-H2···O6	2.856(2)	2.21	136	1/2+,-1/2+Y,1/2+Z			
N5-H5A···O6	2.955(3)	2.11	167	-x,1-y,-z			
N5-H5B···O1	3.048(3)	2.21	164	1/2-x,3/2-y,1/2-z			
	<b>ETP-INAM</b> (1:1)						
O1-H1···O5	2.643(3)	1.79	172	3/2-x,1/2+y,1/2-z			
O2-H2···N4	2.707(3)	1.75	157	2-x,1-y,-z			
N5-H5A···N2	3.142(3)	2.24	161	1-x,-y,-z			
N5-H5B···O6	2.952(3)	2.10	173	3/2-x,-1/2+y,1/2-z			
C7-H7···O4	3.261(3)	2.45	146	1-x,1-y,-z			
C15-H15···O1	3.009(3)	2.37	125	2-x,1-y,-z			
ETP-THP-HYD (1:1:1)							
O1-H1A···O8	2.560(5)	1.74(4)	176(6)	x,1+y,z			
O2–H2A···O3	2.589(4)	1.77(6)	148(6)	Intra			
O2–H2A···O3	3.029(4)	2.40(7)	126(5)	-1+x,-1+y,z			
N6-H6A···O1	2.873(4)	1.99(4)	168(3)	xyz			
O8–H8A···O5	2.733(5)	1.90(7)	178(11)	1+x,y,z			
O8–H8B···O7	2.756(5)	1.90(7)	165(7)	x,-1+y,z			
C4-H4···O6	3.313(5)	2.44	156	x,-1+y,z			
C7-H7···O6	3.382(5)	2.52	154	-1+x,1+y,z			
C20-H20B···O8	3.533(6)	2.59	166	Intra			
ETP-PYZ (1:1)							
O1–H1A···N4	2.671(11)	1.95	144	3/2+x,1-y,1/2+z			
O2–H2A···O3	2.616(11)	1.88	146	Intra			
O2-H2A···O6	2.709(11)	2.19	120	1+x,y,1+z			
N6-H6A···O5	2.925(12)	2.17	146	1+x,y,z			
N6-H6A···O3	3.083(13)	2.28	155	X,y,-1+z			
C17-H17···O1	3.285(14)	2.50	142	-1+x,y,z			
C18-H18···O6	3.285(14)	2.50	161	-1/2+x,1-y,1/2+z			

## **2.3 Crystal Structure Analysis**

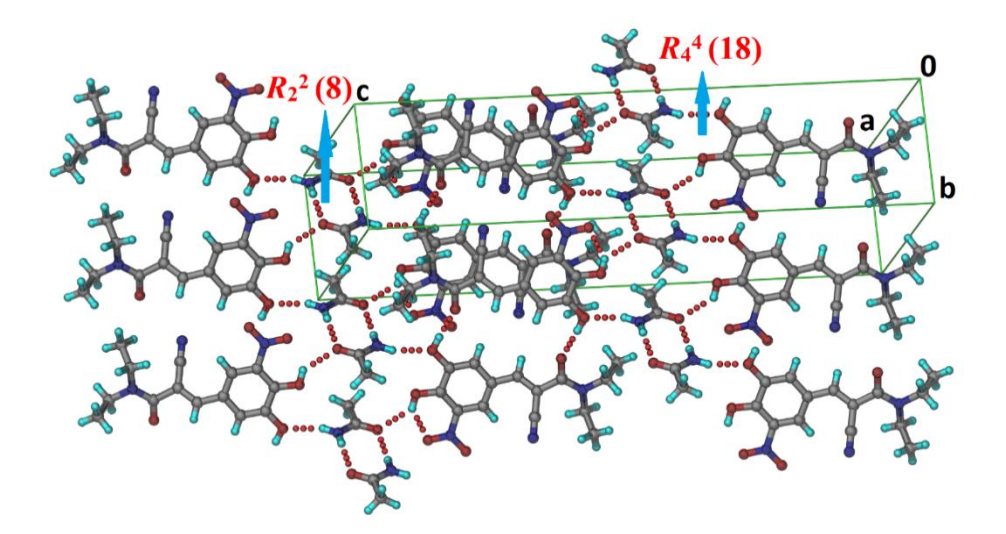
The X-ray crystal structure of ETP (CSD Refcode OFAZUQ) was reported in 2000 by Leppanen et al.<sup>19</sup> Inversion related ETP molecules in the triclinic space group P-1 are connected via O–H···N (O3–H2···N2, 2.93 Å, 153°) hydrogen bonds in a  $R_2^2(20)$  ring motif <sup>38</sup> (Figure 2.1a). Such dimers are associated through bifurcated O–H···O (O2–H1···O1, 2.62 Å, 173°) H-bonds in a 1D chain along the c-axis (Figure 2.1b).



**Figure 2.1:** Inversion related ETP dimers connected by strong O–H···N interactions (a) and such dimers connected by bifurcated O–H···O bonds in a chain along the c-axis (b).

## Entacapone-Acetamide (ETP-ACT, 1:1) Cocrystal

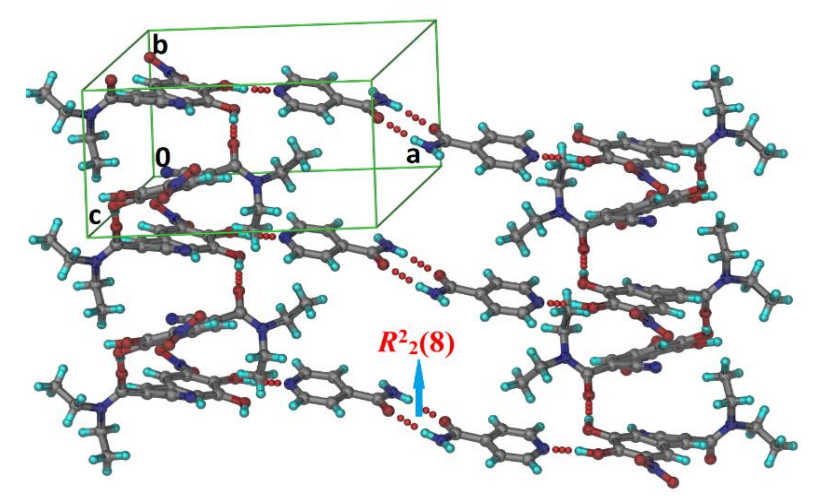
The X-ray crystal structure of ETP-ACT was solved and refined in the monoclinic space group  $I_2/a$ . ACT coformer binds to ETP drug via a single point amide-phenol N–H···O bond (N5–H5A···O1, 2.23 Å, 158°). Adjacent molecules in the cocrystal structure are connected by ACT amide dimer (N5–H5B···O6, 2.08 Å, 168°) in  $R_2^2$ (8) ring motif (Figure 2). The structure extends in a layer through O–H···O (O2–H2···O6, 2.60 Å, 159°) bonds in a  $R_4^4$  (18) tetrameric ring motif and such layers are further connected by O–H···O (O1–H1···O5, 1.86 Å, 171°) bonds.



**Figure 2.2:** Layered structure of ETP-ACT cocrystal is sustained by O–H···O and N-H···O=C hydrogen bonds.

## Entacapone-Isonicotinamide (ETP-INAM, 1:1) Cocrystal

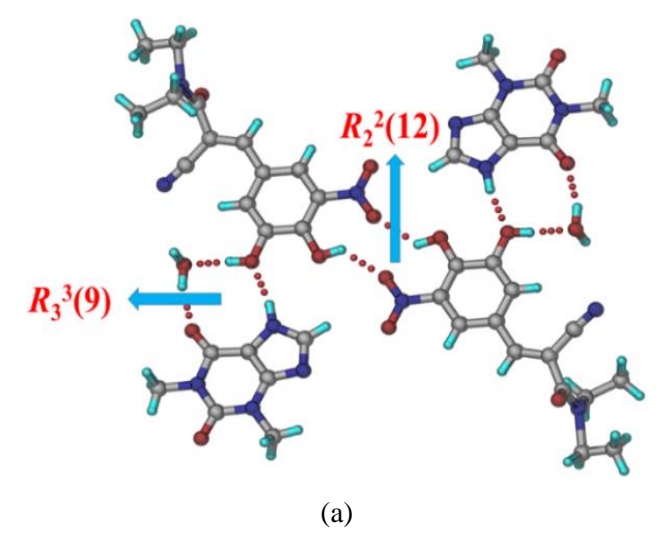
This molecular complex is in the monoclinic  $P2_1/n$  space group. ETP and INAM molecules associate through O–H···N (O2–H2A···N4, 1.76 Å, 156°) hydrogen bond in the structure. The molecules are connected via O–H···O (O1–H1A···O5, 1.77 Å, 171°) motif along the screw axis. Such linear chains are bridged by INAM amide dimer N–H···O (N5–H5A···O6, 2.09 Å, 172°) hydrogen bond in  $R_2^2(8)$  ring motif (Figure 2.3).



**Figure 2.3:** Screw axis related molecules in the cocrystal structure are bridged by amide dimer N–H···O hydrogen bonds via  $R_2^2(8)$  ring motif.

## Entacapone-Theophylline hydrate (ETP-THP-HYD, 1:1:1) Cocrystal

The 1:1:1 cocrystal hydrate was solved and refined in the triclinic P-1 space group. A molecules ETP, THP and water are linked in a trimeric  $R_3^3(8)$  ring motif through N–H···O (N6–H6A···O1, 1.98 Å, 171°) and O–H···O (O1–H1A···O8, 1.75 Å, 169° and O8–H8B···O7, 1.87 Å, 164°) hydrogen bonds. Such molecular adduct hydrate dimers aggregate through O–H···O (O8–H8B···O7, 1.81 Å, 146°) hydrogen bond in a  $R_2^2(12)$  ring motif in sheet structure (Figure 2.4a). The dimers stack to make a ladder structure via O–H···O (O8–H8A···O5, 1.93 Å, 178°) bonds (Figure 2.4b).



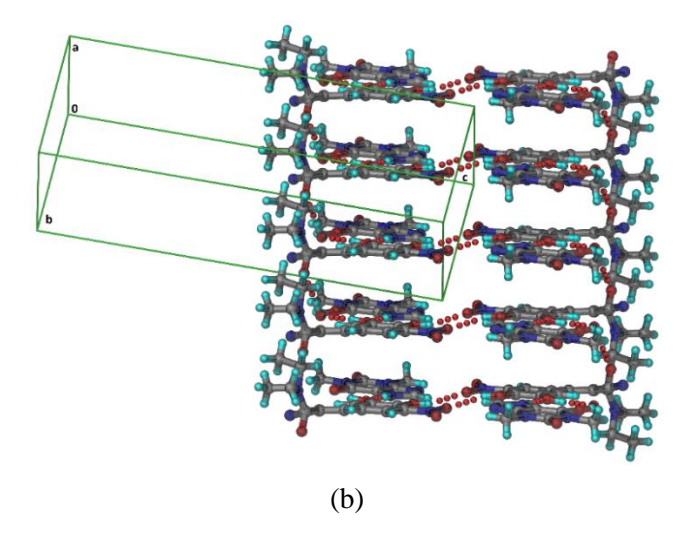


**Figure 2.4:** Inversion center related cocrystal hydrate dimers are bridged through O–H···O hydrogen bond  $R_2^2(12)$  ring motif (a) and such dimers 2D patterns connected via O–H···O interaction and make a ladder structure (b).

#### Entacapone-Pyrazinamide (ETP-PYZ, 1:1) Cocrystal

Plate morphology of crystals of ETP-PYZ was solved and refined in *Pn* space group with one molecule of ETP and PYZ in the asymmetric unit. ETP and PYZ are linked by hydroxyl-pyridine O–H···N (O1–H1A···N4, 1.93 Å, 150°) hydrogen bond in the structure (Figure 2.5). The molecular adducts are connected by O–H···O (O2–H2A···O6, 2.21 Å, 116°) and C–H···O (C18–H18···O6, 2.51 Å, 161°) bonds in a layer structure.

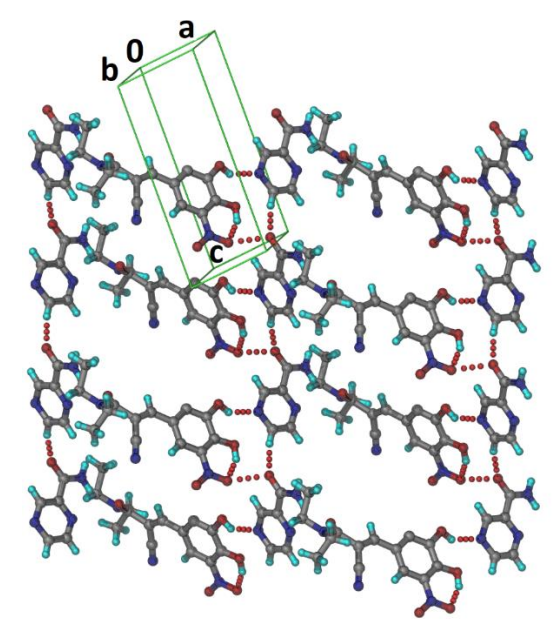


**Figure 2.5:** ETP-PYZ layer structure connected by O–H···O and C–H···O interactions.

Generally, heteromeric interactions with coformer in the crystal structure changes the conformation of the drug due to systematic effects. The presence of phenol OH, cyano and diethylacrylamide groups in ETP suggests that it can adopt potentially different conformations and orientations in the cocrystal crystal structures due to the flexibility of these groups' rotations. Indeed, different conformations of ETP have observed in its cocrystals and torsion angles displayed in Figure 2.6 and listed in Table 2.4.

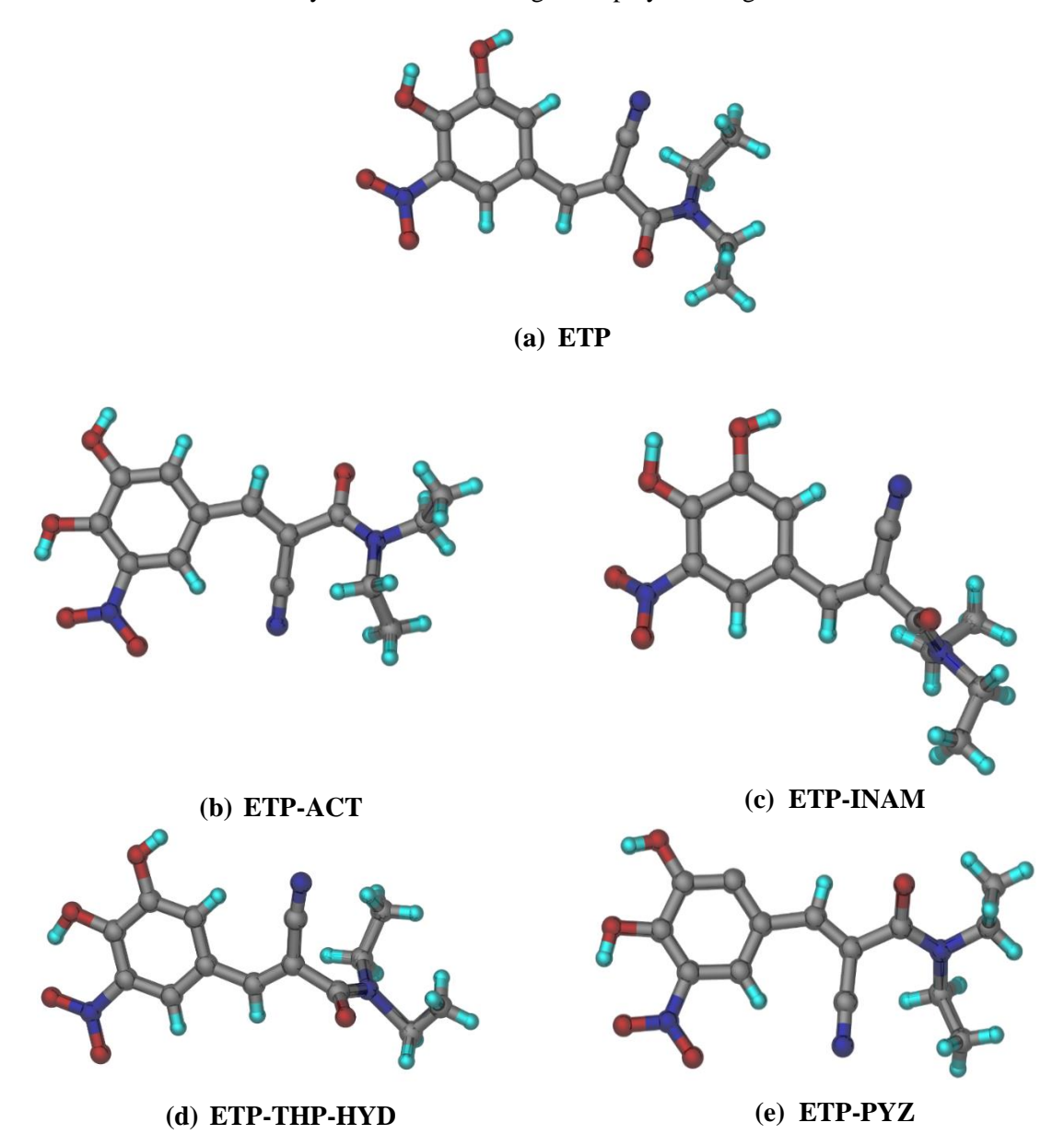


Figure 2.6: Conformational representation of ETP in its cocrystals.

Table 2.4: Torsion angles of ETP and its cocrystals

 $\tau_1$ C5C7, C8, C10,  $\tau_2$  C5, C7, C8, C9,  $\tau_3$  C10, C8, C9, O5,  $\tau_4$  C9, N3, C13, C14,  $\tau_5$  C9, N3, C11, C12

	$ au_1$	$ au_2$	τ <sub>3</sub>	τ4	τ <sub>5</sub>
ETP	2.73	172.57	131.97	81.50	119.18
ETP-ACT	0.77	174.29	141.09	114.00	95.37
ETP-INAM	3.34	172.90	53.34	98.98	98.98
ETP-THP-HYD	6.45	178.60	88.28	89.92	-103.81
ETP-PYZ	-5.30	-173.22	-137.80	-79.05	-118.73

# 2.4 FT-IR Spectroscopy

Infrared spectroscopy provides information about the vibration modes of a molecule due to changes in molecular conformations and hydrogen bonding.<sup>37</sup> The tertiary amide carbonyl (C=O) stretching vibrations of ETP appears at 1627 cm<sup>-1</sup> and the nitrile group stretching band is at 2216 cm<sup>-1</sup>. The phenolic hydroxyl OH stretching band appears as a broad band at 3335 cm<sup>-1</sup>. All these functional groups showed significant changes in their vibration peaks upon cocrystal formation (Table 2.5 and Figure 2.7a-f). Especially, two cocrystals of ETP-NAM and ETP-INZ for which single crystals for single crystal X-ray diffraction were not available, were characterized by their unique powder X-ray diffraction pattern and molecular level interactions in FT-IR spectra. In ETP-NAM cocrystal, NH<sub>2</sub> and OH region, sym and asym stretching bands are at 3257 and 3330 cm<sup>-1</sup> for NH<sub>2</sub> (NAM) group and phenolic hydroxyl OH at 3449 cm<sup>-1</sup> are significantly shifted compared to API. Whereas ETP-INZ cocrystal is in the same region at 3275 and 3312 cm<sup>-1</sup> there are differences compared to the starting materials. The stretching bands of C=N and C=O are shifted significantly to indicate hydrogen bonding. These differences support the presence of O-H···N bonding between ETP and coformer (NAM and INZ). Similarly, there is a red shift in the nitrile functional group including fingerprint region stretching bands in all the cocrystals when compared to ETP and coformer. The stoichiometry of ETP-NAM and ETP-INZ was confirmed by <sup>1</sup>H-NMR integration (Figure 2.7g-k).

**Table 2.5** IR stretching frequencies of ETP/coformer in the crystalline forms (Figure 2.7a-f).

Solid form	CONH <sub>2</sub> /CON R <sub>2</sub> v <sub>C=O</sub> in ETP/coformer (cm <sup>-1</sup> )	CONH <sub>2</sub> /CON R <sub>2</sub> v <sub>C=0</sub> in Cocrystal (cm <sup>-1</sup> )	OH/NH/NH <sub>2</sub> v NH (cm <sup>-1</sup> ) in ETP/coforme r (cm <sup>-1</sup> )	OH/NH/NH <sub>2</sub> v <sub>NH</sub> (cm <sup>-1</sup> ) in Cocrystal (cm <sup>-1</sup> )	Nitrile v <sub>CN</sub> in ETP/Cocryst al (cm <sup>-1</sup> )
ETP	1627		3335		2216
ETP-ACT	1670	1686	3194, 3376	3189, 3410	2208
ETP- INAM	1677	1686	3182, 3371	3194, 3417	2212
ETP-NAM	1698	1689	3161, 3366	3211, 3339, 3461	2206
ETP-THP- HYD	1667, 1717	1652, 1703	3121	3211, 3402	2198
ETP-PYZ	1715	1694	3290, 3413	3257, 3330, 3449	2205
ETP-INZ	1667	1666,1624	3232, 3303, 3419	3275, 3312	2206

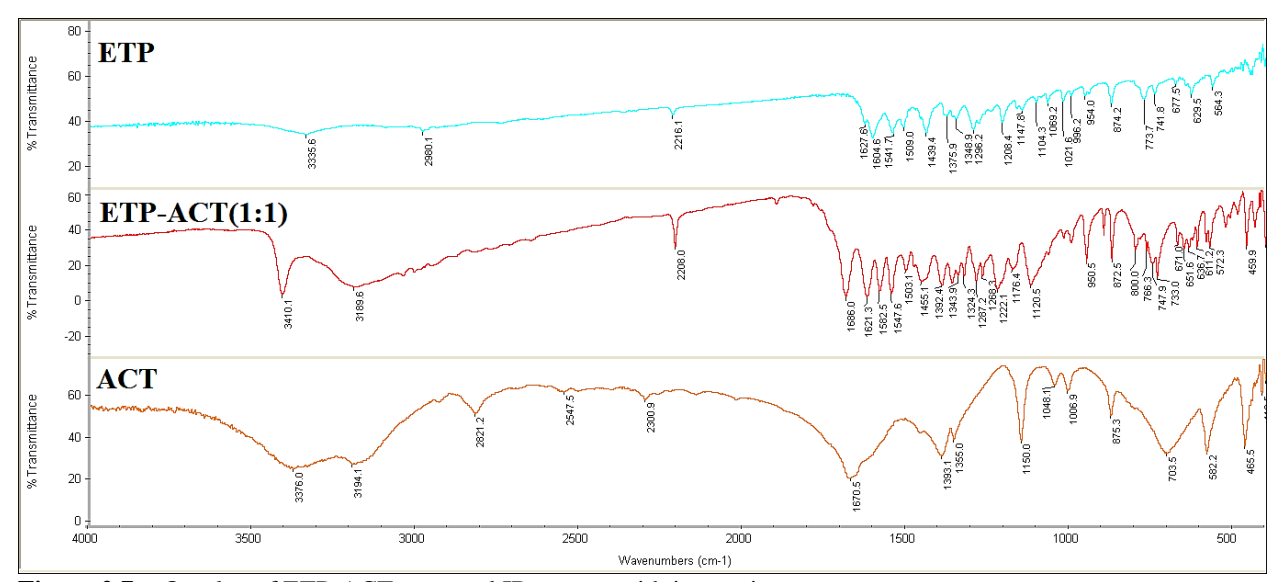
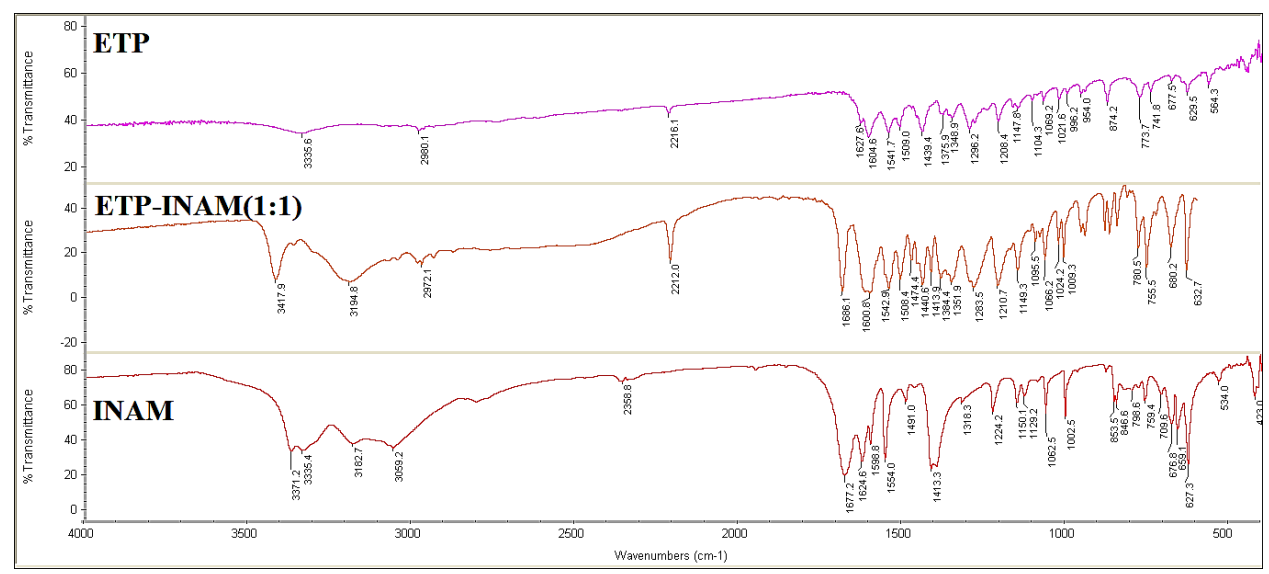


Figure 2.7a: Overlay of ETP-ACT cocrystal IR spectra with its starting components.



**Figure 2.7b:** Overlay of ETP-INAM cocrystal IR spectra with its starting components.

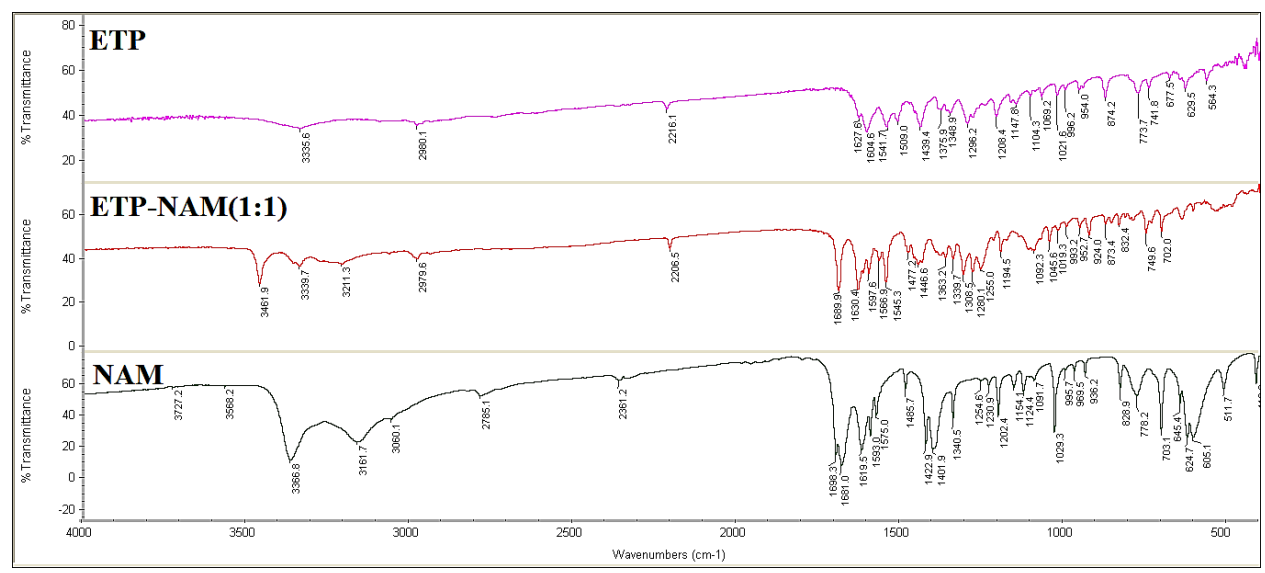


Figure 2.7c: Overlay of ETP-NAM cocrystal IR spectra with its starting components.

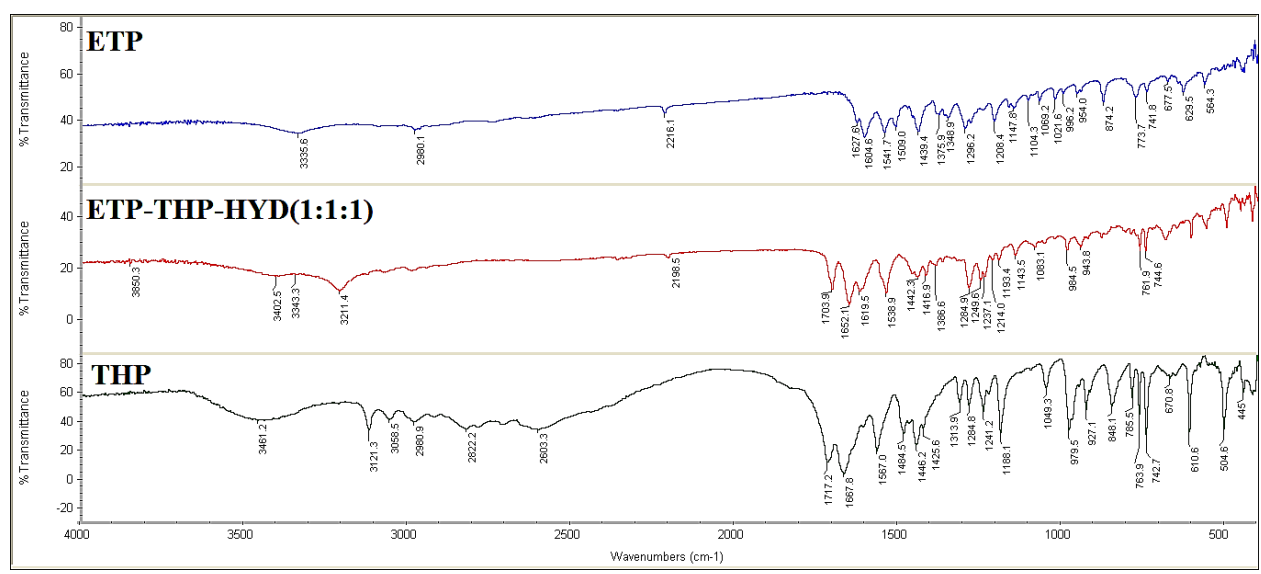


Figure 2.7d Overlay of ETP-THP-HYD cocrystal IR spectra with its starting components.

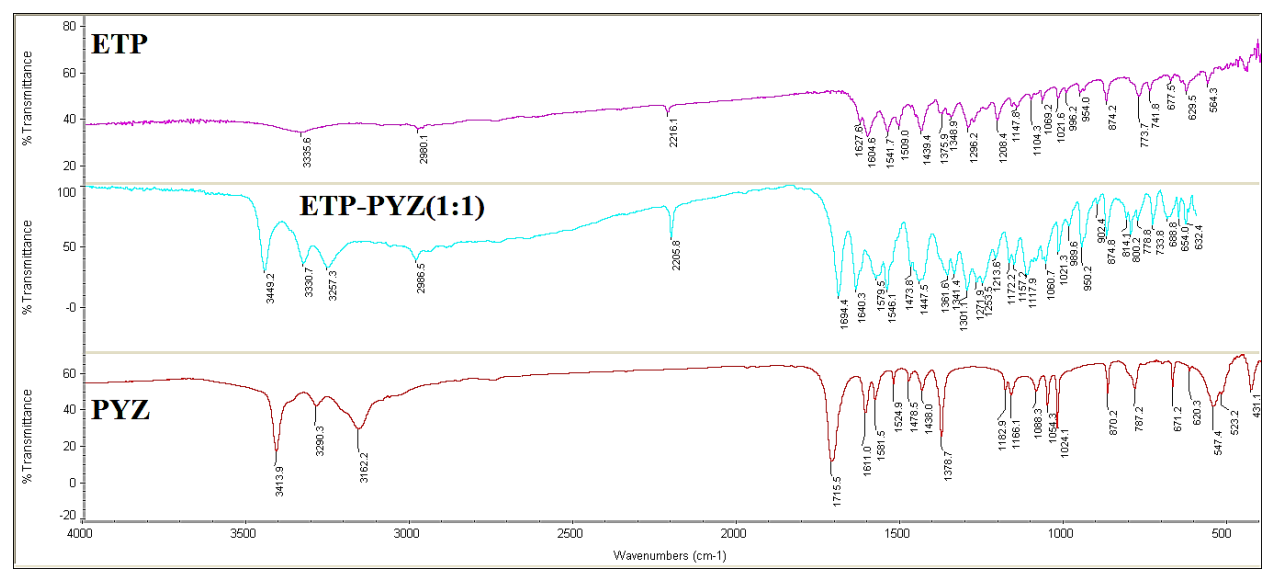


Figure 2.7e: Overlay of ETP-PYZ cocrystal IR spectra with its starting components.

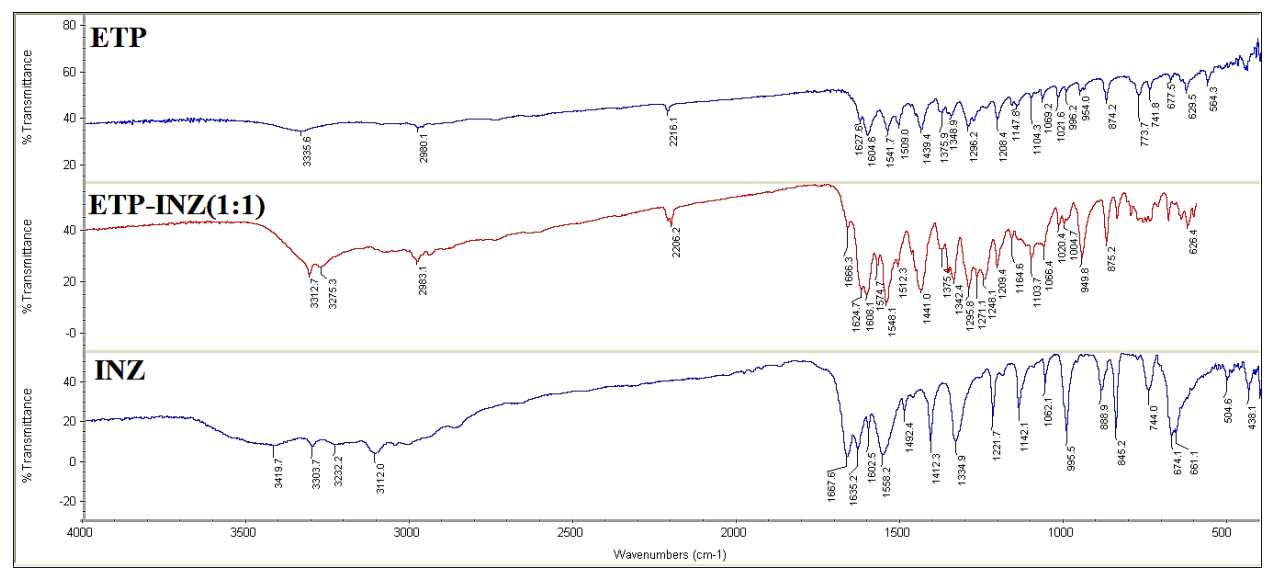
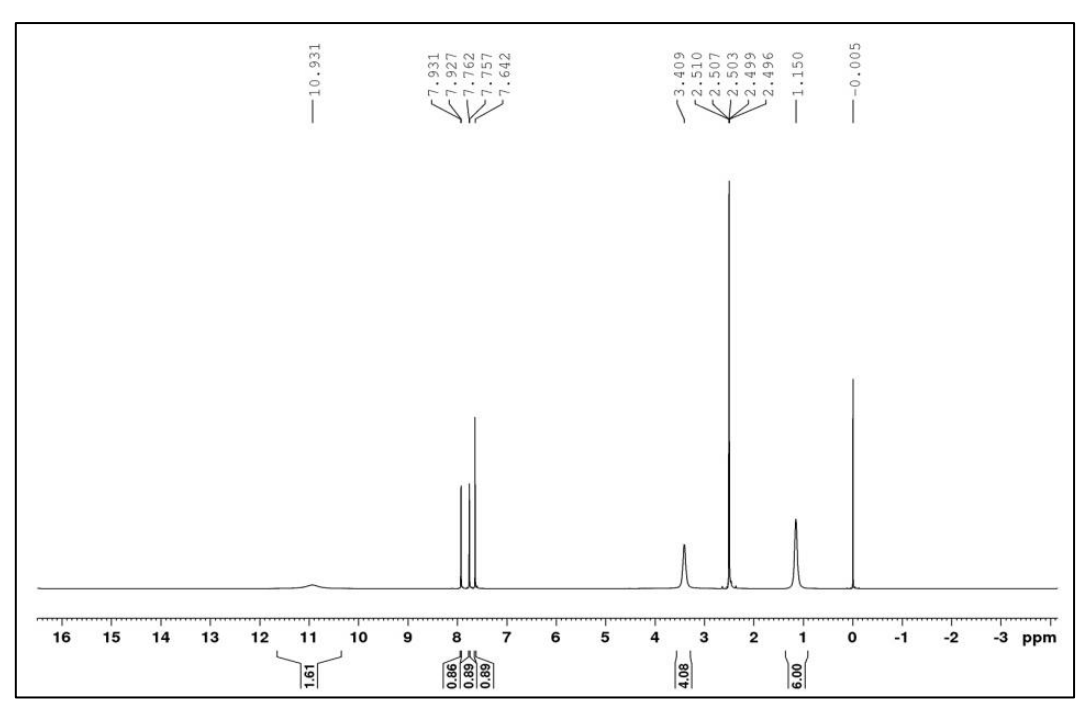
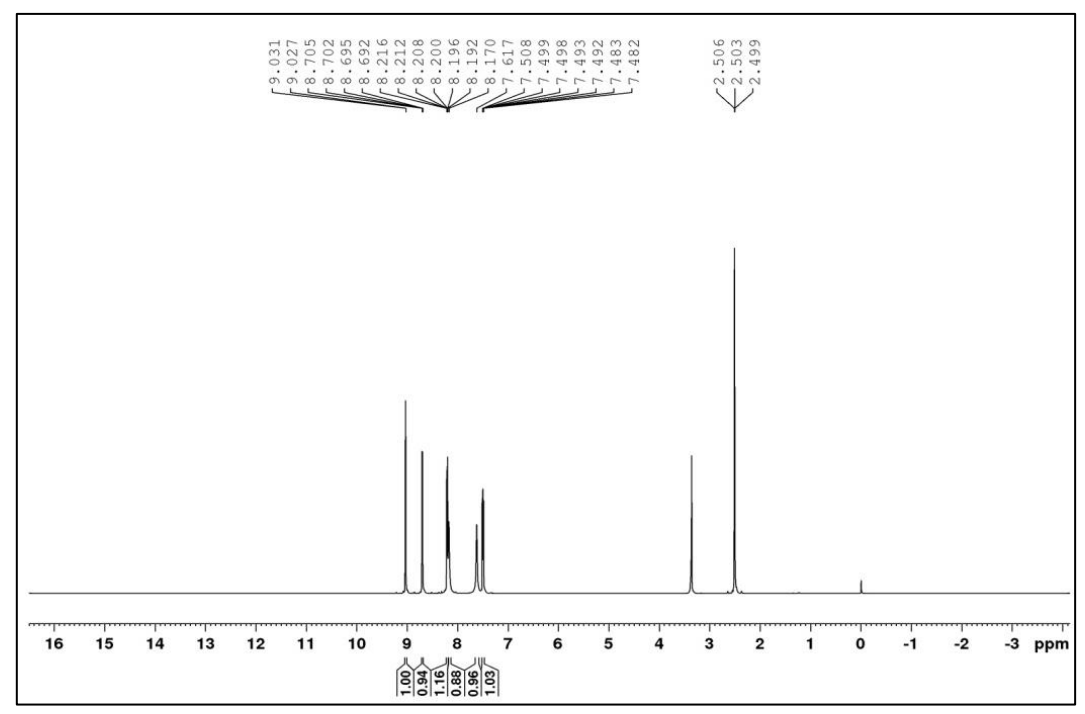


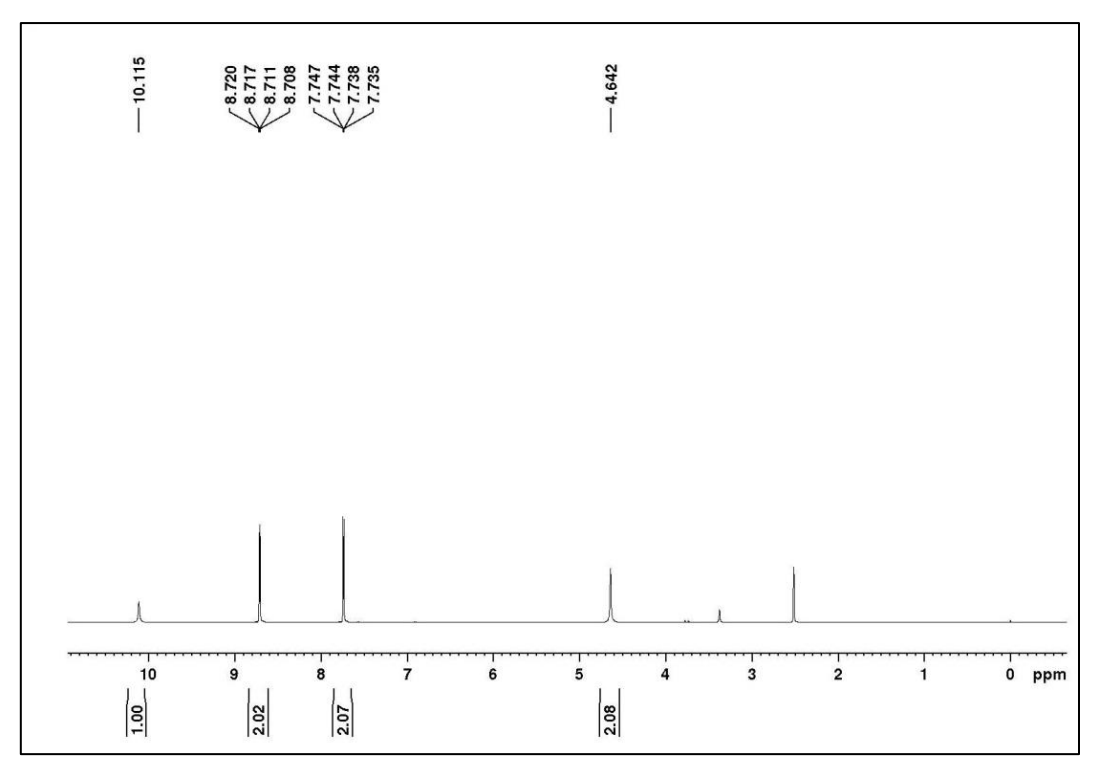
Figure 2.7f: Overlay of ETP-INZ cocrystal IR spectra with its starting components.



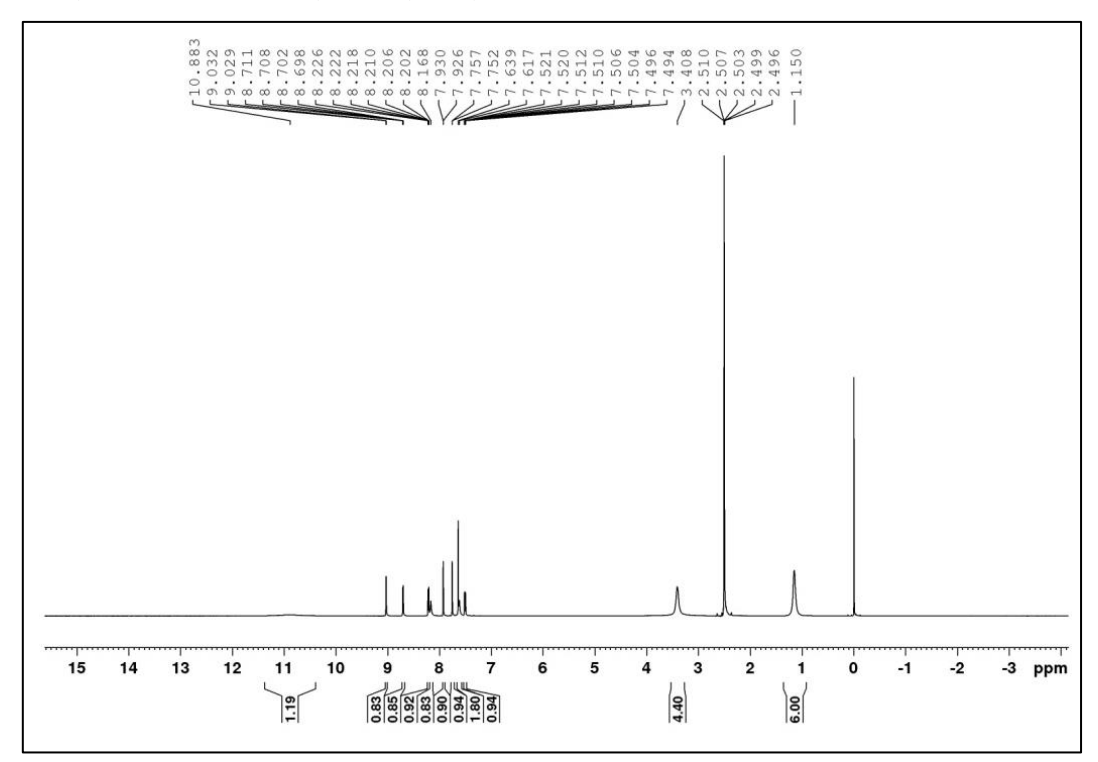
**Figure 2.7g:** ETP proton NMR spectrum; **ETP (DMSO-d<sub>6</sub>, δ, ppm):** 10.9 (s, 2H); 7.93 (d, J=2Hz, 1H); 7.76 (d, J=2Hz, 1H); 7.64 (s, 1H); 3.4 (s, 4H); 1.15 (s, 6H).



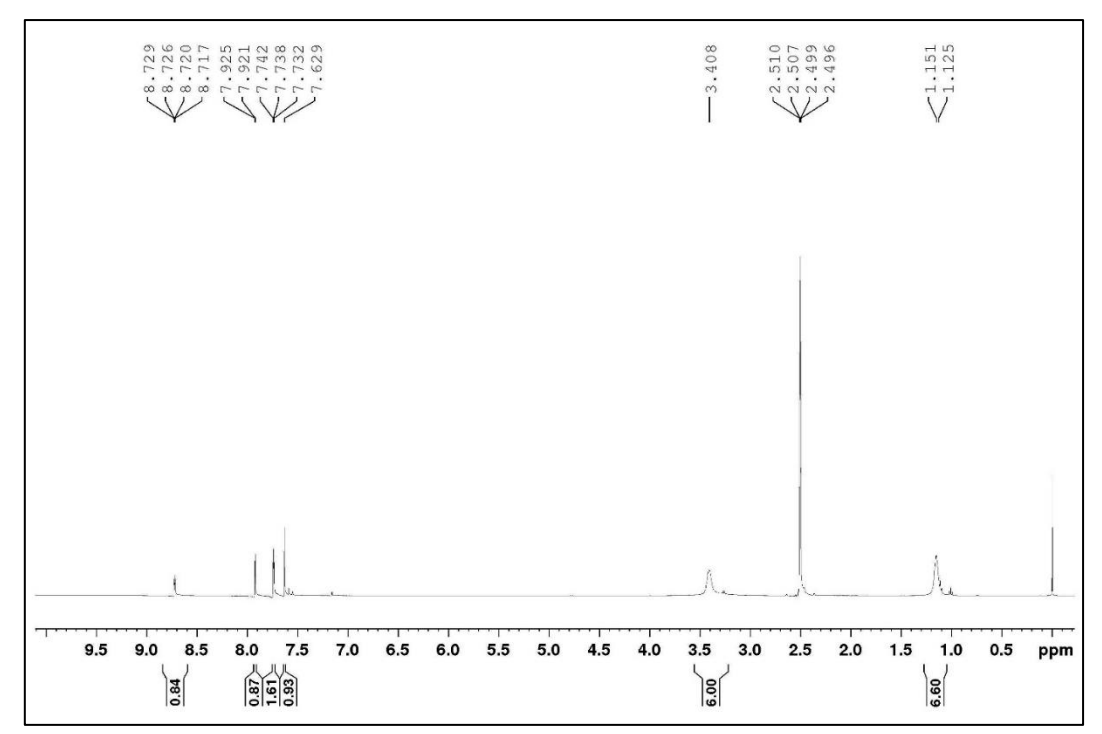
**Figure 2.7h:** NAM proton NMR spectrum; **NAM (DMSO-d<sub>6</sub>, δ, ppm):** 9.02 (d, J=2Hz, 1H); 8.69 (dd, J=3.2,1.5Hz, 1H); 8.20 (dt, J=4.0,1.7Hz, 1H); 8.16 (s, 1H); 7.16 (s, 1H); 1.15 (s, 6H); 7.49 (qd, J=2.5,0.6Hz, 1H).



**Figure 2.7i:** INZ proton NMR spectrum; **INZ (DMSO-d<sub>6</sub>, δ, ppm):** 10.1 (s, 1H); 8.70 (dd, J=2.3,1.5Hz, 2H); 7.72 (dd, J=2.3,1.5Hz, 2H); 4.63 (s, 2H).

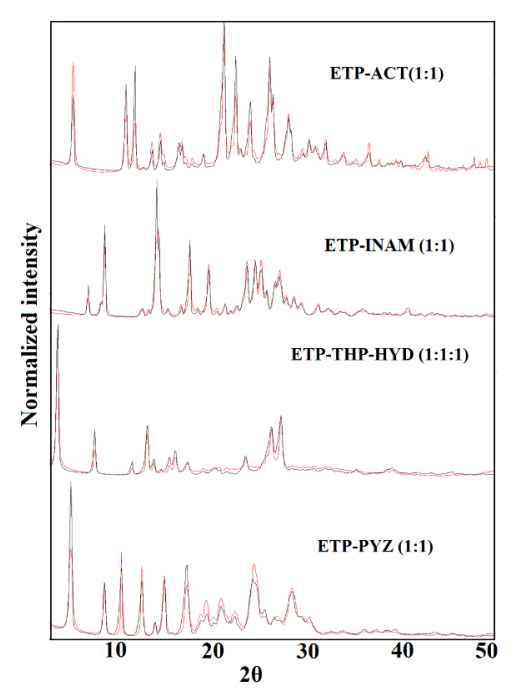


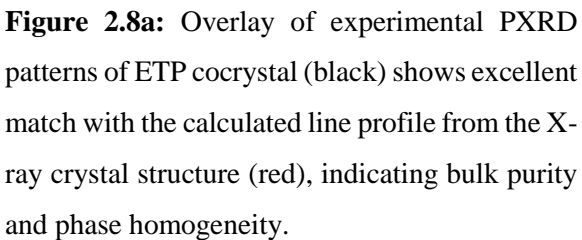
**Figure 2.7j:** ETP-NAM proton NMR spectrum; **ETP-NAM (1:1) (DMSO-d<sub>6</sub>, δ, ppm**): 10.88 (s,1H); 9.03 (d, J=2Hz, 1H); 8.70 (dd, J=5.0,1.5Hz, 1H); 8.21 (dt, J=4.0,1.8Hz, 1H); 8.16 (s, 1H);1.15 (s, 6H); 7.92 (d, J=2Hz, 1H); 7.75 (d, J=2Hz, 1H); 7.63 (s, 1H); 7.61 (s, 1H); 7.51 (qd, J=4.0,1.0Hz, 1H); 3.4 (s, 4H); 1.15 (s, 6H).



**Figure 2.7k:** ETP-INZ proton NMR spectrum; **ETP-INZ** (**1:1**) (**DMSO-d<sub>6</sub>**, δ, **ppm**): 8.72 (dd, J=4.5,1.6Hz, 1H); 7.92 (d, J=2.1Hz, 1H); 7.75-7.73 (m, 2H); 7.63 (s, 1H); 3.41 (s, 6H); 1.15 (s, 7H).

# 2.5 Powder X-ray Diffraction





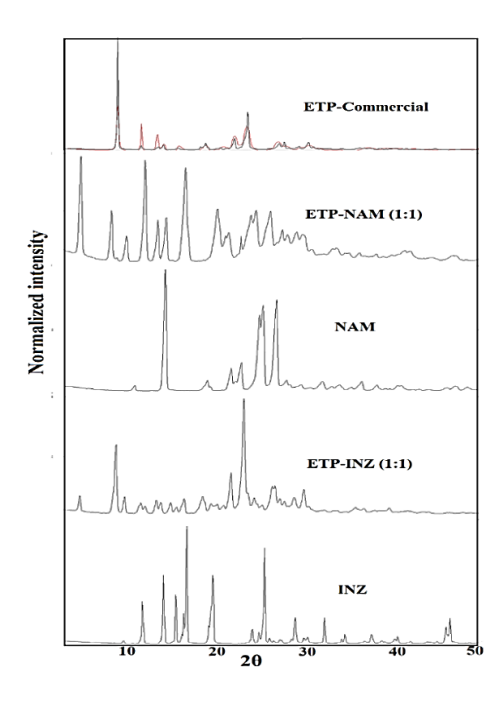


**Figure 2.8b:** Experimental PXRD plots of ETP, ETP-NAM, ETP-INZ, and coformers NAM and INZ to compare  $2\theta$  values in the new crystalline phases.

The bulk phase purity of all cocrystals was confirmed by Powder X-ray diffraction. PXRD lines of the four cocrystals exhibited excellent match by using PCW Software<sup>39</sup> of the experimental pattern with the calculated lines from the X-ray crystal structure (Figure 2.8a). The other two cocrystals of ETP-NAM and ETP-INZ showed diffraction peaks at  $2\theta$  values different and unique from that of the starting components, indicating new crystalline phases (Figure 2.8b).

## **2.6 Differential Scanning Calorimetry**

The cocrystals were analyzed by DSC to measure accurate melting point/decomposition of the solid (Figure 2.9 and Table 2.6). The melting point of ETP-ACT and ETP-NAM are intermediate compared to the drug and coformer, whereas ETP-INAM and ETP-INZ cocrystals exhibit lower melting point than either of the starting components. ETP-THP-HYD (hydrate) exhibited a broad endotherm at 64 °C prior to the melting endotherm at 147 °C which is due to dehydration of one water molecule as observed from the weight loss of the material in TGA at the same temperature (Obsd. 3.51% and Calc. 3.57% for 1 mole of water, Figure 2.10 a-c). Surprisingly when ETP-PYZ cocrystal was subjected to DSC the PYZ coformer eliminated from the crystal lattice and sublimed at 115 °C and the remaining ETP melted at 162 °C. This coformer dissociation during heating was confirmed by controlled heating experiment followed by powder X-ray diffraction analysis (Figure 2.11).

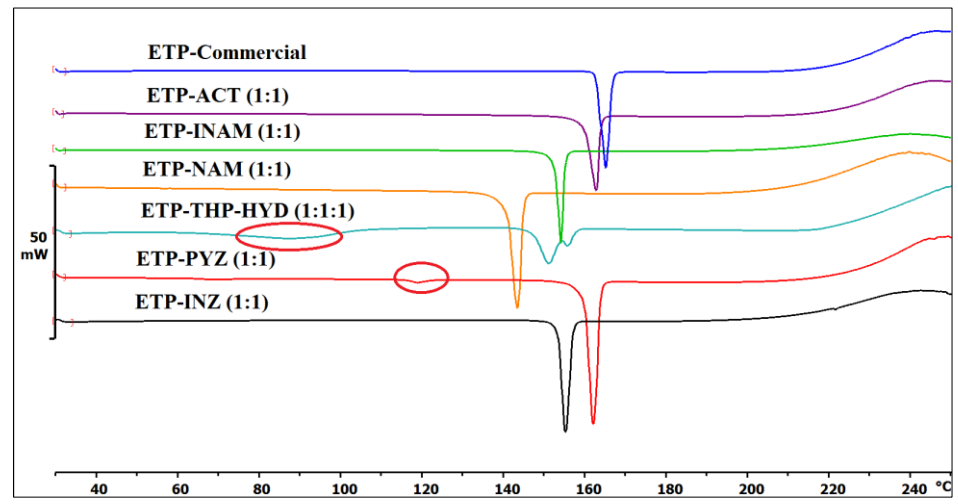


**Figure 2.9:** Overlay of DSC thermograms of ETP and cocrystals showing their unique melting behaviour and sharp endotherms.

**Table 2.6:** Melting point of ETP, cocrystals and coformers.

- word - word in the control of the				
	ETP/Cocrystal	<b>m.p.</b> (° <b>C</b> )	Coformer	<b>m.p.</b> (°C)
1	ETP	162-164		
2	ETP-ACT (1:1)	159-161	ACT	79-81
3	ETP-INAM (1:1)	152-153	INAM	155-157
4	ETP-NAM (1:1)	140-142	NAM	128-131
5	ETP-THP-HYD (1:1:1)	147-150	THP	271-274
6	ETP-PYZ (1:1)	159-160	PYZ	189-191
7	ETP-INZ (1:1)	153-154	INZ	171-173

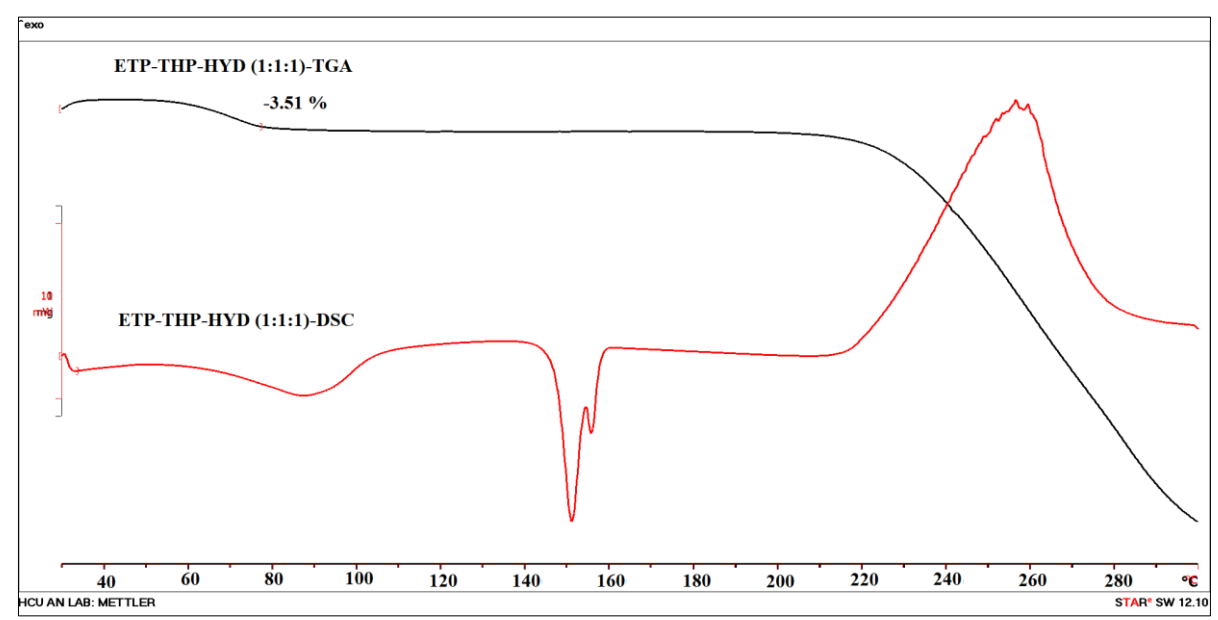


**Figure 2.10a:** DSC (red) and TGA (black) of ETP-THP-HYD. The weight loss in TGA is consistent with one H<sub>2</sub>O molecule in the cocrystal hydrate structure.

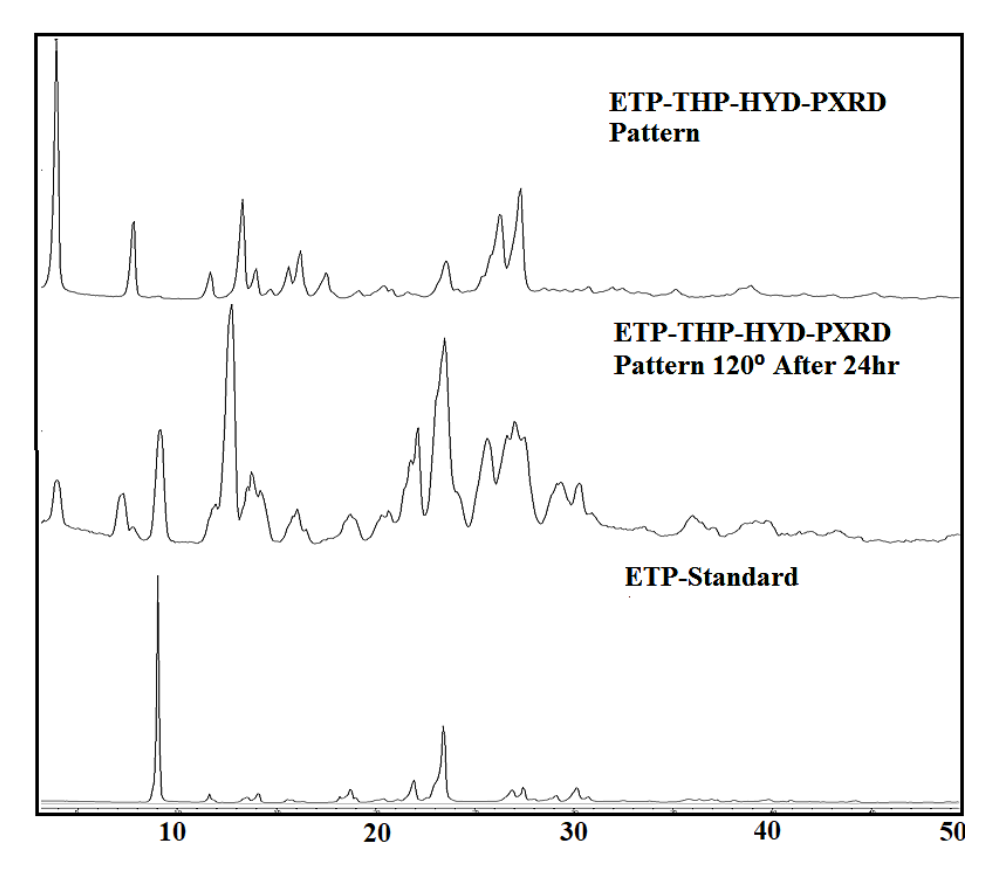


Figure 2.10b ETP-THP-HYD PXRD pattern after controlled heating experiment.

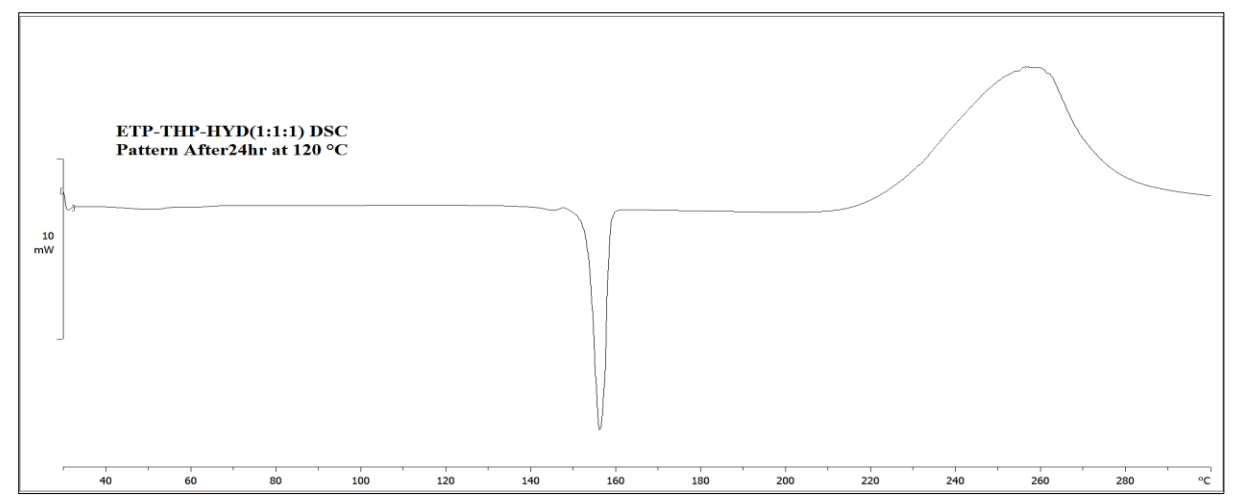
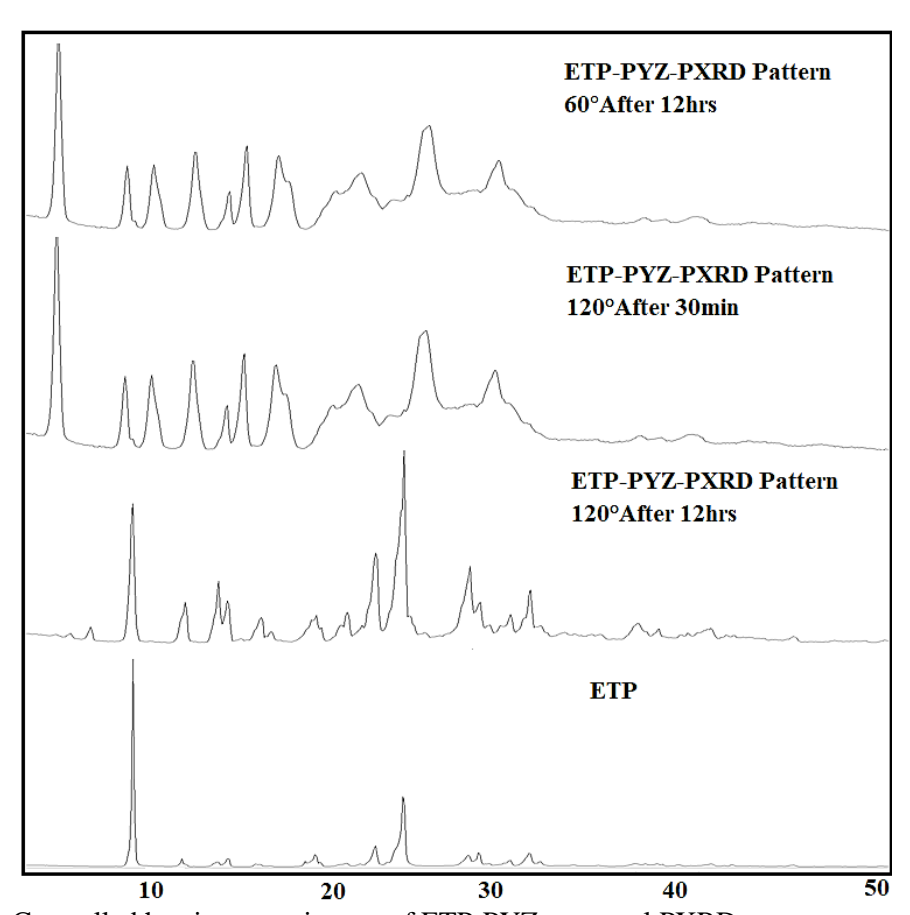


Figure 2.10c: ETP-THP-HYD DSC pattern after 24 h at 120 °C shows a sharp endotherm obtained after loss of water molecule.



**Figure 2.11:** Controlled heating experiments of ETP-PYZ cocrystal PXRD patterns compared with ETP standard material.

#### 2.7 Solubility and Dissolution

High solubility and fast dissolution are essential for better pharmacokinetics and improved therapeutic efficacy. 40 Dissolution rate enhancement can be modulated via cocrystals through high solubility of the coformer. Solubility and dissolution rate were measured in phosphate buffer (pH 7) medium. Equilibrium solubility was measured at the end of 24 h and dissolution rate measurements were performed for 4 h by the rotating disk intrinsic dissolution rate (DIDR) method at 37 °C in phosphate buffer (pH 7). Both solubility and IDR concentration of the drug were measured by UV spectroscopy (using the  $\lambda_{max}$  of ETP at 376 nm) and undissolved materials were characterized by PXRD to confirm the phase nature/ stability during the experiment. Only two cocrystals, ETP-THP-HYD and ETP-PYZ were stable during the equilibrium solubility experiment for 24 h, while the remaining four cocrystals dissociated into the individual compounds as confirmed by PXRD (Figure 2.13a-g). The stable cocrystals of ETP-THP-HYD and ETP-PYZ displayed 1.5-fold higher solubility compared to pure ETP (Table 2.7). In dissolution study, the stable cocrystals ETP-PYZ and ETP-THP-HYD exhibited 2 & 1.7fold faster dissolution rate compared to ETP. The improved solubility of cocrystals has been ascribed to supramolecular interactions N-H···O, O-H···N and O-H···O different conformational changes in the crystal structure as well as the high solubility of the coformer.<sup>41</sup> The remaining cocrystals showed only a slight increase in dissolution rate (Figure 2.12 and Table 2.7). The undissolved material at the end of the dissolution experiment was stable as confirmed by PXRD as the starting cocrystal, except ETP-ACT which showed partial dissociation at 4 h (Figure 2.14a-g). Usually, stability and solubility tend to be inversely correlated, because the high thermodynamic function imparts faster dissolution. In case of dissociated cocrystals under physiological conditions exhibit greater dissolution rate because dissociation leads drug molecules in aperiodic arrangement which comprehensibly exhibit high free energy of the system leads to faster dissolution rate. However, this study is contra to the trend in that the stable phases exhibit high solubility and dissolution rate.

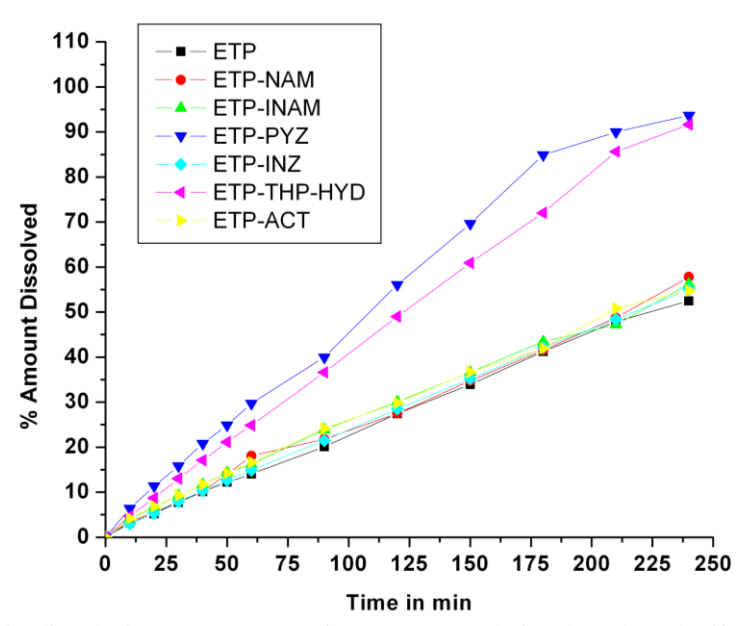


**Figure 2.12:** Intrinsic dissolution rate curves of ETP cocrystals in phosphate buffer (pH 7).

Compound	Solubility of the drug / coformer (mg/mL)	Molar Extinction coefficient (mM <sup>-1</sup> cm <sup>-1</sup> )	Equilibrium Solubility in pH 7 medium (mg/mL)	Intrinsic dissolution rate, IDR (mg/cm²/min)	Cumulative amount dissolved per unit area (mg/500mL)
ETP	0.08	25.21	4.03	1.21	131.26
ETP-ACT	2000	23.77	Unstable	1.41	136.92
ETP-INAM	191	24.91	unstable	1.40	140.49
ETP-NAM	1000	23.98	Unstable	1.31	144.48
ETP-THP- HYD	8.3	24.33	5.86 (x1.45)	2.08 (x1.71)	229.13 (x1.74)
ETP-PYZ	22	27.44	5.89 (x1.46)	2.46 (x2.03)	234.57 (x1.78)
ETP-INZ	125	27.44	unstable	1.24	137.71

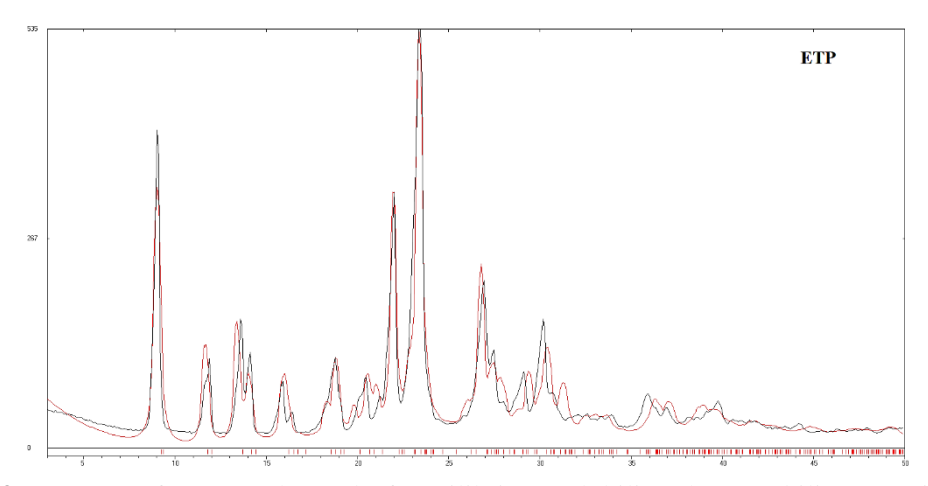


**Figure 2.13a:** PXRD of ETP at the end of equilibrium solubility/phase stability experiment (24 h, black) in phosphate buffer (pH 7) media matches with the calculated XRD pattern of ETP (red) indicating phase stability.

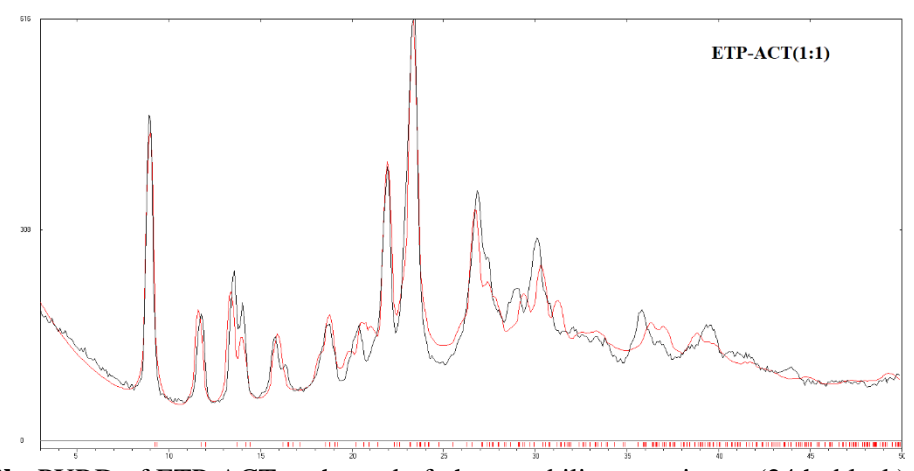


**Figure 2.13b:** PXRD of ETP-ACT at the end of phase stability experiment (24 h, black) in phosphate buffer (pH 7) media matches with the calculated XRD pattern of ETP (red) indicating cocrystal phase is completely dissociated in 24 h.

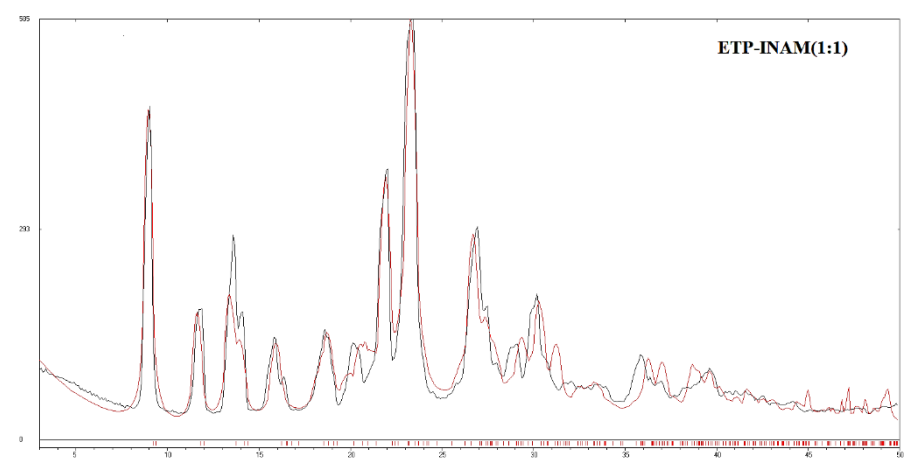


**Figure 2.13c:** PXRD of ETP-INAM at the end of phase stability experiment (24 h, black) in phosphate buffer (pH 7) media matches with the calculated XRD pattern of ETP (red) indicating cocrystal phase is completely dissociated in 24 h.

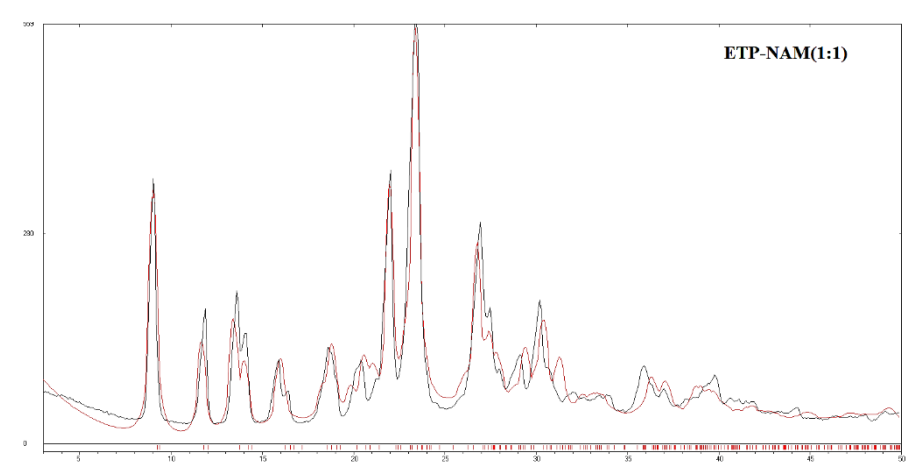


**Figure 2.13d:** PXRD of ETP-NAM at the end of phase stability experiment (24 h, black) in phosphate buffer (pH 7) media matches with the calculated XRD pattern of ETP (red) indicating cocrystal phase is completely dissociated in 24 h.

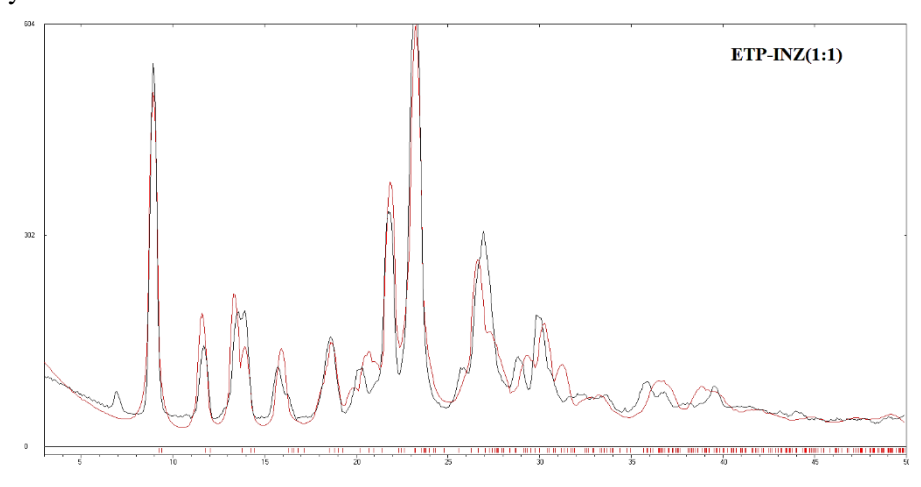


**Figure 2.13e:** PXRD of ETP-INZ at the end of phase stability experiment (24 h, black) in phosphate buffer (pH 7) media matches with the calculated XRD pattern of ETP (red) indicating cocrystal phase is completely dissociated in 24 h.

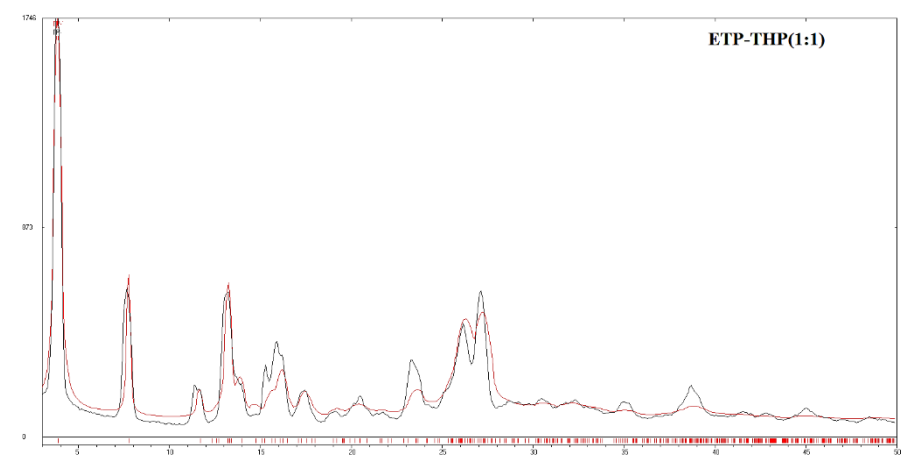


**Figure 2.13f:** PXRD of ETP-THP-HYD at the end of equilibrium solubility/phase stability experiment (24 h, black) in phosphate buffer (pH 7) media matches with the calculated XRD pattern of ETP-THP-HYD (red) indicating phase stability.

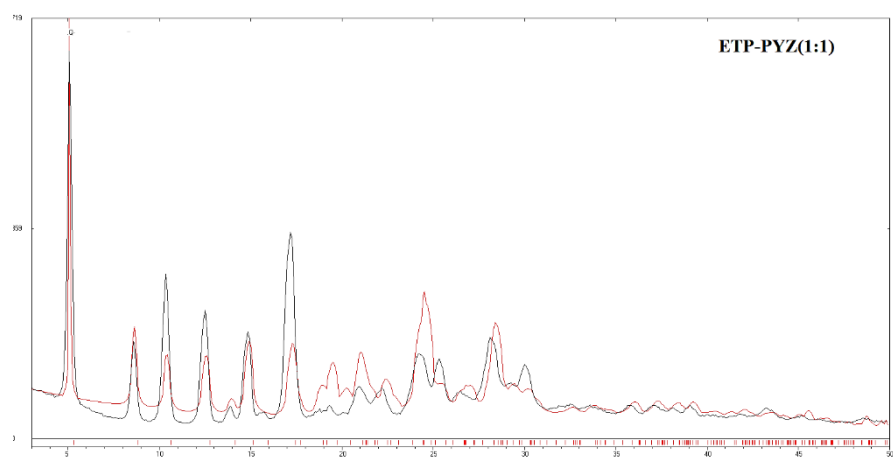


**Figure 2.13g:** PXRD of ETP-PYZ at the end of equilibrium solubility/phase stability experiment (24 h, black) in phosphate buffer (pH 7) media matches with the calculated XRD pattern of ETP-PYZ (red) indicating phase stability.

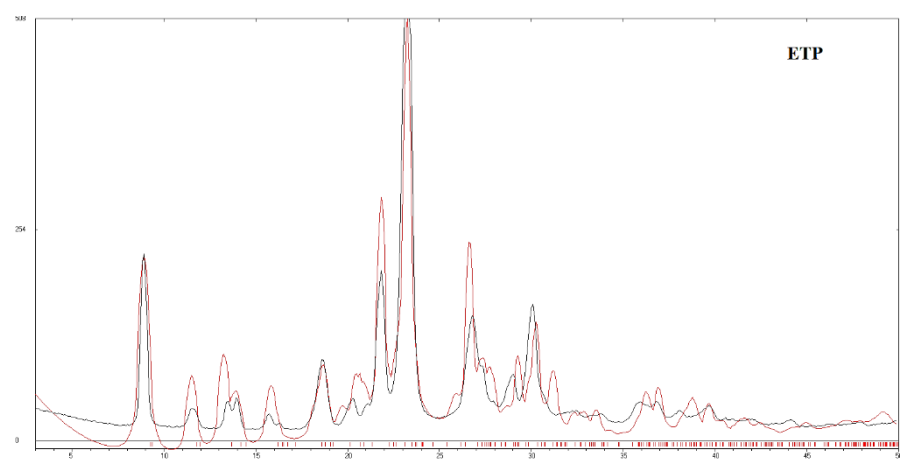


**Figure 2.14a:** PXRD of ETP at the end of dissolution experiment (4h, black) matches with the calculated XRD pattern of ETP (red) indicating phase stability.

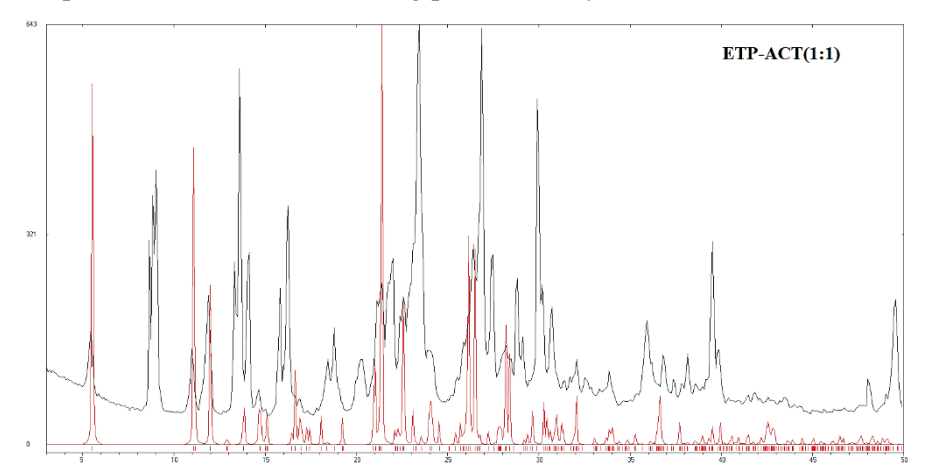


**Figure 2.14b:** PXRD of ETP-ACT at the end of dissolution experiment (4h, black) matches with the calculated XRD pattern of ETP-ACT (red) and pure ETP peaks were also present indicating mixture of cocrystal and dissociated physical mixture.

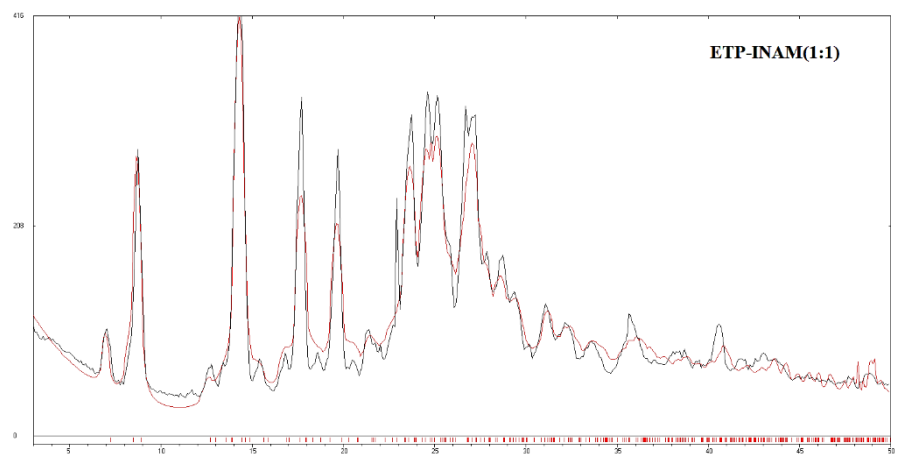


**Figure 2.14c:** PXRD of ETP-INAM at the end of dissolution experiment (4h, black) matches with the calculated XRD pattern of ETP-INAM (red) indicating phase stability.

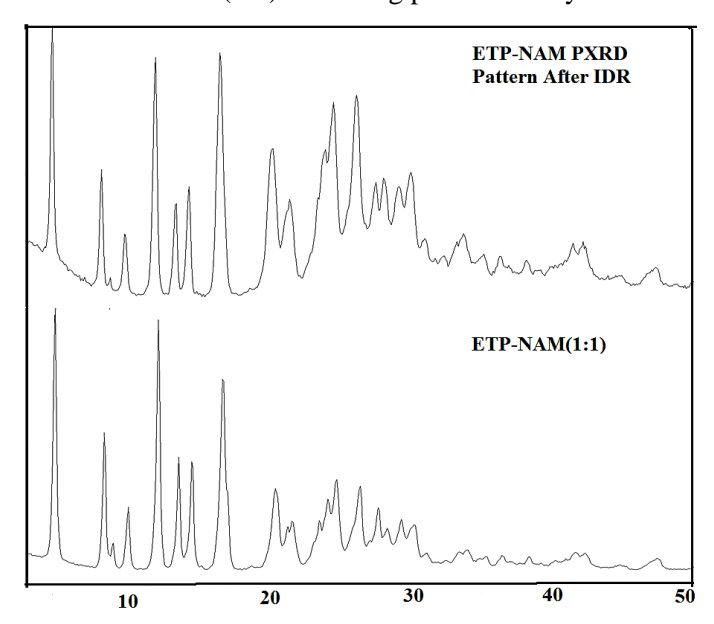


**Figure 2.14d:** PXRD of ETP-NAM at the end of dissolution experiment (4 h, black) matches with the experimental XRD pattern of ETP-NAM indicating phase stability.

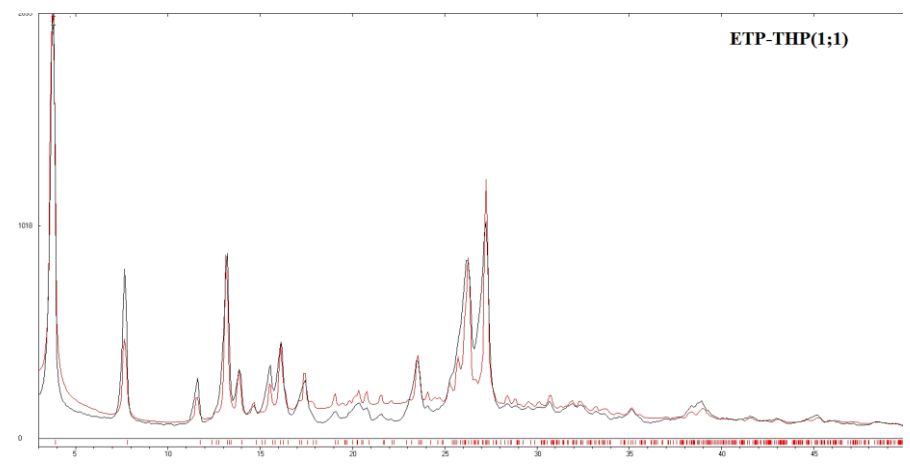


**Figure 2.14e:** PXRD of ETP-THP-HYD at the end of dissolution experiment (4h, black) matches with the calculated XRD pattern of ETP-THP-HYD (red) indicating phase stability.

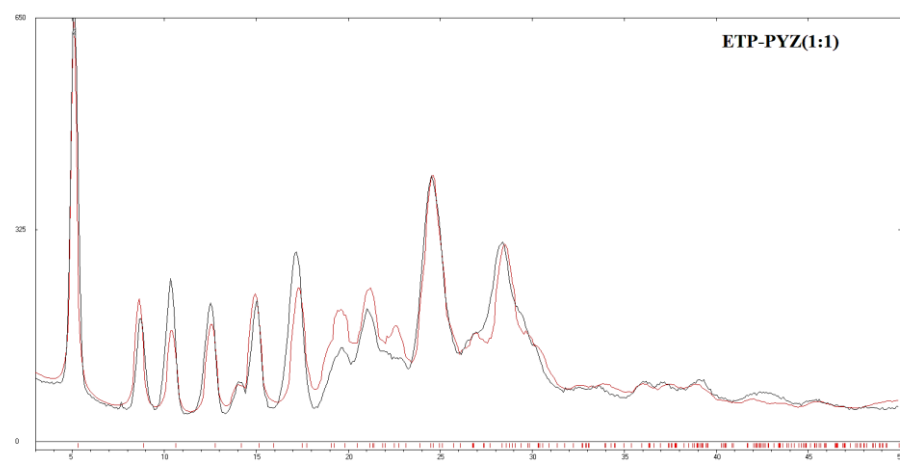


**Figure 2.14f:** PXRD of ETP-PYZ at the end of dissolution experiment (4h, black) matches with the calculated XRD pattern of ETP-PYZ (red) indicating phase stability.

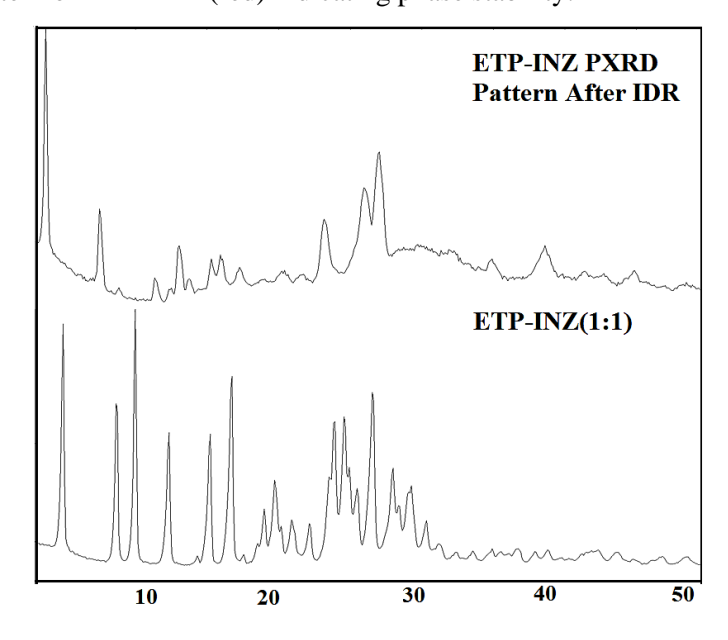


**Figure 2.14g:** PXRD of ETP-INZ at the end of dissolution experiment (4 h, black) matches with the experimental XRD pattern of ETP-INZ indicating phase stability.

# 2.8 Diffusion and Permeability Flux

Drug absorption is defined as the process of movement of the drug from the site of administration (oral) to systematic circulation. This is mainly influenced by solubility, stability, bioavailability, and membrane permeability. The last of these parameters is measured for the cocrystals and compared with their dissolution rate and cocrystal stability. The permeation of cocrystals was measured by in vitro diffusion using a Franz diffusion cell which gives an idea of permeation property. 42, 43 Any molecule either API or coformer will have a lag time which expresses the rate of permeation through the membrane and diffusion into the receptor medium, which is reflected by a sharp peak and then drop to a steady state profile. Subsequently, there is a near constant movement of permeation across the membrane. The diffusion of cocrystals and ETP was measured in phosphate buffer medium over 4 h. No substantial pH changes were observed in the receptor compartment during the experiment. The two plots are drawn with cumulative drug diffused vs. time (Figure 2.15) and flux of the drug vs. time it is calculated by the formula j=Q/(A\*t) where 'Q' is the quantity of the compound traversing the membrane in time 't' and 'A' is the area of exposed membrane in cm<sup>2</sup>. (Figure 2.16). These plots show that the cocrystals exhibit higher diffusion rate than pure ETP. Specifically, ETP-THP-HYD exhibits the highest diffusion rate compared to all other cocrystals. This may be explained by the high solubility and high permeability of the coformer theophylline. The apparent permeability value of ETP  $1.58 \pm 0.01$  at pH 5.0 and 0.18 $\pm$ 0.02 at pH 7.4<sup>16</sup> theophylline 4.05  $\pm$  0.06<sup>44</sup>). Theophylline is BCS class I molecule of high solubility and high permeability. The high dissolution rate and solubility of ETP-PYZ cocrystal displayed lower diffusion rate compared to ETP-THP-HYD. This is because PYZ coformer is less permeable being a BCS class III molecule of high solubility and low permeability (PYZ log P-1.53<sup>43</sup>). The coformers with high permeability and high solubility can tune the stability of the cocrystal together with solubility, faster dissolution rate, and better diffusion permeability. These results indicate that cocrystals of ETP provide a platform to improve the physicochemical properties and of BCS class IV drugs.

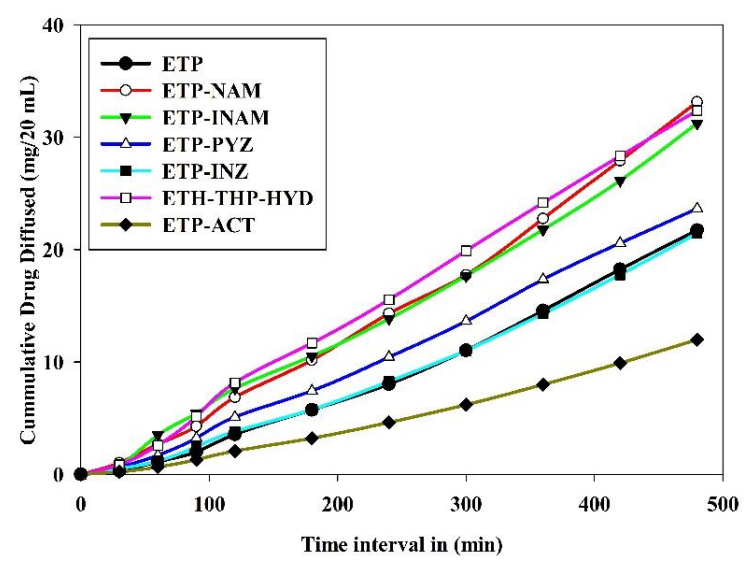


Figure 2.15: Cumulative amount of ETP cocrystal diffused vs. time.

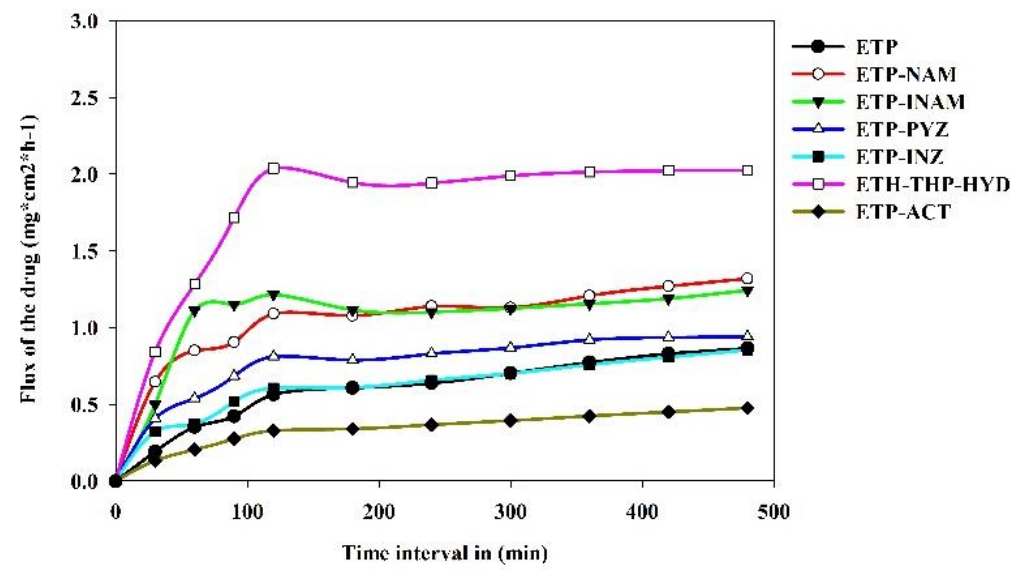


Figure 2.16: Flux of ETP and its cocrystal vs. time.

#### 2.9 Conclusions

Six pharmaceutical cocrystals of ETP in a 1:1 stoichiometry was crystallized and structurally characterized. ETP-THP-HYD and ETP-PYZ displayed enhanced solubility and dissolution rate together with good stability due to stronger hydrogen bonds and different ETP conformation changes in the crystal structure. Furthermore, ETP-THP-HYD cocrystal exhibits high diffusion and flux rate for possible BBB cross over. ETP-THP-HYD scores on high solubility, good stability and high permeability criteria. This case study presents a crystal engineering approach to solve solubility and permeability challenges in BCS class IV drugs.

#### 2.10 Experimental Section

Entacapone (purity >99.8%) was obtained as a gift sample from Hetero Drugs (Hyderabad, India) and coformers were purchased from Sigma-Aldrich (Hyderabad, India). All solvents (purity >99%) were purchased from Finar chemicals (Hyderabad, India).

# 2.10.1Preparation of cocrystals

**Entacapone–Acetamide (ETP–ACT):** The cocrystal was obtained by grinding ETP and ACT in 1:1 stoichiometry with a few drops of CH<sub>3</sub>CN added in a solvent-assisted method for 30 min. Single crystals were obtained by dissolving 40 mg of the ground product in 6 mL of iso-butanol and left for slow evaporation over 4-5 days.

**Entacapone–Isonicotinamide (ETP–INAM):** This cocrystal was obtained by grinding ETP and INAM in 1:1 stoichiometry with a few drops of CH<sub>3</sub>CN added in a solvent-assisted method for 30 min. Single crystals were obtained by dissolving40 mg of the ground product in 6 mL of methanol and left for slow evaporation over 4-5 days.

**Entacapone–Theophylline hydrate (ETP–THP-HYD):** The cocrystal was obtained by grinding ETP and THP in 1:1 stoichiometry with a few drops of CH<sub>3</sub>CN added in a solvent-assisted method for 30 min. Single crystals were obtained by dissolving 40 mg of the ground product in 6 mL of methanol and left for slow evaporation over 4-5 days.

**Entacapone–Pyrazinamide (ETP–PYZ):** The cocrystal was obtained by grinding ETP and PYZ in 1:1 stoichiometry with a few drops of water added in a solvent-assisted method for 30 min. Single crystals were obtained by dissolving 40 mg of the ground product in isobutanol-ethyl-methyl ketone (1:1 v/v, 6 mL) solvent mixture and left for slow evaporation over 4-5 days.

**Entacapone–Nicotinamide** (**ETP–NAM**): The cocrystal was obtained by grinding ETP and NAM in 1:1 stoichiometry with a few drops of CH<sub>3</sub>CN added in a solvent-assisted method for 30 min. The formation of cocrystal was confirmed by PXRD, DSC, FT-IR, and NMR. Diffraction quality single crystals could not be harvested.

**Entacapone–Isoniazid (ETP–INZ):** The cocrystal was obtained by grinding ETP and INZ in 1:1 stoichiometry with a few drops of CH<sub>3</sub>CN added in a solvent-assisted method for 30 min. The formation of cocrystal was confirmed by PXRD, DSC, FT-IR, and NMR. Diffraction quality single crystals could not be harvested.

# 2.10.2 X-ray crystallography

X-ray reflections were collected on Bruker D8 QUEST, CCD diffractometer equipped with a graphite monochromator and Mo-K $\alpha$  fine-focus sealed tube ( $\lambda$  = 0.71073 Å) and reduction was performed using APEXII Software. Intensities were corrected for absorption using SADABS and the structure was solved and refined using SHELX97. All non-hydrogen atoms were refined anisotropically. Hydrogen atoms on hetero atoms were located from difference electron-density maps and all C–H hydrogen atoms were fixed geometrically. Hydrogen-bond geometries were determined in PLATON. All Crystal

parameters (Table 1) and hydrogen bond distances shown in Table 3 are neutron normalized to fix the D–H distance to its accurate neutron value in the X-ray crystal structures (O–H 0.983 Å, N–H 1.009 Å, and C–H 1.083 Å). X-Seed was used to prepare packing diagrams.<sup>50,51</sup> Crystallographic cif files are available at <a href="https://www.ccdc.cam.ac.uk/data">www.ccdc.cam.ac.uk/data</a> or as part of the Supporting Information (CCDC Nos. 1848761-1848764).

#### 2.10.3 Powder X-ray diffraction

Powder X-ray diffraction was recorded on Bruker D8 Advance diffractometer (Bruker-AXS, Karlsruhe, Germany) using Cu-K $\alpha$  X-radiation ( $\lambda$  = 1.5406 Å) at 40 kV and 30 mA power. X-ray diffraction patterns were collected over the 2 $\theta$  range 3–50° at a scan rate of 3.9°/min. Powder Cell 2.4<sup>45</sup> (Federal Institute of Materials Research and Testing, Berlin, Germany) was used for Rietveld refinement of experimental PXRD and calculated lines from the X-ray crystal structure. The Rp and Rwp values of cocrystals shown here ETP-INAM (Rp=19.96 Rwp=29.34), ETP-PYZ (Rp=14.50 Rwp=20.27) ETP-THP-HYD (Rp=23.50 Rwp=30.50) ETP-ACT (Rp=29.97 Rwp=40.18).

#### 2.10.4 Vibrational spectroscopy

Thermo-Nicolet 6700 FT-IR-NIR spectrometer with NXR FT-Raman module (Thermo Scientific, Waltham, MA) was used to record IR spectra. IR spectra were recorded on samples dispersed in KBr pellets. Data were analyzed using the Omnic software (Thermo Scientific, Waltham, MA).

#### 2.10.5 Thermal analysis

DSC was performed on a Mettler Toledo DSC 822e module and TGA on a Mettler Toledo TGA/SDTA 851e module. The typical sample size is 3-5 mg for DSC and 5-12 mg for TGA. Samples were placed in sealed pin-pricked aluminum pans for DSC experiments and alumina pans for TGA experiments. A heating rate of 10 °C min<sup>-1</sup> in the temperature range 30-300 °C was applied. Samples were purged by a stream of dry nitrogen flowing at 80 mL min<sup>-1</sup> for DSC and 50 mL min<sup>-1</sup> for TGA.

#### 2.10.6 Solubility and dissolution measurements

The solubility of ETP and its cocrystals was measured using the Higuchi and Connor method<sup>52</sup> in (phosphate buffer (pH 7) media at 37 °C. First, the absorbance of a known concentration of the ETP and its salts was measured at the given  $\lambda_{max}$  (ETP 376 nm) in purified pH 7 phosphate buffer medium on Thermo Scientific Evolution 300 UV-vis spectrometer (Thermo Scientific, Waltham, MA) respectively. These absorbance values were plotted against several known concentrations to prepare the concentration vs. intensity calibration curve. From the slope of the calibration curves, molar extinction coefficients for PEF and its salts were calculated. Intrinsic dissolution rate (IDR) of ETP and cocrystals were carried out on a USP certified Electro lab TDT-08L Dissolution Tester (Electro lab, Mumbai, MH, India). In intrinsic attachment unit 400 mg sample (PEF/salts) is compressed between the smooth surfaces under a pressure of 2.5 ton/inch<sup>2</sup> for 4 min in an area of 0.5 cm<sup>2</sup>. Then the pellets were dipped

into 500mL of pH7.0 phosphate buffer medium at 37 °C with rotating paddle of 100 rpm. A 5mL of dissolution medium was collected at an interval of 10, 20, 30, 40, 50, 60, 90, 120, 150, 180, 210, 240 min by replacing each with same amount of fresh pH 7.0 phosphate buffer. The absorbance is plotted against time for samples collected at regular intervals for ETP and cocrystals was calculated. An excess amount of the sample (ETP/cocrystals) was added to 3 mL of purified pH 7 phosphate buffer medium and pH 1.2 HCl medium. The supersaturated solution was stirred at 800 rpm using a magnetic stirrer at 30 °C. After 24 h, the suspension was filtered through Whatmann 0.45µm syringe filter. Then equilibrium solubility is calculated as per procedure and remaining residues of ETP and its cocrystals were characterized by PXRD.

#### 2.10.7 Diffusion study

The diffusion studies were conducted using a diffusion apparatus (Model EMFDC-06, Orchid Scientific, Maharashtra, India). ETP and its cocrystals was carried out through a dialysis membrane-135 (dialysis membrane-135, average flat width 33.12 mm, average diameter 23.8 mm, capacity approx. 4.45 mL/cm) obtained from HiMedia, India. The dialysis membrane was pre-treated with 2% NaHCO<sub>3</sub> at 80 °C for 30 min to remove traces of sulphides, followed by 10 mM of EDTA at 80 °C for 30 min to remove traces of heavy metal and another 30 min of treatment with deionized water at 80 °C to remove glycerin. The treated dialysis membrane was then mounted in clips and placed in diffusion cells with an effective surface area of 3.14 cm<sup>2</sup>. Suspensions of the drug ETP and its cocrystal materials were prepared and placed on the dialysis membrane in donor compartment. The temperature of diffusion medium was thermostatically maintained at 37 °C  $\pm$  1°C throughout the experiment. The drug and/or cocrystal solution was then allowed to stir at 600 rpm and diffuse through the membrane towards the receptor compartment containing 20 mL of phosphate-buffered solution (PBS, pH = 7). The release of the compounds at predetermined intervals (30, 45, 60, 90, 120, 150,180, 210 and 240 min) were withdrawn (0.5 mL for each interval) and replaced by equal volume. The samples collected from receptor compartment through the dialysis tube was analyzed by UV-Vis spectrophotometer (JASCO Spectrophotometer V-730) at  $\lambda_{max}$  of 376 nm.

#### 2.11 References

- 1. <u>Sveinbjornsdottir, S.</u>: The clinical symptoms of Parkinson's disease. <u>J. Neurochem.</u> **2016**, *139*, 318–324.
- 2. Samii, A.; Nutt, J.G.; Ransom, B.R.; Parkinson's disease. *The Lancet.* **2004**, *363*, 1783–1793
- 3. Factor S.A.; Weiner W.J.; Parkinson's disease: *Diagnosis & Clinical Management, Second Edition* (Google eBook). Demos Medical Publishing, New York, **2008**.
- 4. Hiroshima, Y.; Miyamoto, H.; Nakamura F.; Masukawa D.; Yamamoto, T.; Muraoka, H.; Yamashita, N.; Suzuki, T.; Matsuzaki, S.; Endo, I.; Goshima, Y. The protein Ocular albinism1 is

- the orphan GPCR GPR143 and mediate depressor and bradycardic responses to DOPA in the nucleus tractus solitarii. *Br. J. Pharmcol.* **2014**, *171*, 403–414.
- 5. Lopez, V.M.; Decatur, C.L.; Stamer, W.D.; Lynch, R.M; McKay, B.S. L-DOPA Is an Endogenous Ligand for OA1. *PLoS Biol.* **2008**, *6*: e236, 1861–1869.
- 6. Männistö P.; Kaakkola S. Rationale for selective COMT inhibitor as adjuncts in the drug treatment of Parkinson's disease. *Pharmacol. Toxicol.* **1990**, *66*, 317–323.
- 7. Hamilton, R.J. *Tarascon Pharmacopoeia* (14 Eds.).Jones& Bartlett Learning, Burlington, MA, **2013**.
- 8. WHO Model List of Essential Medicines (19th List). *World Health Organization*. April **2015**. http://www.who.int/medicines/publications/essentialmedicines/en/ (accessed 29 May 2018).
- 9. Drug Reference for FDA Approved Parkinson's Disease Drugs Retrieved 2010-4-1.
- 10. Gilbert, J.A.; Frederick, L.M.; Ames, M.M.; The aromatic-L-amino acid decarboxylase inhibitor carbidopa is selectively cytotoxic to human pulmonary carcinoid and small cell lung carcinoma cells. *Clin. Canc. Res.* **2000**, *6*, 4365–4372.
- 11. Myllylä V.V.; Sotaniemi K.A.; Illi, A.; Suominen, K.; Keränen, T. Effect of entacapone, a COMT inhibitor, on the pharmacokinetics of levodopa and on cardiovascular responses in patients with Parkinson's disease. *Eur. J. Clin. Pharmacol.* **1993**, *45*, 419–423.
- 12. Nutt, J.G.; Woodward, W.R.; Beckner, R.M.; Stone C.K.; Berggren, K.; Carter, J.H.; Gancher, S.T.; Hammerstad, J.P.; Gordin, A. Effect of peripheral catochol-O-methyltransferase inhibition on the pharmacokinetics and pharmacodynamics of levodopa in Parkinsonian patients. *Neurology* **1994**, *44*, 913–919.
- 13. Stalevo® (entacapone/carbidopa/levodopa): Ongoing Safety Review Retrieved on 2010-4-2.
- 14. Anjan Kumar, M.; Murthy, P.N.; Sameeraja, N.H.; Narayan, P.N. Dissolution rate enhancement of entacapone and formulation of its oro-Dispersible tablets applying statistical design. Ind. *J. Pharma. Edu. Res.* **2016**, *50*, 549–562.
- 15. Savolainen, J.; Forsberg, M.; Taipale, H.; Männistö, P.T.; Järvinen, K.; Gynther, J.; Jarho, P.; Järvinen, T. Effects of Aqueous Solubility and Dissolution Characteristics on Oral Bioavailability of Entacapone. *Drug Dev. Res.* **2000**, *49*, 238–244.
- 16. Forsberg, M.M.; Huotari, M.; Savolainen, J.; Mannisto, P.T. The role of physicochemical properties of entacapone and tolcapone on their efficacy during local intrasriatal administration. *Eur. J Pharm. Sci.* **2005**, *24*, 503–511.
- 17. Vadlamudi, H.C.; Yalavarthi, P.R.; Venkata, B.R.M.; Thanniru, J.; Vandana, K.R.; Sundaresan, C.R. Potential of micro emulsified entacapone drug delivery systems in the management of acute Parkinson's disease. *J. Acute Disease* **2016**, *5*, 315–325.
- 18. CSD version 2017, Feb 2017 update. www.ccdc.cam.ac.uk
- 19. LeppaÈnena, J.; Wegeliusb, E.; Nevalainena, T.; JaÈrvinena, T.; Gynthera, J.; Huuskonen, J. Structural studies of acyl esters of Entacapone. *J. Mol. Struct.* **2001**, *562*, 129–135.

- 20. Jaweed, M.S.M.; Khan, R.A.R.; Yadav, R.P.; Shaikh, Z.G. Stable polymorphs of (E)-N,N-diethyl-2-cyano-3-(3,4-dihydroxy-5-nitrophenyl)acrylamide Patent application No. WO 2005/066117 A1.
- 21. Kwokal, A.; Nguyen, T.T.H.; Roberts, K.J. Polymorph-Directing Seeding of Entacapone Crystallization in Aqueous/Acetone Solution Using a Self-Assembled Molecular Layer on Au (100). *Cryst. Growth Des.* **2009**, *9*, 4324–4334.
- 22. Kwokal, A.; Roberts, K.J. Direction of the polymorphic form of entacapone using an electrochemical tuneable surface template. *CrystEngComm* **2014**, *16*, 3487–3493.
- 23. Desiraju, G.R.; Vittal, J.J.; Ramanan, A. *Crystal Engineering. A Textbook*, World Scientific Publishing, Singapore, **2011**.
- 24. S. Aitipamula et al. Polymorphs, Salts, and Cocrystals: What's in a Name? *Cryst. Growth Des.* **2012**, *12*, 2147–2152.
- 25. http://www.fda.gov/Food/IngredientsPackagingLabeling/GRAS/. (accessed 29 May 2018).
- 26. Bolla, G.; Nangia, A. Pharmaceutical cocrystals: walking the talk. *Chem. Commun.* **2016**, *52*, 8342–8360.
- 27. Suresh K.; Minkov V.S.; Namila, K.K.; Derevyannikova, E.; Losev, E.; Nangia, A.; Boldyreva, E.V. Novel Synthons in Sulfamethizole Cocrystals: Structure–property Relations and Solubility. *Cryst. Growth Des.* **2014**, *15*, 3498–3510.
- 28. Suresh K.; Mannava M.K.C.; Nangia A. Cocrystals and Alloys of Nitazoxanide: Enhanced Pharmacokinetics. *Chem. Commun.* **2016**, *52*, 4223–4226.
- 29. Gopi, S.P.; Ganguly, S.; Desiraju, G.R. A Drug–Drug Salt Hydrate of Norfloxacin and Sulfathiazole: Enhancement of in Vitro Biological Properties via Improved Physicochemical Properties. *Mol. Pharm.* **2016**, *13*, 3590–3594.
- 30. Suresh K.; Goud, N.R.; Nangia, A. Andrographolide: Solving Chemical Instability and Poor Solubility by Means of Cocrystals. *Chemistry—An Asian J.* **2011**, *8*, 3032–3041.
- 31. Fala L.; Entresto (Sacubitril/Valsartan); First-in- Class Angiotensin Receptor Neprilysin Inhibitor FDA Approved For Patients with Heart Failure. Am Health Drug Benefits. 2015, 8(6), 330-334.
- 32. Bernhardson D.; Brandt T. A.; Hulford C A.; Lehner R. S.; Preston B. R.; Price K Sagal J.F.; St. Pierre. M. J.; Thompson P. H.; Thuma B.; Development of an Early- Phase Bulk Enabling Route to sodium- Dependent Glucose Cotransporter 2 Inhibitor Ertugliflozin. *Org. Process Res. Dev* 2014, 18, 1, 57-65.
- 33. Desiraju, G. R. Angew. Chem., Int. Ed. Engl. 1995, 34, 2311–2327.
- 34. Desiraju, G.R.; Steiner, T. *The Weak Hydrogen Bond in Structural Chemistry and Biology*, IUCr Monographs in Crystallography, **1999**.
- 35. Cherukuvada, S.; Babu, N.J.; Nangia A. Nitrofurantoin–p-aminobenzoic acid cocrystal: Hydration stability and dissolution rate studies. *J. Pharm. Sci.* **2011**, *100*, 3233–3244.
- 36. Savjani K.T.; Gajjar A.K.; Savjani J.K. Drug Solubility: Importance and Enhancement Techniques. *ISRN Pharmaceutics.* **2012**, 1-10. doi:10.5402/2012/195727.

- 37. Silverstein, R. M. *Spectrometric Identification of Organic Compounds*, 6<sup>th</sup> Ed., John Wiley, New York, **2002**.
- 38. Etter, M. C.; MacDonald, J. C.; Bernstein, J.; Graph-set analysis of hydrogen-bond patterns in organic crystals. *Acta Cryst.* B 1990, 46, 2, 256-262.
- 39. Kraus, W.; Nolze, G. Powder cell– a program for the representation and manipulation of crystal structures and calculation of the resulting X-ray powder patterns.(1996). J. Appl. Cryst. 29, 301–303.
- 40. Sanphui, P.; Devi K.; Clara D.; Malviya N.; Ganguly S.; Desiraju G.R. Cocrystals of Hydrochlorothiazide: Solubility and Diffusion/Permeability Enhancements through Drug–Coformer Interactions. *Mol. Pharmaceutics* **2015**, *12*, 1615–1622.
- 41. Jagadeesh Babu N.; Sreenivas Reddy L.; Nangia A Amide- N-Oxide Heterosynthon and Amide Dimer Homosynthon in Cocrystals of Carboxamide Drugs and Pyridine N-Oxides. 2007. 4(3), *Molecular Pharmaceutics* 417-434.
- 42. Saikia, B.; Bora, P.; Khatioda, R.; SarmaB. Hydrogen Bond Synthons in the Interplay of Solubility and Membrane Permeability/Diffusion in Variable Stoichiometry Drug Cocrystals. *Cryst. Growth Des.* **2015**, *15*, 5593–5603.
- 43. Kinnings S L.; Liu N.;Buchmeier N.;Tonge P J.; Xie L.; Bourne P E.; Drug Discovery Using Chemical Systems Biology Repositioning the Safe Medicine Comtan to Treat Multi-Drug and Extensively Drug Resistant Tuberculosis. *PloS Computat. Biol.* **2009**, *5*, e1000423.
- 44. Corti G.; Maestrelli F.; Cirri M.; Zerrouk N.; Mura P.; Development and evaluation of an in vitro method for prediction of human drug absorption II. Demonstration of the method suitability. *Eur. J. Pharm. Sci.* **2006**, *27*, 354-362.
- 45. Powder Cell, A program for structure visualization, powder pattern calculation and profile fitting. www.ccp14.ac.uk/tutorial/powdercell. (accessed 29 May 2018).
- 46. Bruker SMART, Version 5.625, SHELXTL, Version 6.12. Bruker AXS Inc., Madison, Wisconsin, USA. **2000**.
- 47. Sheldrick, G. M. *Program for Refinement of Crystal Structures*, University of Göttingen, Germany, **1997**.
- 48. Sheldrick, G. M. A short history of SHELX. Acta Crystallogr., Sect. A. 2008, 64, 112–122.
- 49. Sheldrick, G. M.Crystal structure refinement with SHELXL. *Acta Cryst., Sect. C: Struct. Chem.* **2015**, *71*, 3–8.
- 50. Barbour, L.J. Supramol. Chem., 2001, 1, 189–191.
- 51. Barbour, L.J. *X-Seed, Graphical Interface to SHELX-97 and POV-Ray;* University of Missouri-Columbia, Columbus, MO, **1999**.
- 52. Higuchi, T.; Connors, K.A. Phase Solubility Techniques, Advanced Analytical Chemistry of Instrumentation. *Adv. Anal. Chem. Instrum.* **1965**, *4*, 117–212.

# **CHAPTER THREE**

# Entacapone Polymorphs: Crystal Structures, Dissolution, Permeability and Stability



Entacapone (ETP) is a catechol-O-methyltransferase (COMT) drug used to treat Parkinson's disease. ETP is available in the marketplace under the brand name Comtan since 2010, and ETP form-I was first reported in a patent published in 2001. However, analysis of its X-ray crystal structures and stability relationship of ETP polymorphs and their dissolution and permeability profile have not yet been reported. We crystallized two new conformational polymorphs of ETP from a water and acetone mixture and studied the structural origin of polymorphism and their phase transformations, stability, equilibrium solubility, dissolution, and permeability properties. The ETP molecule adopts different conformations in the polymorphic structures with slight changes in carbonyl and nitrile group orientations. Thermal analysis suggests that form-III and form-IV are enantiotropically related to form-I, which is the thermodynamically stable form at ambient conditions. In contrast, form-II is monotropically related to form-I. Equilibrium solubility, dissolution, and permeability studies show that form-II persists in the slurry medium and dissolves faster with a high flux rate compared to the stable form-I in phosphate buffer solution at  $37 \pm 0.5$  °C.

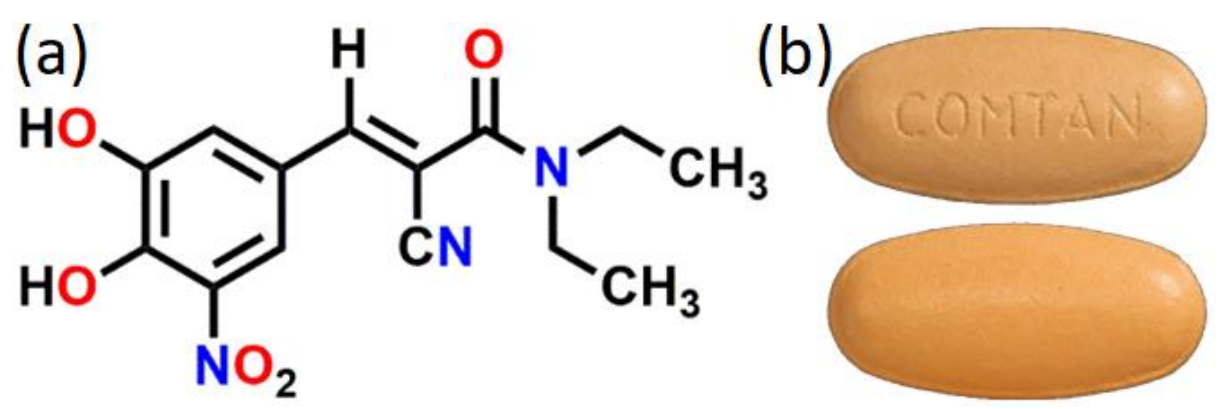
#### 3.1 Introduction

Entacapone (brand name Comtan®) has a nitro catechol structure (Scheme 3.1) and exhibits potent, selective inhibition of catechol-O-methyltransferase (COMT) enzyme. The drug is administered orally for the treatment of Parkinson's disease to reduce the so-called 'wearing off' effect, <sup>1,2</sup> or the loss in the effectiveness of levodopa until the next dose is given. The recommended dose of entacapone 200 mg is co-administered with levodopa (50-200 mg) and/or carbidopa (10-50 mg). The maximum daily recommended dose of entacapone is 2000 mg/day³. Currently, a fixed dose combination of levodopa, carbidopa and entacapone is marketed by Novartis (brand name: Stalevo®)⁴. However, due to low solubility of ETP 0.08 mg/mL (80  $\mu$ g/mL)⁵ and apparent permeability log P<sub>app</sub> of 0.18±0.02 cm/s, ⁶ the drug is practically insoluble in water and categorized under Biopharmaceutics Classification System (BCS) class IV.⁵ The wide use of entacapone tablets, either in single dose or as combination therapy, makes it important to have a detailed understanding of the different crystalline forms (polymorphs) of entacapone.

Modifications in the solid-state and conversion from one polymorph to another occur due to deliberate change in conditions or unintentional incidents during drug development. The ability of polymorphs to exist in different hydrogen bonding, crystal packing and/or in molecular conformations, significantly changes the thermodynamic and physicochemical properties of drugs, such as color, density, dissolution rate, solubility, melting point, flowability, hygroscopicity and compaction. The solubility and dissolution rate of polymorphs are influenced by hydrogen bonding, crystal packing, lattice energy, and interplay of solute-solute (crystal structure) vs. solute-solvent (solvation) interactions. Cenerally, the more soluble metastable polymorph recrystallizes to the less soluble and thermodynamically stable form as the system reaches equilibrium stability. Thus, selection of the thermodynamically stable polymorph is preferred in drug formulation to avoid polymorphic changes during process development, storage and marketing. For poorly soluble drugs, a metastable form of higher solubility could offer improved bioavailability. The stability of the polymorph is preferred in drug formulation to avoid polymorphic changes during process development, storage and marketing. For poorly soluble drugs, a metastable form of higher solubility could offer improved bioavailability.

Six polymorphs of entacapone (ETP) have been characterized and reported (forms A, D,  $\alpha$ ,  $\beta$ ,  $\gamma$  and  $\delta$ ). The Among these, form A is the only polymorph characterized by single crystal X-ray diffraction (CCDC Refcode OFAZUQ) and is the thermodynamically stable polymorph. Since ETP molecule has sufficient flexibility with 6 rotatable single bonds and several hydrogen bond synthons are possible for the amide, nitro, nitrile and hydroxyl groups, there is ample scope for conformational and/or synthon polymorphs with different molecular packing arrangements. From a pharmaceutical point of view, the determination of X-ray crystal structure (or high-resolution powder X-ray diffraction data) is important and necessary to fully understand physicochemical behavior of the drug such as solubility, dissolution rate and form stability. The presence of minute amounts of a second polymorph can complicate analysis of structure-property correlation, and so quantitative determination of the bulk solid using powder X-ray diffraction (PXRD) is mandatory. Comparison of the

experimental PXRD with the calculated XRD lines from the crystal structure gives a reliable fingerprint overlay match to infer the presence of other polymorphs.<sup>24-27</sup> In the present work, ETP was found to crystallize in a broad range of solvents and the structures were solved by single crystal X-ray diffraction (SC-XRD). Further, quantitative intermolecular interactions using Hirshfeld surface analysis of the crystal structures was analyzed and the solubility, dissolution and stability of the characterized polymorphs was determined in this study.



**Scheme 3.1:** (a) Chemical structure of the E-configuration of 2-cyano-3-(3,4-dihydroxy-5-nitrophenyl)-N,N-diethyl-2-propenamide (ETP); and (b) a typical 200 mg marketed Comtan® tablet with an oval shape of 17 mm x 6 mm size. https://www.drugs.com/imprints/comtan-1339.html.

#### 3.2 Results and Discussion

The ETP molecule has three hydrogen bond acceptors (C=O of amide, N=O of nitro and C=N of cyano group) and two donors (O-H of phenol) which can form strong hydrogen bonds in the crystal structure. There is also the possibility of weak C-H···O interactions from aromatic C-H donors to O acceptors. The hydrogen bond synthons and their graph set analysis are shown in Figure 3.1 to anticipate possible hydrogen bond patterns in the crystal structures. Due to intramolecular O-H···O hydrogen bonding motifs S(6) and S(5) (Figure 3.1, a-d), the second hydroxyl group can form intermolecular hydrogen bond motif D with carbonyl or nitrile group as shown in Figure 3.1, e-h and combinations of these D motifs can produce binary graph sets C/R. Ring motifs are expected with sp<sup>2</sup>-C-H hydrogen bonds. Figure 3.1i shows a centrosymmetric  $R_2^2(10)$  unitary graph set formed by aromatic hydrogen and carbonyl oxygen atom. Similarly, aromatic hydrogen atom forms a centrosymmetric  $R_2^2(10)$  graph set with oxygen of the nitro group (Figure 3.1j).

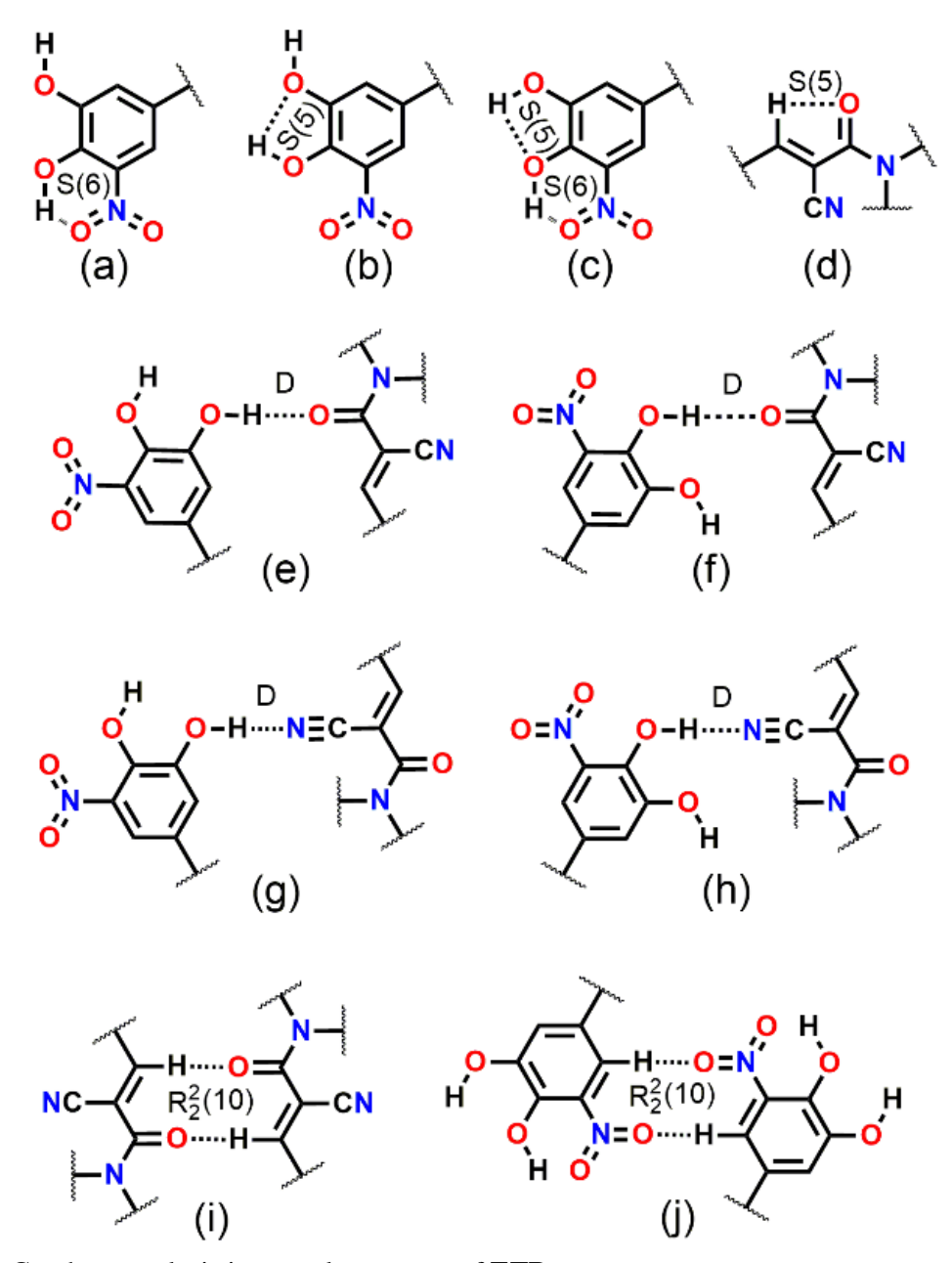


Figure 3.1: Graph set analysis in crystal structures of ETP.

#### 3.3 Crystal structure analysis

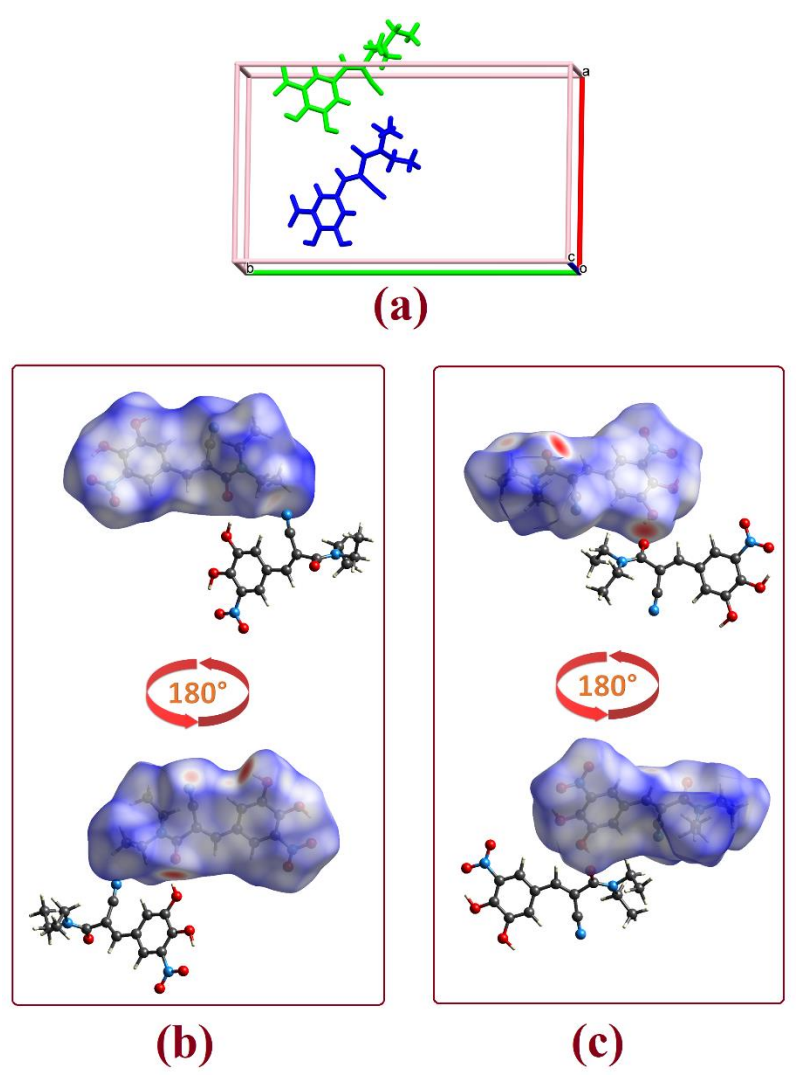
The only reported X-ray crystal structure of ETP (ref code: OFAZUQ)<sup>15</sup> is form-A. We refer to this known crystal structure as form-I and two new crystal structures reported in this paper as form-II and form-III, based on the chronology of results in our lab. The reported form-I was recrystallized in triclinic space group *P*-1 with cell parameters similar to that reported.<sup>15</sup> Novel form-II and III were crystallized in orthorhombic crystal system with space group *Pna2*<sub>1</sub> and *Pbca*, respectively (Table 3.1). The room temperature crystal data (296 K, RT) is discussed for all three polymorphs in this paper. The low temperature (100 K, LT) X-ray crystal structure of the known from-I determined by us is also included for comparison.<sup>15</sup> The RT structure of known form-I showed a slight disorder in terms of two

orientations of the NO<sub>2</sub> group which was cleanly resolved in the LT structure (details may be viewed in the .cif files). Whereas form-I and III have one ETP molecule in the asymmetric unit cell (Z'=1) form-II has two symmetry independent molecules (Z'=2) (Figure 3.2). A comparison of cell parameters and cell volume shows that form-II has slightly larger volume and lower density than form-III; the unit cell dimensions of the two cells are very different. Figure 3.3a shows the atom numbering and dihedral angles ( $\Phi 1 = O1\text{-}C9\text{-}C8\text{-}C14$ ,  $\Phi 2 = C9\text{-}N1\text{-}C10\text{-}C11$  and  $\Phi 3 = C9\text{-}N1\text{-}C12\text{-}C13$ ) through which variation in molecular conformation is observed. Comparison of molecular conformation by overlaying the molecules (Figure 3.3b) clearly shows that form-I ( $\Phi 1 = 130.145(11)^\circ$ ,  $\Phi 2 = 120.84(13)^\circ$ ,  $\Phi 3 = 83.94(13)^\circ$ ,) has a different molecular conformation than form-II (molecule 1:  $\Phi 1 = 133.8(6)^\circ$ ,  $\Phi 2 = 125.6(6)^\circ$ ,  $\Phi 3 = 83.4(7)^\circ$ ; molecule 2:  $\Phi 1' = 94.2(7)^\circ$ ,  $\Phi 2' = 103.3(6)^\circ$ ,  $\Phi 3' = 82.8(6)^\circ$ ), and form-III ( $\Phi 1 = 94.2(3)^\circ$ ,  $\Phi 2 = 99.9(3)^\circ$ ,  $\Phi 3 = 94.1(3)^\circ$ ). Orthorhombic structures form-II and form-III do not show significant variation in the conformation but it appears to be local conformation adjustments. The overlay of two molecules of form-II shows slight deviation in the carbonyl and nitrile groups positions; however, one of the ethyl side chain methyl groups is flipped by 180° through  $\Phi 2$  (Figure 3.3b).

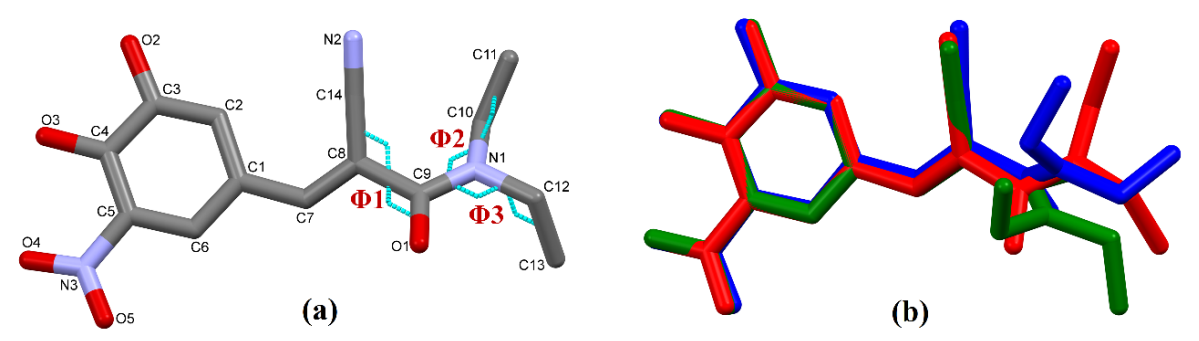
Since molecular conformations play an important role in crystal packing and the inter -and intramolecular interactions in the crystal structure, quantitative intermolecular interactions analysis was performed in Mercury, a crystal structure visualization software bundled with the CCDC software, and by Hirshfeld surface analysis in Crystal Explorer. Figure 3.4 shows the molecular packing along the a-axis and intra/ inter molecular interactions in three ETP polymorphs. Form-I contains the five-membered S(5) motif of O3–H2···O2 interaction. The molecules are oriented in a 1D linear chain stabilized by O2–H1···O1, O3–H2···N2 and aromatic C3–H3···O1 interactions and 2D inter-chain of C12–H12···O4 interactions (Figure 3.4a, b and c, Table 3.2). The 1D linear chain of O2–H1···O1 in graph-set  $C_1^4$ (9) and O3–H2···N2 shows a dimeric construct of  $R_2^2$ (20) ring. A tetrameric second level  $C_4^4$ (22) chain is connected by O2–H1···O1 and O3–H2···N2 interactions (Table 3.2).

Form-II and III have intramolecular hydrogen bond between oxygen acceptor of nitro group and hydroxyl hydrogen donor at ortho position as S(6) motif (Figure 3.1c) of O3–H3···O4 hydrogen bonds, and motifs S(5) (Figure 3.1b) is absent in form-II and III. Form-I is somewhat surprising in that the 6-member intramolecular O–H···O hydrogen bond (Figure 3.1c) is absent (in both RT and LT structures). In fact, the nitro(O4)···(O3) hydroxy distance is significantly longer in the LT structure (2.5981(14) Å) than the RT structure (2.582(2) Å) due to repulsion. This is a major hydrogen bonding difference between the molecular conformations of form-I compared to novel forms-II and III. Since form-II has two symmetry independent molecules it is important to know whether both molecules form identical hydrogen bond patterns in the asymmetric unit or different hydrogen bonding patterns; whether they form identical hydrogen bond patterns or different synthons. Symmetry-independent molecules in form-II are connected via O7–H7···O1 hydrogen bond from hydroxyl donor to carbonyl group of another molecule, and O2–H2···O6 from second to first, which leads to a  $C_2^2(18)$  chains (Table

3.2). The other interactions which further stabilize the crystal structure of form-II are aromatic C2–H2A···O6, vinylic C21–H21···O7, aliphatic C12–H12A···N5 and C22–H26B···N2.  $\pi$ ··· $\pi$  stacking between the aryl rings in form-II is significant and shows two different Cg···Cg distances of 3.70 Å and 4.10 Å (Table 3.1). In case of form-III, the major intermolecular hydrogen bond which stabilizes the crystal structure is O2–H2···O1 and is extended in a linear chain as C(9) graph set (Table 3.2). Another weak intermolecular interaction in form-III is C6–H6···O3 between a aromatic hydrogen and carbonyl oxygen (Figure 3.4h).  $\pi$ ··· $\pi$  stacking between the aryl rings in form-III is stronger than in form-II, with Cg···Cg distances of 3.54 Å (Table 3.3).



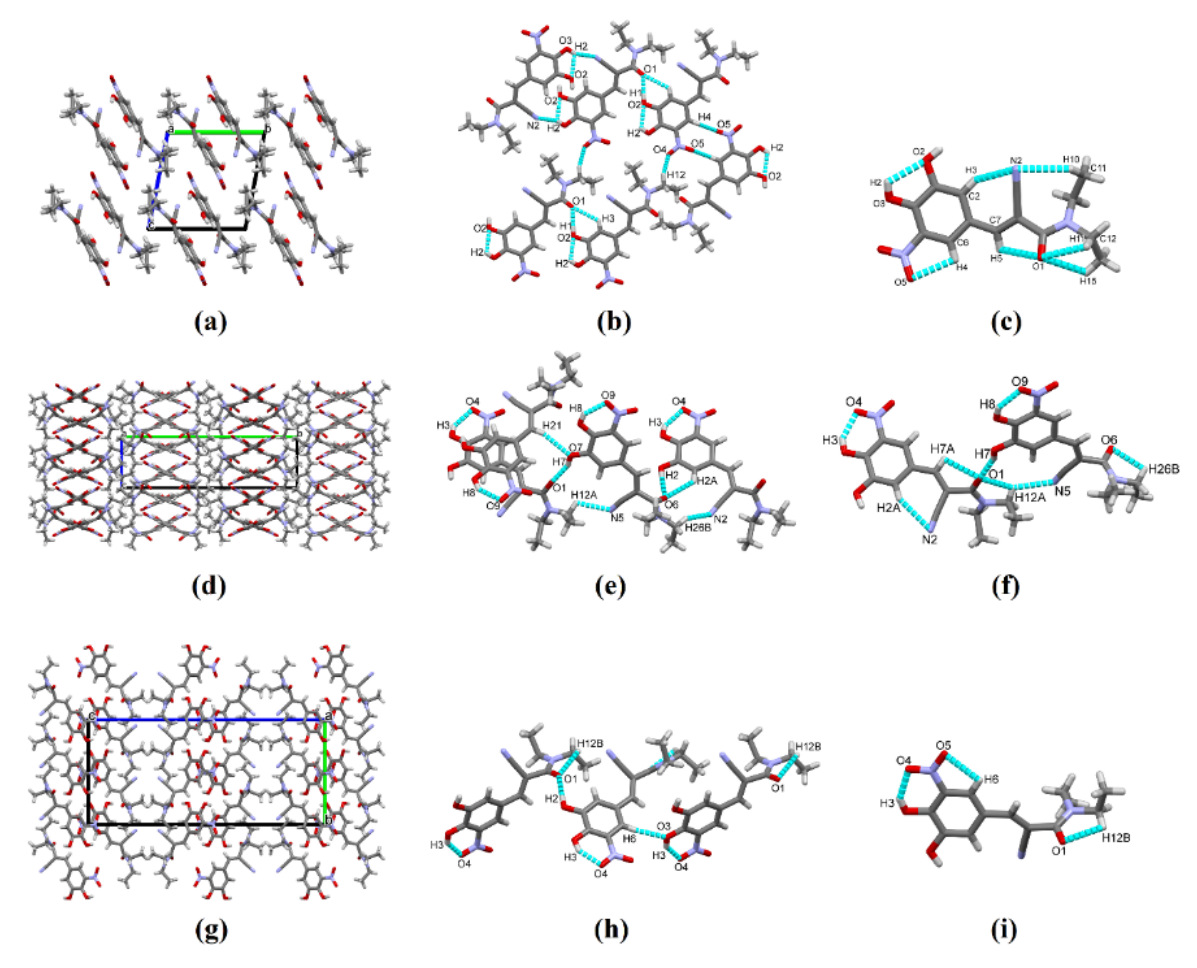
**Figure 3.2:** (a) Crystal structure of form-II with asymmetric unit cell, (b & c) represent the Hirshfild surfaces generated over  $d_{norm}$  for blue and green structures, respectively.



**Figure 3.3:** (a) Molecular structure of ETP with atom numbering and selected dihedral angles ( $\Phi$ 1,  $\Phi$ 2,  $\Phi$ 3), and (b) molecular overlay diagram of form-I (red), II (blue) and III (green). Hydrogen atoms are omitted for clarity.

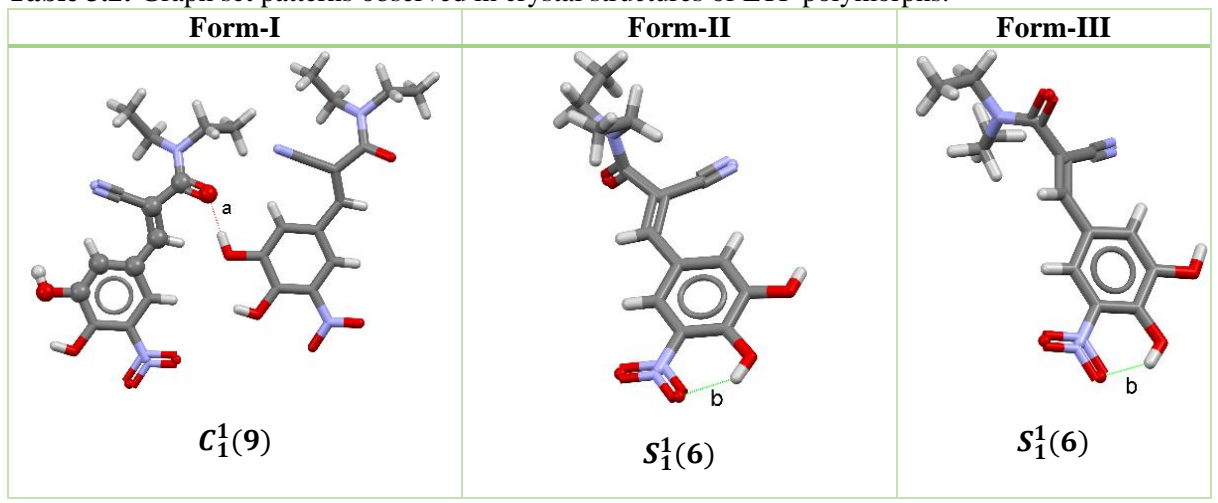
**Table 3.1:** Crystallographic parameters of ETP polymorphs form-I, form-II and form-III (all at 296 K, RT). Form-I data at 100 K (LT) is added to compare the molecular conformations at two temperatures.

Parameters	Form-I (RT)	Form-II (RT)	Form-III (RT)	Form-I (LT)
Emp. form.	$C_{14}H_{15}N_3O_5$	$C_{14}H_{15}N_3O_5$	$C_{14}H_{15}N_3O_5$	$C_{14}H_{15}N_3O_5$
Form. wt.	305.29	305.29	305.29	305.29
Cryst. system	triclinic	orthorhombic	orthorhombic	Triclinic
Space group	P-1	Pna2 <sub>1</sub> Pbca		P-1
T (K)	296(2)	295.8(4)	296(2)	100(2)
a (Å)	7.5772(12)	15.1908(8)	7.390(2)	7.5315(3)
<b>b</b> (Å)	9.8383(15)	25.6909(15)	13.170(3)	9.6146(4)
c (Å)	9.9324(16)	7.4942(5)	29.796(6)	9.9201(5)
α (deg)	99.915(5)	90	90	100.038(2)
β (deg)	95.402(5)	90	90	99.310(2)
γ (deg)	99.720(5)	90	90	95.873(2)
$\mathbf{V}(\mathring{\mathbf{A}}^3)$	713.1(2)	2924.7(3)	2900.0(12)	691.70(5)
Z	2	8	8	2
$\rho_{\rm calc}~({\rm g/cm^3})$	1.422	1.387	1.398	1.466
Reflns. collect	25785	12650	26715	49372
Independent reflections	$4373 [R_{int} = \\ 0.0219, R_{sigma} \\ = 0.0153]$	$4873 [R_{int} = \\ 0.0486, R_{sigma} = \\ 0.0991]$	$\begin{array}{c} 2385 \; [R_{int} = \\ 0.0892,  R_{sigma} = \\ 0.0458] \end{array}$	$2440 [R_{int} = \\ 0.0287, R_{sigma} \\ = 0.0090]$
Data/restraints/parameters	4373/0/248	4873/1/405	2385/0/203	2440/0/209
GOF on F <sup>2</sup>	1.081	0.900	1.130	1.458
Final R indexes [I>=2σ (I)]	$R_1 = 0.0445,$ $wR_2 = 0.1337$	$R_1 = 0.0538,$ $wR_2 = 0.0775$	$R_1 = 0.0604,$ $wR_2 = 0.1038$	$R_1 = 0.0363,$ $wR_2 = 0.1495$
Final R indexes [all data]	$R_1 = 0.0527,$ $wR_2 = 0.1454$	$R_1 = 0.1198,$ $wR_2 = 0.0983$	$R_1 = 0.1003,$ $wR_2 = 0.1141$	$R_1 = 0.0390,$ $wR_2 = 0.1547$
Large diff. peak/hole /e Å-3	0.39/-0.40	0.19/-0.14	0.17/-0.22	0.26/-0.31
CCDC No.	2095588	2074821	2074791	2074862



**Figure 3.4:** (a, d and g) Molecular packing along the a-axis and (b, c, e, f, h and i) selected hydrogen bond interactions in ETP form-I (Refcode: OFAZUQ), form-II and form-III.

**Table 3.2:** Graph set patterns observed in crystal structures of ETP polymorphs.



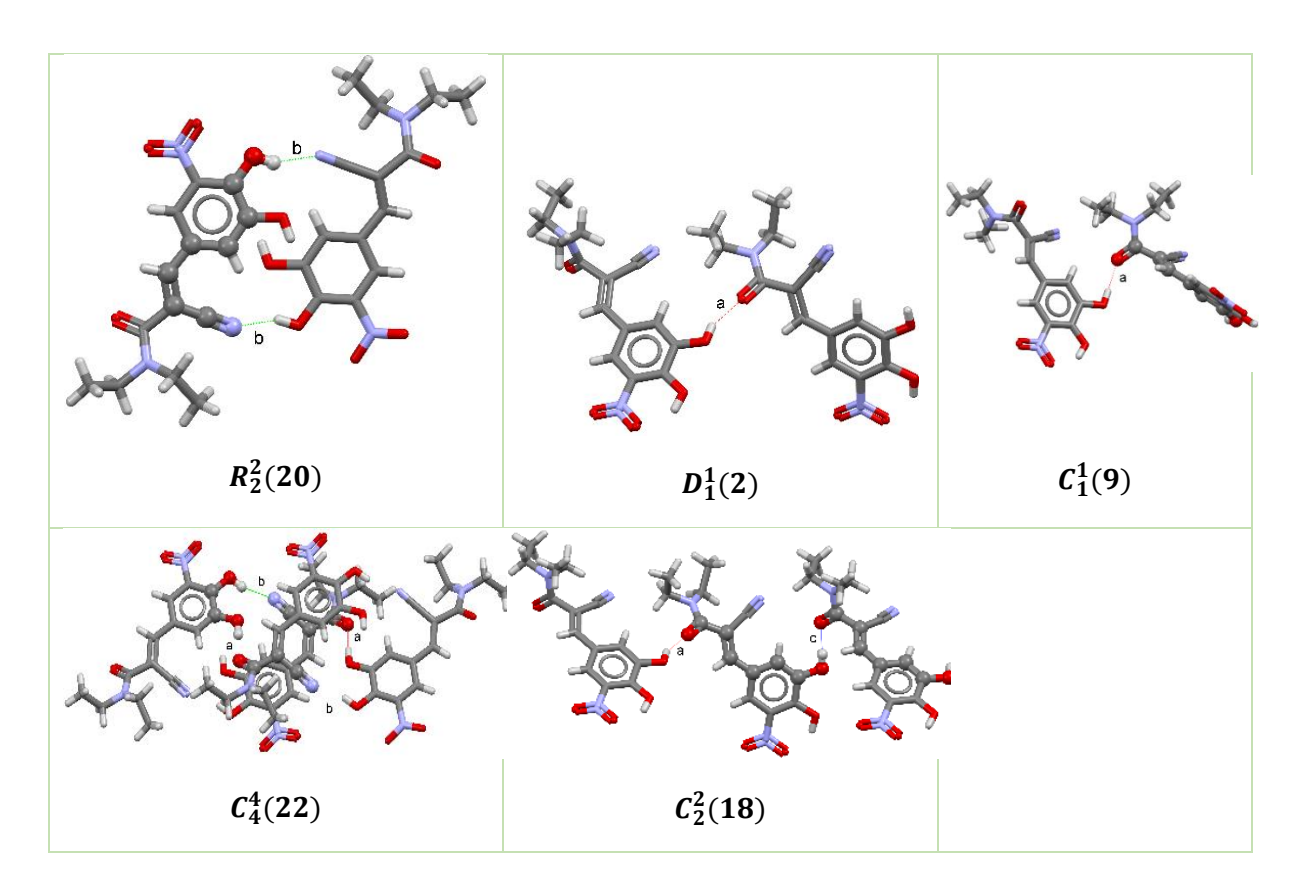


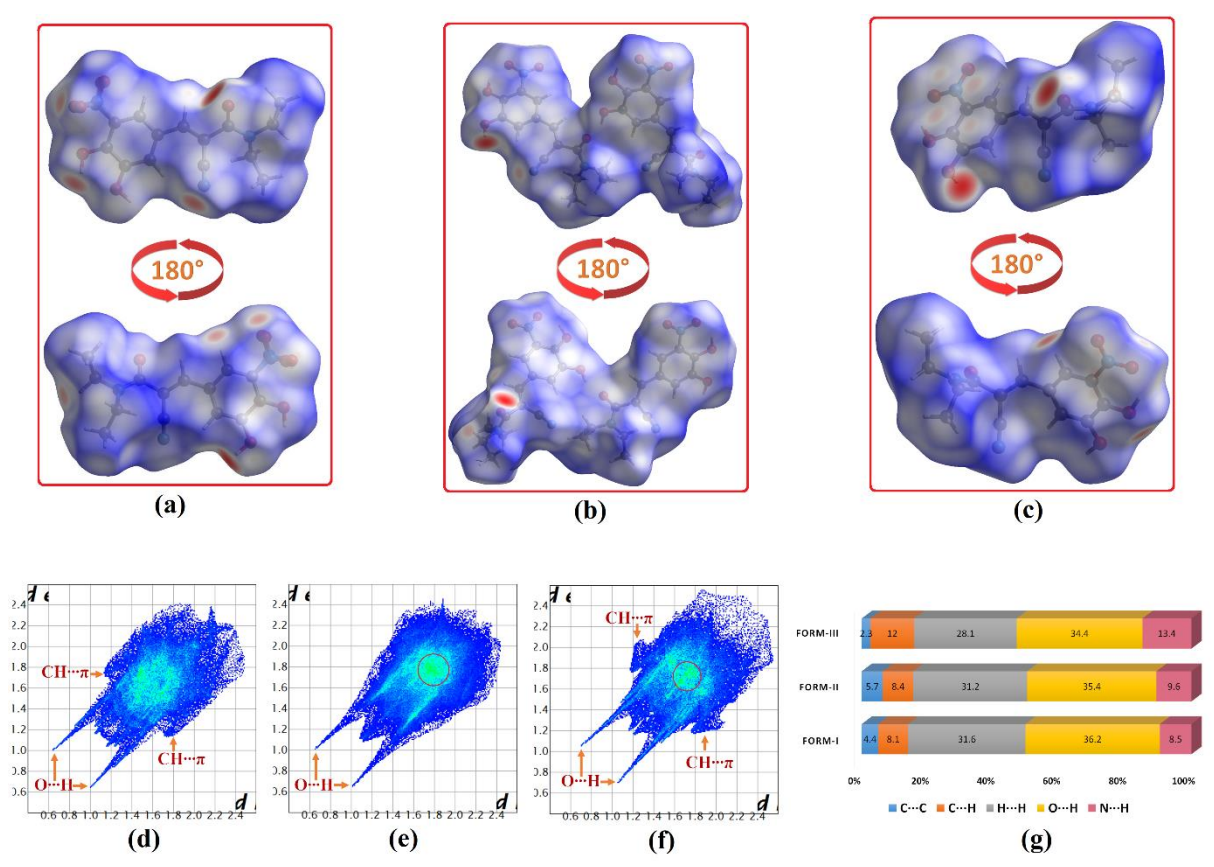
Table 3.3: Hydrogen bond interactions in ETP form-I, II and III (RT data).

D-H···A	H…A (Å)	D…A (Å)	D-H···A (deg)	symmetry code		
Form-I						
O2–H1···O1	1.76	2.6309(4)	176	1+x,y,z		
O3–H2···O2	2.15	2.6347(4)	114	Intra		
O3–H2···N2	2.16	2.9363(5)	147	2-x,1-y,1-z		
C6–H4···O5	2.55	3.2049(5)	145	1-x,1-y,1-z		
C12-H12···O4	2.29	3.1412(5)	146	-x,-y,-z		
		Form-II				
O2–H2···O6	1.83	2.6494(2)	176	x,y,1+z		
O3–H3···O4	1.88	2.5673(2)	141	Intra		
O7–H7···O1	1.84	2.5865(2)	151	1+x,y,-1+z		
O8–H8···O9	1.88	2.5763(2)	142	Intra		
C2–H2A···O6	2.58	3.2406(2)	128	x,y,1+z		
C12–H12A···N5	2.56	3.0598(2)	112	-1+x,y,1+z		
C21–H21···O7	2.58	3.4114(2)	149	-1/2+x,1/2-y,z		
C26-H26B···N2	2.48	3.3383(2)	147	x,y,-1+z		
$\pi(Cg1)\cdots\pi(Cg2)^*$		3.6978(2)		-1/2+x,1/2-y,z		
$\pi(Cg2)\cdots\pi(Cg1)^*$		4.1025(3)		1/2+x,1/2-y,-1+z		
		Form-III				
O2–H2···O1	1.92	2.7334(7)	174	5/2-x,1/2+y,z		
O3–H3···O4	1.88	2.5763(7)	142	Intra		
C6-H6···O3	2.31	3.2304(9)	171	3/2-x,-1/2+y,z		
C12–H12B···O1	2.40	2.7457(7)	100	Intra		
$\pi(Cg1)\cdots\pi(Cg1)**$		3.5453(10)		2-x,1-y,-z		
*Cg1= C1-C2-C3-C4-C5-C6, *Cg2 = C15-C16-C17-C18-C19-C20; **Cg1 = C1-C2-C3-C4-C5-C6						

# 3.4 Hirshfeld surface analysis

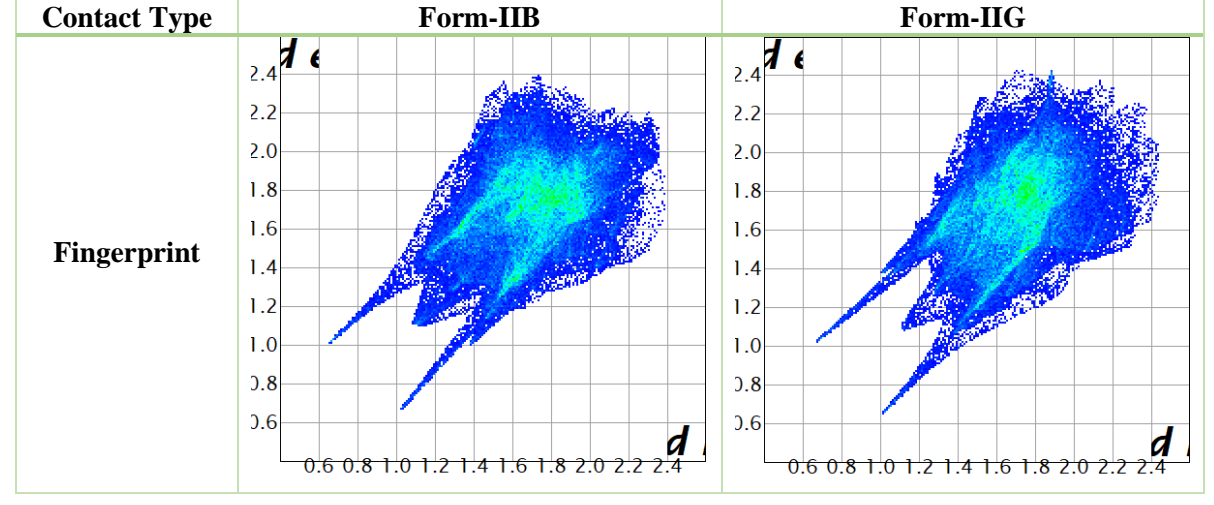
A reliable tool for the rapid and visual comparison of polymorphic crystal structures in terms of intermolecular interactions is Hirshfeld surface analysis and the associated 2D fingerprint plots. This analysis imprints the "whole of the structure view" of intermolecular contacts, rather than specific hydrogen bonds only. Further, Hirshfeld surface analysis enables the quantitative analysis of intermolecular interactions by the breakdown of 2D fingerprint plots into specific atom...atom contacts in the structure which are important for structural discrimination. Since Hirshfeld surfaces directly depend on the molecular environment in the crystal structure, the number of surfaces that can be unique in a given crystal structure depends on the number of independent molecules in the asymmetric unit (i.e. Z'). Hirshfeld surfaces mapped over d<sub>norm</sub> for ETP form-I, II and III are shown in Figure 3.5a, b &c. The brightest red spots appear over meta-hydroxy donor and carbonyl acceptor (i.e. for O-H···O interaction) in all the polymorphs. Further, among all the short contacts the O-H···O interactions show widest area which means that H···O distance is much shorter than the sum of van der Waals radii of donor (H atom) and acceptor (O atom). From the 2D fingerprint plots (Figure 3.5d, e & f), the H···O distance in form-I and II at ~1.65 Å (i.e.  $d_i + d_e$ ) and is slightly shorter than in form-III ( $d_i + d_e \approx 1.75$ Å). Compared to O–H···O contacts, the red spot above the nitrile synthon is less intense and narrower in form-I which indicates the weak nature of the O-H···N interaction. From the intensity of the red spots in the Hirshfeld surface maps, the H···N contact in form-I  $(d_i + d_e \approx 2.0 \text{ Å})$  is stronger than in form-II  $(d_i + d_e \approx 2.4 \text{ Å})$ , however the red spot is absent for form-III indicating no such short interaction below the van der Waals radii sum. The activated hydrogen donor ortho to the nitro group is engaged in the centrosymmetric R<sub>2</sub><sup>2</sup>(10) ring of C-H···O interactions. This interaction is significant in form-I (red spots near oxygen and hydrogen atoms), but is absent in form-II and III, perhaps due to offset stacking of aromatic rings which inhibits the in-plane parallel construction of centrosymmetric  $R_2^2(10)$  ring. A red spot over the ortho-hydrogen atom in form-III is observed where C-H···O interaction is formed with the oxygen atom of hydroxy group ortho to the nitro group. The aromatic stacking is seen in the decomposed 2D fingerprint plots of C···C contacts which contribute 4.4 %, 5.7 % and 2.3 % in form-I, II and III, respectively (Figure 3.5g). The luminous red bins (i.e. highlighted by red circle) for the  $\pi \cdots \pi$ stacking are observed at de + di  $\approx 3.6$  Å in form-II and at 3.4 Å in form-III. The contribution of C···H contacts are 8.1 %, 8.4 % and 12.0 % in form-I, II and III. A detailed analysis of interactions maps is given in Table 3.4 and Figure 3.6. The  $C-H\cdots\pi$  interactions of form-I and III are visualized in the side wings of C···H contacts at de + di  $\approx 2.8$  Å in form-I and  $\approx 3.0$  Å in form-III. The C-H··· $\pi$  interactions are most significant in form-III. C-H··· $\pi$  interactions between aliphatic hydrogen and C=N bond is observed in form-III only and augments the  $C-H\cdots\pi$  interactions. From a distribution of strong and weak interactions, the contribution of polar (O···H and N···H) is 44.7 %, 45.0 % and 47.8 % in form-I,

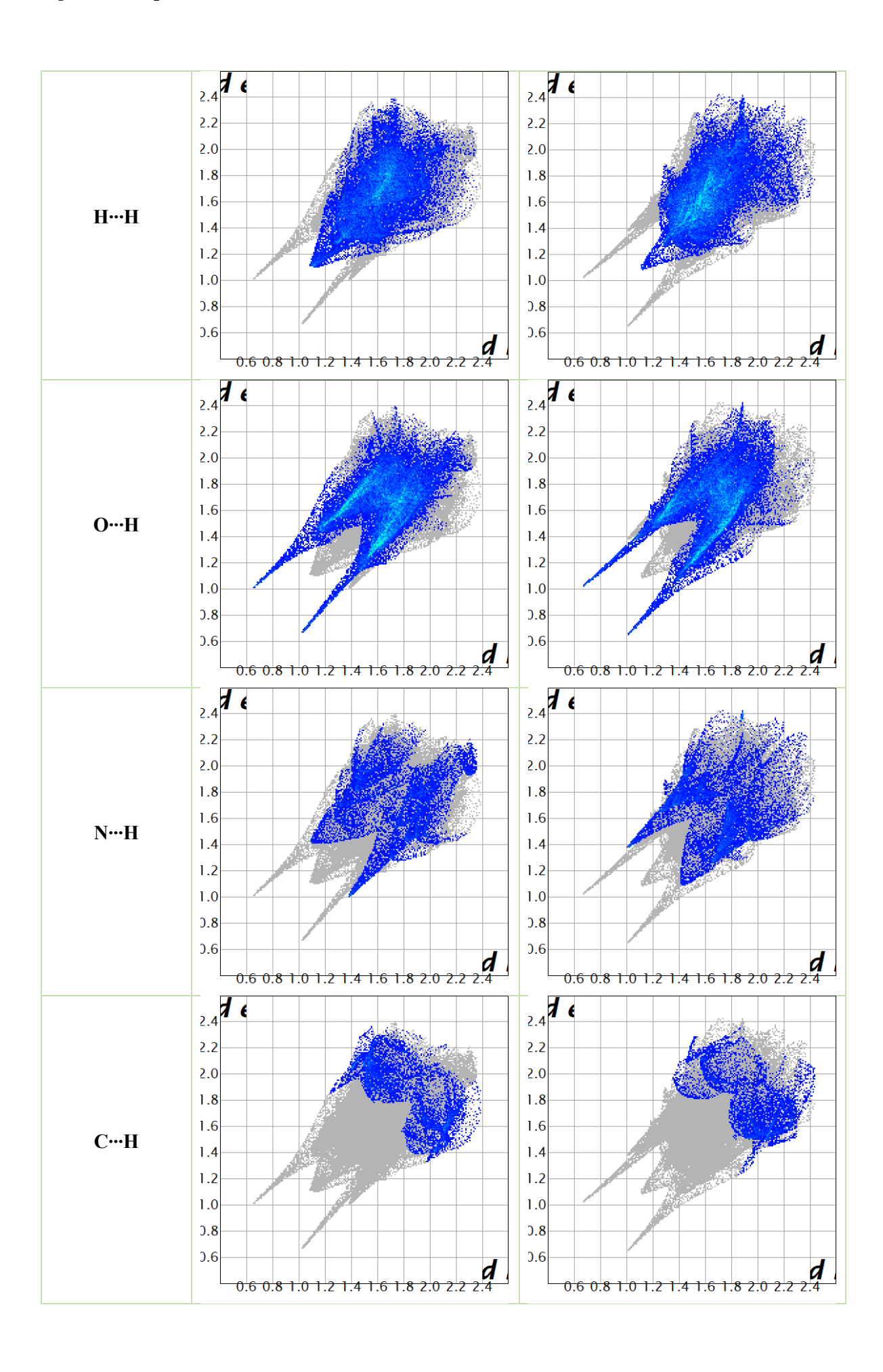
II and III (Figure 3.5g). Hydrophobic interactions (H···H) are nearly comparable in the three polymorphs at 31.6%, 31.2% and 28.1%.



**Figure 3.5:** Hirshfeld surfaces generated over  $d_{norm}$  for form-I (a), II (b) and III (c), the two surfaces are flipped 180° to show the opposite side surfaces of the same molecule. 2D fingerprint plots of form-I (d), II (e) and III (f), and percentage contribution of some selected interactions (g).

**Table 3.4:** Fingerprint plots and decomposed plots for form-IIB and IIG (Blue and Green are symmetry independent molecules).





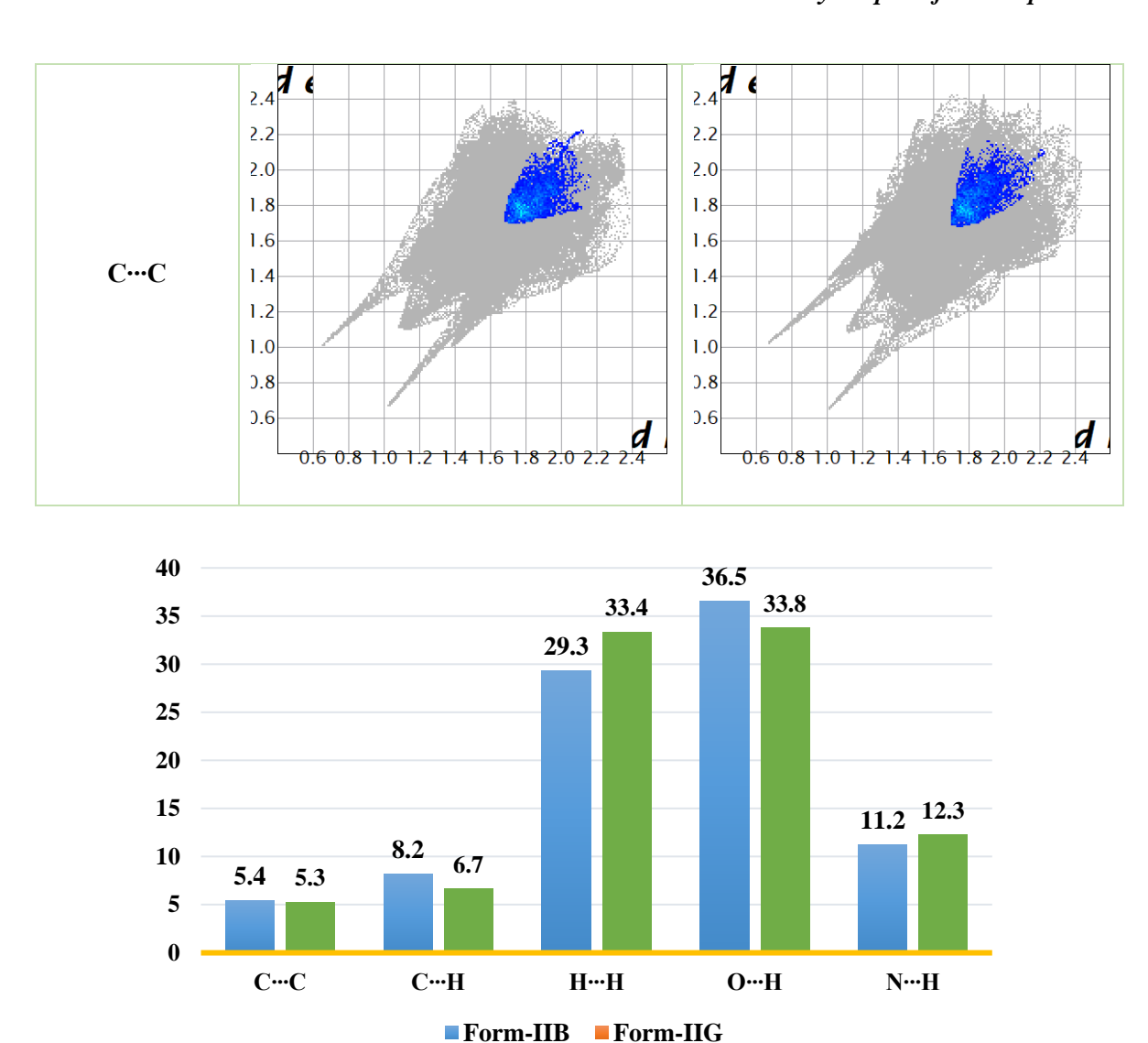


**Figure 3.6:** Percentage contribution of different interactions in crystal structure of form-II in blue and green molecules of the crystal structure (blue and green are for symmetry-independent molecules).

## 3.5 FT-IR spectroscopy

The tertiary amide carbonyl (C=O) stretching vibration in form-I appears at 1627 cm<sup>-1</sup> and this resonance is red shifted to 1634 cm<sup>-1</sup> in form-II and at 1632 cm<sup>-1</sup> in form-III. The fourth form-IV which was characterized by PXRD only (Figure 3.15) but without single crystal X-ray data shows IR C=O peak at 1630 cm<sup>-1</sup>. The nitrile group stretching band of form-I is at 2216 cm<sup>-1</sup> which is blue shifted to 2210 cm<sup>-1</sup> in form-II and form-III (2208 cm<sup>-1</sup>) but at similar value in form-IV (2215 cm<sup>-1</sup>). The phenolic OH stretching band of form-II and form-III at 3091 cm<sup>-1</sup> and 3072 cm<sup>-1</sup> is blue shifted at 3335 cm<sup>-1</sup> in form-I while in form-IV the hydroxyl OH peak is at same frequency as in form-I. All these functional groups showed significant changes in their vibration peaks upon conformational changes in their molecular packing (Table 3.5 and Figure 3.7).

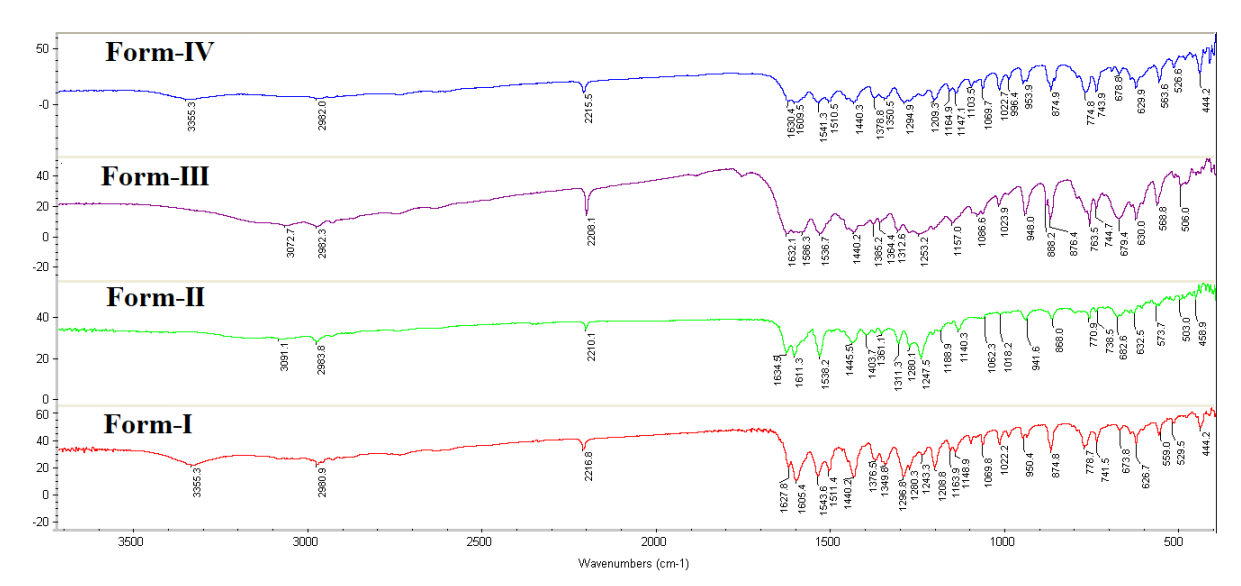


Figure 3.7: IR spectra of novel ETP polymorphs compared with commercially available ETP form-I.

**Table 3.5:** IR stretching frequency of ETP polymorphs.

Solid form	C-N Stretching (cm <sup>-1</sup> )	C=O Stretching (cm <sup>-1</sup> )	OH Stretching (cm <sup>-1</sup> )
Form-I	2216	1627	2980, 3355
Form-II	2210	1634	2983, 3091
Form-III	2208	1632	2982, 3072
Form-IV	2215	1630	2982, 3355

## 3.6 Thermal analysis

Differential scanning calorimetry (DSC) analysis of the neat polymorphs was done to correlate the thermodynamic relations and melting/ solidification during heating and cooling cycles. Figure 3.8 shows the stack plots of different forms with their heating, cooling and subsequent re-heat cycles. The DSC thermogram of form-I shows a single sharp melting endotherm peak at 165 °C (Tonset 164 °C, Tendset 167 °C) with  $\Delta H_{\text{fus}} = 44.79 \text{ kJ/mol}$  in the first heating cycle but no transition was observed during the cooling run (Figure 3.8a). The same sample was re-run from 30 °C to 200 °C, which melted at ~160 °C (Tonset 155 °C, Tendset 162 °C) through an exothermic transition at ~91 °C with onset at 79 °C and endset at 98 °C. The second heating cycle shows that the melted phase of form-I crystallizes to a relatively stable crystalline phase at ~90 °C and then melts at ~160 °C (about 4-5 °C lower than the original melting temperature). The crystal structure of form-II has two independent molecules in the asymmetric unit cell (Z'=2) and lower crystal density, which relates with its relatively lower lattice energy than form-I and III. However, DSC did not show any phase transition before melting which indicates its thermodynamic stability (Figure 3.8b). DSC experiments were run for all polymorphs at lower temp rate of 5 °C/min to check for any changes but similar transitions and peaks behavior was observed. Form-II shows melting endotherm at 159 °C ( $T_{onset}$  158 °C,  $T_{endset}$  161 °C) with  $\Delta H_{fus} = 34.14$  kJ/mol (calculated form the melting endotherm because there is no phase change prior to melting). Based on melting point and heat of fusion values (Table 3.6), form-II is monotropically related to form-I. A melting endotherm was observed for form-III at 164-166 °C with an endothermic phase transition seen at ~88 °C (Figure 3.8c). These evidences suggest that form-III is enantiotropically related to form-I. Form-III  $\Delta H_{\text{fus}} = 59.89 \text{ kJ/mol}$  as calculated in the Experimental Section ( $\Delta H_{\text{tra} \text{ (IIItoI)}} = 15.10 \text{ kJ/mol}$ ). The phase transition in form-III is very broad with an onset-endset range ~25 °C (75-100 °C) indicating its slow phase conversion. Further insight on the temperature mediated conversion was studied by heating form-III at above the transition temperature in a hot oven at 155 °C for 2 h (kept below the melting temperature). PXRD pattern of the resulting solid showed match with form-I, which confirms that form-III transforms to form-I above the transition temperature (Figure 3.9). A notable observation in the DSC temperature cycle is the exothermic transition of the starting polymorph and then melting endotherm of the stable polymorph in the second heating cycle. These observations mean that after melting, each solid form is converting to the thermodynamically stable solid which melts at ~160 °C. The PXRD pattern of form-IV shows peaks for a distinct polymorph (Figure 3.15b). DSC thermogram of form-IV shows an endothermic solid-solid transition at 158 °C (Tonset 154 °C, Tendset 160 °C) and ΔH<sub>tra (IVtoI)</sub> = 6.09 kJ/mol followed by an immediate melting endotherm at 165 °C (T<sub>onset</sub> 164 °C, T<sub>endset</sub> 167 °C).  $\Delta H_{\text{fus}}$  value of 50.88 kJ/mol was recorded for form-IV in the first heating cycle (Figure 3.8d). These events indicate that form-IV is enantiotropically related to form-I with a transition at 155-160 °C. The cooling and subsequent heating cycles follow the same pattern as in form-I, except a slightly broader exotherm during the second heating cycle. The discussion of DSC thermograms at 10 °C heating rate (Figure 9) summarized in Table 6 follows similar trends and profile at a lower temperature rate of 5 °C.

One last point to be confirmed was the outcome of polymorph modification after the heat-cool-reheat cycles in DSC. The melting point of the reheat (blue) curve is consistently at ~160 °C for all the four forms. The slight lowering of the melting endotherm temperature by a few °C in the reheat run is not due to any impurity or by products of ETP from the thermal cycles as confirmed by proton NMR. We surmise that after the solid melts in the DSC pan, it has much better contact with the sample pan over a larger surface area, and hence its melting point is lower by a few degrees in the reheat cycle. Even though the lower temperature of ~160 °C coincides with the melting endotherm for form-II, the product is actually form-I after confirmation by PXRD comparison. Thus, the stable polymorph after multiple heating cycles is the commercial drug polymorph form-I.

**Table 3.6:** Thermal events and stability relationship of entacapone polymorphs I-IV.

ETP Form	ΔH <sub>fus</sub> (kJ/mol)	ΔH <sub>tra</sub> (kJ/mol)	m.p. °C in 1st heat cycle	Stability relationship
I	44.79		163-164	Stable polymorph
II	34.14		158-159	Monotropic with I
III	59.89	15.10	164-166	Enantiotropic with I
IV	50.88	6.09	164-166	Enantiotropic with I

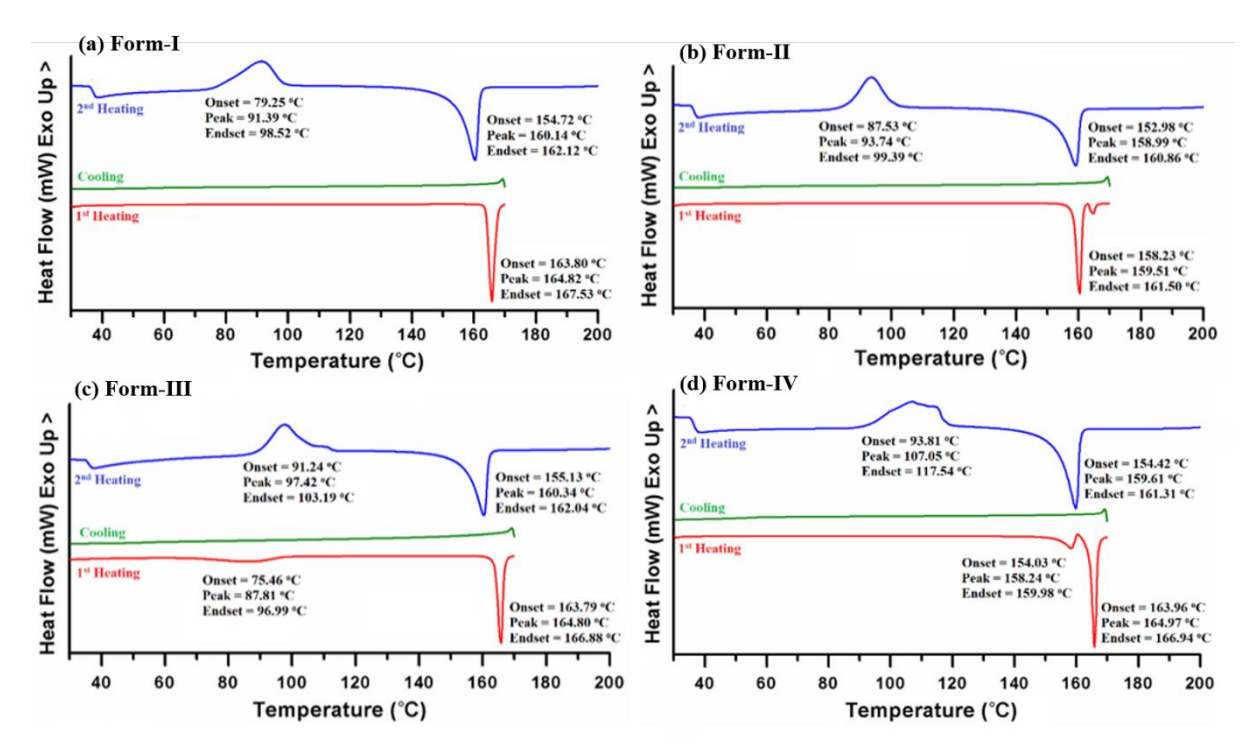


**Figure 3.8:** Stack plots of heating and cooling cycles of DSC thermogram of (a) form-I (b) form-II, (c) form-III, and (d) form-IV. First heating up to 170 °C (red) followed cooling to 30 °C (green) and subsequent second heating up to 200 °C (blue). Heating rate was set at 10 °C/ min.

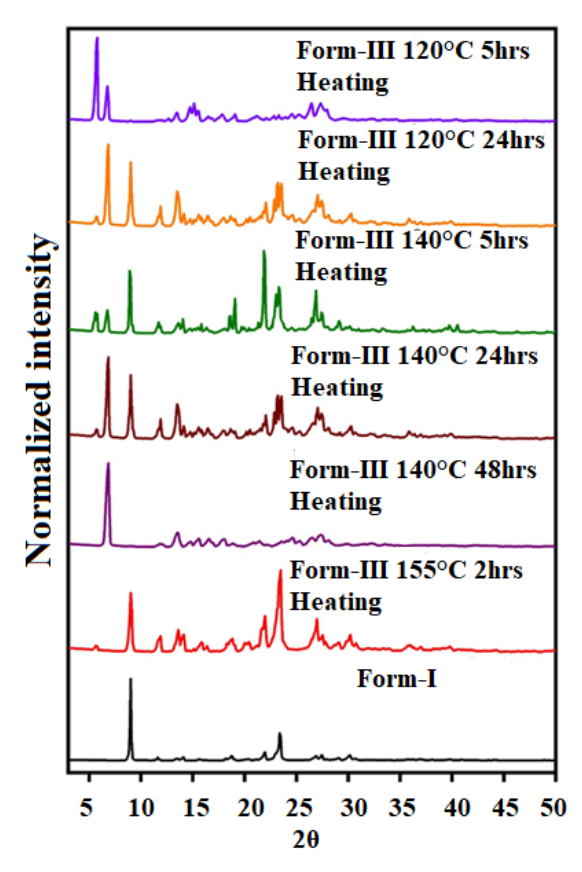
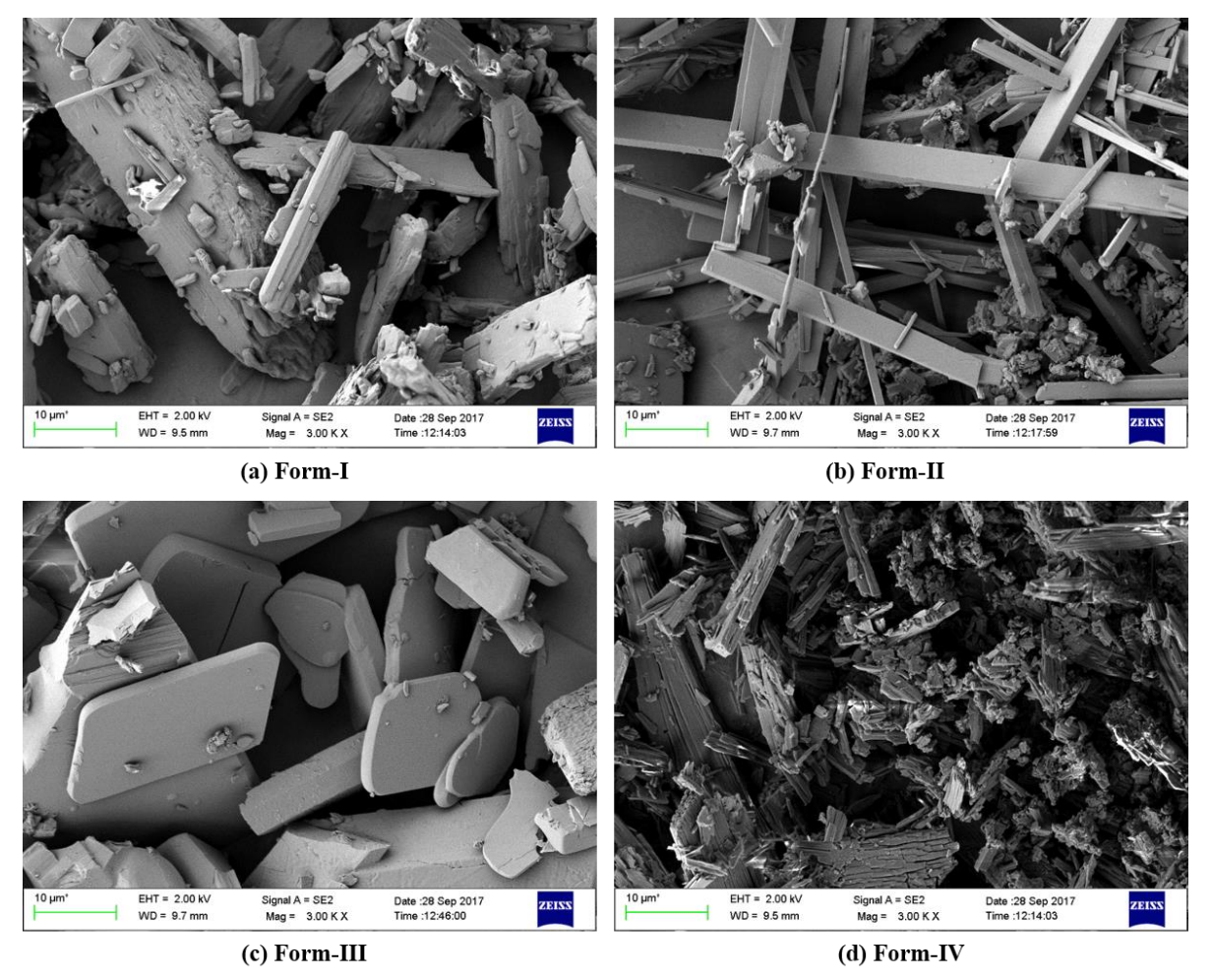


Figure 3.9: ETP-form-III PXRD pattern after controlled heating experiment

## 3.7 Field emission scanning electron microscope analysis

FE-SEM micrographs of the four polymorphic forms of entacapone (Figure 10 a-d) clearly show differences in crystal habit such as shape and surface texture. The reference form-I images display a non-homogeneous particle size of the sample in irregular twinned rod-like or columnar habit with approximately 2-100  $\mu$ m length and 1-10  $\mu$ m width and a rough surface. Form-II has well defined homogeneous long columnar rods with smooth surface of dimensions 2-50  $\mu$ m and 2-5  $\mu$ m (1 x b). Form-III is composed of homogeneous sub-rounded tabular with smooth surface in 5-30  $\mu$ m range. Form-IV shows irregular surface of non-ordered multi-layered rods that overlap and are coarse due to aggregation / agglomeration of small rods. The morphology variations in the crystal habits are due to differences in crystal growth conditions which influence external shape (crystal habit) of the internal structure.



**Figure 3.10:** FE-SEM images of ETP polymorphs (a) form-I, (b) form-II, (c) form-III and (d) form-IV. The four images are at the same magnification (3.00 K X) in order to compare the size and nature of the surfaces of the polymorph particles.

# 3.8 Solubility and dissolution

Solubility and dissolution rate of polymorphic crystal forms are important in the transport and absorption (i.e. bioavailability) of the drug.<sup>33,34</sup> Solubility and intrinsic dissolution rate (IDR) of the novel ETP polymorphs was measured and compared with the marketed form-I in phosphate buffer solution (PBS) at pH 7.0±0.5 at 37±0.5 °C. After 24 h to establish equilibrium solubility in slurry experiments, it was found that both ETP form-I and form-II polymorphs are stable in PBS media, with no detectable phase transitions. ETP form-II exhibited 1.3-fold higher solubility than the reference drug form-I (Figure 3.12a and Table 3.7). The phase stability after equilibrium slurry experiments (of the undissolved material) was analyzed by PXRD (Figure 3.11a&b). Form II persists for up to 24 h in the PBS medium but was converted to form-I after 48 h (Figure 3.11c). However, forms III and IV are not stable in PBS media, and showed rapid conversion to form-I.

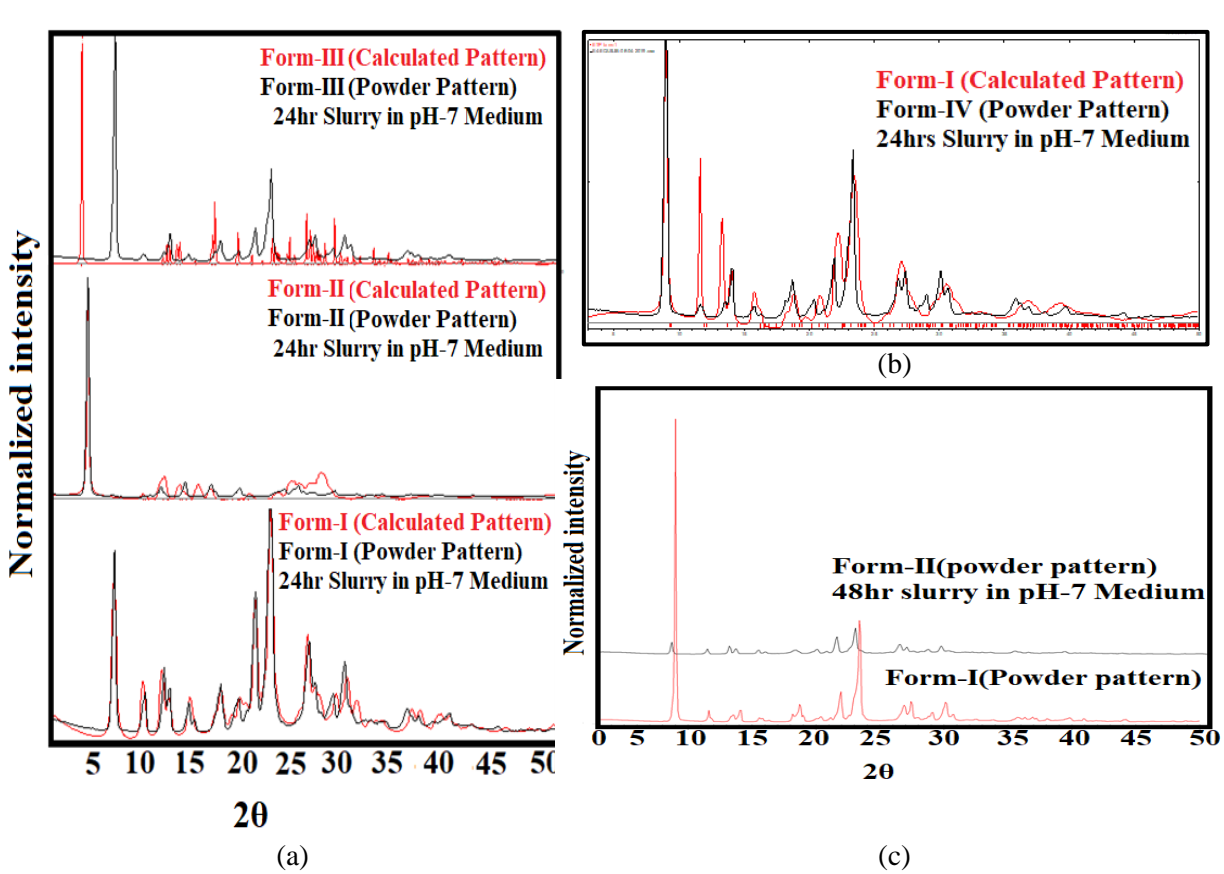


**Figure 3.11:** (a) Equilibrium Solubility of ETP Polymorphs form-I, form-II and form-III PXRD's After 24h Experiment, (b) Experimental Pattern of ETP-form-IV is matching with ETP-form-I Simulate Pattern, (c) Conversion of form-II to form-I after 48 h in pH-7 slurry buffer medium.

Intrinsic dissolution rate curves of ETP polymorphs are displayed in Figure 12b for a shorter period of 4 h as a function of cumulative drug amount dissolved (mg/ 500 mL) versus time (min). ETP polymorphs form-I, II and III exhibited faster dissolution rate with time; form-IV initially matched with

form-II and III up to 90 min, but later exhibited a gradual reduction compared with other forms in the dissolution media throughout the experiment duration (240 min). Form-II shows relatively faster dissolution at all time points compared to the commercial form-I which in turn shows faster dissolution than both form-III and form-IV. The average release of ETP from pellet to the dissolution media was analyzed for 4 h, which indicates that the concentration of the dissolved drug for form-I is 80 mg/500 mL (26.6% release w.r.t. total pellet amount), form-III is the highest at 124 mg/500 mL (41.3% release w.r.t. total pellet amount), form-III is 79 mg/500 mL (26.3% release w.r.t. total pellet amount,) and form-IV is 60 mg/500 mL (19.9% release w.r.t. total pellet amount). The phase stability and phase transformation after dissolution (the undissolved residue at 4 h) were analyzed by PXRD (Figure 3.13). Forms I and II were stable at this stage, but forms III and IV showed transformation to form-I and this is a reason for the reduced dissolution rate of form-IV after 90 min.

The above measurements show that the highest solubility and dissolution rate of form-II over other forms may be ascribed to the difference in their enthalpy, with form-II having the lowest enthalpy of fusion ( $\Delta H_{fus}$ : form-II < form-IV < form-III, Table 3.6). Other reasons also contribute such as the lower crystal density of form-II (Table 3.1), which suggest its relatively lower lattice energy (loose packing) than form-I and III. Different molecular conformations in form-II (Z' = 2, awkward packing)<sup>35</sup> result in lower melting point (158-159 °C) than form-I (163-164 °C). Thus, both stronger intermolecular interactions with water and lower melting point and somewhat loose crystal packing contribute the highest solubility / dissolution rate of form-II. Further, the rod-shaped morphology and comparatively smaller size particles of form-II favor higher solubility and dissolution due to larger surface contact area. Even though form-IV has much smaller particle size compared to form-II, the aggregation/ agglomeration of such irregular shape small particles eventually reduces the dissolution rate of form-IV (as well its transformation during dissolution/ solubility to form-I). There is thus an optimal range of particle size for high solubility and faster dissolution rate which are realized in ETP form-II.

**Table 3.7:** Equilibrium Solubility and Intrinsic dissolution of ETP polymorphs and n-fold enhancement compared to form-I is given in parenthesis.

ETP Polymorph	Molar Extinction coefficient (mM/cm) at $\lambda_{max}$ 376 nm	Equilibrium solubility in pH 7 after 24 h slurry (mg/ mL)	Intrinsic dissolution rate, IDR mg/cm²/min
Form-I	2.33	1.71	8.14
Form-II	2.33	2.14	10.74 (>1.31-fold)
Form-III	2.33	unstable	2.71 (0.33-fold)
Form-IV	2.33	unstable	5.43 (0.66-fold)

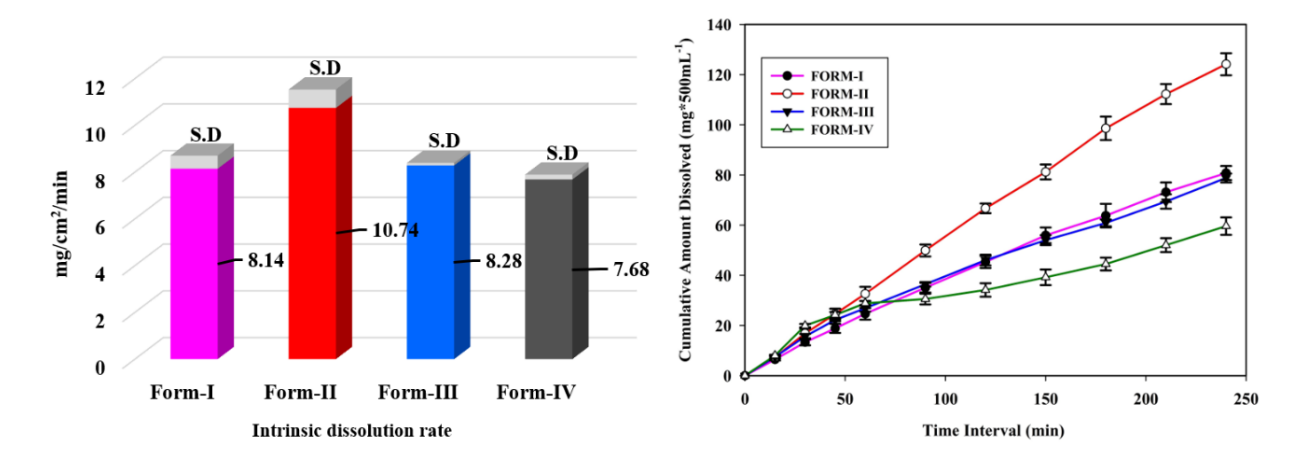


**Figure 3.12:** (a) Intrinsic dissolution rate of ETP polymorphs in pH  $7\pm0.5$  phosphate buffer medium. (b) Cumulative amount ETP dissolved in pH  $7\pm0.5$  PBS.

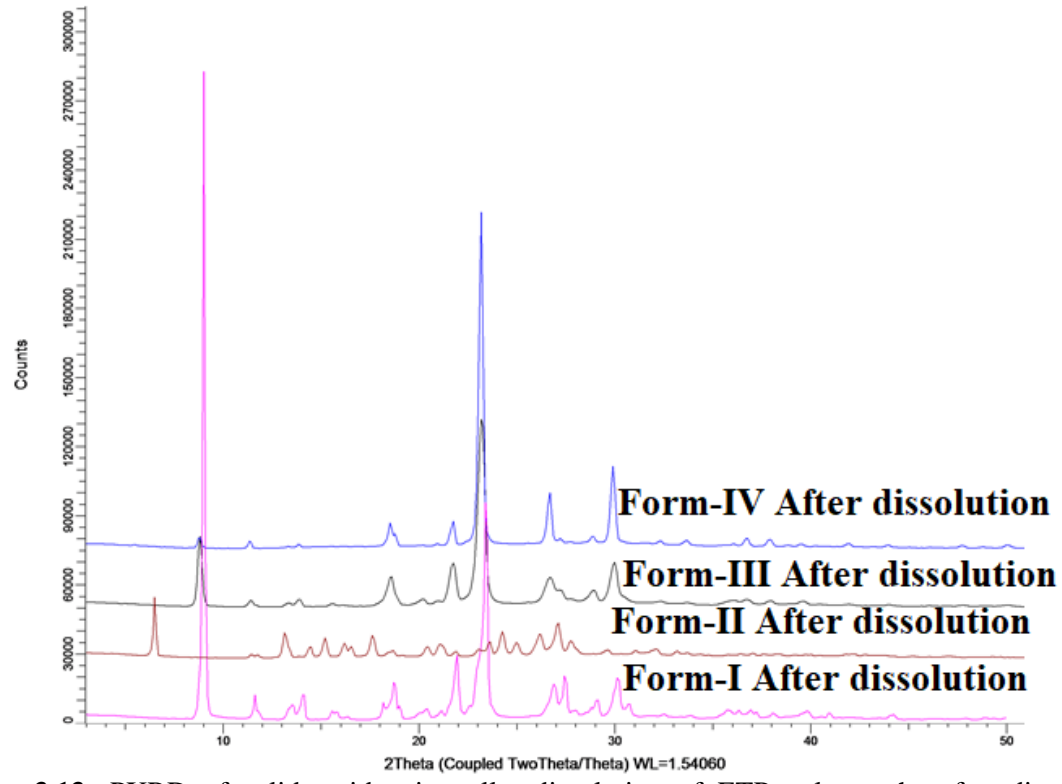


**Figure 3.13:** PXRD of solid residue in pellet dissolution of ETP polymorphs after dissolution experiment (4 h).

## 3.9 Permeability

Solubility and permeability are two important parameters for optimal drug adsorption to achieve high bioavailability. The change in flux across the dialysis membrane gives a measure of drug permeability, or log P. A significant change in the flux of ETP polymorphs (Figure 3.14a) is attributed to the variation in crystal packing, which in turn leads to changes in the cumulative polar interactions, namely O···H

plus N···H in order to bring the solid into the solution phase by crossing of the semi-permeable membrane. The sum of polar interactions (O···H and N···H) in form-I (44.7%), form-II (45.0%), and form-III (47.8%) (Hirshfeld analysis in Figure 3.5g). Therefore, due to greater lipophilic interactions the drug permeability is higher due to surface contact between solute-membrane-solvent interactions (Figure 3.14b): form-I (2.65 mg/mL), form-II (11.22 mg/mL), form-III (7.53 mg/mL) and form-IV (8.78 mg/mL) (values at 420 min in Figure 3.14b). Furthermore, higher dissolution rate and lower enthalpy of fusion of form-II also contribute to its highest membrane permeability and flux pass. Compared with the commercial form-I, the above results demonstrate that the permeability of novel ETP form-II is superior to that of the marketed form-I. Permeability of the commercial form-I is lower than that of the other polymorphs, and this observation prompts further studies to enhance not just solubility/dissolution but also drug permeability/flux pass in pharmaceutical crystal forms. <sup>36-39</sup>

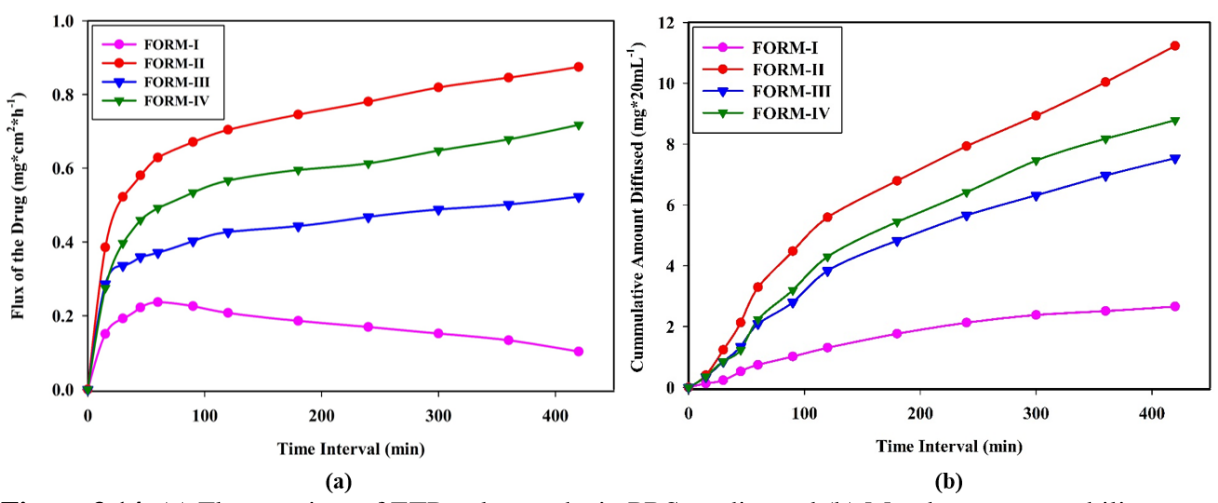


Figure 3.14: (a) Flux vs. time of ETP polymorphs in PBS media, and (b) Membrane permeability.

#### 3.10 Conclusions

From a pharmaceutical prospective, we have systematically investigated the ETP polymorphs which is an essential and significant step in any formulation to understand the relative thermodynamic stability of polymorphs, and if the polymorphs are enantiotropically related, thus the determination of thermodynamic transition point is crucial to analyze the crystalline form of the raw material to be most stable, acceptable and effective crystal form should be known for drug development. The above study, we have shown the structural origin of polymorphism in entacapone. Out of three novel polymorphs, form-II and form III crystals, are successfully solved which are obtained concomitantly from water and acetone solvent combination, and the inter ETP molecule conformation changes in the crystal lattice is found to be different. Thus, the hydrogen bonding is significantly different in the polymorphs. The thermal behavior of the polymorphs is investigated with DSC to detect the phase transformation from the metastable to the stable polymorph by performing heat-cooled-heat controlled experiments and found that, the form-IV and form-III are enantiotropically related to form-I. Whereas, the form-II is

monotrpically realted to form-I. However, from the post equilibrium solubility helped to make definite conclusions on the stability relationship and the polymorphic phase transformations at ambient temperatrure  $37 \pm 0.5$  °c. The reported ETP form-I and the novel form-II is found to be the thermodynamically stable polymorph at ambient conditions, and the form-III is converted to form-II and form-IV to form-I respectively. From the dissolution and permeability experiments, form II dissolves and diffused faster than the form-I, form-III and form-IV due to variation in crystal packing (i.e Z'=2 for form-II and Z'=1 for form-I and form-III) which implies its relatively lower lattice energy to dissolve and diffused. Therefore, form II is superior among the four polymorphic forms isolated so far. Thus, selection of the thermodynamically stable ETP polymorph-II is preferred in drug formulation to avoid polymorphic changes with superior solubility, dissolution and permeability during process development, formulation and marketing.

## 3.11 Experimental Section

ETP was obtained from Hetero Drugs (Hyderabad, India). Solvents (Purity >99%) and PBS (phosphate buffer solution) capsules were purchased from Finar Laboratories (Hyderabad, India) and used for the experiments.

# 3.11.1 Preparation of Polymorphs

**ETP form-I**: Entacapone was obtained from Hetero Drugs (Hyderabad, India) and analyzed by PXRD to know the polymorphic identity and it matches with form-I, or the commercial form (see Figure 3.15). Single crystals of form-I were obtained by slow solvent evaporation at room temperature after dissolving 40 mg of ETP in 60 mL methanol.

ETP form-II: ETP form-II was obtained by dissolving 1 g of form-1 in 1:1 volume ratio of several solvent mixtures such as methanol-toluene, methanol-acetone, methanol-chloroform, iso-butanol-benzene, iso-butanol-methyl ethyl ketone and then the solvent was evaporated in vacuum rotavapor at 50-55 °C temperature with constant rpm. The resultant solid product was characterized as crystalline form-II by PXRD (see Figure 3.15 and Figure 3.16). Form-II was also isolated by spray drying using acetone solvent to disperse the product. The rotavapor method with methanol-toluene was suitable to obtain bulk quantity of form-II for further experiments. Single crystals were obtained by dissolving 40 mg of powder obtained from rotavapor in a mixture of solvents (60 mL water and 40 mL acetone) by maintaining 60 °C in hot air oven left for slow evaporation over 2 days.

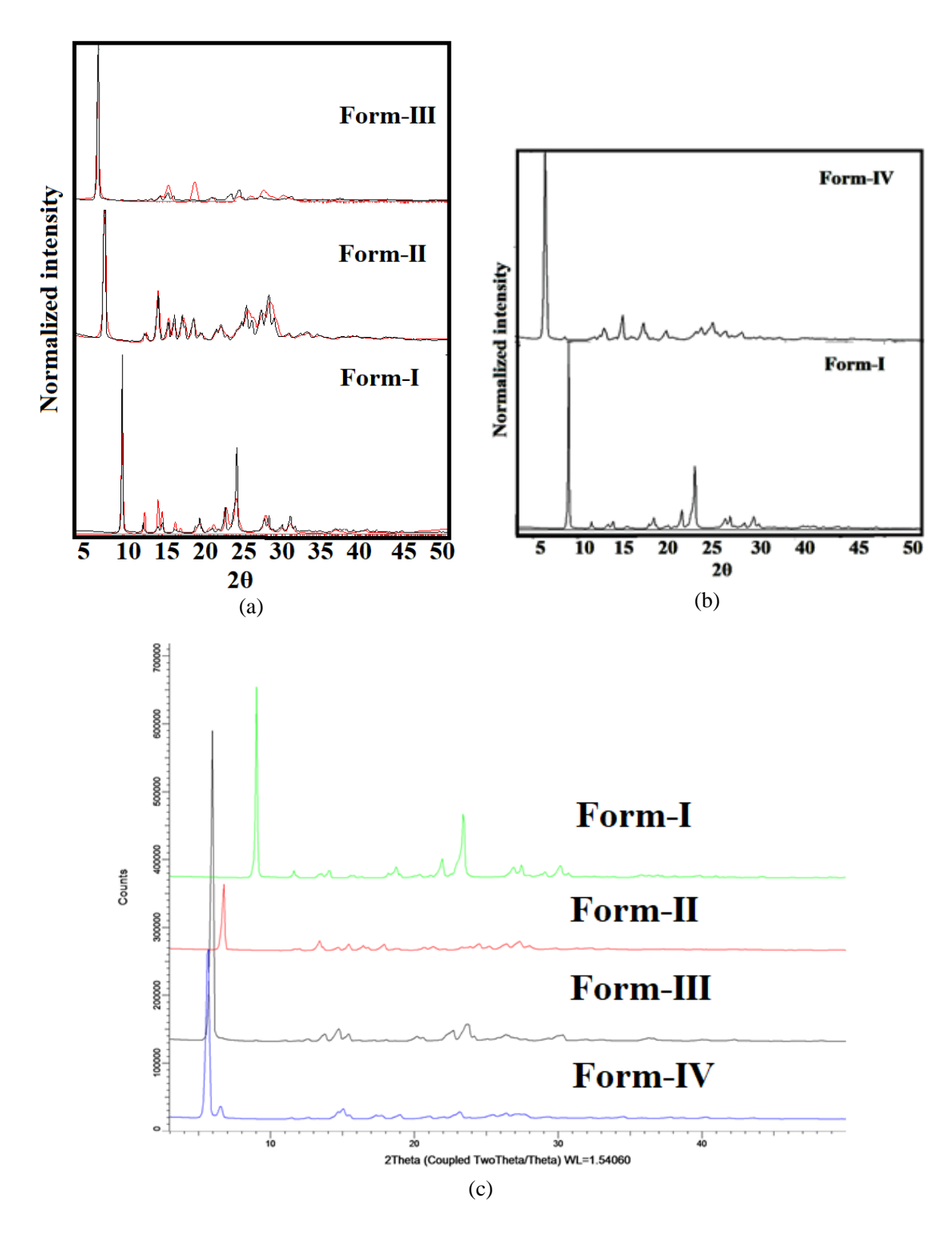


**Figure 3.15:** (a) PXRD of ETP polymorph (black trace, experimental) show excellent match with the calculated line profile from the X-ray crystal structure (red trace) for from-I, II and III. (b) Comparison of experimental PXRD of ETP form-IV with commercially available form-I shows a new phase. (c) PXRD overlay of ETP all forms.

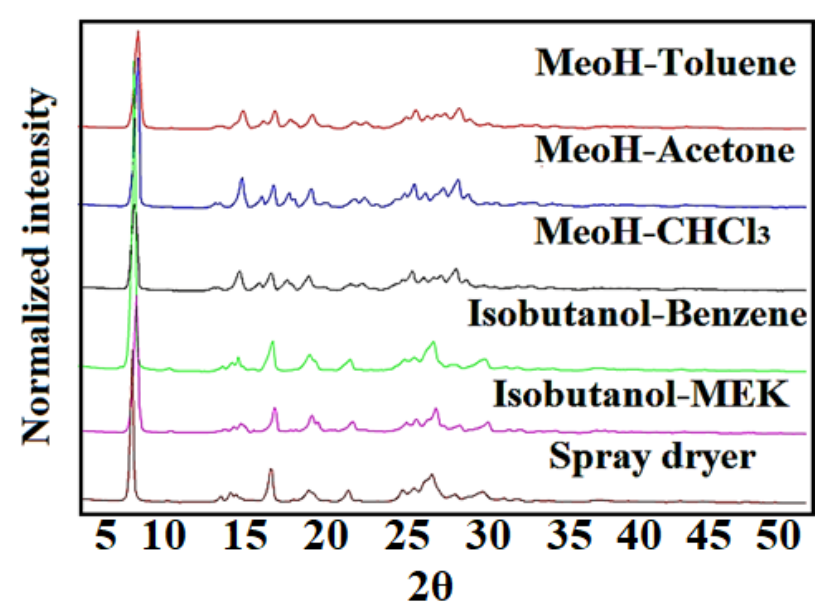
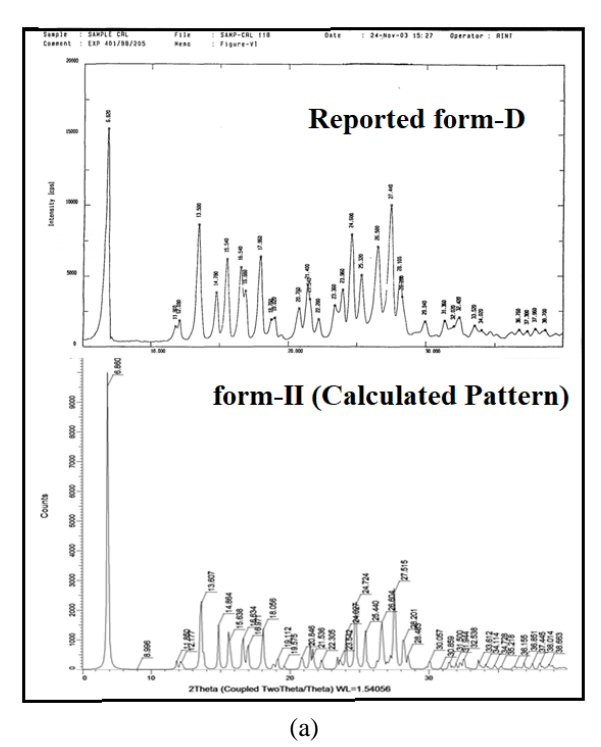


Figure 3.16: Comparison of form-II Powder Pattern in different solvent.

**ETP form-III**: 1 g of form-1 ETP was dissolved in toluene in a 100 mL beaker followed by solubilizing the drug by heating. After filtration the solvent was transferred to a 250 ml RB flask, and flash distillation using Heidolph vacuum rotavapor to maintain 70 °C for the complete evaporation of the solvent, so that a fine shiny product precipitated at the bottom of the flask, which was characterized and confirmed as form-III by PXRD (Figure 3.15). Single crystals were obtained by dissolving 40 mg of powder obtained from rotavapor in a mixture of solvents (60 mL water and 40 mL acetone) by maintaining 60 °C in hot air oven left for slow evaporation over 2 days.

**ETP form-IV**: A combination of toluene, nitromethane and acetone in 1:1:0.5 volume ratio was used to dissolve 1 g of ETP form-I to provide form-IV after vacuum rotavapor and maintain 70 °C temperature, similar to the above procedure (Figure 3.15). Even after repeated attempts we were unable to crystallize diffraction quality crystals of form-IV.

A comparison of entacapone polymorphs crystallized in this study compared to those reported in the literature <sup>16,26</sup> is shown in Figure 3.17. Form-1 correlates with form-A and form-II with form-D, while form-III and IV appear to be novel in the prior art.



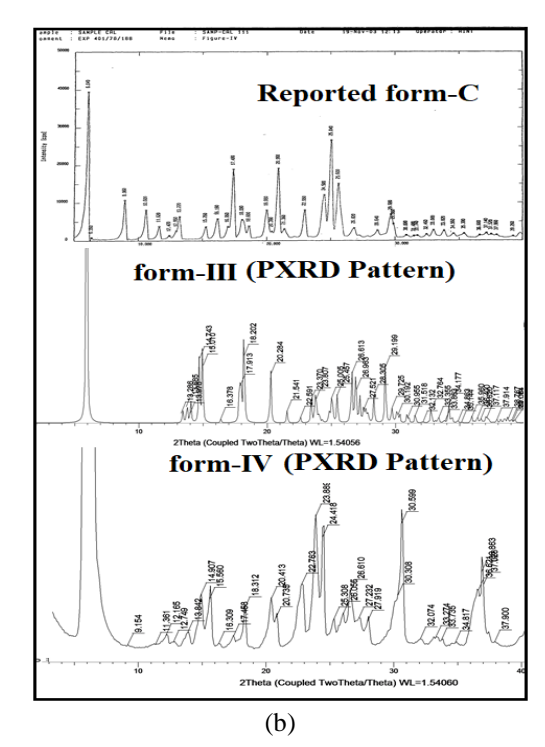


Figure 3.17:(a) PXRD of form-II (calculated/ experimental) produced in our lab matches with form-D reported in patent WO/2005/066117 (ref. 16) and in SI of Kevin Roberts paper (Cryst. Growth Des. 2009, ref. 26). (b) However, reported form-C (ref. 16) does not match with any of new form-III or IV in this study.

### 3.11.2 Powder X-ray diffraction

PXRD was recorded on Bruker D8 Advance diffractometer (Bruker-AXS, Karlsruhe, Germany) with Cu-K $\alpha$  radiation of  $\lambda$  =1.5406 Å and an acceleration voltage of 40 kV and current of 30 mA power. All polymorphic forms of ETP were scanned in the reflectance mode range from 3° to 50° (20) at scan rate of 5°/min (see Figure 3.15).

#### 3.11.3 Single crystal X-ray diffraction

Single-crystal X-ray diffraction data were collected on a Bruker SMART APEX II single-crystal X-ray CCD diffractometer having graphite monochromatized (Mo-K $\alpha$ ,  $\lambda$  = 0.71073 Å) radiation. The X-ray generator was operated at 50 kV and 0.8 mA. Data reduction was performed using APEX-II Software.<sup>28</sup> Intensities for absorption were corrected with SADABS and the structures were solved and refined using SHELXL-97<sup>29</sup> with anisotropic displacement parameters for non-H atoms. Hydrogen atoms on O and N were experimentally located in all crystal structures. Hydrogen atoms were experimentally located through the Fourier difference electron density maps in all crystal structures. All O–H and C–H atoms were fixed geometrically with HFIX command in SHELX-TL program of Bruker-AXS. Crystal parameters (Table 3.1) and hydrogen bond distances listed in Table 3.3 are neutron normalized to fix the D–H distance to its accurate neutron value in the X-ray crystal structures (O–H 0.983 Å, N–H 1.009 Å, and C–H 1.083 Å). A check of the final CIF file using PLATON<sup>30,31</sup> for any missed symmetry. Mercury software was used to prepare packing diagrams. Crystal data of form-I, II and III

at 296 K (room temperature) and additionally form-I at 100 K (low temperature are reported in this study. Crystallographic .cif files are available at <a href="www.ccdc.cam.ac.uk/data\_such">www.ccdc.cam.ac.uk/data\_such</a> as part of the Supporting Information (CCDC Nos. 2074791, 2074821, 2074862, 2095588).

# 3.11.4 Vibrational spectroscopy

Infrared spectra of ETP polymorphic forms are acquired by FT-IR spectroscopy Thermo-Nicolet 6700 FT-IR-NIR spectrometer by physically mixing each polymorphic form of ETP with KBr by using spatula and later applied 2.5 ton pressure in KBr press machine for 3 min to prepare the sample pellet. Omnic software (Thermo Scientific, Waltham, MA) was utilized to analyze the data. Each sample pellet was scanned 120 times in the range 400–4000 cm<sup>-1</sup> with, and spectra were normalized with background correction (see Figure 3.7).

# 3.11.5 Thermal analysis

Mettler-Toledo DSC 822e module, (Mettler-Toledo, Columbus, OH) was used for thermal analysis. The temperature of the instrument and heat flow were calibrated using Indium (calibration standard, purity > 99.999 %) with melting point onset at  $156.60 \pm 0.3$  °C and heat flow  $28.45 \pm 0.6$  J/g. The temperature range for each polymorph was preprogramed from 30-200 °C for the 1<sup>st</sup> cycle heating at rate of 10 °C/ min, then cooled down to 30 °C and 2<sup>nd</sup> cycle heating rate of 10 °C/ min from 30-200 °C. A few samples were repeated at a heating rate of 5 °C/ min to compare the thermal events and phase transitions. Samples were purged with dry nitrogen flowing at 80 mL/min. Each thermal DSC run was repeated 3 times with consistent and reproducible results. The standard deviation for temperature is 0.3 °C and enthalpy 0.5 J/g.

Enthalpy of fusion ( $\Delta H_{fus}$ ) of form-I and form-II was determined directly from DSC, since they do not show any phase transformation (see Thermal analysis section).  $\Delta H_{fus}$  for form-III and form-IV were calculated using Hess's law of heat summation.

 $\Delta H_{\text{fus}}$  values of form-III and IV were calculated as follows.

 $\Delta H_{fus}$  (form-III) =  $\Delta H_{fus \text{ (form-I)}} + \Delta H_{tra \text{ (form-III)}}$ 

 $\Delta H_{fus}$  (form-IV) =  $\Delta H_{fus \text{ (form-I)}} + \Delta H_{tra \text{ (form-IV)}}$ 

Enthalpy values from DSC thermogram were converted using the formula.

 $\Delta H (kJ/mol) = \Delta H (J/g, normalized value from DSC) x 305.29 (mol. wt.) / 1000$ 

The measured and calculated values of  $\Delta H_{fus}$  are given below.

 $\Delta H_{fus}$  (form-I) = 44.79 kJ/mol

 $\Delta H_{fus}$  (form-II) = 34.14 kJ/mol

 $\Delta H_{fus}$  (form-III) = 44.79 + 15.10 = 59.89 kJ/mol

 $\Delta H_{fus}$  (form-IV) = 44.79 + 6.09 = 50.88 kJ/mol

## 3.11.6 FESEM morphology

The morphology and size of the microstructures of ETP polymorphs were examined by FESEM analysis on a Carl Zeiss field emission scanning electron microscope model 6027 with MERLIN compact using a beam voltage of 5 kV. The ETP polymorphs were deposited on carbon tape and sputtered with gold to avoid charging. The same samples were used for morphology analysis.

## 3.11.7 Equilibrium solubility and dissolution rate measurements

Equilibrium solubility and dissolution rate studies were carried in triplicate (n = 3). An excess amount of the sample of ETP polymorphs was added to 5 mL of purified pH 7 phosphate buffer saline medium. The supersaturated solution was stirred at 800 rpm using a magnetic stirrer at 37  $\pm$  0.5 °C. After 24 h, the suspension was filtered through Whatmann 0.45 µm syringe filter. Equilibrium solubility was calculated by the absorbance value of ETP at  $\lambda_{max}$  of 376 nm using Thermo Scientific Evolution 300 UV-vis spectrometer (Thermo Scientific, Waltham, MA) and plotted against several known concentrations to prepare the concentration vs. intensity calibration curve. From the slope of the calibration curves, molar extinction coefficient for ETP was calculated and the remaining residues of ETP polymorphs were characterized by PXRD to know their stability. Intrinsic dissolution rate (IDR) of ETP form-II, form-III and form-IV were carried out on a USP certified Electro lab TDT-08L Dissolution Tester (Electro lab, Mumbai, MH, India). In intrinsic attachment unit 300 mg of ETP polymorph was compressed between the smooth surfaces under a pressure of 2.5 ton/inch for 4 min in an area of 0.5 cm<sup>2</sup>. The compressed pellets were analyzed by PXRD to know the stability of the polymorphic form or any changes in XRD line pattern after powder compression (Figure 3.17). The pellets were dipped in 500 mL of pH 7.0 phosphate buffer saline at  $37 \pm 0.5$  °C with rotation of 100 rpm. 5 mL of dissolution medium was collected at interval of 15, 30, 45, 60, 90, 120, 150, 180, 210, 240 min by replacing each time with the same amount of fresh pH 7.0 phosphate buffer. The absorbance is plotted against time for samples collected at regular intervals.

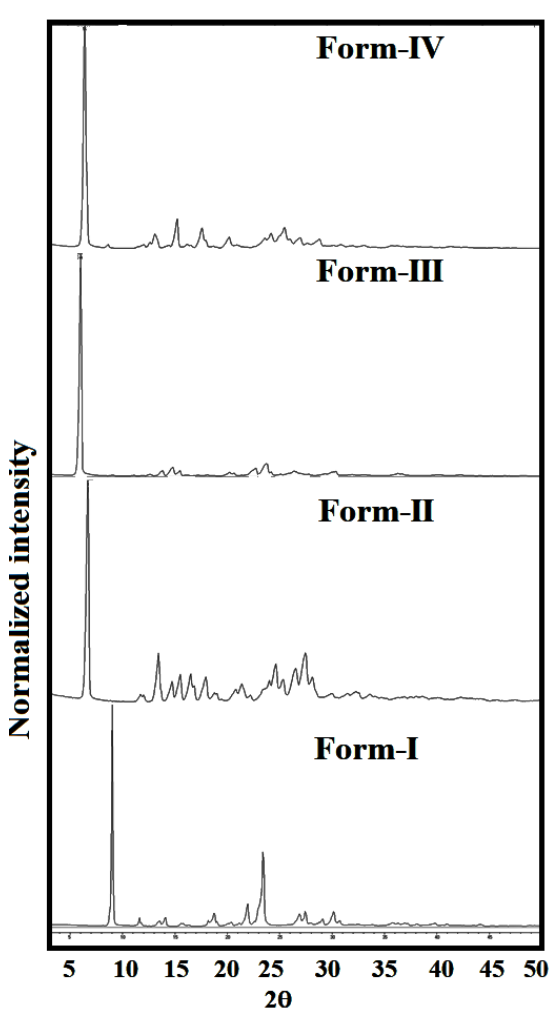


**Figure 3.17:** Compressed pellets were recorded and analyzed by PXRD to know the stability of polymorphs to compression and found to be stable to run solubility and dissolution experiments.

## 3.11.8 Diffusion measurements

Diffusion studies were carried out in a glass Franz diffusion cell (Model JFDC-07, Orchid Scientific, Maharashtra, India) with 20 mL volume. The membrane used are dialysis membrane-135 [width 33.12 mm, and diameter 23.8 mm, capacity 4.45 mL/cm] purchased from HiMedia, India. The dialysis membrane is placed between the two compartments fixed by a stainless-steel clamp with an effective mass transfer area of  $3.14 \, \text{cm}^2$ . The receptor compartment is filled with (PBS) phosphate buffer solution, and air bubbles are removed. The donor compartment was loaded with 20 mg polymorph sample and 2 mL of PBS was added. The temperature of diffusion medium is thermostatically maintained at  $37 \pm 0.5 \,^{\circ}$ C throughout the experiment at 600 rpm and permitted to diffuse through the membrane towards the receptor compartment. Aliquots of 1 mL were withdrawn from the receptor compartment at set time periods (15, 30, 45, 60, 90, 120,180, 240, 300, 360 and 420 min) and fresh PBS was added to replenish the volume. The diffused concentration of sample was determined by UV spectroscopy.

### 3.12 References

- 1. Holm, K. J.; Spencer, C. M. Entacapone. A Review of Its Use in Parkinson's Disease. *Drugs*, **1999**, *58*, 159-177.
- 2. Schrag, A. Entacapone in the Treatment of Parkinson's Disease, *Lancet Neurol.* **2005**, *4*, 366–370
- 3. https://www.accessdata.fda.gov/drugsatfda\_docs/label/2016/020796s026lbl.pdf
- 4. https://www.accessdata.fda.gov/drugsatfda\_docs/label/2010/020796s15lbl.pdf
- 5. Savolainen, J.; Forsberg, M.; Taipale, H.; Männistö, P.T.; Järvinen, K.; Gynther, J.; Jarho, P.; Järvinen, T. Effects of Aqueous Solubility and Dissolution Characteristics on Oral Bioavailability of Entacapone. *Drug Dev. Res.* **2000**, *49*, 238–244.
- Forsberg, M. M.; Huotari, M.; Savolainen, J.; Mannisto, P. T. The Role of Physicochemical Properties of Entacapone and Tolcapone on Their Efficacy During Local Intrasriatal Administration. *Eur.J Pharm.Sci.* 2005, 24, 503–511.
- 7. Anjan Kumar, M.; Murthy, P. N.; Sameeraja, N. H.; Narayan, P. N. Dissolution Rate Enhancement of Entacapone and Formulation of Its Oro-Dispersible Tablets Applying Statistical Design. *Ind. J. Pharma. Edu. Res.* **2016**, *50*, 549–562.
- 8. Snider, D. A.; Addicks, W.; & Owens, W, Polymorphism in generic drug product development. *Advanced drug delivery reviews*, **2004**,56(3), 391-395.
- 9. Kawabata, Y.; Wada, K.; Nakatani, M.; Yamada, S.; & Onoue, S, Formulation design for poorly water-soluble drugs based on biopharmaceutics classification system: basic approaches and practical applications. *International journal of pharmaceutics*, **2011**, *420*(1), 1-10.
- 10. Yan, Y.; Dai, X.-L.; Jia, J.-L.; Zhao, X.-H.; Li, Z.-W. Lu, T.-B.; Chen, J.-M. Crystal Structures, Stability, and Solubility Evaluation of Two Polymorphs of a 2:1 Melatonin-Piperazine Cocrystal. *Cryst. Growth Des.* **2020**, *20*, 1079–1087.
- 11. Bolla, G.; & Nangia, A. Clofazimine mesylate: a high solubility stable salt. *Crystal growth & design*, **2012**, 12(12), 6250-6259.
- 12. Brittain, H. G.; Grant, D. J. R.; Myrdal, P. B. Effects of Polymorphism and Solid-State Solvation on Solubility and Dissolution Rate. Polymorphism in Pharmaceutical Solids: Second Edition, CRC Press. **2016**, 436-480.
- 13. Nicoud, L.; Licordari, F.; Myerson, A. S. Estimation of the Solubility of Metastable Polymorphs: A Critical Review. *Cryst. Growth Des.* **2018**, *18*, 7228–7237.
- 14. Singhal, D.; Curatolo, W. Drug polymorphism and dosage form design: A practical perspective. Adv. Drug Delivery Rev. 2004, 56, 335–347.
- 15. Leppanen, J.; Wegelius, E.; Nevalainen, T.; Jarvinen, T.; Gynther, J.; Huuskonen, J. *J.* Structural studies of acyl esters of entacapone. *Journal of Molecular Structure*, **2001,**562(1-3), 129-135.

- 16. Jaweed, M. S. M.; Khan, R. A. R.; Yadav, R. P.; Shaikh, Z. G. Patent application No. WO 2005/066117 A1.
- 17. Samec-Skalec, D.; Marinkovic, M.; Siljkovic, Z.; Horvat, M. Patent application No. WO 2007/135406 A1.
- 18. Bommaka, M. K., Mannava, M. C., Suresh, K., Gunnam, A., & Nangia, A. Entacapone: Improving aqueous solubility, diffusion permeability, and cocrystal stability with theophylline. *Crystal Growth & Design*, **2018**, *18*(10), 6061-6069.
- 19. Suresh, K.; Goud, N. R.; Nangia, A. Andrographolide: Solving Chemical Instability and Poor Solubility by Means of Cocrystals. *Chem. Asian J.* **2011**, *8*, 3032–3041.
- 20. Bernhardson, D.; Brandt, T. A.; Hulford, C. A.; Lehner, R. S.; Preston, B. R.; Price, K.; Sagal, J. F.; St. Pierre, M. J.; Thompson, P. H.; Thuma, B. Development of an Early- Phase Bulk Enabling Route to Sodium- Dependent Glucose Cotransporter 2 Inhibitor Ertugliflozin. *Org. Process Res. Dev.* 2014, 18, 57–65.
- 21. Desiraju, G. R. Angew. Chem., Int. Ed. Engl. 1995, 34, 2311–2327. 627 (34)
- 22. Desiraju, G. R.; Steiner, T. The Weak Hydrogen Bond in Structural Chemistry and Biology, IUCr Monographs in Crystallography, **1999**.
- 23. Tiwari, M., Chawla, G., & Bansal, A. K. Quantification of olanzapine polymorphs using powder X-ray diffraction technique. *Journal of pharmaceutical and biomedical analysis*, **2007** *43*(3), 865-872.
- 24. Etter, M. C.; MacDonald, J. C.; & Bernstein, J. Graph-set analysis of hydrogen-bond patterns in organic crystals. *Acta Crystallographica Section B: Structural Science*, 1990, 46(2), 256-262.
- 25. Thalluri, C. S.; Bontha, V. K.; Devanna, N. Enhancement of entacapone bioavailability by polymorphism. *International Journal of Pharmacy and Technology* **2013**, 5(3), 5753-5760
- 26. Kwokal, A.; Nguyen, T. T. H.; Roberts, K. J. Polymorph-Directing Seeding of Entacapone Crystallization in Aqueous/Acetone Solution Using a Self-Assembled Molecular Layer on Au (100). *Cryst. Growth Des.* **2009**, *9*, 4324-4334.
- 27. Kwokal, A.; Čavužić, D.; Roberts, K. J. Surface Adsorbed Templates for Directing the Crystal Growth of Entacapone as Monitored Using Process Analytical Techniques. Cryst. Growth Des. **2013**, *13*, 5324–5334.
- 28. Jednačak, T.; Hodzic, A.; Scheibelhofer, O.; Marijan, M.; Khinast, J. G.; Novak, P. Fast Real-Time Monitoring of Entacapone Crystallization and Characterization of Polymorphs via Raman Spectroscopy, Statistics and SWAXS. *Acta Pharm.* **2014**, *64*, 1-13.
- 29. Kwokal, A.; Roberts, K. J., Direction of the Polymorphic Form of Entacapone Using an Electrochemical Tuneable Surface Template. *CrystEngComm* **2014**, *16*, 3487-3493.

- 30. Bruker SMART v 5.625, SHELXTL v 6.12; Bruker AXS Inc.: 669 Madison, Wisconsin, USA. 2000.
- 31. Sheldrick, G. M. Program for Refinement of Crystal Structures; 671 University of Göttingen: Germany, 1997.
- 32. Reichelt R. Scanning electron microscopy. Science of Microscopy. Springer. 2007,133-272.
- 33. Rao Khandavilli, U. B.; Gangavaram, S.; Rajesh Goud, N.; Cherukuvada, S.; Raghavender, S.; Nangia, A.; Manjunatha, S. G.; Nambiar, S.; Pal, S. High solubility crystalline hydrates of Na and K furosemide salts. *Cryst Eng Comm* **2014**, 16, 4842–4852.
- 34. Suresh, K.; Minkov, V. S.; Namila, K. K.; Derevyannikova, E.; Losev, E.; Nangia, A.; Boldyreva, E. V. Novel Synthons in Sulfamethizole Cocrystals: Structure–Property Relations and Solubility. *Cryst. Growth Des.* **2015**, 15, 3498–3510.

# **CHAPTER FOUR**

# Improvement of Physiochemical Properties of Pimozide through Co-crystalization with Dicarboxylic Acids

Pimozide is a BCS class II drug of the diphenyl-butyl piperidine class. This antipsychotic drug is used in schizophrenia and chronic psychosis, Tourette syndrome, and resistant tics, and it can be also used to treat Delusional parasitosis. Cocrystal screening experiments of PMZ resulted in the formation of five binary molecular salts with the coformers oxalic acid (OA), succinic acid (SA), glutaric acid (GA), adipic acid (AA) and fumaric acid (FA). It was observed that PMZ-SA salt exhibited superior performance for both solubility and dissolution experiments. In diffusion permeability (Franz diffusion cell, pH 7.0) experiment also PMZ-SA salt exhibited highest permeability among all the complexes of PMZ. PMZ-SA salt is a high bioavailability formulation for PMZ.

# 4.1 Introduction

Pimozide (PMZ, Scheme 4.1), a FDA-approved drug is used for the treatment of Tourette syndrome (a neurological disorder with uncontrolled repetitive muscle movements and sounds known as tics) and chronic psychosis. Besides, it has been found that this drug can be used for the treatment of different types of cancers such as hepatocellular carcinoma<sup>2</sup>, colorectal cancer<sup>3</sup>, osteosarcoma<sup>4</sup>, myelogenous leukemia<sup>5,6</sup> and prostate cancer<sup>7,8</sup> due to its ability to inhibit cancer cell proliferation by decreasing signal transducer and activator of transcription activity. PMZ compound appears as white crystalline solid. Though this drug is highly effective for the treatment of the above-mentioned diseases, it suffers from low aqueous solubility which directly affects its oral bioavailability. PMZ is a BCS (Biopharmaceutical Classification System) class II drug (low solubility and high permeability) and it is almost insoluble in water (solubility: 0.00173 mg/mL, < 2 mg/L) whereas it is found to be freely soluble in chloroform and sparingly soluble in ether and alcohol. Only 20, it is very essential to enhance its solubility applying suitable methods to achieve improved bioavailability. There are several conventional methods such as particle size reduction, solid dispersion, nanosuspension, supercritical fluid process, cryogenic techniques, synthesis of inclusion complexes, micellar solubilisation, hydrotrophy<sup>20</sup> etc. to improve solubility or dissolution of poorly water-soluble drugs.

Besides these conventional methods, crystal engineering <sup>21</sup> approach is regarded as a novel, emerging and promising technique to ameliorate physicochemical properties of drugs. Crystal engineering method includes the preparation of polymorphs, cocrystals, salts, hydrates and solvates. In addition to intermolecular interactions and crystal packing in these materials, other factors which can also influence physicochemical properties of a drug are particle size distribution, crystal habit, crystal form, surface nature etc.<sup>22</sup> In the past two decades, pharmaceutical cocrystals have gained significant attention from academia as well as pharmaceutical industries because of efficiency of those materials to enhance physicochemical properties of drugs. <sup>23</sup> According to US-FDA, pharmaceutical cocrystal is defined as crystalline solid material composed of two or more components including at least one API in a stoichiometric ratio in their crystal lattices where the molecules/species are assembled through noncovalent interactions. <sup>24</sup> Pharmaceutical salts are formed when proton transfer takes place between API and coformer. Formation of cocrystal or salt depends on  $\Delta p K_a$  value of the components and it can be predicted based on the  $\Delta p K_a$  value such as- for  $\Delta p K_a > 3$  and  $\Delta p K_a < 0$ , the expected products are salt and cocrystal respectively whereas for  $\Delta p K_a$  value between 0 and 3, the product may be salt or cocrystal or mixed-ionic complex.<sup>25-27</sup> GRAS (Generally Regarded as Safe) coformers are used in the syntheses of pharmaceutical cocrystals. The cocrystallization techniques widely used include solvent evaporation<sup>28</sup>, antisolvent method<sup>29</sup>, cooling crystallization<sup>30</sup>, slurry conversion<sup>31</sup>, liquid-assisted grinding<sup>32</sup> and melting crystallization <sup>33</sup>. Recent approval of some pharmaceutical cocrystals such as Suglat<sup>34</sup>, Entresto <sup>35</sup> Steglatro<sup>36</sup> explicitly reveals the importance and usefulness of pharmaceutical cocrystals in the quality improvement of drug products. Plenty of literature reports have delineated

about improvement of solubility or physicochemical properties of low water-soluble drugs via formation of pharmaceutical cocrystals and organic salts.<sup>37-42</sup>

Scheme 4.1: Molecular structures and acronyms of Pimozide and coformers.

Pharmaceutical cocrystal of PMZ has not been reported to date. Few attempts have been made to improve solubility of PMZ using other formulation strategies. Manohari and coworkers prepared self-micro emulsifying drug delivery system (SMEDDS) formulation of PMZ to improve its solubility or dissolution using Capmul MCM NF as oily phase, Cremophor RH 40 as Surfactant and PEG-8000 as Co-Surfactant.<sup>43</sup> Further, Bera et al. attempted to ameliorate the solubility of PMZ by synthesizing binary (PMZ and β-cyclodextrin) and ternary (PMZ, β-cyclodextrin and polyvinylpyrrolidone (PVP-K30)) inclusion complexes, and from the solubility studies, it was revealed that the ternary inclusion complex had better efficiency to enhance the solubility compared to the binary inclusion complex.<sup>44</sup> A Cambridge Structural Database (CSD) search of PMZ displayed one structure of PMZ-perchlorate.<sup>45</sup> In this study, our aim was to improve solubility as well as permeability of PMZ through formation of pharmaceutical cocrystals or salts using various coformers. Cocrystal/salt screening study of PMZ resulted in the formation of five crystalline organic salts with the following coformers- adipic acid, fumaric acid, succinic acid, oxalic acid and glutaric acid. These novel salts were characterized by spectral, thermal, diffractive techniques. Further we studied the solubility, dissolution and permeability through franz diffusion were explained in these chapter.

## **4.2 Results and Discussion**

PMZ is a weak basic molecule at the piperazine N atom and its calculated (Marvin Sketch) acid dissociation constant pKa is 7.32. A summary of the experimental methods and crystallization conditions are given in the section 4.10.1 and the coformers are shown in Scheme 4.1 and  $\Delta$ pKa values listed in Table 4.5. The five binary salts PMZ-GA (1:1), PMZ-AA (1:1), PMZ-SA (1:1), PMZ-OA (1:1) and PMZ-FA (1:1) were characterized by spectroscopic, thermal, and powder X-ray diffraction techniques. All of these solids' crystal structures are characterized by single crystal X-ray diffraction and selected crystal data, data collection and refinement parameters are summarized in Table 4.1 hydrogen bonds are listed in Table 4.2. The solubility, *invitro* dissolution measurements and permeability studies were carried out for these novel complexes and the results were compared with the pristine PMZ compound.

**Table 4.1** Single crystal X-ray diffraction and crystallographic table of PMZ salts.

Table 4.1 Single crys	PMZ-AA	PMZ-FA	PMZ-SA	PMZ-OA	PMZ-GA
Empirical Formula	C <sub>28</sub> H <sub>29</sub> F <sub>2</sub> N <sub>3</sub> O	$C_{28}H_{30}F_2N_3O$	C <sub>28</sub> H <sub>30</sub> F <sub>2</sub> N <sub>3</sub> O	$C_{28}H_{30}F_2N_3O$	C <sub>28</sub> H <sub>30</sub> F <sub>2</sub> N <sub>3</sub> O
Formula weight	534.61	520.59	520.59	551.58	629.69
Crystal System	Monoclinic	Monoclinic	Monoclinic	Triclinic	Triclinic
Space Group	P 21/n	P 21/n	P 21/n	P-1	P-1
T (K)	293 K	293 K	293 K	293 K	293 K
a (Å)	11.744(2)	10.345(2)	10.357(2)	8.2872(19)	10.992(3)
<b>b</b> (Å)	18.703(4)	17.804(4)	17.697(5)	11.143(3)	12.562(3)
c (Å)	12.064(2)	14.032(3)	14.054(4)	15.787(3)	12.562(3)
α (°)	90	90	90	102.946(10)	94.411(10)
<b>β</b> (°)	96.433(6)	93.209(10)	93.211(10)	92.93(1)	105.349(10)
γ(°)	90	90	90	108.024(1)	106.955(9)
$V(\mathring{ m A}^3)$	2633.2(8)	2580.4(9)	2571.9(11)	1339.6(6)	1577.5(7)
$D_{\rm calc}({ m g~cm^{-3}})$	1.349	1.340	1.344	1.367	1.326
Z	4	4	4	2	2
Rflns. collect	12778	14553	13842	10204	5544
Unique rflns.	12733	14477	13804	10152	5507
Obsd. rflns.	9539	11510	8571	7905	4781
Parameters	464	496	502	479	425
$R_1$	0.0609	0.0438	0.0599	0.0565	0.0790
$w\mathbf{R}_2$	0.1814	0.1328	0.1467	0.1537	0.2332
Goodness of fit	1.105	1.102	1.047	1.085	1.076
X-ray diffractometer	Bruker APEX2	Bruker APEX2	Bruker APEX2	Rigaku OD	Bruker APEX2

**Table 4.2** Selected geometric parameters of hydrogen bonds in PMZ salts.

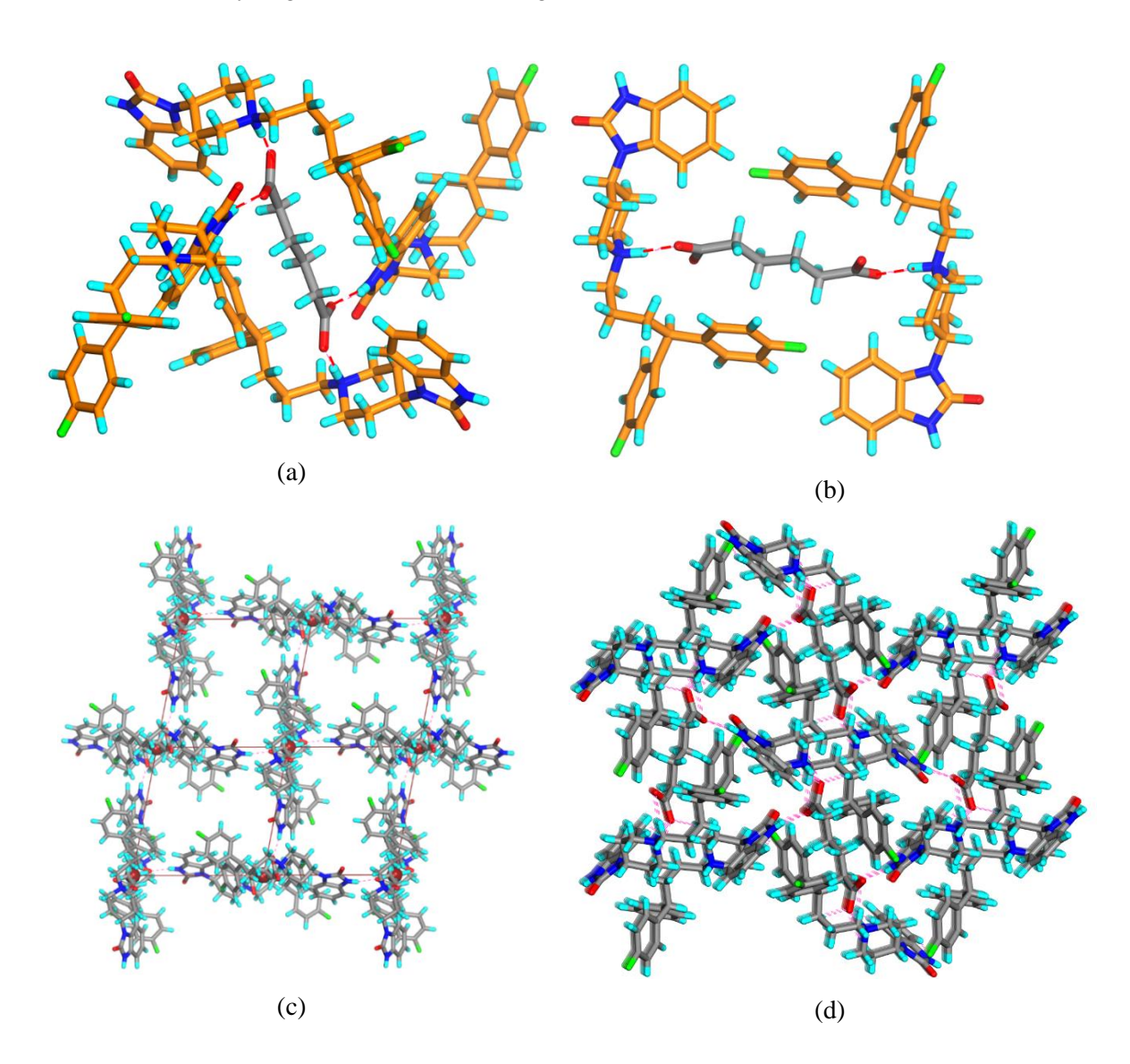
Table 4.2 Selected geometric parameters of hydrogen bonds in PMZ salts.					
D–H···A	D…A (Å)	H…A (Å)	D-H···A (°)	symmetry code	
PMZ-AA (1:0.5)					
O1–HA···O5	2.670(4)	1.86	171	1/2-x,3/2-y,1-z	
O2–H2···N5	3.382(3)	2.60	159	1/2-x,3/2-y,1-z	
N5-H5A···O1	3.048(3)	2.23	158	1/2-x,3/2-y,1-z	
N5-H5B···O6	2.952(3)	2.08	168	-x,1-y,1-z	
		PMZ-FA (1:0.5)			
O1-H1A···O5	2.642(3)	1.77	171	3/2-x,1/2+y,1/2-z	
O2-H2A···O1	2.673(3)	2.23	105	Intra	
O2-H2A···N4	2.708(3)	1.76	156	2-x,1-y,-z	
N5-H5A···O6	2.952(3)	2.09	172	1-x,-y,-z	
N5-H5B···N2	3.141(3)	2.24	161	3/2-x,-1/2+y,1/2-z	
C7-H7···O4	3.261(3)	2.45	146	1-x,1-y,-z	
C15-H15···O1	3.010(3)	2.37	125	2-x,1-y,-z	
		PMZ-SA (1:0.5)	)		
O1-H1A···O8	2.5594(1)	1.75	169	x,1+y,z	
O2-H2A···O1	2.6092(1)	2.13	117	Intra	
O2-H2A···N6	3.3427(1)	2.54	167	1+x,1+y,z	
N6-H6A···O1	2.8720(1)	1.98	171	-1+x,-1+y,z	
O8-H8A···O5	2.7353(1)	1.94	176	xyz	
O8-H8B···O7	2.7548(1)	1.89	164	1+x,y,z	
C4-H4···O6	3.3117(1)	2.44	155	x,-1+y,z	
С7-Н7…О6	3.3814(1)	2.52	154	x,-1+y,z	
C20-H20A···O8	3.5311(1)	2.59	166	-1+x,1+y,z	
C21-H21A···N7	2.9388(1)	2.50	108	Intra	
		PMZ-OA (1:1)			
O1-H1A···N4	2.665(11)	1.93	150	3/2+x,1-y,1/2+z	
O2-H2A···N4	3.092(13)	2.29	168	3/2+x,1-y,1/2+z	
N6-H6A···O5	2.927(12)	2.17	146	1+x,y,z	
N6-H6B···O3	3.085(13)	2.29	155	x,y,-1+z	
C17-H17···O1	3.293(14)	2.51	142	-1+x,y,z	
C18-H18···O6	3.403(14)	2.51	161	-1/2+x,1-y,1/2+z	
O2-H2A···O6	2.707(11)	2.21	116	1+x,y,1+z	
		PMZ-GA-2H <sub>2</sub> O (1:	1:2)		
O1-H1A···N4	2.665(11)	1.93	150	3/2+x,1-y,1/2+z	
O2-H2A···N4	3.092(13)	2.29	168	3/2+x,1-y,1/2+z	
N6-H6A···O5	2.927(12)	2.17	146	1+x,y,z	
N6-H6B···O3	3.085(13)	2.29	155	x,y,-1+z	
C17-H17···O1	3.293(14)	2.51	142	-1+x,y,z	
C18-H18···O6	3.403(14)	2.51	161	-1/2+x,1-y,1/2+z	
O2-H2A···O6	2.707(11)	2.21	116	1+x,y,1+z	
O1-H1A···N4	2.665(11)	1.93	150	3/2+x,1-y,1/2+z	

# **4.3** Crystal Structure Analysis

# Pimozide-Adipic acid (PMZ-AA, 1:0.5) Salt:

PMZ-AA salt which crystallizes in  $P2_1$ /n space group. Its asymmetric unit is constituted by one unit of protonated PMZ at the piperazine N and half unit of adipate ion. Each adipate ion is connected with

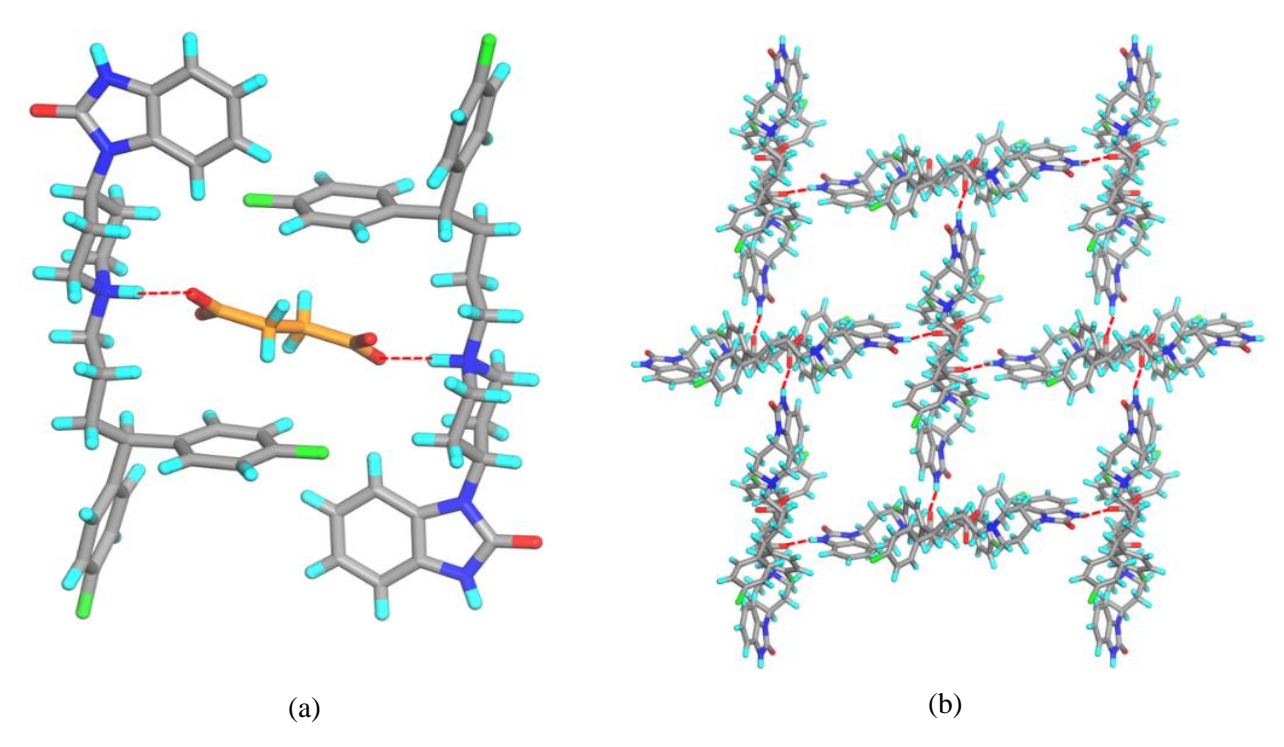
four PMZ cation through –N+H... OOC- interactions and charge-assisted –N-H... OOC- hydrogen bonding (Figure 4.1a). Among four PMZ ions connected to a same adipate ion, two are found to be connected with the adipate ion in such a way that these two PMZ ions act as molecular tweezers to encapsulate the adipate ion (Figure 4.1b). Here, the other two PMZ units also act as molecular clips to encapsulate an adipate ion remaining almost perpendicular from the plane of that adipate and those PMZ molecular clips. So, two consecutive pairs of PMZ tweezers containing adipate ions remain in perpendicular to each other. Each of the unit [(PMZ)<sub>2</sub>(AA)] i.e. a pair of PMZ clips with an encapsulated adipate ion is connected with four such type of units through charge-assisted N-H...-OOC- hydrogen bonding which leads to the formation of hydrogen-bonded two-dimensional square grid type (4,4-connected) network (Figure 4.1c). If we consider AA as a node and connect these nodes according to the hydrogen bonding interactions of the protonated PMZ ions, then we can obtain the simplified view of the 2D square grid network. F atoms of PMZ units are found to be involved in C-H...F weak hydrogen bonding interaction with other PMZ units leading to the extension of the above-mentioned 2D network to 3D hydrogen bonded network (Figure 4.1d).



**Figure 4.1:** Illustrations for the crystal structure of PMZ-AA: (a) Hydrogen bonding of one adipate dianion surrounded by four PMZ cations through  $-N^+H\cdots^-OOC^-$  interactions, (b) PMZ molecular tweezers to encapsulate the adipate ion, (c) Formation of 2D rhomboid grid type network via charge-assisted N-H····OOC- hydrogen bond between PMZ cation and adipate di-anion, (d) 3D hydrogen bonded network.

# Pimozide-Succinic acid (PMZ-SA, 1:0.5) Salt:

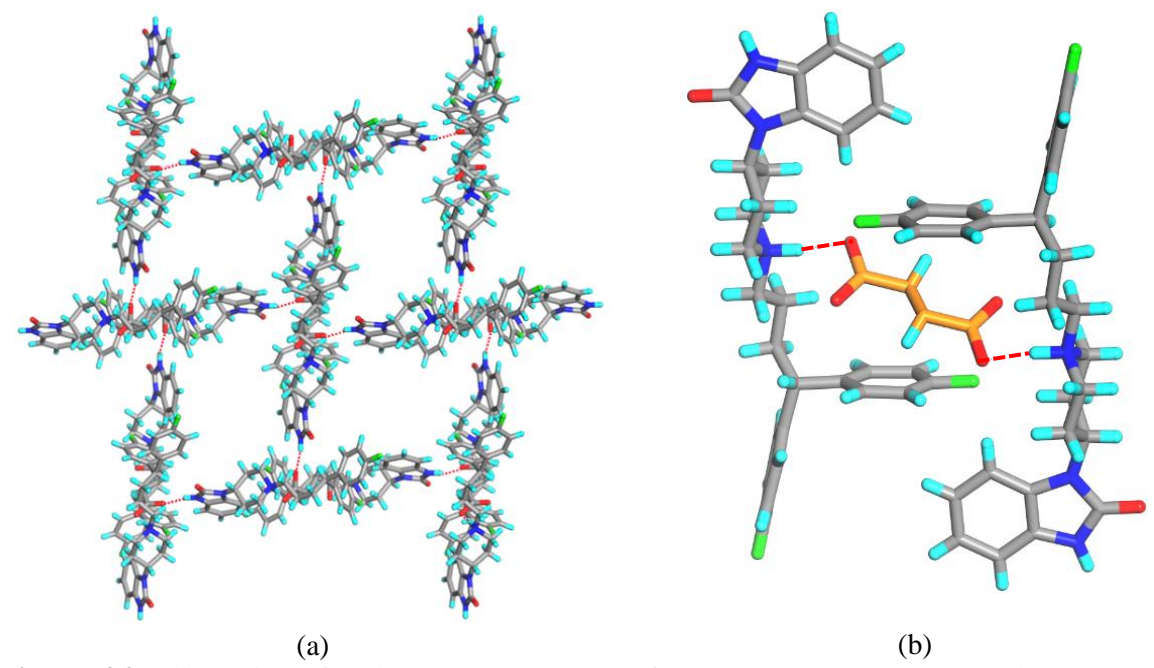
The salt of PMZ and SA crystallizes in  $P2_1$ /n space group and its asymmetric unit comprises one unit of protonated PMZ and half unit of succinate (Figure 4.2a). Like the PMZ-AA salt previous complex, in this complex also, the PMZ ions act as molecular tweezers to encapsulate the succinate ions and the hydrogen bonded networks (2D square grid network) are isostructural with that of PMZ-AA salt (Figure 4.2b).



**Figure 4.2:** Illustrations for the crystal structure of PMZ-SA: (a) PMZ molecular tweezers to encapsulate the succinate ion; (b) hydrogen bonded 2D rhomboid grid network.

#### Pimozide- Fumaric acid (PMZ-FA, 1:0.5) Salt:

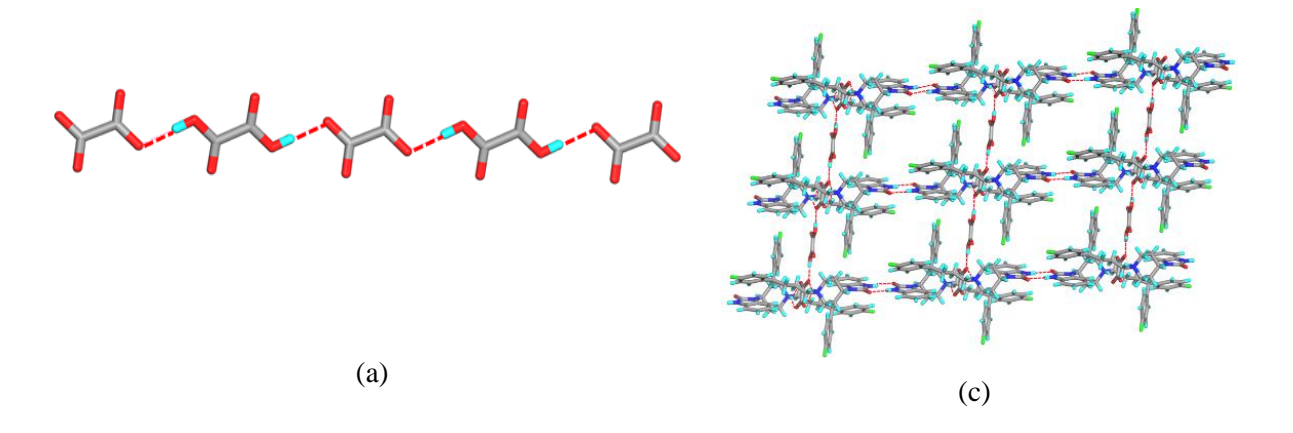
This complex crystallizes in  $P2_1$ /n space group and its asymmetric unit is composed of one-unit protonated PMZ and half unit of fumarate ion. In terms of hydrogen bonded networks, this complex is isostructural with the previously mentioned two complexes PMZ-AA and PMZ-SA (Figure 4.3a & b).



**Figure 4.3:** Illustrations for the crystal structure of PMZ-FA: (a) PMZ molecular tweezers to encapsulate the fumarate ion; (b) hydrogen bonded 2D rhomboid grid network.

## Pimozide-Oxalic acid (PMZ-OA, 1:1) Salt:

PMZ-OA crystallizes in *P*-1 space group and its asymmetric unit is constituted by one unit of protonated PMZ and half unit each of oxalic acid and oxalate ion. Crystal structure analysis reveals that oxalic acid and oxalate ions form one dimensional hydrogen bonded chain along y-axis through charge-assisted O-H... OOC- hydrogen bonding interactions (Figure 4.4a). From these 1D chains formed by the coformer protonated PMZ ions remain as pendant via bifurcated N+-H...-OOC- interactions. These 1D chains containing the pendant are further connected to each other through hydrogen-bonded amide-amide homosynthon (Figure 4.4b) which leads to the formation of 2D hydrogen-bonded rectangular grid type layered network along yz-plane (Figure 4.4c). Among PMZ ions, C-H...F hydrogen bonds are observed where these interactions play pivotal role towards the formation of 3D hydrogen-bonded network (Figure 4.4.e).



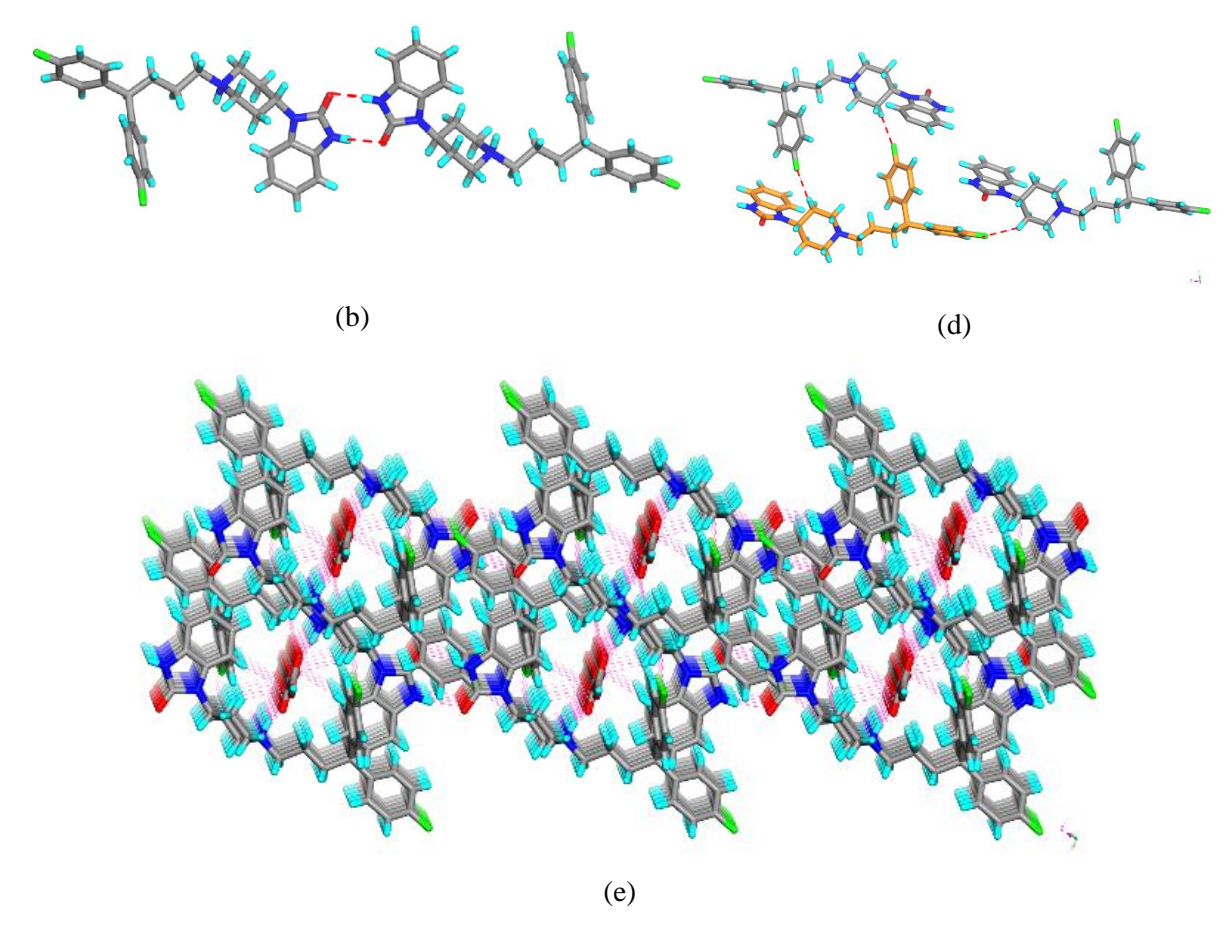


**Figure 4.4:** Illustrations for the crystal structure of PMZ-OA: (a) 1D linear chain formed by hydrogen bonding between oxalic acid and oxalate ion; (b) hydrogen-bonded amide-amide dimer; (c) 2D rectangular grid type layered network; (d) C-H...F hydrogen bonds between PMZ units; (e) Hydrogen-bonded 3D network shown along b-axis.

## Pimozide-Glutaric acid Salt Hydrate (PMZ-GA-2H<sub>2</sub>O, 1:1:2):

PMZ-GA crystallizes in P-1 space group and its asymmetric unit is composed of one unit each of protonated PMZ, singly deprotonated glutaric acid and two water molecules. Each PMZ ion is connected with two GA via –N+H...·OOC- interactions (between trialkyl ammonium cation of PMZ and carboxylate of GA) and charge-assisted –N-H...·OOC- hydrogen bonding (between imidazole N-H of PMZ and carboxylate of GA), and one water molecule via O-H...O hydrogen bonding (between O-H of water and –C=O of PMZ) (Figure 4.5a). Each singly deprotonated glutaric acid is connected with two PMZ ions and two water molecules (Figure 4.5b). PMZ and GA form a one-dimensional chain where the components themselves remain in translational symmetry (Figure 4.5c). These 1D chains are further connected to each other through water bridging leading to the construction of 2D hydrogen-bonded layered network (Figure 4.5d). Here, the two crystallographically independent water molecules remain as a dimer through O-H...O hydrogen bonding. Each water dimer is connected to three 1D chains (formed by PMZ and singly deprotonated GA) via O-H...O and charge-assisted O-H...·OOC-

hydrogen bonding (Figure 4.5e). F-atoms of PMZ are found to be involved in C-H...F weak hydrogen bonding as well as C-F... $\pi$  interactions (Figure 4.5f).

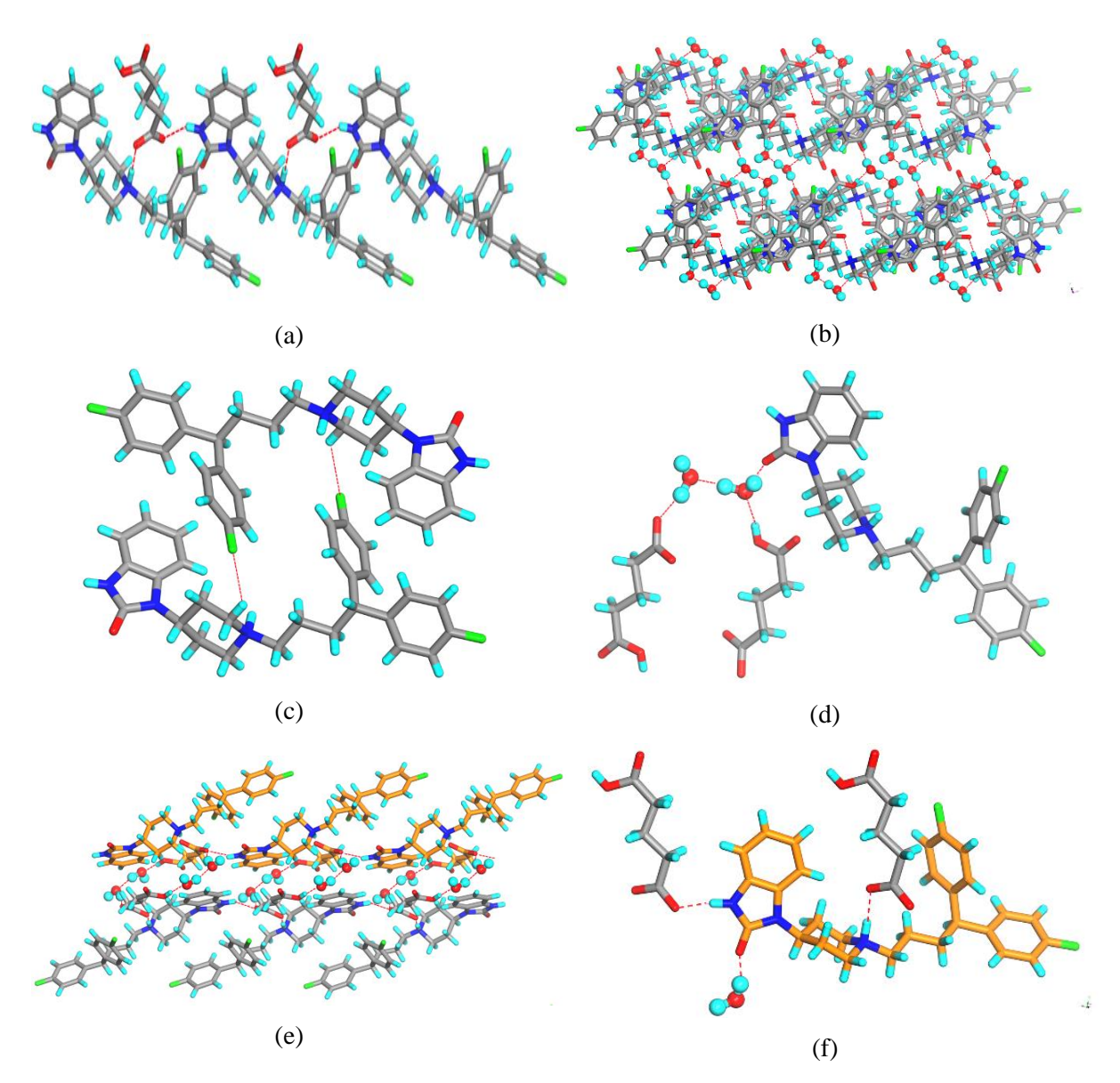


**Figure 4.5:** Illustrations for the crystal structure of PMZ-GA-HYD: Hydrogen bonding of (a) PMZ and (b) GA; (c) 1D chain formed by PMZ and GA; (d) 2D layered network formed via water bridging; (e) hydrogen bonding of water dimer; (f) C-H···F interactions between PMZ units.

## **4.4 FT-IR Spectroscopy**

The hydrogen bonding patterns of a molecule are found to be changed after formation of a salt, which in turn changes the vibrational modes of the associated functional groups, and the IR frequencies (Figure-4.6a-d).<sup>3</sup> It is possible to study supramolecular synthons of hydrogen bonded dimer or catemer motifs of acids or amides and ions by IR spectroscopy.<sup>4</sup> The changes in IR frequencies correlate with hydrogen bond synthons in the crystal structures. -C=O, O-H/N-H and aliphatic/aromatic C-H

stretching frequencies of PMZ and the coformers are found to be shifted after complex formation due to strong or weak hydrogen bonds or intermolecular interactions (Table 4.3).

**Table 4.3** IR stretching frequencies of PMZ/coformer in the crystalline forms (Figure 4.6a-e).

Compound	CO(NHR)(NR2), $COOH, COO^{-}$ $(v_{C=0}, cm^{-1})$	OH, NH ( v <sub>NH/OH</sub> , cm <sup>-1</sup> )	Aliphatic and aromatic CH (v <sub>CH</sub> , cm <sup>-1</sup> )
PMZ	1689	3361	2936
AA	1693		3037, 2963
PMZ-AA	1692		3149, 2956
SA	1731, 1693		3047, 2932
PMZ-SA	1695	3376	3140, 3098
FA	1695		3084, 3000
PMZ-FA	1694		3135, 3097
OA	1666	3476, 3423	3023, 2968
PMZ-OA	1693, 1624		3131, 3039
GA	1697		3045, 2955
PMZ-GA-2H <sub>2</sub> O	1693, 1623		3147, 3058, 2983

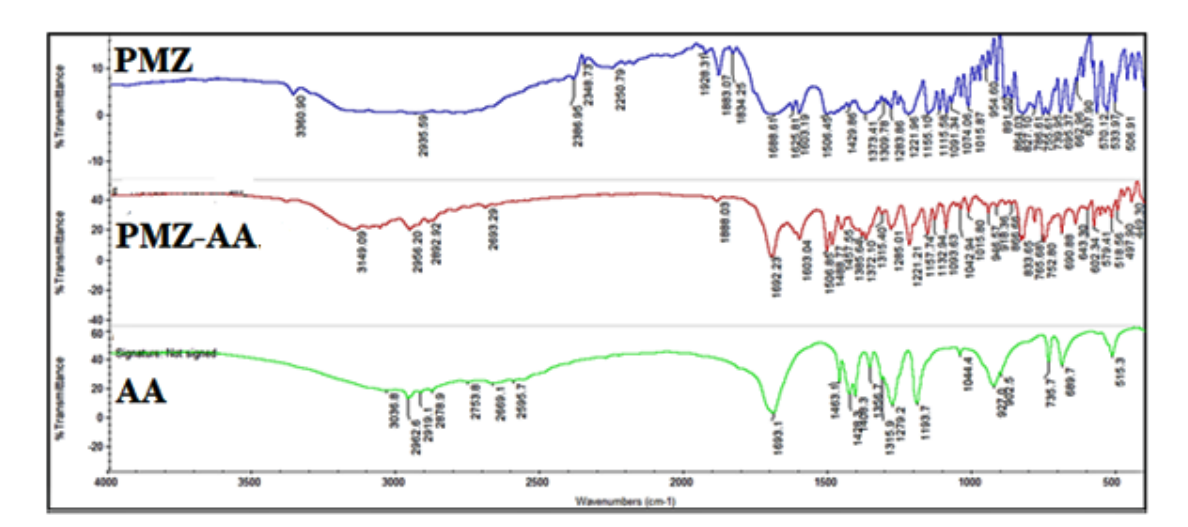
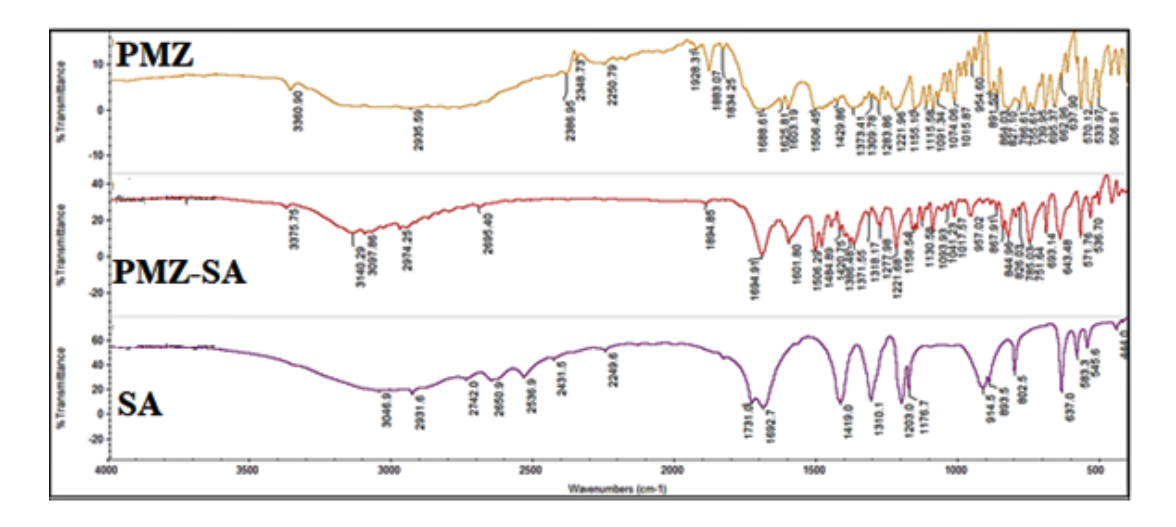


Figure 4.6a: Overlay of PMZ-AA Salts IR spectra with its starting components.



**Figure 4.6b:** Overlay of PMZ-SA Salts IR spectra with its starting components.

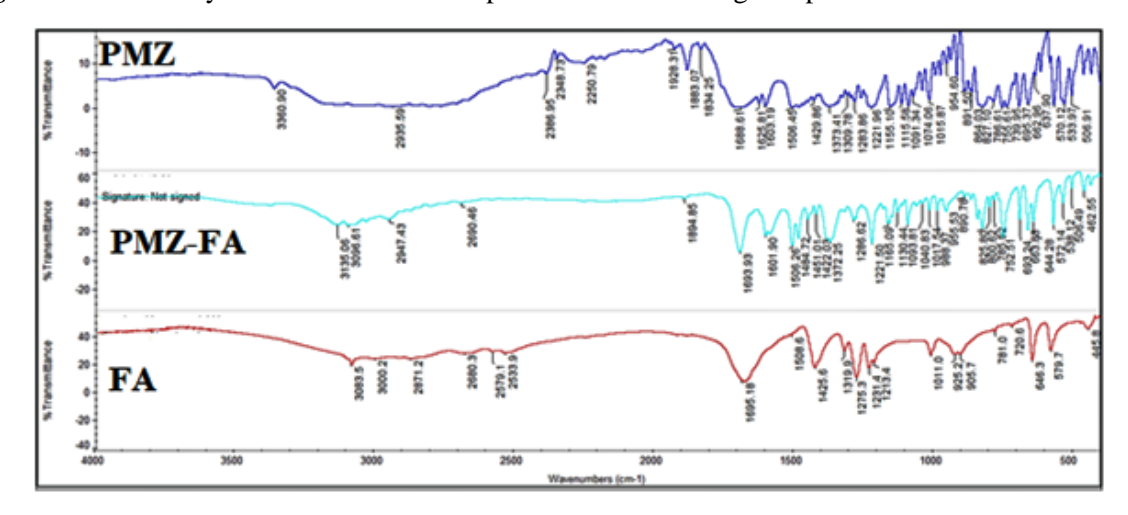


Figure 4.6c: Overlay of PMZ-FA Salts IR spectra with its starting components.

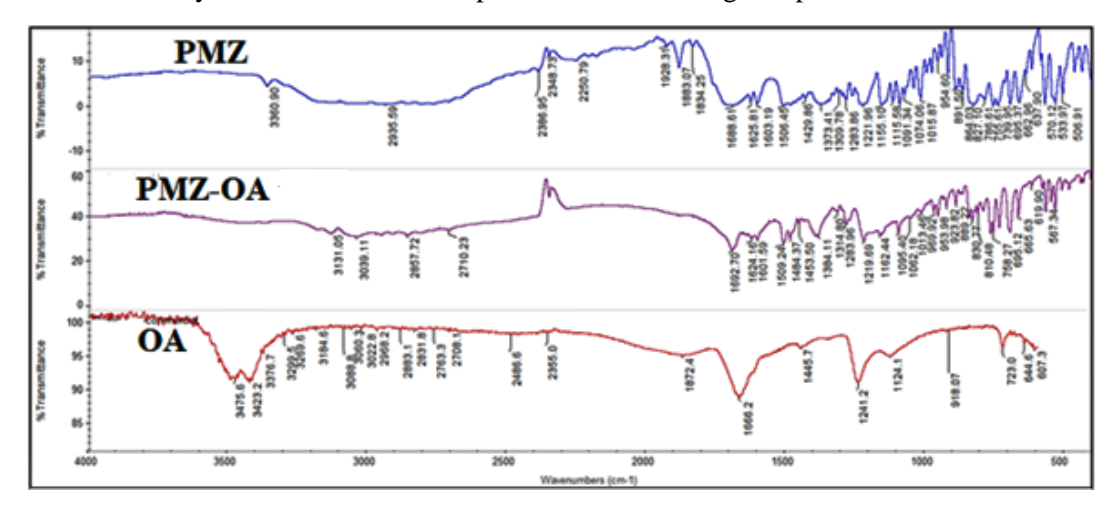
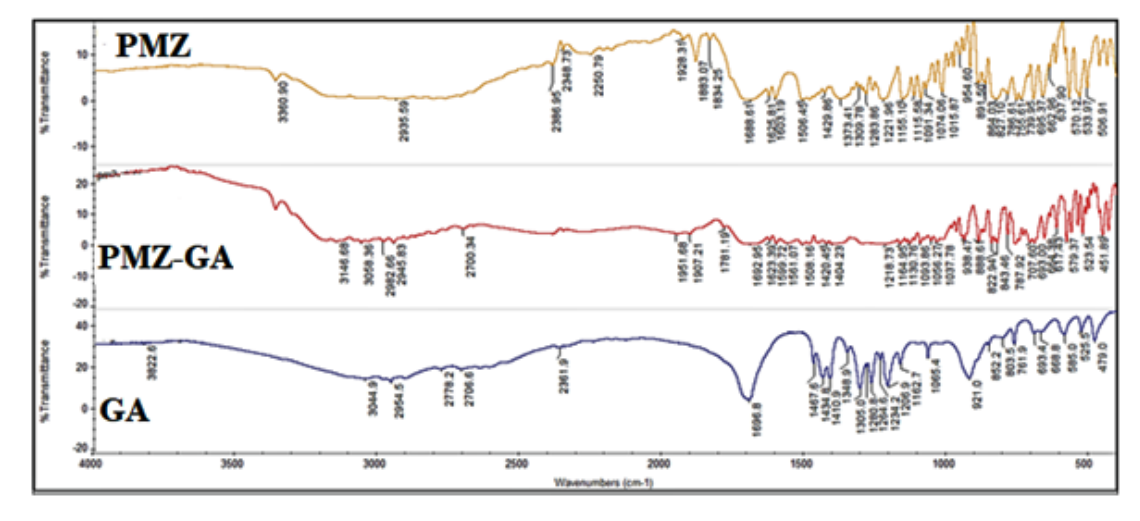


Figure 4.6d: Overlay of PMZ-OA Salts IR spectra with its starting components.



**Figure 4.6e:** Overlay of PMZ-GA Salts IR spectra with its starting components.

# 4.5 Powder X-ray Diffraction

It is needless to say that PXRD is an indispensable characterization technique in the field of pharmaceutical materials for examining generation of new phase, bulk-phase purity and homogeneity, and in some cases, for determining structures. Solvent-assisted mechano-ground materials composed of the API (PMZ) and the coformers containing carboxylic acid functionalities are found to exhibit new PXRD patterns indicating the formation of new phase. Further, simulated PXRD pattern for the single crystals of the cocrystals and salts of PMZ completely matches with the experimental PXRD pattern (for powdered material of the synthesized crystals) and the solvent-assisted mechano-ground material as well which clearly ensures bulk phase purity of the synthesized materials. PXRD lines of the five Salts exhibited excellent match by using PCW Software<sup>46</sup> of the experimental pattern with the calculated lines from the X-ray crystal structure (Figure 4.7).

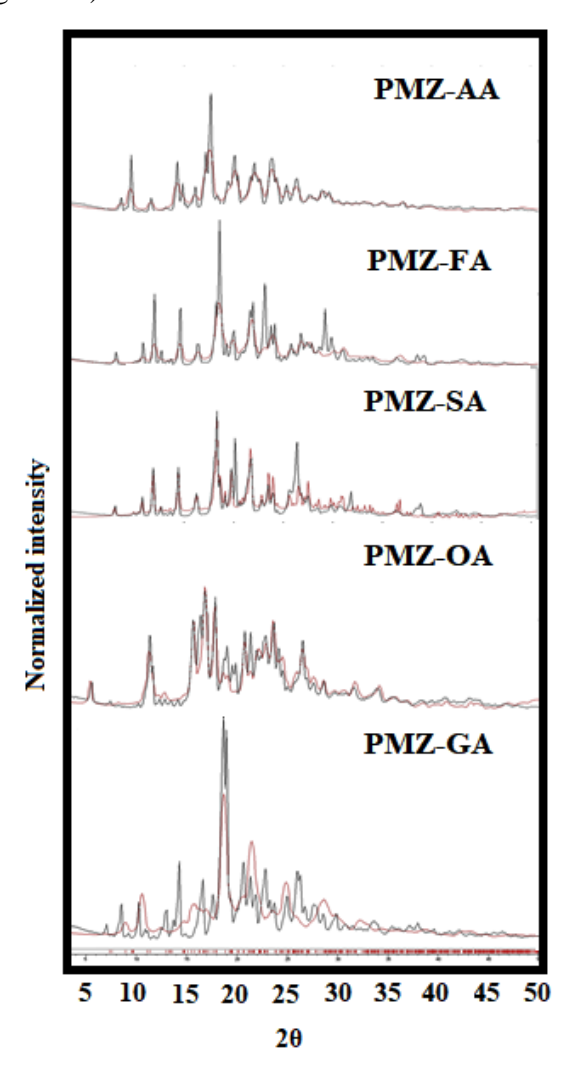


**Figure 4.7:** Overlay of experimental PXRD patterns of PMZ Salts (black) shows excellent match with the calculated line profile from the X-ray crystal structure (red), indicating bulk purity and phase homogeneity.

## **4.6 Differential Scanning Calorimetry**

In order to delineate thermal behaviour, DSC studies were carried out for the synthesized binary crystalline salts, and API and coformers as well. In DSC thermograms, it is observed that each of the complexes exhibit single endothermic peak which ensures that apart from melting, other phase transformations do not take place (Figure 4.8). Among the five binary complexes, PMZ-GA, PMZ-AA, PMZ-SA and PMZ-FA have melting points at 189, 194, 216 and 216 °C respectively which are in between the melting points of the API (218 °C) and the coformers (98, 151, 188 and 287 °C for GA, AA, SA and FA respectively). Whereas in case of PMZ-OA complex, melting temperature (254 °C) is found higher than melting temperature of API (218 °C) and the coformer (189.5 °C) as well (Table 4.4). This could be attributed to the strong hydrogen bonding interactions such as bifurcated –N<sup>+</sup>-H... OOC- interaction between API and the coformer observed this complex.

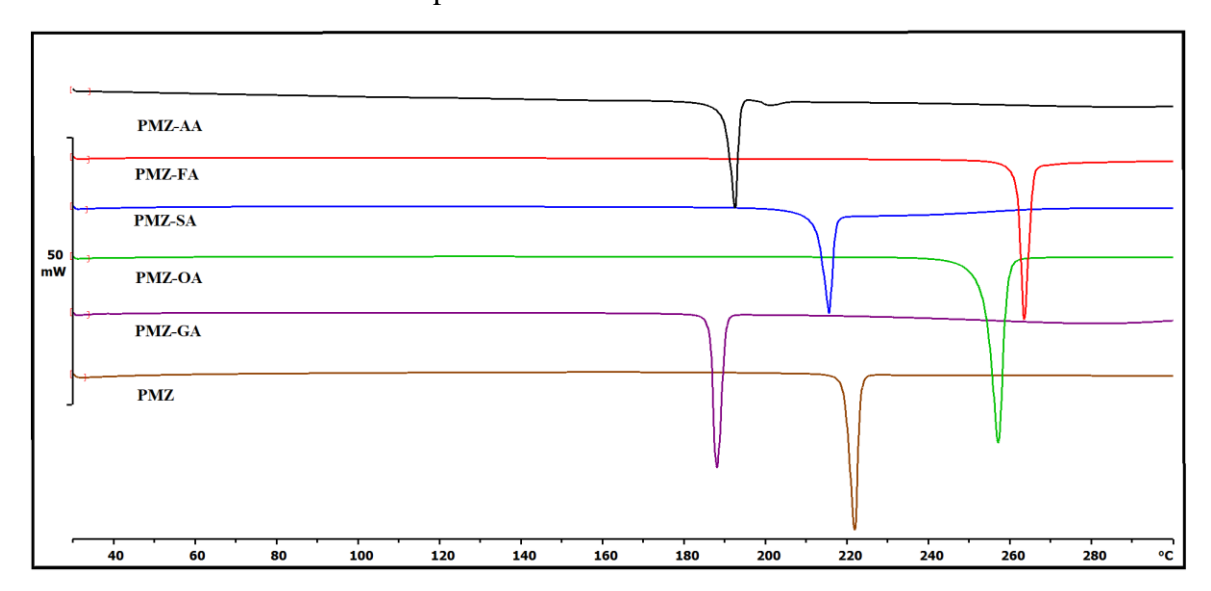


**Figure 4.8:** Overlay of DSC thermograms of PMZ and Salts showing their unique melting behaviour and sharp endotherms.

Table 4.4: Melting point of PMZ, Salts and coformers.

	PMZ/Salts	m.p. (°C)	Coformer	m.p. (°C)
1	PMZ-AA (1:0.5)	189-193	AA	151-154
2	PMZ-FA (1:0.5)	261-265	FA	287-288
3	PMZ-SA (1:0.5)	212-217	SA	184-190
4	PMZ-OA (1:1)	252-258	OA	102-103
5	PMZ-GA-2H <sub>2</sub> O (1:1:2)	186-189	GA	95-98
6	PMZ	218-223		

## 4.7 Solubility and dissolution

Solubility is a thermodynamic factor that usually taken as the concentration of the solute at 24h after mixing in a solvent. Dissolution rate studies rely on the supersaturation phenomenon that is the peak concentration of the drug delivered through a suitable carrier in a short period of time depending on the stability of the drug form being tested. Significantly, solubility and dissolution rate were influenced mainly strength of crystal lattice and solvation of components in salts or cocrystals. Therefore, these two factors can control the salt/cocrystal solubility in the media. The PMZ and its salts equilibrium solubility and dissolution rates were measured in PBS medium at 37°C and quantified the concentration of the drug through high performance liquid chromatography (HPLC). The initial drug form during the course of the equilibrium solubility test conditions at 0 h, and the later phase stability after 24 h at the end of the experiment, has been verified independently by PXRD (Figure 4.10). It has been found that in PBS media PMZ and its binary salts PMZ-AA, PMZ-SA and PMZ-FA are showed phase stability and others such as PMZ-GA, and PMZ-OA were unstable.

Then IDR measurements were performed for 8h at the rate of 100 rpm at 37 °C. The dissolution rate advantage is moderate (about two-fold faster in pH-7). Ever since there is indication of the salt stability for extended periods of time up to 8h, the dissolution measurement at chosen time points can be used as a reference to estimate the higher aqueous exposure of salts compared with the pure drug PMZ. The dissolution rate from the linear graph region of the IDR curve is presented in figure 4.9. During dissolution, all binary solid forms exhibited study state increase over 8h than pure PMZ and the dissolution order in PBS as follows, PMZ-SA>PMZ-GA>PMZ-AA>PMZ-OA>PMZ-FA>PMZ and the PXRD analysis of post dissolution were presented in figure 4.11. The improved solubility and dissolution rate of new solid forms are attributed to N<sup>+</sup>H... OOC charge assisted bond in case of all salts. In addition, coformer solubility too played significant role for improving new solid form solubility. Potentially, among phase stability new solids, the aliphatic coformers derivatives PMZ-SA, PMZ-GA, PMZ-AA, PMZ-OA and PMZ-FA salt form show the enhanced dissolution rate than its pure PMZ.

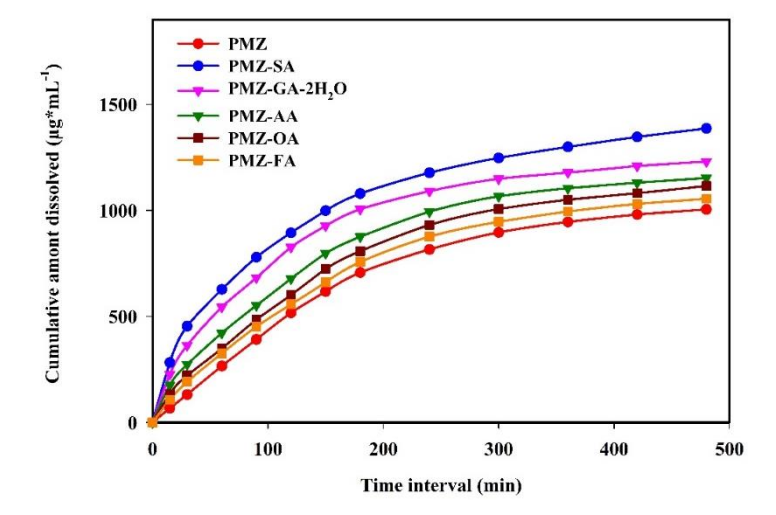
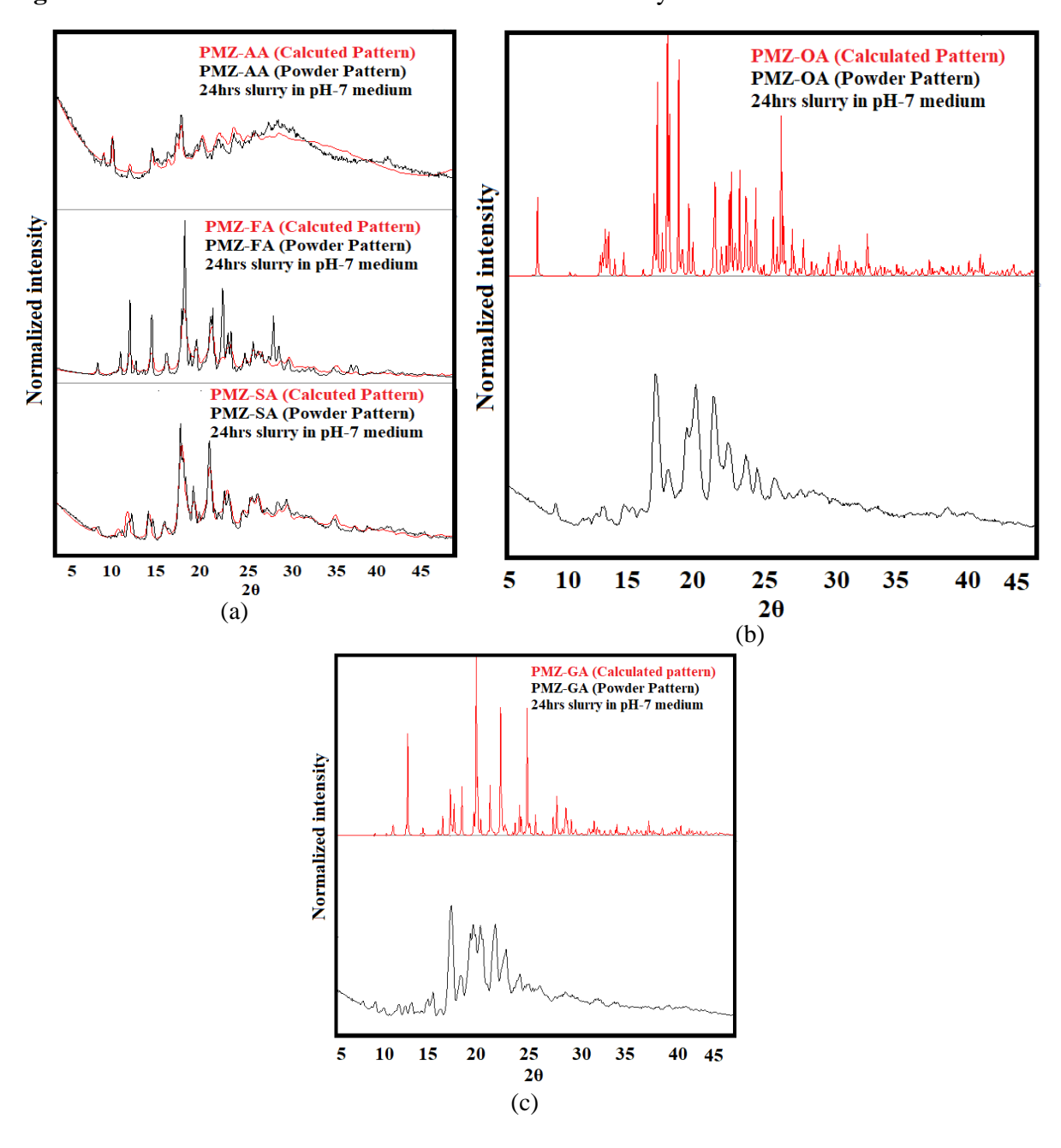
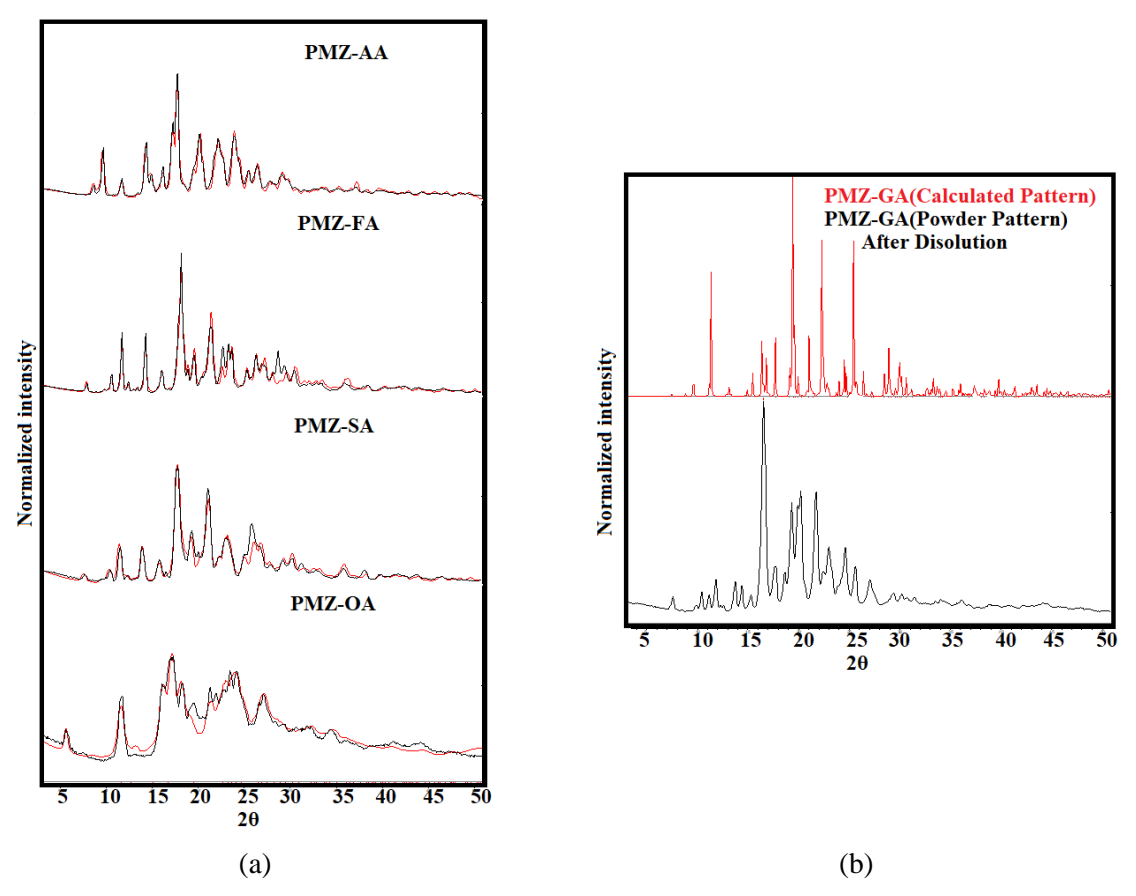


Figure 4.9: Intrinsic dissolution rates of PMZ and its binary salts in PBS medium.



**Figure 4.10:** (a) PXRD patterns of PMZ-AA, PMZ-FA and PMZ-SA at the end of equilibrium solubility experiment (24 h, black) in phosphate buffer (pH 7) media match with the calculated PXRD patterns of PMZ-AA, PMZ-FA and PMZ-SA (red) indicating phase stability. (b) and (C) PXRD patterns of PMZ-OA and PMZ-GA at the end of equilibrium solubility experiment (24 h, black) in phosphate buffer (pH 7) media don't match with the calculated XRD pattern of PMZ-OA and PMZ-GA.



**Figure 4.11:** (a) PXRD patterns of PMZ-AA, PMZ-FA, PMZ-SA and PMZ-OA at the end of dissolution experiment (black) match with the calculated PXRD patterns of PMZ-AA, PMZ-FA, PMZ-SA and PMZ-OA (red) indicating phase stability. (b) PXRD pattern of PMZ-GA at the end of dissolution experiment (black) does not match with the calculated PXRD pattern of PMZ-GA (red) indicating mixture of salts and dissociated physical mixture.

#### 4.8 Diffusion

The diffusion behavior of salts of PMZ were studied using a Franz diffusion cell which gives a relative idea of permeation property. Usually, any molecule whether the drug or the coformer will have a lag time which expresses the increasing rate of permeation through the membrane and diffusion into the receptor medium. This is reflected by a sharp peak which stabilizes once steady state diffusion is reached. Subsequently, there is a near constant profile of the permeation behavior across the membrane. The diffusion of salt of PMZ such as PMZ-SA, PMZ-GA, PMZ-AA, PMZ-OA and PMZ-FA were

carried out over 8 h. PMZ exists in neutral form in PBS media and exhibits less membrane permeability and flux rate due to poor solubility and dissolution rate. Contrastingly, PMZ salts are marginally better than the reference drug (Figure 4.12a). The succinate form of PMZ salt exhibit higher permeability than the rest of the salts displayed lower permeability. We expected that PMZ salts will show better flux rate than PMZ in PBS due to coformer permeation nature. From the (Figure 4.12b). it clearly indicates that dissolved for all the salts of PMZ drug availability or high drug concentration in donor compartment showed high flux rate to receiver compartment across the membrane which is ascribed to strong ionic N+H...\*OOC charge assisted bond drug-coformer hydrogen bonds. The enhanced flux rates of PMZ molecular salts describe the use of carboxylic acids as coformers for binary solids as a means to enhance dissolution rate and diffusion rate of poorly water-soluble drugs.

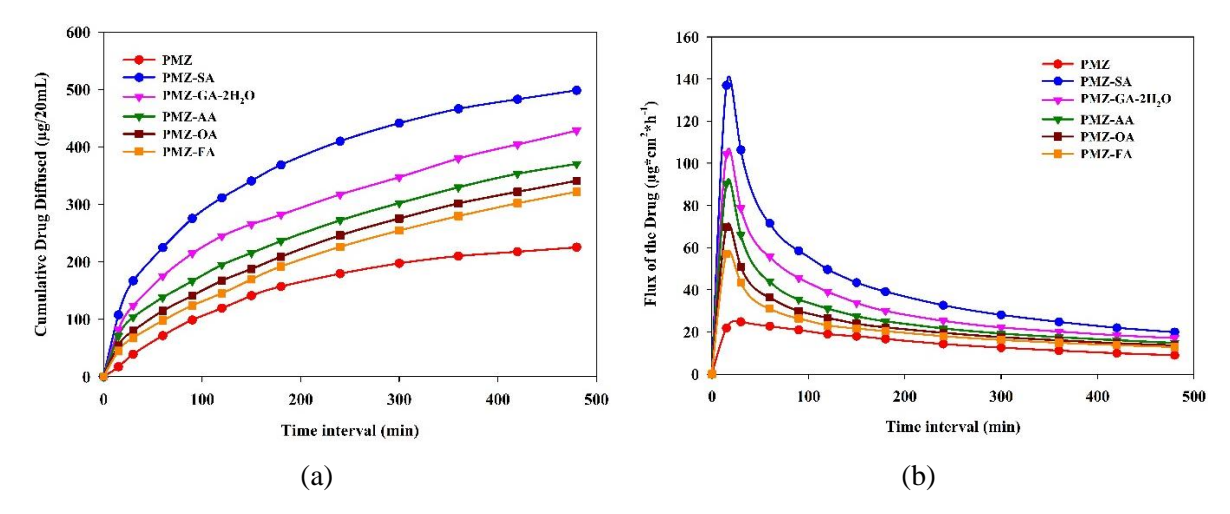


**Figure 4.12:** (a) Cumulative amount of PMZ Salts diffused vs. time. (b) Flux of PMZ and its salts vs. time.

## 4.9 Conclusions

The low solubility limitation of pure PMZ drug have been systematically improved through crystal engineering. Five new multi-component crystalline forms were synthesized, and their X-ray crystal structures confirmed by single crystal X-ray diffraction. Crystal structure analysis showed that the crystalline products exist as salts. NFPD piperazine cation and carboxylate counter anion are bonded through strong, ionic and charge assisted N<sup>+</sup>H... OOC bond hydrogen bonds in the crystal structure. The bulk phase purity of molecular salts was established by PXRD, IR and crystallinity was confirmed by DSC analysis. All the salts exhibited enhanced dissolution and permeability improvement than pure PMZ. Specifically, the pharmaceutically acceptable all coformer salts (GRAS) is a promising candidate with higher dissolution and permeability in oral drug formulation.

# **4.10 Experimental Section**

PMZ is a weak basic molecule and its calculated (Marvin Sketch) acid dissociation constant (pKa) is 7.32. The coformers are shown in Scheme 1 and  $\Delta$ pKa values listed in Table 2. The six binary salts PMZ-AA (1:1), PMZ-FA (1:1), PMZ-SA (1:1), PMZ-OA (1:1), and PMZ-GA-2H2O (1:1:2), and were characterized by spectroscopic, thermal, and powder X-ray diffraction techniques. All of these solids' crystal structures are characterized by single crystal X-ray diffraction and selected crystal data, data collection and refinement parameters are summarized in Table In vitro dissolution, solubility measurements and in vivo pharmacokinetics are also reported.

**Table 4.5:** ΔpK<sub>a</sub>values<sup>a</sup> of dicarboxylic acid coformers and PMZ drug.

APi/Coformers	1 <sup>st</sup> , 2 <sup>nd</sup> pK <sub>a</sub> in water	ΔpKa	Molecular complex
AA	4.43, 5.41	2.89	1:0.5 Salt
FA	3.03	4.29	1:0.5 Salt
SA	4.21	3.11	1:0.5 Salt
OA	1.46, 4.40	2.94	1:1 Salt
GA	4.34	2.98	1:1:2 Salt hydrate
PMZ	7.32		

 $<sup>^</sup>a$ pK<sub>a</sub>'s calculated using Marvin 5.10.1, 2012, ChemAxon, <u>http://www.chemaxon.com</u>. These values are closely matching with pK<sub>a</sub> values compiled by R. Williams.<sup>1</sup>

#### **4.10.1 Preparation of Salts:**

**Pimozide-Adipic acid (PMZ-ADP):** The cocrystal was obtained by grinding PMZ and ADP in 1:1 stoichiometry with a few drops of CH<sub>3</sub>OH added in a solvent-assisted method for 30 min. Single crystals were obtained by dissolving 40 mg of the ground product in 6 mL of methanol and left for slow evaporation over 4-5 days.

**Pimozide-Succinic acid (PMZ-SA):** This cocrystal was obtained by grinding PMZ and SA in 1:1 stoichiometry with a few drops of CH<sub>3</sub>OH added in a solvent-assisted method for 30 min. Single crystals were obtained by dissolving 40 mg of the ground product in 6 mL of methanol and left for slow evaporation over 4-5 days.

**Pimozide-Fumaric acid (PMZ-FA):** The cocrystal was obtained by grinding PMZ and FA in 1:1 stoichiometry with a few drops of CH<sub>3</sub>OH added in a solvent-assisted method for 30 min. Single crystals were obtained by dissolving 40 mg of the ground product in 6 mL of methanol and acetone (1:1 v/v, 6 mL) and left for slow evaporation over 4-5 days.

**Pimozide-Oxalic acid (PMZ-OA):** The cocrystal was obtained by grinding PMZ and OA in 1:1 stoichiometry with a few drops of water added in a solvent-assisted method for 30 min. Single crystals were obtained by dissolving 40 mg of the ground product in methanol and left for slow evaporation over 4-5 days.

**Pimozide- Glutaric acid (PMZ-GA-2H<sub>2</sub>O):** The cocrystal was obtained by grinding PMZ and GA in 1:1 stoichiometry with a few drops of CH<sub>3</sub>OH added in a solvent-assisted method for 30 min. Single crystals were obtained by dissolving 40 mg of the ground product in methanol and left for slow evaporation over 4-5 days.

## 4.10.2 Powder X-ray diffraction

Powder X-ray diffraction was recorded on Bruker D8 Advance diffractometer (Bruker-AXS, Karlsruhe, Germany) using Cu-K $\alpha$  X-radiation ( $\lambda$  = 1.5406 Å) at 40 kV and 30 mA power. X-ray diffraction patterns were collected over the 2 $\theta$  range 3–50° at a scan rate of 3.9°/min. Powder Cell 2.4<sup>47</sup> (Federal Institute of Materials Research and Testing, Berlin, Germany) was used for Rietveld refinement of experimental PXRD and calculated lines from the X-ray crystal structure.

## 4.10.3 Vibrational spectroscopy

Thermo-Nicolet 6700 FT-IR-NIR spectrometer with NXR FT-Raman module (Thermo Scientific, Waltham, MA) was used to record IR spectra. IR spectra were recorded on samples dispersed in KBr pellets. Data were analyzed using the Omnic software (Thermo Scientific, Waltham, MA).

# 4.10.4 Thermal analysis

DSC was performed on a Mettler Toledo DSC 822e module and TGA on a Mettler Toledo TGA/SDTA 851e module. The typical sample size is 3-5 mg for DSC and 5-12 mg for TGA. Samples were placed in sealed pin-pricked aluminum pans for DSC experiments and alumina pans for TGA experiments. A heating rate of 10 °C min<sup>-1</sup> in the temperature range 30-300 °C was applied. Samples were purged by a stream of dry nitrogen flowing at 80 mL min<sup>-1</sup> for DSC and 50 mL min<sup>-1</sup> for TGA.

#### 4.10.5 X-ray crystallography

X-ray reflections were collected on Bruker D8 QUEST, CCD diffractometer equipped with a graphite monochromator and Mo-K $\alpha$  fine-focus sealed tube ( $\lambda$  = 0.71073 Å) and reduction was performed using APEXII Software. Intensities were corrected for absorption using SADABS and the structure was solved and refined using SHELX97. All non-hydrogen atoms were refined anisotropically. Hydrogen atoms on hetero atoms were located from difference electron-density maps and all C–H hydrogen atoms were fixed geometrically. Hydrogen-bond geometries were determined in PLATON. Crystal parameters (Table 1) and hydrogen bond distances shown in Table 2 are neutron normalized to fix the D–H distance to its accurate neutron value in the X-ray crystal structures (O–H 0.983 Å, N–H 1.009 Å, and C–H 1.083 Å). X-Seed was used to prepare packing diagrams. Crystallographic cif files are available at www.ccdc.cam.ac.uk/data or as part of the Supporting Information

## 4.10.6 Solubility and Dissolution

In equilibrium solubility experiment for PMZ and its salts (pH 7, at 37 °C), concentration of PMZ was determined using HPLC technique at  $\lambda_{max}$  of 268 nm. With several known concentrations of PMZ, area under curve (AUC) vs concentration calibration curve was plotted. Unknown concentration of PMZ was calculated using the slope and intercept value of the standard curve. In order to measure the equilibrium solubility, an excess amount of each sample (i.e., pure PMZ and its salts) was added to 5 mL of pH 7 solution and stirred at 600 rpm using a magnetic stirrer at 37 °C  $\pm$  1 to make the solution saturated. After 24 h, the suspension was filtered through a Whatman 0.45  $\mu$ m syringe filter. The filtrate solution was used to calculate the equilibrium solubility from the area under curve (AUC) value plotted against the standard curve. The undissolved residues were air-dried and further characterized with PXRD.

Intrinsic dissolution rate (IDR) of PMZ and its salts were carried out on a USP certified Electro lab TDT-08L Dissolution Tester (Electro lab, Mumbai, MH, India). In intrinsic attachment unit 250 mg sample (PMZ/salts) is compressed between the smooth surfaces under a pressure of 2.5 ton/inch<sup>2</sup> for 4 min in an area of 0.5 cm<sup>2</sup>. Then the pellets were dipped into 500 mL of pH 7 PBS medium at 37 °C with rotating paddle of 100 rpm. A 5 mL of dissolution medium was collected at an interval of 15,30, 60, 90, 120, 150,180, 240,300,360,420 and 480 min by replacing each with same amount of fresh pH 7 PBS medium.

#### 4.10.7 Diffusion and Permeability Flux

The diffusion studies were conducted using a diffusion apparatus (Model EMFDC-06, Orchid Scientific, Maharashtra, India). PMZ and its salts was carried out through a dialysis membrane-135 (dialysis membrane-135, average flat width 33.12 mm, average diameter 23.8 mm, capacity approx. 4.45 mL/cm) obtained from HiMedia, India. The dialysis membrane was pre-treated with 2% NaHCO<sub>3</sub> at 80 °C for 30 min to remove traces of sulphides, followed by 10 mM of EDTA at 80 °C for 30 min to remove traces of heavy metal and another 30 min of treatment with deionized water at 80 °C to remove glycerin. The treated dialysis membrane was then mounted in clips and placed in diffusion cells with an effective surface area of 3.14 cm<sup>2</sup>. Suspensions of the drug PMZ and its salts materials were prepared and placed on the dialysis membrane in donor compartment. The temperature of diffusion medium was thermostatically maintained at 37 °C ± 1°C throughout the experiment. The drug and/or cocrystal solution was then allowed to stir at 600 rpm and diffuse through the membrane towards the receptor compartment containing 20 mL of phosphate-buffered solution (PBS, pH = 7). The release of the compounds at predetermined intervals (15,30, 60, 90, 120, 150,180, 240,300,360,420 and 480 min) were withdrawn (0.5 mL for each interval) and replaced by equal volume. The concentrations of the samples collected from receptor compartment through the dialysis tube were determined by HPLC method.

## **4.10.8 HPLC assay**

Shimadzu LC-20AD liquid chromatography, photodiode array SPD-M20A detector, and degasser DGU-20A3 are performed using reverse-phase (RP) HPLC column  $C_{18}G$  (250 × 4.6 mm, 5 µm particle size). UV absorbance at 268 nm was used to quantify the PMZ drug. The calibration curves are obtained by spiking PMZ (linearity  $R^2 > 0.999$ ). Methanol, acetonitrile and 0.1 M sodium perchlorate in the ratio of 40:30:30 (v/v) at pH 6.1 with 1% perchloric acid were used as mobile phase and delivered at a rate of 1 mL/min. The equilibrium solubility, IDR and diffusion experiment samples were injected into HPLC with a run time of 15 min. Retention time for PMZ was observed at 7.1 min.

## **4.11 References**

- Egolf, A., & Coffey, B. J.. Current pharmacotherapeutic approaches for the treatment of Tourette syndrome. *Drugs of Today (Barcelona, Spain: 1998)*, **2014**, *50*(2), 159-179.
- 2 Chen, J. J., Cai, N., Chen, G. Z., Jia, C. C., Qiu, D. B., Du, C., ... & Zhang, Q. The neuroleptic drug pimozide inhibits stem-like cell maintenance and tumorigenicity in hepatocellular carcinoma. *Oncotarget*, **2017**. *8*(11), 17593.
- Y. Ren, J. Tao, Z. Jiang, D. Guo, J. Tang, Pimozide suppresses colorectal cancer via inhibition of Wnt/beta-catenin signaling pathway, Life Sci. 209. **2018**, 267–273.
- 4 Subramaniam, D., Angulo, P., Ponnurangam, S., Dandawate, P., Ramamoorthy, P., Srinivasan, P., ... & Anant, S. Suppressing STAT5 signaling affects osteosarcoma growth and stemness. *Cell death & disease*, **2020**, *11*(2), 1-15.
- Nelson, E. A., Walker, S. R., Xiang, M., Weisberg, E., Bar-Natan, M., Barrett, R., ... & Frank, D. A. The STAT5 inhibitor pimozide displays efficacy in models of acute myelogenous leukemia driven by FLT3 mutations. *Genes & cancer*, **2012**, *3*(7-8), 503-511.
- Nelson, E. A., Walker, S. R., Weisberg, E., Bar-Natan, M., Barrett, R., Gashin, L. B., ... & Frank, D. A. The STAT5 inhibitor pimozide decreases survival of chronic myelogenous leukemia cells resistant to kinase inhibitors. *Blood, The Journal of the American Society of Hematology*, **2011**, *117*(12), 3421-3429.
- 7 Zhou, W., Chen, M. K., Yu, H. T., Zhong, Z. H., Cai, N., Chen, G. Z., ... & Chen, J. J. The antipsychotic drug pimozide inhibits cell growth in prostate cancer through suppression of STAT3 activation. *International journal of oncology*, **2016**, *48*(1), 322-328.
- 8 Kim, U., Kim, C. Y., Lee, J. M., Ryu, B., Kim, J., Shin, C., & Park, J. H.. Pimozide inhibits the human prostate cancer cells through the generation of reactive oxygen species. *Frontiers in pharmacology*, **2020**, *10*, 1517.
- 9 Smyj, R., Wang, X. P., & Han, F. Pimozide. *Profiles of Drug Substances, Excipients and Related Methodology*, **2012**, *37*, 287-311.

- Pimozide. https://go.drugbank.com/drugs/DB01100, accessed 2022-03-19.
- Pimozide, Merck Index., 14th ed., Merck & Co., Inc., Whitehouse Station, NJ, 2006 pp. 1281–1282.
- Smyj, R., Wang, X. P., & Han, F. Pimozide. *Profiles of Drug Substances, Excipients and Related Methodology*, **2012**, *37*, 287-311.
- Vogt, M., Kunath, K., & Dressman, J. B. Dissolution enhancement of fenofibrate by micronization, cogninding and spray-drying: comparison with commercial preparations. *European Journal of Pharmaceutics and Biopharmaceutics*, **2008**, 68(2), 283-288.
- Gupta, P., Kakumanu, V. K., & Bansal, A. K. Stability and solubility of celecoxib-PVP amorphous dispersions: a molecular perspective. *Pharmaceutical research*, **2004**, *21*(10), 1762-1769.
- Patravale, V. B., Date, A. A., & Kulkarni, R. M. Nanosuspensions: a promising drug delivery strategy. *Journal of pharmacy and pharmacology*, **2004**, *56*(7), 827-840.
- Deshpande, P. B., Kumar, G. A., Kumar, A. R., Shavi, G. V., Karthik, A., Reddy, M. S., & Udupa, N.. Supercritical fluid technology: concepts and pharmaceutical applications. *PDA J Pharm Sci Technol*, **2011**, *65*(3), 333-44..
- Mumenthaler, M., & Leuenberger, H. Atmospheric spray-freeze drying: a suitable alternative in freeze-drying technology. *International Journal of Pharmaceutics*, **1991**, 72(2), 97-110.
- Parikh, R. K., Mansuri, N. S., Gohel, M. C., & Sonlwala, M. M. Dissolution enhancement of nimesulide using complexation and salt formation techniques. *Indian drugs*, **2005**, 42(3), 149-154.
- Hsu, C. H., Cui, Z., Mumper, R. J., & Jay, M. Micellar solubilization of some poorly soluble antidiabetic drugs. *AAPS PharmSciTech*, **2008**, *9*(2), 939-943.
- Badwan, A. A., El-Khordagui, L. K., Saleh, A. M., & Khalil, S. A. The solubility of benzodiazepines in sodium salicylate solution and a proposed mechanism for hydrotropic solubilization. *International journal of Pharmaceutics*, **1982**, *13*(1), 67-74.
- Desiraju, G. R., & Parshall, G. W. Crystal engineering: the design of organic solids. *Materials science monographs*, **1989**, *54*.
- Blagden, N., de Matas, M., Gavan, P. T., & York, P. Crystal engineering of active pharmaceutical ingredients to improve solubility and dissolution rates. *Advanced drug delivery reviews*, **2007**, *59*(7), 617-630.
- 23 Karimi-Jafari, M., Padrela, L., Walker, G. M., & Croker, D. M. Creating cocrystals: A review of pharmaceutical cocrystal preparation routes and applications. *Crystal Growth & Design*, 2018, 18(10), 6370-6387.

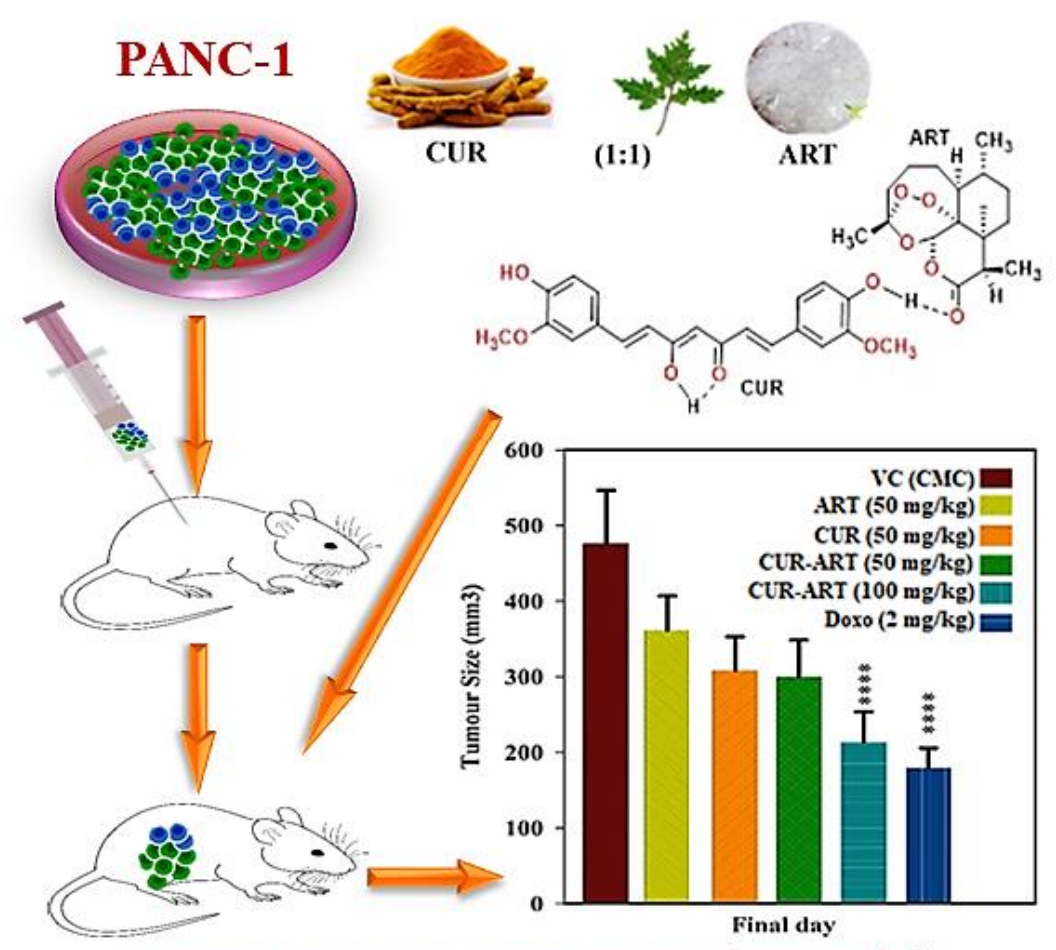
- https://www.fda.gov/files/drugs/published/Regulatory-Classification-of-Pharmaceutical-Co-Crystals.pdf.
- 25 Childs, S. L., Stahly, G. P., & Park, A. The salt– cocrystal continuum: the influence of crystal structure on ionization state. *Molecular pharmaceutics*, **2007**, *4*(3), 323-338.
- Aakeröy, C. B., Fasulo, M. E., & Desper, J. Cocrystal or salt: does it really matter?. *Molecular Pharmaceutics*, **2007**, *4*(3), 317-322.
- 27 Cruz-Cabeza, A. J.. Acid-base crystalline complexes and the p K a rule. *CrystEngComm*, **2012**, *14*(20), 6362-6365.
- Modani, S., Gunnam, A., Yadav, B., Nangia, A. K., & Shastri, N. R. Generation and Evaluation of Pharmacologically Relevant Drug–Drug Cocrystal for Gout Therapy. *Crystal Growth & Design*, **2020**, *20*(6), 3577-3583.
- Chun, N. H., Wang, I. C., Lee, M. J., Jung, Y. T., Lee, S., Kim, W. S., & Choi, G. J. Characteristics of indomethacin–saccharin (IMC–SAC) co-crystals prepared by an antisolvent crystallization process. *European Journal of Pharmaceutics and Biopharmaceutics*, **2013**, 85(3), 854-861.
- Yu, Z. Q., Chow, P. S., & Tan, R. B. Operating regions in cooling cocrystallization of caffeine and glutaric acid in acetonitrile. *Crystal growth & design*, **2010**, *10*(5), 2382-2387.
- Huang, Y., Zhou, L., Yang, W., Li, Y., Yang, Y., Zhang, Z., ... & Yin, Q. Preparation of theophylline-benzoic acid cocrystal and on-line monitoring of cocrystallization process in solution by raman spectroscopy. *Crystals*, **2019**, *9*(7), 329.
- Fischer, F., Scholz, G., Benemann, S., Rademann, K., & Emmerling, F. Evaluation of the formation pathways of cocrystal polymorphs in liquid-assisted syntheses. *CrystEngComm*, **2014**, *16*(35), 8272-8278.
- Yan, Y., Chen, J. M., & Lu, T. B. Thermodynamics and preliminary pharmaceutical characterization of a melatonin–pimelic acid cocrystal prepared by a melt crystallization method. *CrystEngComm*, **2015**, *17*(3), 612-620.
- Approval of Suglat tablets, kotobuki Pharmaceuticals. WWW Document. Available at: https://www.astellas.com/system/files/news/2018-12/181221\_2\_ Eg\_2.pdf (accessed **2014**, 2 10, 21).
- Guo, M., Sun, X., Chen, J., & Cai, T. Pharmaceutical cocrystals: A review of preparations, physicochemical properties and applications. *Acta Pharmaceutica Sinica B*, **2021**, *11*(8), 2537-2564.
- Merck Sharpe & Dohme Corp. Drug trials snapshots: STEGLATRO. Approval date:December 19. **2017**. Available from: https://www.fda.gov/ drugs/drug-approvals-and-databases/drug-trials-snapshots-steglatro.

- Banik, M., Gopi, S. P., Ganguly, S., & Desiraju, G. R. Cocrystal and salt forms of furosemide: solubility and diffusion variations. *Crystal Growth & Design*, **2016**, *16*(9), 5418-5428.
- Gopi, S. P., Banik, M., & Desiraju, G. R. New cocrystals of hydrochlorothiazide: optimizing solubility and membrane diffusivity. *Crystal Growth & Design*, **2017**, *17*(1), 308-316.
- 39 Allu, S., Bolla, G., Tothadi, S., & Nangia, A. K. Novel pharmaceutical cocrystals and salts of bumetanide. *Crystal Growth & Design*, **2019**, 20(2), 793-803.
- Bommaka, M. K., Mannava, M. C., Suresh, K., Gunnam, A., & Nangia, A. Entacapone: Improving aqueous solubility, diffusion permeability, and cocrystal stability with theophylline. *Crystal Growth & Design*, **2018**, *18*(10), 6061-6069.
- 41 Rai, S. K., Allu, S., & Nangia, A. K. Salts and Cocrystal of Etodolac: Advantage of Solubility, Dissolution, and Permeability. *Crystal Growth & Design*, **2020**, 20(7), 4512-4522.
- Khatioda, R., Saikia, B., Das, P. J., & Sarma, B. Solubility and in vitro drug permeation behavior of ethenzamide cocrystals regulated in physiological pH environments. *CrystEngComm*, **2017**, *19*(46), 6992-7000.
- 43 Manohari, P. J., Kunchithapatham, J., Seshadri, V. C., & Muthusamy, C. Pelagia Research Library.
- Bera, H., Chekuri, S., Sarkar, S., Kumar, S., Muvva, N. B., Mothe, S., & Nadimpalli, J. Novel pimozide-β-cyclodextrin-polyvinylpyrrolidone inclusion complexes for Tourette syndrome treatment. *Journal of Molecular Liquids*, **2016**, *215*, 135-143.
- Gorecki, D. K., & Verbeeck, R. K. Trazodone hydrochloride. In *Analytical Profiles of Drug Substances* **1987**, (Vol. 16, pp. 693-730). Academic Press.
- 46 Kraus, W.; Nolze, G. Powder cell– a program for the representation and manipulation of crystal structures and calculation of the resulting X-ray powder patterns. J. Appl. Cryst. 1996, 29, 301–303.
- Powder Cell, A program for structure visualization, powder pattern calculation and profile fitting. www.ccp14.ac.uk/tutorial/powdercell. (accessed 29 May 2018).
- 48 Bruker SMART, Version 5.625, SHELXTL, Version 6.12. Bruker AXS Inc., Madison, Wisconsin, USA. **2000**.
- 49 Sheldrick, G. M. *Program for Refinement of Crystal Structures*, University of Göttingen, Germany, **1997**.
- 50 Sheldrick, G. M. A short history of SHELX. *Acta Crystallogr.*, *Sect. A.* **2008**, *64*, 112–122.
- 51 Sheldrick, G. M.Crystal structure refinement with SHELXL. *Acta Cryst.*, *Sect. C: Struct. Chem.* **2015**, *71*, 3–8.
- 52 Barbour, L.J. Supramol. Chem., **2001**, 1, 189–191.

- Barbour, L.J. *X-Seed, Graphical Interface to SHELX-97 and POV-Ray;* University of Missouri-Columbia, Columbus, MO, **1999**.
- Higuchi, T.; Connors, K.A. Phase Solubility Techniques, Advanced Analytical Chemistry of Instrumentation. *Adv. Anal. Chem. Instrum.* **1965**, *4*, 117–212.

# CHAPTER FIVE

# Curcumin-Artemisinin Coamorphous Solid: Xenograft Model Preclinical Study



Curcumin-Artemisinin Coamorphous Solid: Xenograft Model Preclinical Study

Curcumin-Pyrogallol (CUR-PYR) cocrystal and Curcumin-Artemisinin (CUR-ART) coamorphous solid. Both these solid forms exhibited superior dissolution and pharmacokinetic behavior compared to pure CUR, which is practically insoluble. CUR-ART showed higher therapeutic effect and inhibited approximately 62% of tumor growth at 100 mg/kg oral dosage of CUR in xenograft models, which is equal to the positive control drug, doxorubicin (2mg/kg) by i.v. administration.

#### **5.1 Introduction**

Medicinal plants are gaining interest in the scientific community for health benefits due to their well-known pharmacological action <sup>1,3</sup>. The search for anticancer agents from plant sources began in the 1950s<sup>4</sup>. They are arich and diverse source of chemical constituents with antitumor and cytotoxic properties due to their natural antioxidant and free radical scavenger activity which can reduce or minimize the toxic side effect of chemotherapy<sup>3,5</sup>. The most promising natural herbal extracts withbioactive molecules such as curcumin (turmeric) and artemisinin (qinghao) exhibit pharmacological action, such as antioxidant, antimalarial, antiproliferative, antiangiogenic, anticancer and offer a viable solution to chemotherapeutic drugs <sup>6-8</sup>.

Curcumin (CUR) is a hydrophobic phytochemical polyphenol of bright yellow color found in the rhizome of turmeric (Curcuma longa), chemical diferuloylmethane (C<sub>21</sub>H<sub>20</sub>O<sub>6</sub>). It is generally considered to be the most pharmacologically active constituent of curcuminoids and has many documented activity <sup>8,9</sup>. Artemisinin (ART) is a sesquiterpene lactone natural compound isolated from the plant Artemesia annua in 1972 by Youyou Tu (Nobel Prize 2015) 10. Since 1971, Youyou Tu conducted several antimalarial experiments against artemisinin and their derivatives demonstrated that these compounds exhibit antimalarial activity 11. Recently Padmanabhan et.al. 12, 13 reported synergistic effects of CUR-ART (as a physical mixture) combination having superior antimalarial activity than the individual components. Both compounds CUR and ART are used in traditional medicine in India and China for over 2000 years. Among CUR and ART natural molecules, ART and its derivatives were approved by FDA as antimalarial drugs in the form of single as well as multidrug therapy with a combination of other drugs <sup>14, 15</sup>. However, till today CUR approved as a nutraceutical but not as a drug <sup>16, 17</sup>. Curcumin has poor aqueous solubility (7.8 μg/mL) and low bioavailability (0.051 μg/L) because of rapid metabolism and short half-life 7, 18. Several scientific manuscripts on CUR and ART report potential therapeutic activity as anticancer agents and show cytotoxic activity against a wide range of cancer cell lines including, melanoma, breast, pancreas, and renal cancer cells<sup>19</sup>. Furthermore, xenograft experiments demonstrate the anticancer activity in pancreatic cancer cell lines <sup>20,21</sup>. The insolubility of curcumin makes it a less studied molecule for tumor therapy. In order to enhance its solubility and bioavailability, several formulation strategies have been explored such as polymeric dispersion <sup>22</sup>, nanocrystals <sup>23</sup>, supramolecular gelators <sup>24</sup>, liposomes mixed, suspensions <sup>25</sup>. Our group has reported different solid-state forms of curcumin, i.e polymorphs <sup>26</sup>, cocrystals <sup>27</sup>, eutectics <sup>28</sup> and coamorphous <sup>29</sup>. The therapeutic efficacy of both CUR and ART as an amorphous solid with molecular level interactions is not reported.

In previous studies, curcumin-pyrogallol (CUR-PYR) cocrystal exhibited superior dissolution rate compared to other cocrystals as well as eutectics and polymorphs <sup>27</sup>. Subsequently we reported curcumin-artemisinin (CUR-ART) coamorphous solid which showed enhanced bioavailability than pure CUR in male sprague dwaley (SD) rats at an oral dose of 200 mg/kg. At the same dose, no plasma

concentration for curcumin (crystalline) could detected by HPLC analysis <sup>29</sup> due to its poor aqueous solubility. The present work is a continuation of our previous results on the improved solubility and bioavailability of CUR-PYR cocrystal and CUR-ART coamorphous solid to evaluate the bioavailability of CUR-PYR cocrystals and therapeutic activity of CUR-ART coamorphous solid in xenograft models.

## 5.2 Results and Discussion

CUR-PYR cocrystal and CUR-ART coamorphous solids are associated through intermolecular O—H···O hydrogen bonding (Scheme 1). The crystal structure of CUR-PYR was determined by single crystal X-ray diffraction and the hydrogen bonding synthons are known. Hydrogen bonding in CUR-ART is inferred from IR spectra and preferred hydrogen bonding interaction of strongest donor-strongest acceptor in the crystal structure (in the absence of X-ray data for the amorphous solid) <sup>29</sup>. The bulk phase composition was produced by co-grinding (CUR-PYR) and by fast evaporation under vacuum (CUR-ART) as detailed in the Experimental Section. The bulk phase composition was prepared reproducibly and characterized by powder X-ray diffraction pattern (Figure 1 and 2). The same materials were used in the pharmacokinetic, phase stability, toxicology and xenograft studies.

**Scheme 1:** Molecular structure of CUR-PYR cocrystal (a) and CUR- ART (b) are exist through intermolecular  $O-H\cdots O$  hydrogen bonding respectively.

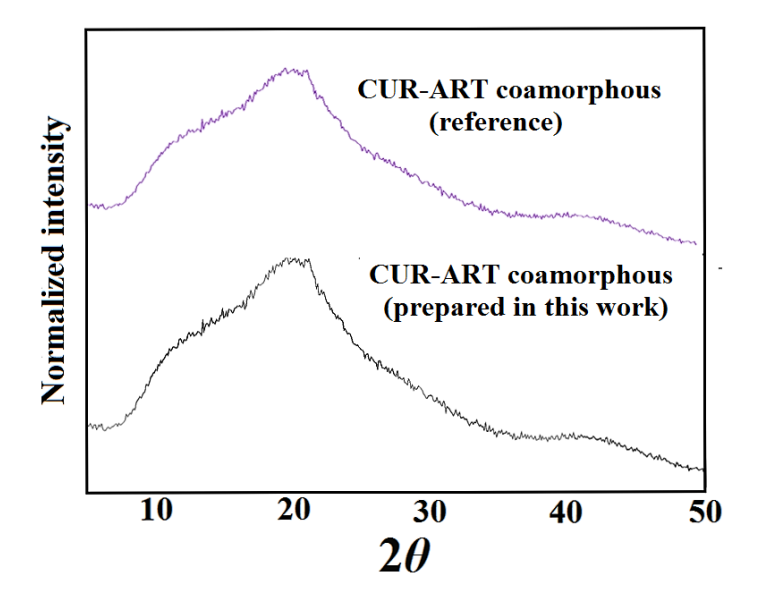
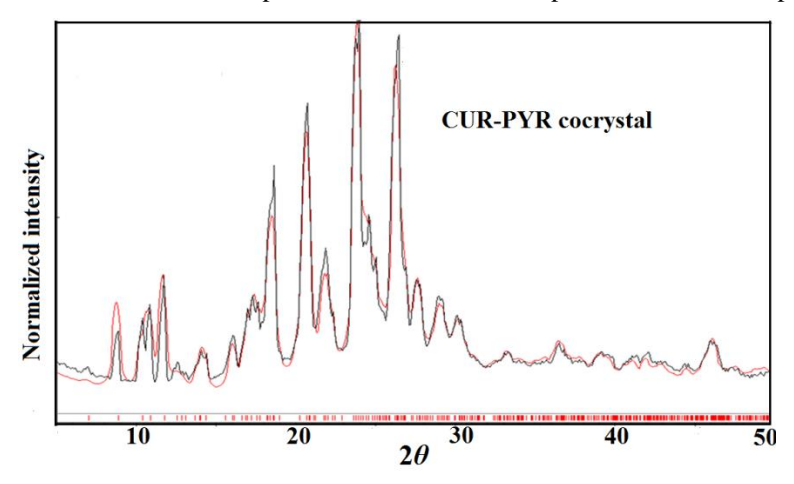


Figure 1: Bulk phase of CUR-ART PXRD pattern matches with the reported reference compound by PXRD <sup>29</sup>.



**Figure 2:** Experimental PXRD (black trace) of CUR-PYR match nicely with the calculated X-ray diffraction lines from the crystal structure (red), indicating the excellent purity of the bulk phase <sup>27</sup>.

# 5.3 Bioavailability studies

Oral bioavailability is the most important property for drug delivery. Over 80% of drugs marketed worldwide as tablets and capsules. Oral bioavailability is the fraction of the solid dose administered which reaches systemic circulation in blood/ plasma. The physicochemical properties of an API or bioactive molecule can be enhanced to give higher solubility and faster dissolution rate through salts, amorphous, cocrystal or coamorphous forms with better absorption and improved bioavailability. With the objective to improve the systemic bioavailability of CUR <sup>30,31</sup> in circulation, we have taken forward the superior dissolution rates of CUR-PYR cocrystal and CUR-ART coamorphous as leads in animal studies. The cocrystal and coamorphous phases of curcumin with a dose of 200 mg/kg (of active curcumin) were administered orally in SD rats (both male and female) to monitor the systemic bioavailability of circulating curcumin. The results of cocrystal and coamorphous solids mean concentrations in the serum are illustrated in Table 1, and Figure 3 and 4. In female SD rats, CUR-ART

coamorphous exhibited superior serum levels of 1.23 µg/mL at 30 min and 0.43 µg/mL of CUR-PYR cocrystal at 45 min post administration, whereas in male rats the CUR-ART value is 0.90 µg/mL and CUR-PYR is 0.53 µg/mL at 30 min respectively. The apparent terminal half-life (T<sub>1/2</sub>) increased significantly to 6-7 hr for both CUR-PYR and CUR-ART, which is much longer than that of pure curcumin <1 h. CUR-ART coamorphous exhibited approximately two-fold superior bioavailability compared to CUR-PYR cocrystal. It is difficult to compare the enhancement with pure curcumin because the soluble fraction is too low to be detected by HPLC method. Sasaki et al. have reported theracurcumin (colloidal dispersion with gum-gatti) <sup>32</sup> formulation at 300 mg/kg oral dosage with high C<sub>max</sub> value of 1.69 μg/mL at T<sub>max</sub> of 120 min and amount of CUR concentration delivered in vivo of AUC (0-∞) 9.3 mg.h/mL. CUR-ART coamorphous (at 200 mg/kg dose) exhibited high C<sub>max</sub> of 0.9-1.2 µg/mL (which is comparable to theracurcumin) at short T<sub>max</sub> (30 min), meaning immediate drug delivery. Specifically AUC<sub>(0-∞)</sub> 35 mg.h/mL for CUR-ART coamorphous solid is 3.7 times greater than that for theracurcumin  $^{32}$ . This is a remarkable improvement in the conc. of the CUR at short  $T_{max}$  of 30 min and total drug delivered AUC<sub>(0-∞)</sub>. Oral administration of pure CUR and CUR-ART physical mixture did not show any detectable levels in the serum attributable to CUR very low solubility and short half-life. This observation is consistent with recent reports wherein pure curcumin could not be detected at even higher dosage levels (>1g/kg) by HPLC. To summarize, the C<sub>max</sub> for CUR-PYR curves do not peak so sharply and rapidly as that for CUR-ART. This is attributed to the coamorphous phase solid-state form of CUR-ART compared to the crystalline state of CUR-PYR. The high free energy of amorphous solids used imparts higher solubility and bioavailability due to high thermodynamic functions.

Table 1: Pharmacokinetic data of CUR-PYR cocrystal vs. CUR-ART coamorphous solids.<sup>a</sup>

Parameters	CUR-PY	R (F)	CUR-AR	CUR-ART (F)		(M)	CUR-ART (M)	
Tarameters	Mean	S.D	Mean	S.D.	Mean	S.D	Mean	S.D.
T <sub>max</sub> (min)	45.00	15.60	30.00	0.00	30.00	8.22	30.00	0.00
C <sub>max</sub> (µg/mL)	0.43	0.15	1.23	0.33	0.53	0.19	0.90	0.39
T <sub>1/2</sub> (h)	7.70	3.27	6.70	0.68	6.00	2.78	7.00	1.66
AUC <sub>(0-24)</sub> (μg.h/mL)	1.91	0.25	3.69	0.69	2.18	0.59	3.45	0.83
$AUC_{(0-\infty)}$ (µg.h/mL)	22.20	6.70	36.40	6.00	19.70	5.72	35.40	5.64

<sup>&</sup>lt;sup>a</sup> Unformulated curcumin @ 340mg/kg oral dosage: T<sub>max</sub> 30 min, C<sub>max</sub> 0.0024μg/mL, AUC4.8 μg min/mL [33].

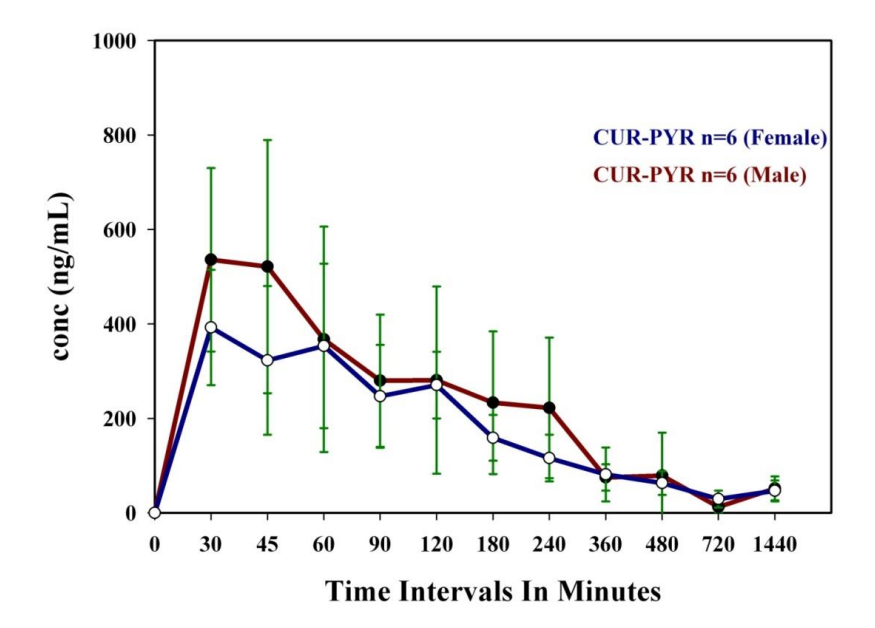


**Figure 3:** Mean Plasma concentration of cocrystal CUR-PYR vs. Time profile obtained from both female and male SD rats.

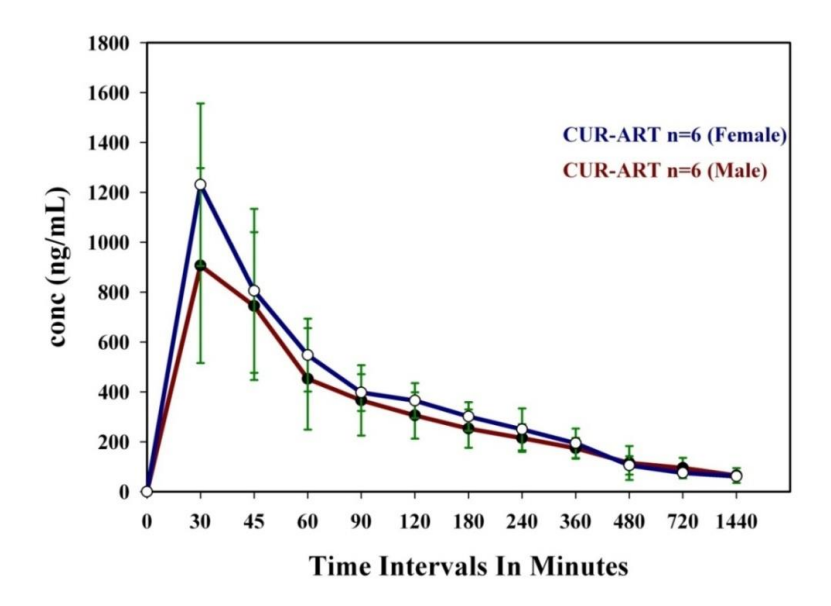


**Figure 4:** Mean Plasma concentration of CUR-ART coamorphous vs. Time profile obtained from both female and male SD rats.

## 5.4 Phase stability in SGF and SIF media

Typically amorphous solids exhibit rapid dissolution rate and high bioavailability in plasma. CUR-ART coamorphous displayed a short  $T_{max}$  but prolonged half-life in vivo (6-7 h). The latter result is significant because the short half-life of pure curcumin (45-60 min) in crystalline form severely limits the active drug delivered. We reasoned that CUR-ART coamorphous is stabilized as dispersion compared to pure curcumin. In vitro slurry experiments in SGF and SIF media (simulated gastric fluid and simulated intestinal fluid of pH 1.2 and 7, respectively) were performed to understand the stability of the amorphous phase by powder X-ray diffraction. PXRD of the reference compound stable form are

shown in Figure 5. In addition, we also conducted supersaturation experiments to find out the soluble curcumin precipitation in both CUR (crystalline) and CUR-ART coamorphous forms.

CUR-ART solid physical stability were conducted in the supersaturated solution of SGF /SIF media at 1000 rpm using magnetic stirrer at 30 °C for different time intervals (1, 2, 3, 6, 12 and 24 h) in separate experiments. At the end point, the suspension was filtered and the solid residue tested by powder X-ray diffraction. CUR-ART coamorphous was noted to be stable for up to 3 h in SGF medium. After about 6 h it dissociated and the ART component precipitated as the crystalline form but CUR component was still present in amorphous/ semi crystalline state as observed by PXRD (Figure 6a). Similarly, in SIF medium CUR-ART coamorphous was stable for up to 12 h (Figure 6b) and after 12 h the ART component precipitated in crystalline state. These results suggest a reason for the high solubility of curcumin in CUR-ART. The amorphous form of CUR is present for a long enough time in the simulated conditions to release high drug concentration over a long period of time (several hours). This explains the longer half-life (up to 6-7 h) of curcumin in SD rats when administered as CUR-ART coamorphous. In contrast, pure curcumin decomposes in less than 1 h. The extended halflife of curcumin which dissociates slowly from CUR-ART is due to the strong intermolecular O-H···O hydrogen bonds in the structure. The phase stability of CUR-ART in SGF and SIG media and its high solubility are explained in Scheme 2 as the "spring and parachute" model of cocrystal solubility for drugs <sup>31</sup>. The mechanism of Scheme 2 for CUR-ART was supported by supersaturation experiments of CUR and CUR-ART in SGF and SIF media (without enzyme) and analyzed by UV spectroscopy (Figure 7). From these experiments we observed that CUR precipitated faster than CUR-ART (Figure 8) at 100 µg/mL concentration of CUR. An additional UV maxima (at 360 nm) was observed in SIF medium, due to degradation of CUR since it is known that curcumin is less stable as the pH increases. These experiments indicate that solubilized CUR in CUR-ART has longer residence time than pure CUR in both SGF and SIF, which is due to noncovalent interactions between CUR and ART in the coamorphous solid.

The particle morphology at time point 1, 2 and 24 h of the precipitated CUR-ART coamorphous was analyzed by FESEM. The high magnification images clearly show that the large particles are actually agglomerates of smaller particles at 1 h and 2 h in SGF medium. There are irregular dense shape particles in both pH media by 24 h (Figure 8).

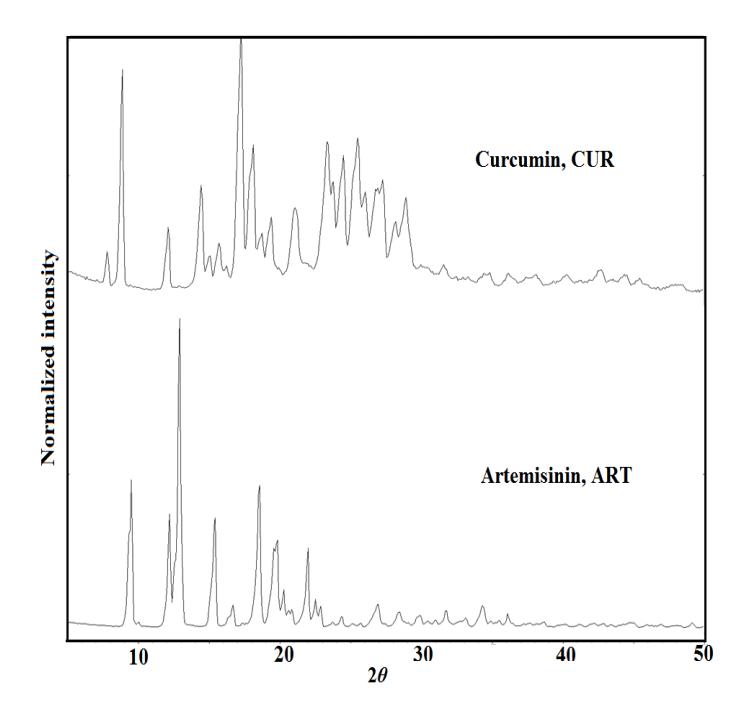
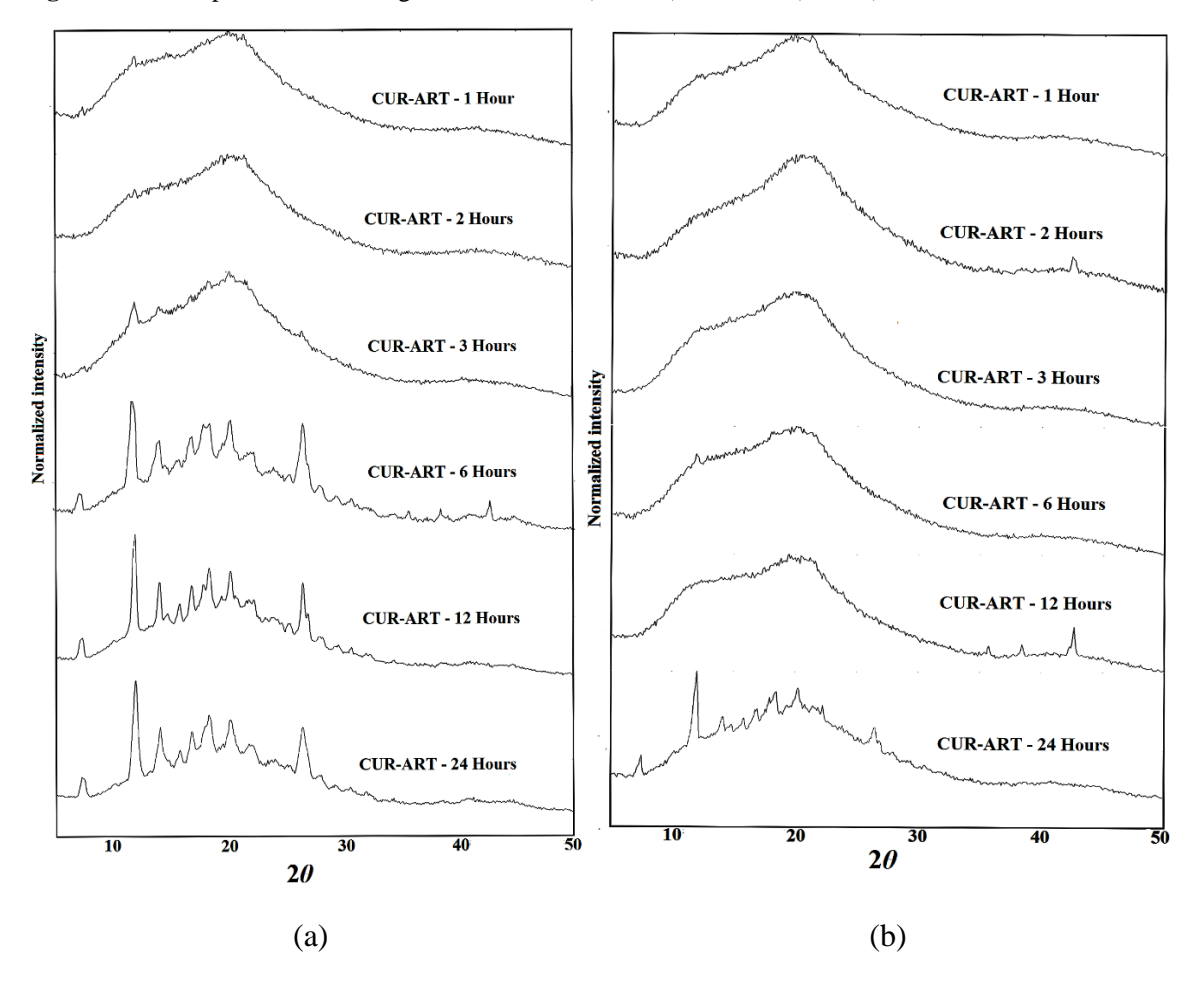
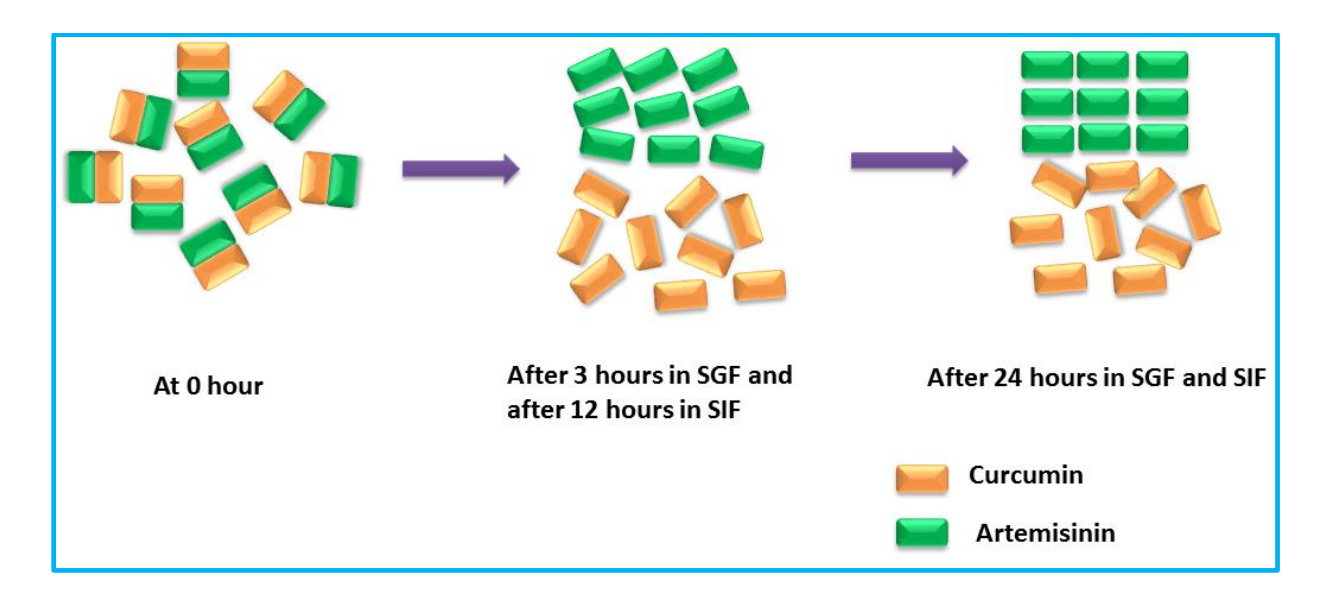


Figure 5: PXRD patterns of starting materials CUR (Form 1) and ART (form 1).



**Figure 6:** CUR-ART phase stability study PXRD patterns at different time intervals in SGF, pH = 1.2 (a), and SIF media, pH = 7 (b).



**Scheme 2:** Pictorial representation of CUR-ART physical stability in simulated fluids.

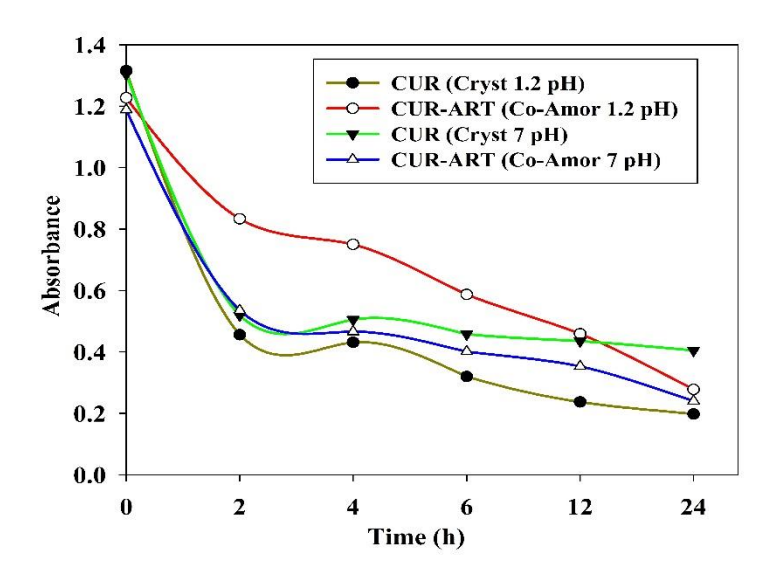


**Figure 7:** Supersaturation experiments of CUR and CUR-ART: UV-Vis plots of Absorbance vs. Time recorded at 420 nm peak intensity for curcumin.

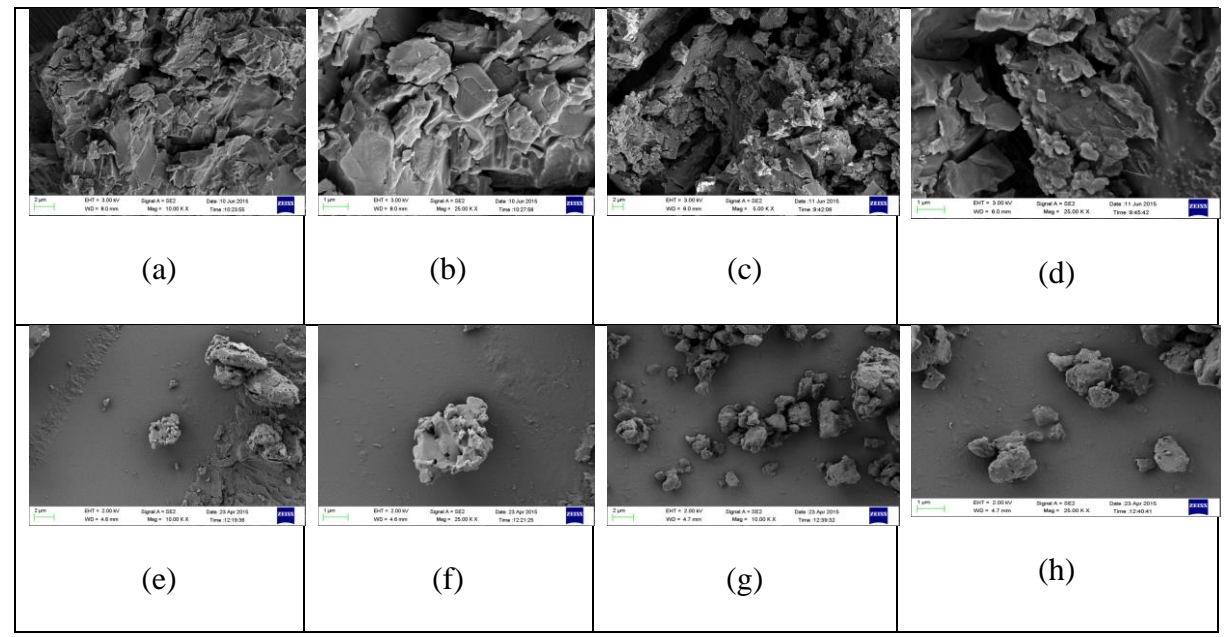


Figure 8: CUR-ART in SGF/SIF at 2  $\mu$ m and 1  $\mu$ m resolution. (a) and (b) are slurry material in SGF at 1 h. (c) and (d) are slurry material in SGF at 2 h. (e) and (f) are slurry material in SGF at 24 h. (g) and (h) are slurry material in SIF at 24 h. The agglomerates of larger particles up to 2 h time point have separated/ dissociated to give smaller particles by 24 h.

# 5.5 Acute toxicity study

In the acute toxicity studies, a high dose of 2000 mg/kg (active curcumin) of CUR-ART coamorphous and CUR-PYR cocrystal was tested in Swiss albino mice and SD rats. During the 15-day observation period of acute oral toxicity and body weight measurements, no toxic were observed in either of the two species (data are shown in Table 2-5). No mortality or morbidity was found in the treated group at the end of the study and no gross pathological abnormalities were observed in rats or mice. Physical, physiological and neurological parameters assessed in the exposed animals were in the normal range and well tolerated without any adverse systemic toxicity. Thus, curcumin-artemisinin is safe at the tested dose and sub-chronic toxicity may be evaluated at different strengths.

**Table 2:** Acute oral toxicity of CUR-PYR cocrystal in Sprague Rats (Male and Female).

# Body weights (g)-Male

Groups	Day 0	Day 4	Day 8	<b>Day 12</b>	<b>Day 15</b>
VC	$210.68 \pm 4.15$	$213 \pm 3.88$	$216.16 \pm 3.79$	$219.25 \pm 3.37$	$220.66 \pm 3.26$
	(6)	(6)	(6)	(6)	(6)
TG	$209.16 \pm 4.03$	$211.83 \pm 1.91$	$215.58 \pm 4.97$	$219.08 \pm 5.31$	219.83 ±5.24
	(6)	(6)	(6)	(6)	(6)

Values are expressed in Mean  $\pm$  S.D

() No. of Animals

() No. of Animals

VC-Vehicle Control

TG-Theraupatic Group

# Body weights (g)-Female

Groups	Day 0	Day 4	Day 8	<b>Day 12</b>	<b>Day 15</b>
VC	$206.91 \pm 3.92$	$210.5 \pm 3.84$	$214.58 \pm 3.74$	$218.0 \pm 3.68$	$218.73 \pm 3.94$
	(6)	(6)	(6)	(6)	(6)
TG	$206.7 \pm 3.34$	$210.16 \pm 3.43$	$213.91 \pm 3.07$	$216.48 \pm 2.96$	$218.83 \pm 2.90$
	(6)	(6)	(6)	(6)	(6)

Values are expressed in Mean  $\pm$  S.D

VC-Vehicle Control

TG-Theraupatic Group

# Organ Weights (g)-Male

Groups	Heart	Lung	Liver	Kidney	Spleen	Brain	Testis
VC	$0.86 \pm 0.03$	$1.17 \pm 0.05$	$9.20 \pm 0.05$	$1.44 \pm 0.01$	$0.84 \pm 0.16$	$1.90 \pm 0.04$	$1.76 \pm 0.07$
	(6)	(6)	(6)	(6)	(6)	(6)	(6)
TG	$0.87 \pm 0.06$	$1.14 \pm 0.01$	$9.10\pm0.12$	$1.39 \pm 0.03$	$0.83 \pm 0.18$	$1.89 \pm 0.03$	$1.73 \pm 0.11$
	(6)	(6)	(6)	(6)	(6)	(6)	(6)

Values are expressed in Mean  $\pm$  S.D

() No. of Animals

VC-Vehicle Control

TG-Theraupatic Group

Organ Weights (g)-Female

Groups	Heart	Lung	Liver	Kidney	Spleen	Brain	Ovaries
VC	$0.80 \pm 0.04$	$1.11 \pm 0.06$	$7.40 \pm 0.09$	$1.33 \pm 0.05$	$0.54 \pm 0.03$	$1.83 \pm 0.06$	$0.05 \pm 0.02$
	(6)	(6)	(6)	(6)	(6)	(6)	(6)
TG	$0.82 \pm 0.02$	$1.10\pm0.03$	$7.43 \pm 0.7$	$1.13 \pm 0.07$	$0.56 \pm 0.08$	$1.82 \pm 0.05$	$0.06 \pm 0.02$
	(6)	(6)	(6)	(6)	(6)	(6)	(6)

Values are expressed in Mean  $\pm$  S.D

VC-Vehicle Control

TG-Theraupatic Group

() No. of Animals

 Table 3: Acute oral toxicity of CUR-ART coamorphous in Sprague Rats (Male and Female).

# Body weights (g)-Male

Groups	Day 0	Day 4	Day 8	Day 12	Day 15
VC	$215.61 \pm 2.8$	$207.08 \pm 2.85$	$209.83 \pm 3.98$	$213.0 \pm 2.75$	$214.41 \pm 2.51$
	(6)	(6)	(6)	(6)	(6)
TG	$214.7 \pm 2.43$	$216.16 \pm 2.18$	$218.5 \pm 2.07$	$220.75 \pm 1.69$	$221.83 \pm 1.47$
	(6)	(6)	(6)	(6)	(6)

Values are expressed in Mean  $\pm$  S.D

VC-Vehicle Control

TG-Theraupatic Group

() No. of Animals

# Body weights (g)-Female

Groups	Day 0	Day 4	Day 8	<b>Day 12</b>	Day 15
VC	$185.85 \pm 2.28$	$187.0 \pm 2.54$	$190.91 \pm 1.88$	$193.28 \pm 1.36$	$196.58 \pm 1.02$
	(6)	(6)	(6)	(6)	(6)
TG	$195.65 \pm 3.18$	$197.83 \pm 2.65$	$201.5 \pm 2.88$	$204.51 \pm 1.62$	$206.35 \pm 2.06$
	(6)	(6)	(6)	(6)	(6)

Values are expressed in Mean  $\pm$  S.D

VC-Vehicle Control

TG-Theraupatic Group

() No. of Animals

## Organ Weights (g)-Male

Groups	Heart	Lung	Liver	Kidney	Spleen	Brain	Testis
VC	$0.82 \pm 0.09$	$1.15 \pm 0.01$	$9.12 \pm 0.01$	$1.42 \pm 0.07$	$0.83 \pm 0.05$	$1.95 \pm 0.03$	$1.75 \pm 0.09$
	(6)	(6)	(6)	(6)	(6)	(6)	(6)

# Cur-Art Coamorphous Solid...143

1	TG	$0.87 \pm 0.06$	$1.14 \pm 0.01$	$9.10 \pm 0.12$	$1.39 \pm 0.03$	$0.83 \pm 0.18$	$1.89 \pm 0.03$	$1.73 \pm 0.11$
		(6)	(6)	(6)	(6)	(6)	(6)	(6)

Values are expressed in Mean  $\pm$  S.D

VC-Vehicle Control

TG-Theraupatic Group

## Organ Weights (g)-Female

Groups	Heart	Lung	Liver	Kidney	Spleen	Brain	Ovaries
VC	$0.82 \pm 0.08$	$1.12 \pm 0.13$	$7.50 \pm 0.07$	1.30 v 0.01	$0.61 \pm 0.07$	$1.88 \pm 0.017$	$0.07 \pm 0.01$
	(6)	(6)	(6)	(6)	(6)	(6)	(6)
TG	$0.81 \pm 0.02$	$1.05\pm0.06$	$7.56 \pm 0.4$	$1.28 \pm 0.09$	$0.59 \pm 0.07$	$1.87 \pm 0.015$	$0.05 \pm 0.01$
	(6)	(6)	(6)	(6)	(6)	(6)	(6)

Values are expressed in Mean  $\pm$  S.D

VC-Vehicle Control

TG-Theraupatic Group

() No. of Animals

() No. of Animals

Table 4: Acute oral toxicity of CUR-ART coamorphous in Swiss Albino Mice (Male and Female).

## Body weights (g)-Male

Groups	Day 0	Day 4	Day 8	<b>Day 12</b>	Day 15
VC	$18.8 \pm 0.4$	$19.75 \pm 0.52$	$21.4 \pm 0.37$	$24.0 \pm 0.63$	$25.58 \pm 0.58$
	(6)	(6)	(6)	(6)	(6)
TG	$20.81 \pm 0.9$	$21.7 \pm 0.89$	$23.41 \pm 0.37$	$24.66 \pm 0.25$	$26.43 \pm 0.38$
	(6)	(6)	(6)	(6)	(6)

Values are expressed in Mean  $\pm$  S.D

VC-Vehicle Control

TG-Theraupatic Group

() No. of Animals

## Body weights (g)-Female

Groups	Day 0	Day 4	Day 8	<b>Day 12</b>	<b>Day 15</b>
VC	$17.83 \pm 0.12$	$19.0 \pm 0.44$	$19.9 \pm 0.49$	$21.91 \pm 0.49$	$23.5 \pm 0.44$
	(6)	(6)	(6)	(6)	(6)
TG	$19.03 \pm 0.50$	$20.41 \pm 0.37$	$22.16 \pm 0.40$	$23.83 \pm 0.25$	$24.91 \pm 0.73$
	(6)	(6)	(6)	(6)	(6)

Values are expressed in Mean  $\pm$  S.D

VC-Vehicle Control

TG-Theraupatic Group

() No. of Animals

# Organ Weights (g)-Male

Groups	Heart	Lung	Liver	Kidney	Spleen	Brain	Testis
VC	$0.14 \pm 0.05$ (6)	$0.41 \pm 0.07$ (6)	$1.3 \pm 0.04$ (6)	$0.4 \pm 0.05$ (6)	$0.06 \pm 0.01$ (6)	$0.4 \pm 0.005$ (6)	0.22 ± 0.03 (6)
TG	$0.14 \pm 0.01$ (6)	$0.34 \pm 0.06$ (6)	$1.30 \pm 0.03$ (6)	$0.49 \pm 0.05$ (6)	0.061 ± 0.01 (6)	0.47 ± 0.005 (6)	$0.22 \pm 0.02$ (6)

Values are expressed in Mean  $\pm$  S.D

VC-Vehicle Control

TG-Theraupatic Group

# Organ Weights (g)-Female

	Groups	Heart	Lung	Liver	Kidney	Spleen	Brain	Ovaries
Ì	VC	$0.11 \pm 0.013$	$0.30 \pm 0.07$	$1.03 \pm 0.08$	0.30 v 0.026	$0.07 \pm 0.002$	$0.47 \pm 0.06$	$0.05 \pm 0.01$
		(6)	(6)	(6)	(6)	(6)	(6)	(6)
	TG	$0.11 \pm 0.012$	$0.32 \pm 0.05$	$1.06 \pm 0.04$	$0.38 \pm 0.022$	$0.07 \pm 0.002$	$0.45\pm0.08$	$0.02 \pm 0.01$
		(6)	(6)	(6)	(6)	(6)	(6)	(6)

Values are expressed in Mean  $\pm$  S.D

VC-Vehicle Control

TG-Theraupatic Group

() No. of Animals

() No. of Animals

**Table 5:** Acute oral toxicity of CUR-PYR cocrystal in Swiss Albino Mice (Male and Female).

## Body weights (g)-Male

Groups	Day 0	Day 4	Day 8	Day 12	<b>Day 15</b>
VC	$18.93 \pm 1.57$	$20.5 \pm 1.94$	$23.08 \pm 2.17$	$25.41 \pm 2.51$	$25.38 \pm 3.24$
	(6)	(6)	(6)	(6)	(6)
TG	$19.23 \pm 1.70$	$21.11 \pm 1.35$	$23.73 \pm 1.32$	$26.25 \pm 1.89$	$26.4 \pm 1.41$
	(6)	(6)	(6)	(6)	(6)

Values are expressed in Mean  $\pm$  S.D

VC-Vehicle Control

TG-Theraupatic Group

() No. of Animals

Body weights (g)-Female

Groups	Day 0	Day 4	Day 8	Day 12	Day 15
VC	$20.0 \pm 1.44$	$21.41 \pm 1.15$	$23.65 \pm 1.14$	$25.75 \pm 1.3$	$26.11 \pm 1.70$
	(6)	(6)	(6)	(6)	(6)
TG	$18.75 \pm 1.44$	$20.58 \pm 1.90$	$22.83 \pm 1.63$	$25.0 \pm 1.34$	$25.25 \pm 1.80$
	(6)	(6)	(6)	(6)	(6)

Values are expressed in Mean  $\pm$  S.D

VC-Vehicle Control

TG-Theraupatic Group

() No. of Animals

Organ Weights (g)-Male

Groups	Heart	Lung	Liver	Kidney	Spleen	Brain	Testis
VC	$0.14 \pm 0.06$	$0.42 \pm 0.06$	$1.40 \pm 0.07$	$0.41 \pm 0.07$	$0.05 \pm 0.02$	$0.52 \pm 0.06$	$0.27 \pm 0.02$
	(6)	(6)	(6)	(6)	(6)	(6)	(6)
TG	$0.15 \pm 0.03$	$0.44 \pm 0.03$	$1.41 \pm 0.05$	$0.43 \pm 0.03$	$0.06 \pm 0.02$	$0.52 \pm 0.004$	$0.25 \pm 0.03$
	(6)	(6)	(6)	(6)	(6)	(6)	(6)

Values are expressed in Mean  $\pm$  S.D

VC-Vehicle Control

TG-Theraupatic Group

Organ Weights (g)-Female

Groups	Heart	Lung	Liver	Kidney	Spleen	Brain	Ovaries
VC	$0.12 \pm 0.02$	$0.37 \pm 0.05$	$0.97 \pm 0.06$	$0.4 \pm 0.03$	$0.07 \pm 0.001$	$0.45 \pm 0.03$	$0.03 \pm 0.01$
	(6)	(6)	(6)	(6)	(6)	(6)	(6)
TG	0.14 ± 0.012	$0.32 \pm 0.05$ (6)	$1.06 \pm 0.04$ (6)	$0.38 \pm 0.022$ (6)	$0.07 \pm 0.002$ (6)	$0.45 \pm 0.08$ (6)	$0.02 \pm 0.01$ (6)
	(6)	. ,	,		, ,	, ,	, ,

Values are expressed in Mean  $\pm$  S.D

VC-Vehicle Control

TG-Theraupatic Group

# 5.6 In vivo antitumor effect of CUR-ART against Panc-1 Xenograft

With enhanced bioavailability, improved stability and low toxicity of CUR-ART, the coamorphous solids was tested in xenograft animal study (n=7) to know its therapeutic efficacy. This study was investigated in the induced pancreas xenograft (tumor was developed by Panc-1 cells) model in nude mice. The compounds were administered systemically with CUR-ART (50 and 100mg/kg) coamorphous relative to the control (vehicle control, VC, 1% CMC, sodium carboxymethyl cellulose), CUR (50 mg/kg), ART (50 mg/kg), (CUR-ART 50 and 100 mg/kg) and doxorubicin (DOXO,

() No. of Animals

() No. of Animals

2mg/kg).Doxorubicin, a standard drug for pancreatic cancer, was used as positive control. CUR-ART, CUR and ART were administered orally with 1% CMC solution while doxorubicin was delivered through the tail vein (i,v). All drugs were administered daily for 5 weeks. A schematic representation of the six groups employed in this study (Figure 9a) shows that CUR-ART coamorphous and doxorubicin decreased tumor size significantly (P<0.0001) compared to all other solids and controls. The percentage of inhibition of CUR-ART (100mg/kg) is 61.87% which is close to doxorubicin 69.97% (2 mg/kg). The inhibition in other treated groups (at 50 mg/kg) is ART 29.22%, CUR 41.23% and CUR-ART coamorphous 41.41%. Based on these in vivo experiments, it is clear that CUR-ART coamorphous can be an effective treatment to inhibit tumor growth in Panc-1 xenograft mice model at 100 mg/kg dose. On day 28, the experimental mice were euthanized and tumors were excised from each group. The picture of these dissected tumors shows that the size of the tumor treated with 100 mg/kg CUR-ART coamorphous and 2 mg/kg doxorubicin is the smallest among other treated and non-treated groups (Figure 9b and 10). The body weight was similar in all the treated and non-treated groups (Figure 11, Supporting Information). Significant inhibition of tumor growth was evident in nude mice by treatment with CUR-ART coamorphous (p.o.) and Doxorubicin (i.v.) at 100 mg/kg/day and 2 mg/kg/day respectively (Figure 10). This indicates that solo or combination therapies could be considered to achieve fast treatment of cancer with minimal side effects.

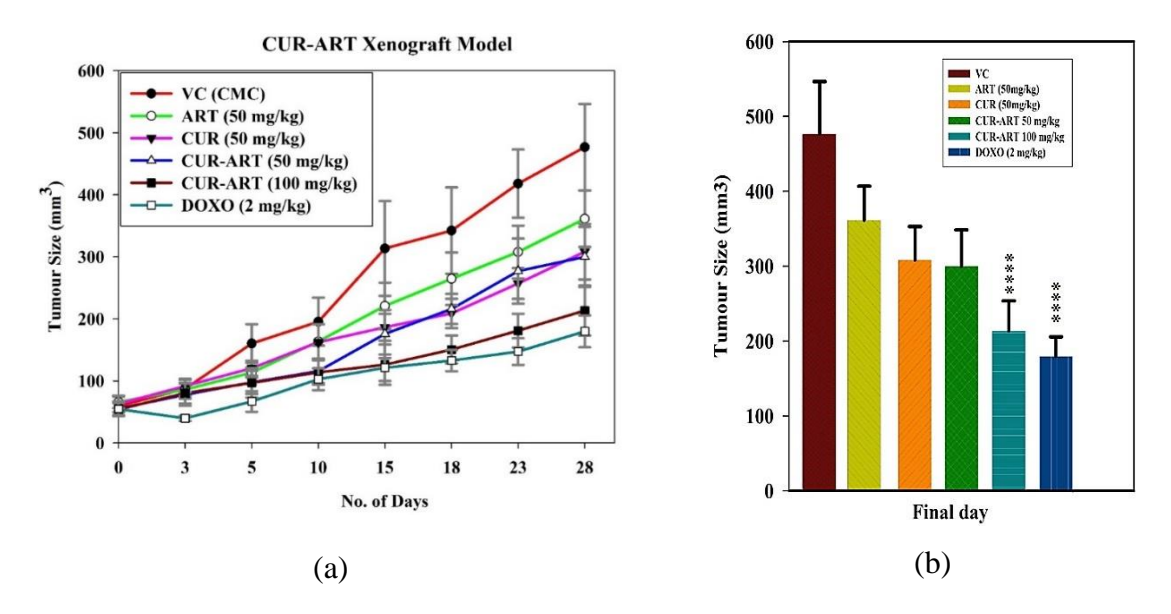


**Figure 9:** (a) Effect of VC, ART, CUR, CUR-ART and DOXO on tumor size during the study period. (b) Comparison of tumor size on day 28.

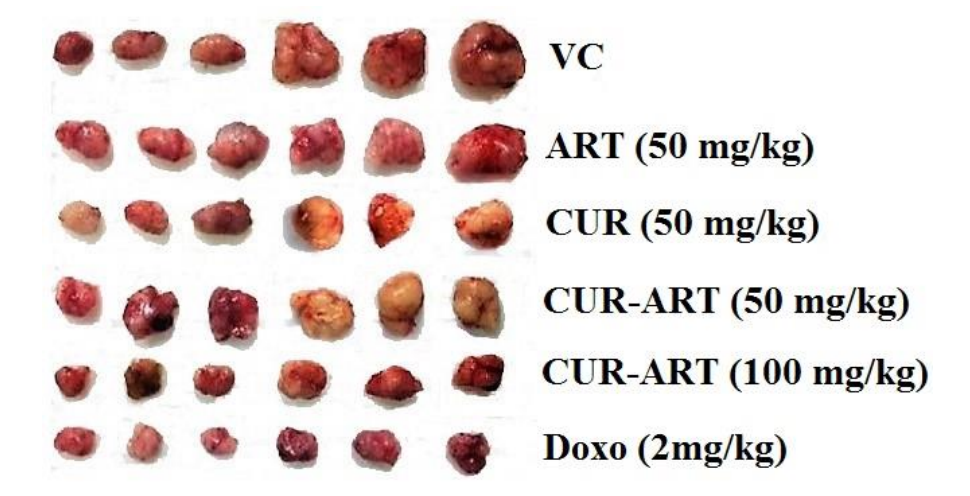


**Figure 10:** Tumor volume of established Panc-1 xenograft model in nude mice during therapy under different treatments.

# Body weights in (g) for Xenograft study

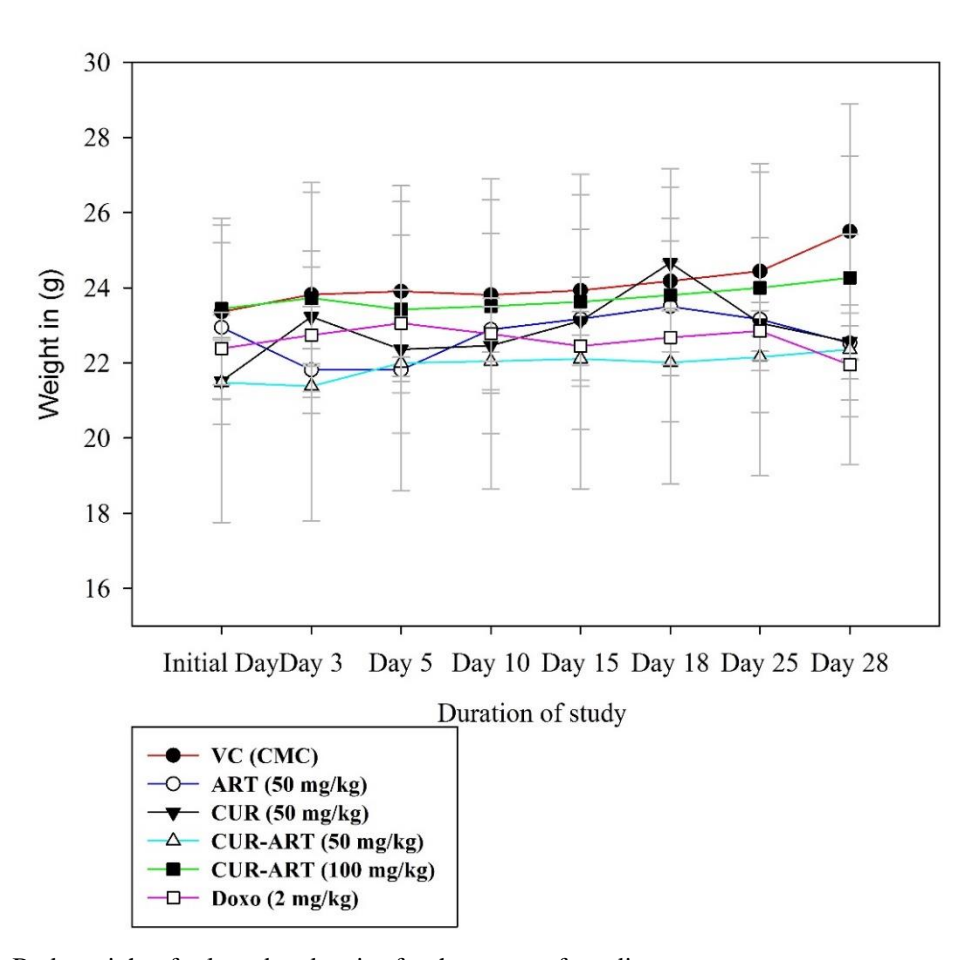


Figure 11: Body weight of selected nude mice for the xenograft studies.

#### 5.7 Materials and Methods.

#### **5.7 Materials**

Curcumin (purity > 99.8%) was obtained from Sigma-Aldrich (Hyderabad, India) and Artemisinin was purchased from Mangalam Drugs (Mumbai, India). Solvents (purity > 99%) were purchased from Merck (India). Water filtered through a double deionized purification system (Aqua DM, Bhanu, Hyderabad, India) was used for all experiments.

#### 5.8 Methods

# 5.8.1 Curcumin solids preparation method

CUR-PYR cocrystal: The cocrystal was obtained by grinding of CUR (1mmol) and PYR (1 mmol) in 1:1 stoichiometry with a few drops of EtOH added in a liquid-assisted method for 60 min. The resultant product was characterized cocrystal by PXRD and used in next experiments.

CUR-ART coamorphous:CUR (1mmol) and ART (1mmol) were taken in a 1:1 stoichiometric ratio and dissolved in 100 ethanol and rotavaporized at 50-55°c temperature. The resultant product was characterized as a coamorphous solid by PXRD and used in next experiments.

## 5.8.2 Characterization of multicomponent systems of Curcumin by PXRD

Powder X-ray diffraction (PXRD) was recorded on Bruker D8 Advance diffractometer (Bruker-AXS, Karlsruhe, Germany) using Cu-K $\alpha$  X-radiation ( $\lambda$  = 1.5406 Å) at 40 kV and 30 mA power. X-ray diffraction patterns were collected over the 2 $\theta$  range 5–50° at a scan rate of 5°/min.

#### 5.9 In Vivo Study Design and Drug Administration

Sprague-Dawley rats (200±50g) were obtained from Sainath Agencies Limited (Hyderabad, India). Animals were acclimatized for 1 week prior to experimentation in a temperature-controlled, 12/12 h light/dark room, and were allowed standard laboratory food and water. The rats were fasted overnight (~18 h) with free access to water before the experiment. The study was conducted in compliance with standard animal use practices at Virchow Biotech Private Limited, Department of preclinical toxicology, Hyderabad, India (Registration No.546/02/A/CPSCEA, India). IAEC Approval No. VB/UH/PCT/CUR-ART-2015/PT-3 dated 24-03-2015.

Pharmacokinetic studies of CUR-PYR, CUR-ART physical mixture/ coamorphous were conducted in Sprague Dawley rats (male and female) weighing (200±50g) (n=6) in crossover design. All compounds (200mg/kg) were suspended in 1% sodium carboxymethylcellulose (CMC) separately and administered by oral gavage. Blood (0.4 mL) was withdrawn from retro-orbital plexus into lithium heparin tube at the following times after drug administration: 30, 45, 60, 90, 120,180,240,360,480 and 720 min. After centrifugation for 2000g for 15 min, an aliquot of 0.2mL plasma was collected and

extracted curcumin from plasma by deproteination. The resulting plasma was frozen at  $-80^{\circ}$ C until HPLC analysis.

#### 5.9.1 Determination of Curcumin Plasma concentration

Curcumin Plasma concentrations of CUR were analyzed by HPLC. The area under the curve (AUC) for serum concentration versus time plots was calculated by linear trapezoidal rate. The maximum plasma concentration,  $C_{\text{max}}$ , and the time  $T_{\text{max}}$ , required to reach  $C_{\text{max}}$  were obtained from the plasma concentration curve.

## **5.9.2** Chromatographic Conditions

The HPLC analyses were performed using a Shimadzu Prominence model LC-20AD equipped with 20-mL injection loop, and a photodiode array detector and CUR detected at 420nm. Data acquisition and analysis were carried out using LC solution software. A C18 reversed-phase column (250mm×4.6 mm, particle size 5μm) preceded by a C18 guard column (33mm×4.6mm) was used for analysis. The mobile phase consisted of Acetonitrile- 5% acetic Acid (75:25, v/v) was run through the column at flow rate of 1.0 mL/min.

## 5.10Preparation of SGF and SIF media

Simulated Gastric Fluid (SGF): SGF was prepared according to USP specifications (Test Solutions, United States Pharmacopeia 35, NF 30, 2012). Sodium chloride (0.2 g) has to be added to a 100 mL flask and dissolved in 50 mL of water. Then 0.7 mL of 10 M HCl should add to adjust the pH of the solution to 1.2. To this, 0.32 g of pepsin should be added and dissolve with gentle shaking and the volume made up to 100 mL with water. Add pepsin only after the pH was adjusted to 1.2.

Simulated Intestinal Fluid (SIF): SIF was prepared according to USP specifications (Test Solutions, United States Pharmacopeia 35, NF 30, 2012). Monobasic potassium phosphate (0.68 g) dissolve in 25 mL of water, then 7.7 mL of 0.2 N NaOH will be added to adjust the pH to 6.8. To this, 1 g of pancreatin should add and shake gently until dissolve and the volume can be adjusted to 100 mL with water. Add Pancreatin after adjusting the pH of the solution to 6.8 to avoid precipitation of the enzyme.

## **5.10.1** Supersaturation study

Supersaturation of CUR and CUR-ART were measured in SGF and SIF (without enzyme) medium at 30 °C. The supersaturated solution (CUR 100  $\mu$ g/mL dissolved in 5 mL of SGF/SIF fluid) was stirred at 800 rpm using a magnetic stirrer at 30 °C. After regular intervals of time 2 h, 4 h, 6 h, 12 h and 24 h the solution concentration of curcumin was determined at 420 nm maxima on a Thermo Scientific Evolution 300 UV-Vis spectrometer (Thermo Scientific, Waltham, MA).

## 5.11 Acute Toxicity Study

In two different acute toxicity studies, Sprague Dwaley (SD) and Swiss albino mice (female and male) were used and obtained from Sainath Agencies Limited (Hyderabad, India). The study was conducted as per norms of the institutional guideline, quality assurance officer (QAO) with animal welfare regulations under an approved protocol by the Institutional Animal Care and Use Committee at Virchow Biotech Private Limited, Department of preclinical toxicology, Hyderabad, India (Registration No. 546/02/A/CPSCEA, India).

In two acute studies, Sprague Dwaley (SD) rats (6M+6F/group: 6-8 weeks of age; body weight range: 180–220 g) and Swiss albino mice (6M+6F/group; 6-8 weeks of age; body weight range: 18–21 g) were administered a single oral (gavage) dose of CUR-ART coamorphous and CUR-PYR cocrystal suspended in sodium carboxymethyl cellulose (CMC) at levels of 0 and 2000 mg/kg body weight. In all these experiments, animals were observed for 15 days for clinical signs as well as for morbidity and mortality. On day 15 at completion, all the animals were euthanized and gross pathological examinations were undertaken.

### 5.12 In Vitro Cell culture

The PANC-1 cells derived from human pancreatic carcinoma of ductal cell origin were obtained from National Center for Cell Science, Pune. The cells were cultured in Dulbecco's modified medium (DMEM) supplemented with 10% v/v fetal bovine serum (FBS), 1 % penicillin, and 1% streptomycin. Cultures (Figure 12) were maintained at 37°C in a humidified atmosphere with 5% CO<sub>2</sub>.

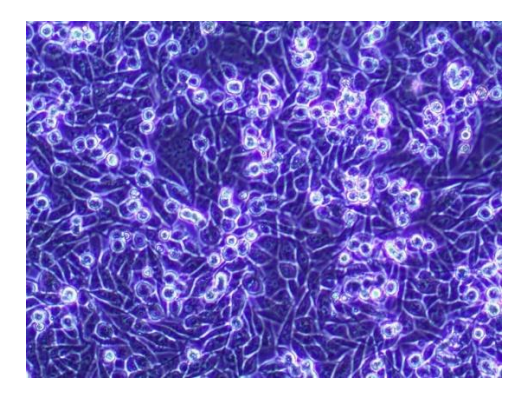


Figure 12: Morphology of PANC-1 cells.

# 5.13 In vivo PANC-1 Tumor Growth Xenograft Model

Female athymic nude mice were obtained from the National Centre for Laboratory Animal Sciences (NCLAS), National Institute of Nutrition (ICMR), Hyderabad, and were selected after careful initial screening for any external signs of disease or injuries. They were housed in individual cages in the conventional animal facilities of NCLAS, a registered facility with Committee for the Purpose of Control and Supervision of Experimentation on Animals (CPCSEA) (154/1999), Government of India.

The environmental conditions were kept at 21±2 °C, with 10-15 air changes per hour and relative humidity of 50-55 percent with 12 h light/dark cycle water. Animals were quarantined for 4 days and all the animals had free access to sterile formulated feed pellets and filtered potable clean water.

PANC-1 cells ( $1 \times 10^6$ ) using matrigel were injected subcutaneously into the flanks of mice (Figure 13). Tumor-bearing mice were then divided randomly into six treatment groups (six mice per group) and treatment initiated when the xenografted solid tumors reached a volume of about 80-100 mm<sup>3</sup>. Each mouse was administered orally (p.o) every day with either control vehicle (CMC), CUR (50 mg/kg), ART (50mg/kg), CUR-ART (50 and 100 mg/kg) and Intravenous (i.v.) route doxorubicin (2 mg/kg).All mice were cared for and maintained in accordance with animal welfare regulations under an approved protocol by the Institutional Animal Care and Use Committee at Virchow Biotech Private Limited, Department of preclinical toxicology, Hyderabad, India (Registration No. 546/02/A/CPSCEA, India).

After xenograft transplantation, mice exhibiting tumors were monitored (Figure 14) and tumor size was measured once every 3 and 5 days using caliper. The tumor volume in each animal was estimated according to the formula: tumor volume (mm<sup>3</sup>) =  $L \times W^2/2$  (where L is the length and W are the widths) with the final measurement taken 4 weeks after tumor cell inoculation. At the same time, the body weight of each animal was measured. At the end of the experiment (4 weeks after cell inoculation), the animals were euthanized by  $CO_2$  and sacrificed. Tumors from each animal were removed and measured.

## Implantation of cells by S.C. (Subcutaneous) route

PANC-1 xenograft tumors were implanted using martigel in 6-8-week-old Female nude mice by implanting  $1 \times 10^6$  PANC-1 cells s.c.





Figure 13: Implantation of cells through subcutaneous route (S.C.) using Matrigel.

## PANC-1 cells Implantation for tumour development

We observed tumour development while implanting PANC-1 cell lines after 4 weeks of observation (by implanting  $1 \times 10^6$  PANC-1 cells).





Figure 14: Tumor development of PANC-1 implanted cell lines in mice.

#### 5.14 Statistical Analysis

## 5.14.1 Bioavailability study

The standard curve was calculated by a linear relationship between concentration and area with regression factor R=0.999. The Area under the curve (AUC) for serum concentration vs. Time plots was calculated by the linear trapezoidal rule. The maximum plasma concentration  $C_{max}$  and the time  $T_{max}$  required to reach  $C_{max}$  were obtained from the plasma concentration curve. Statistical analysis was carried out, where matched paired t–test comparison and repeated measures of ANOVA were applied for different time points.

## 5.14.2 Xenograft Studies

Each value represents mean  $\pm$  SD. The control and experimental animal groups were compared by paired *t*-test. \*\*\*\*p < 0.0001 was considered significant.

## **5.15 Conclusions**

Examples of coamorphous drugs are as such rare in the literature <sup>34-37</sup>. Curcumin and artemisinin are herbal drugs of Indian and Chinese origins. The low solubility and short half-life of curcumin, and hence high dosage administered, have been a limitation to making drug formulations of curcumin. We have overcome the multiple disadvantages of curcumin in the designed CUR-ART coamorphous dispersion. This novel binary solid exhibits high solubility and bioavailability, extended half-life and action of bioactive curcumin at normal drug dose regime of 100 mg/kg. The therapeutic activity of CUR-ART in Xenograft models of Panc-1 is comparable to commercial drug doxorubicin. Given the

diverse biological action of curcumin and artemisinin, the high quantity of net drug delivered as coamorphous solid could open opportunity for an herbal formulation in cancer, malaria and several other treatments.

#### **5.16 References:**

- 1. Vikram, P.; Chiruvellam K.K.; Ripain, I.H.; Arifullah, M. A recent review on phytochemical constituents and medicinal properties of kesum (*Polygonum minus* Huds.) *Asian Pac. J. Trop Biomed.* 2014, 4, 430–435.
- 2. Newman, D.J.; Cragg G.M., Natural Products as Sources of New Drugs from 1981 to 2014. *J Nat Prod.* 2016, 79, 629–661.
- 3. Gurib-Fakim, A. Medicinal plants: traditions of yesterday and drugs of tomorrow. *Mol Aspects Med.* 2006, 27, 1–93.
- 4. Cragg, G.M.; Newman D.J. Plants as a source of anti-cancer agents. *J Ethnopharm* 2005, 100, 72–79.
- 5. Jin, D.; Russell, J.M. Plant Phenolics: Extraction, Analysis and Their Antioxidant and Anticancer Properties. *Molecules*. 2010, 15, 7313–7352.
- Isacchi, B.; Bergonzi, M.C.; Grazioso, M.; Righeschi, C.; Pietretti, A.; Severini, C. Bilia, A.R. Artemisinin and artemisinin plus curcumin liposomal formulations: Enhanced antimalarial efficacy against Plasmodium berghei-infected mice. *Eur J Pharm Biopharm*. 2012, 80, 528–534.
- 7. Anand, P.; Kunnumakkara, AB.; Newman, R.A.; Aggarwal, B.B. Molecular Bioavailability of Curcumin: Problems and Promises. *Mol Pharmaceutics*. 2007, 4, 807–818.
- 8. Shanmugam, M.K.; Rane, G.; Kanchi, M.M.; Arfuso, F.; Chinnathambi, A.; Zayed, M.E.; Alharbi, S.A.; Tan, B.K.H.; Kumar, A.P.; Sethi, G. The Multifaceted Role of Curcumin in Cancer Prevention and Treatment. *Molecules*. 2015, 20, 2728–2769.
- 9. Sharma, R.A.; Euden, S.A.; Platton, S.L.; Cooke, D.N.; Shafayat, A.; Hewitt, H.R.; Marczylo, T.H.; Morgan, B.; Hemingway, D.; Plummer, S.M. Phase I clinical trial of oral curcumin: Biomarkers of systemic activity and compliance. *Clin Cancer Res.* 2004, 10, 6847–6854.
- 10. Tu, Y. Artemisinin-A Gift from Traditional Chinese Medicine to the World (Nobel Lecture). *Angew Chem Int Ed.* 2016, 55, 10210 –10226.
- 11. The National Leading Group Office for Malaria Control, Communication on Malaria Control Research, 5th November 1972.
- 12. Padmanabam, G.; Nagaraj, V.A.; Rangarajan, P.N. Artemisinin-based combination with curcumin adds a new dimension to malaria therapy. *Current Science*. 2012, 102, 704–711.
- 13. Nandakumar, D.N.; Nagaraj, V.A.; Vathsala, P.G.; Rangarajan, P.; Padmanaban, G. Curcumin-Artemisinin Combination Therapy for Malaria. *Antimicrob Agents Chemother*. 2006, 50, 1859–1860.

- 14. WHO, Guidelines for the Treatment of Malaria, 3<sup>rd</sup> Ed. April 2015.
- 15. Xu, Q,; Bauer, R,; Hendry, B.M,; Fan, T.P,; Zhao, Z,; Duez, P,; Simmonds, M.S.J,; Witt, CM,; Lu, A,; Robinson, N,; Guo, D,; Hylands, P.J. The quest for modernization of traditional Chinese medicine. *BMC Complementary and Alternative Medicine*. 2013, 13(132),1–11.
- 16. Rapport, L.; Lockwood, B. Nutraceutical. Pharmaceutical Press, London, 2002.
- 17. Lockwood, B. Nutraceuticals. Pharmaceuticals Press: London, UK, 2007.
- 18. Qureshi, S.; Shah, A.H.; Ageel, A.M. Toxicity studies on Alpinia galanga and Curcuma longa. *Planta Med.* 1992, 58, 124-127.
- 19. Ravindran, J.; Prasad, S.; Aggarwal, B.B.; Curcumin and Cancer Cells: How Many Ways Can Curry Kill Tumor Cells Selectively? *The AAPS Journal*. 2009, 11, 495–510.
- 20. Epelbaum, R,; Schaffer, M,; Vizel, B,; Badmaev, V,; Bar-Sela, G. Curcumin and gemcitabine in patients with advanced pancreatic cancer. *Nutr Cancer*. 2010. 62, 1137–1141.
- 21. Dhillon, N.; Aggarwal, B.B.; Newman, R.A.; Wolff, R.A.; Kunnumakkara, A.B.; Abbruzzese, J.L.; Ng, C.S.; Badmaev, V.; Kurzrock, R. Phase II trial of curcumin in patients with advanced pancreatic cancer. *Clin Cancer Res.* 2008, 14, 4491–4499.
- 22. Rachmawati, H.; Edityaningrum, C.A.; Mauludin, R. Molecular inclusion complex of curcumin-beta-cyclodextrin nanoparticle to enhance curcumin skin permeability from hydrophilic matrix gel. *AAPS Pharm Sci Tech.* 2013, 14, 1303-1312.
- 23. Khalil, N.M.; Do.; N.T.C.; Casa, D.M.; Dalmolin, L.F.; De, M.A.C.; Hoss, I. Pharmacokinetics of curcumin-loaded PLGA and PLGA-PEG blend nanoparticles after oral administration in rats. *Colloids Surf Biointerfaces*. 2013, 101, 353–360.
- 24. Li, C,; Zhang, Y,; Su, T,; Feng, L,; Long, Y,; Chen, Z. Silica-coated flexible liposomes as a nanohybrid delivery system for enhanced oral bioavailability of curcumin. *Int. J. Nanomed.* 2012, 7, 5995–6002.
- 25. Yang, C,; Wang, Z,; Ou, C,; Chen, M,; Wang, L,; Yang, Z. The first supramolecular hydrogelator of curcumin. *Chem Commun.* 2014, 50, 9413—9415.
- 26. Sanphui, P.; Goud, N.R.; Khandavilli, U.B.R.; Bhanoth, S.; Nangia, A. New polymorphs of curcumin. *Chem Commun.* 2011, 47, 5013–5015.
- 27. Sanphui, P,; Goud, N.R,; Khandavilli, U.B.R,; Nangia, A. Fast Dissolving Curcumin Cocrystals. *Cryst Growth Des.* 2011, 11, 4135–4145.
- 28. Goud, N.R.; Suresh, K.; Sanphui, P.; Nangia, A. Fast dissolving eutectic compositions of curcumin. *Int J Pharm.* 2012, 439, 63–72.
- 29. Suresh, K.; Mannava, M.K.C.; Nangia, A. A novel curcumin–artemisinin coamorphous solid: physical properties and pharmacokinetic profile. *RSC Adv.* 2014, 4, 58357–58361
- 30. Tong, W.Q.; Wen, H.; Liu, R, E.d. Preformulation aspects of insoluble compounds. In Water-Insoluble Drug Formulation; *CRC Press*, Taylor and Francis: Boca Raton, FL. 2008, 63.

- 31. Babu, N.J.; Nangia, A. Solubility Advantage of Amorphous Drugs and Pharmaceutical Cocrystals. *Cryst Growth Des.* 2011, 11, 2662–2679.
- 32. Sasaki, H.; Sunagawa, Y.; Takahashi, K.; Imaizumi, A.; Fukuda, H.; Hashimoto, T.; Wada, H.; Katanasaka, Y.; Kakeya, H.; Fujita, M.; Hasegawa, K.; Morimoto, T. Innovative preparation of curcumin for improved oral bioavailability. *Biol Pharm Bull*. 2011, 34, 660–665.
- 33. Marczylo, T.H.; Verschoyle, R.D.; Cooke, D.N.; Morazzoni, P.; Steward, W.P.; Gescher, A.J. Comparison of systemic availability of curcumin with that of curcumin formulated with phosphatidylcholine. *Cancer Chemother Pharmacol.* 2007, 60, 171–177.
- 34. Dengale, S.J.; Grohganz, H.; Rades, T.; Löbmann, K.; Recent advances in co-amorphous drug formulations. *Adv. Drug Deliv Rev.* 2016, 100, 116–125.
- 35. Ueda, H,; Muranushi, N,; Sakuma, S,; Ida, Y,; Endoh, T,; Kadota, K,; Tozuka, Y. A Strategy for Co-former Selection to Design Stable Co-amorphous Formations Based on Physicochemical Properties of Non-steroidal Inflammatory Drugs. *Pharm Res.* 2016, 33, 1018–1029.
- 36. Laitinen, R,; Löbmann, K,; Grohganz, H,; Strachan, C,; Rades, T. Amino Acids as Coamorphous Excipients for Simvastatin and Glibenclamide: Physical Properties and Stability. *Mol Pharmaceutics*. 2014, 11, 2381–2389.
- 37. Kasten, G.; Grohganz, H.; Rades, T.; Löbmann, K. Development of a screening method for co-amorphous formulations of drugs and amino acids. *Eur J Pharm Sci.* 2016, 95, 28–35.

### **CHAPTER SIX**

# Ribociclib: Crystal Structure Analysis of Ribociclib Salts

Ribociclib (RBC), a BCS class IV drug, was crystallized with different coformers such as benzoic acid (BA), 3-methoxybenzoic acid (3-MBA), 4-hydroxybenzoic acid (4-HBA) and 3,4,5-tryhydroxybezoic acid (345-THBA). The salts of RBC were prepared utilizing the solvent-assisted grinding method. In addition to the single-crystal X-ray diffraction studies, these solids were characterized by powder X-ray diffraction (PXRD), Infrared spectroscopy (IR) and differential scanning calorimetry (DSC). Single crystals of the binary salts were obtained in various solvents by solution crystallization.

### **6.1 Introduction**

Crystal engineering is a fascinating technique for constructing various multi-component solid-state forms using non-covalent interactions. <sup>1,2,3</sup> The design and synthesis of pharmaceutical solid forms such as polymorphs, salts, cocrystals, hydrates and solvates of active pharmaceutical ingredients (APIs) have been mostly manifested supramolecular synthons, in which one acidic/accepter component and another one basic/donor component are utilized. <sup>4</sup> Pharmaceutical salt establishment is the most efficient method for modifying the physicochemical and pharmacological activities of APIs, such as solubility, stability and bioavailability. <sup>5</sup> It has been shown that stoichiometrically combined in a ratio of molecular or ionic API and a GRAS <sup>6</sup> coformer (generally regarded as safe) in a crystalline state wherein the solubility of salt former can improve 10 times or more than the pure API. <sup>7</sup> Hence, crystalline salt formation can modify solubility more than 2000 fold compared to cocrystals and polymorphs. <sup>8</sup>

Ribociclib<sup>9</sup> (**RBC**) named as chemically 7-cyclopentyl-N,N-dimethyl-2-{[5-(piperazine-1-yl)piperidine-2-yl]amino}-7H-pyrrole[2,3-d]pyrimindine-6-formamide belongs to the Biopharmaceutics Classification System (BCS) <sup>10</sup> Class IV drug of poor solubility (0.231 mg/mL) and low permeability (log P 2.38, Chemaxon calculator). **RBC** is a selective cyclin-dependent kinase inhibitor, containing two proteins called cyclin-dependent kinase 4 and 6 (CDK4/6) and which inhibit the progression of cancer slowly. This drug first marketed by Novartis Pharmaceuticals Corporation under the brand name Kisqali (LEE011). Kisqali (**RBC**) is a safe and effective anticancer drug (200 mg dose) but has significant antitumor activity in metastatic breast cancer and advanced breast cancer. Pharmaceutical solid-forms of **RBC** are essential drugs which are very less explored in the published literature. Few polymorphs, hydrates and solvates of **RBC**-Succinate have been reported as crystalline salts.<sup>11</sup> So far, there is no report on crystal structures of **RBC** and it's solid-state forms.

### 6.2 Results and Discussion

Ribociclib (7-cyclopentyl-N,N-dimethyl-2-{[5-(piperazine-1-yl)piperidine-2-yl]amino}-7H-pyrrole [2,3-d]pyrimindine-6-formamide, RBC, Scheme 6.1) is a conformationally flexible and chemically diverse functionally (piperazine and carbonyl functional groups) for the formation of intermolecular interactions and supramolecular synthons. The carbonyl (-C=O), piperazine (-NH) tendency to form multiple supramolecular synthons, such as N-H<sup>+--</sup>O<sup>-</sup>, O-H<sup>--</sup>O and O-H<sup>--</sup>O<sup>-</sup> in salts with acid functional group of the coformers. In this background, the synthesis and crystal structure investigation for pharmaceutical salts (Scheme 6.1) of Ribociclib (RBC) with acid based coformers (full list of coformers in Table 6.1) such as benzoic acid (BA), 3-methoxybenzoic acid (3-MBA), 4-hydroxybenzoic acid (4-HBA) and 3,4,5-trihydroxybenzoic acid (345-THBA). RBC containing basic (-NH) group of piperazine which is found to show a strong tendency toward the subtract proton from acid (-COOH) group of coformer, whereas formation of salt-bridge determined through supramolecular synthon.<sup>12</sup> the salts of RBC were prepared utilizing the solvent-assist grinding. All the solids were characterized by powder

X-ray diffraction (PXRD), Infrared spectroscopy (IR) and differential scanning calorimetry (DSC) to support the crystalline phases. Single crystals of the binary salts were obtained in various solvents by solution crystallization, and their structures were studied by single crystal X-ray diffraction (SC-XRD) (Table 6.2). In Addition, These binary salts are carried out for improvement in the physicochemical properties.

**Scheme 6.1**: Molecular structures and acronyms of Ribociclib and coformers.

**Table 6.1:** List of coformers attempted for salts with RBC in this study. The successful molecules which gave crystalline products are shown in bold font.

Hydroquinone	Histidine
Apocyanin	Phloroglucinol
Catechol	Hydroquinone
Benzoic acid	Theophylline
Maleic acid	Thymine
Fumaric acid	3-Methoxy benzoic acid
Piperazine	4-Hydroxy benzoic acid
Adenine	Saccharin
Guaiacol	Isoniazid
Adipic acid	Caffeine
Succinic acid	Adenine
Urea	3,4,5-Tryihydroxy benzoic acid
Cytosine	Nicotinamide
L-Tartaric acid	D-Glucose
Ethyl vanillin	Vanillyl alcohol
Vanillin	Pyrazinamide

**Table 6.2:** Crystallographic parameters of RBC salts.

	RBC-BA(1:1)		RBC-4HBA(1:1)	RBC- 345THBA(1:1)
Emp. form.	$C_{60}H_{67}N_{16}O_{7}$	$C_{62}H_{79}N_{16}O_{10}$	$C_{30}H_{35}N_8O_4$	C <sub>51</sub> H <sub>54</sub> N <sub>8</sub> O <sub>21</sub>
Form. wt.	1124.30	427.42	503.48	1115.02
Cryst. system	Triclinic	Triclinic	Triclinic	Triclinic
Space group	P -1	P -1	P 21/n	P -1
T (K)	297	299	296	299
a (Å)	10.6804(9)Å	11.0894(4)	11.5474(8)	11.0823(13)
<b>b</b> (Å )	15.3427(17Å	15.6906(7)	8.1010(8)	12.6131(12)
c (Å )	20.179(2) Å	19.9563(9)	30.949(3)	18.980(2)
a (°)	107.284(11)	111.589(2)	90	94.416(4)
β (°)	105.064(9)	95.991(2)	91.241(7)	100.945(5)
γ (°)	92.495(8)	97.094(2)	90	90.645(4)
Z	2	2	4	2
$\mathbf{V}(\mathbf{\mathring{A}}^3)$	3022.6(6)	3161.6(2)	2894.5(4)	2596.2(5)
Rflns. collect	13159	14908	5921	10677
Unique rflns.	12574	14649	5891	10658
Obsd. rflns.	2553	7054	2483	7016
Parameters	796	807	385	724
$R_1$	0.1187	0.0863	0.0852	0.1354
$\mathbf{w}\mathbf{R}_2$	0.3988	0.2470	0.2526	0.3788
GOF	0.927	1.022	0.917	1.511
Diffractometer	Bruker APEX-II CCD detector	Bruker APEX-II CCD detector	Bruker APEX-II CCD detector	Bruker APEX- II CCD detector

### 6.3 Crystal Structure Analysis '

### **RBC-HYD** (1:1):

RBC-hydrate crystallizes in  $P2_1/n$  space group and its asymmetric unit consists of one unit each of RBC and H<sub>2</sub>O molecule. Each RBC molecule is strongly hydrogen bonded with two water molecules and one RBC molecule, whereas each H<sub>2</sub>O is found to participate in strong hydrogen bonding with two RBC molecules (Figure ...a and b). RBC molecules remain pairwise through the formation of hydrogen bonded homosynthons composed of N-H···N hydrogen bonds (N-H···N: 2.23 Å, 165°) between the amino-pyridine moieties with  $R_2^2$ (8) ring motif (Figure 6.1a). Each H<sub>2</sub>O is connected to two RBC via O-H···N (O-H···N: 2.03 Å, 161°) and O-H···O (O-H···O: 1.86 Å, 166°) hydrogen bonding (Figure 6.1b). Such type of hydrogen bonding of RBC and water molecule leads to the formation of 2D corrugated layered type network (Figure 6.1c).

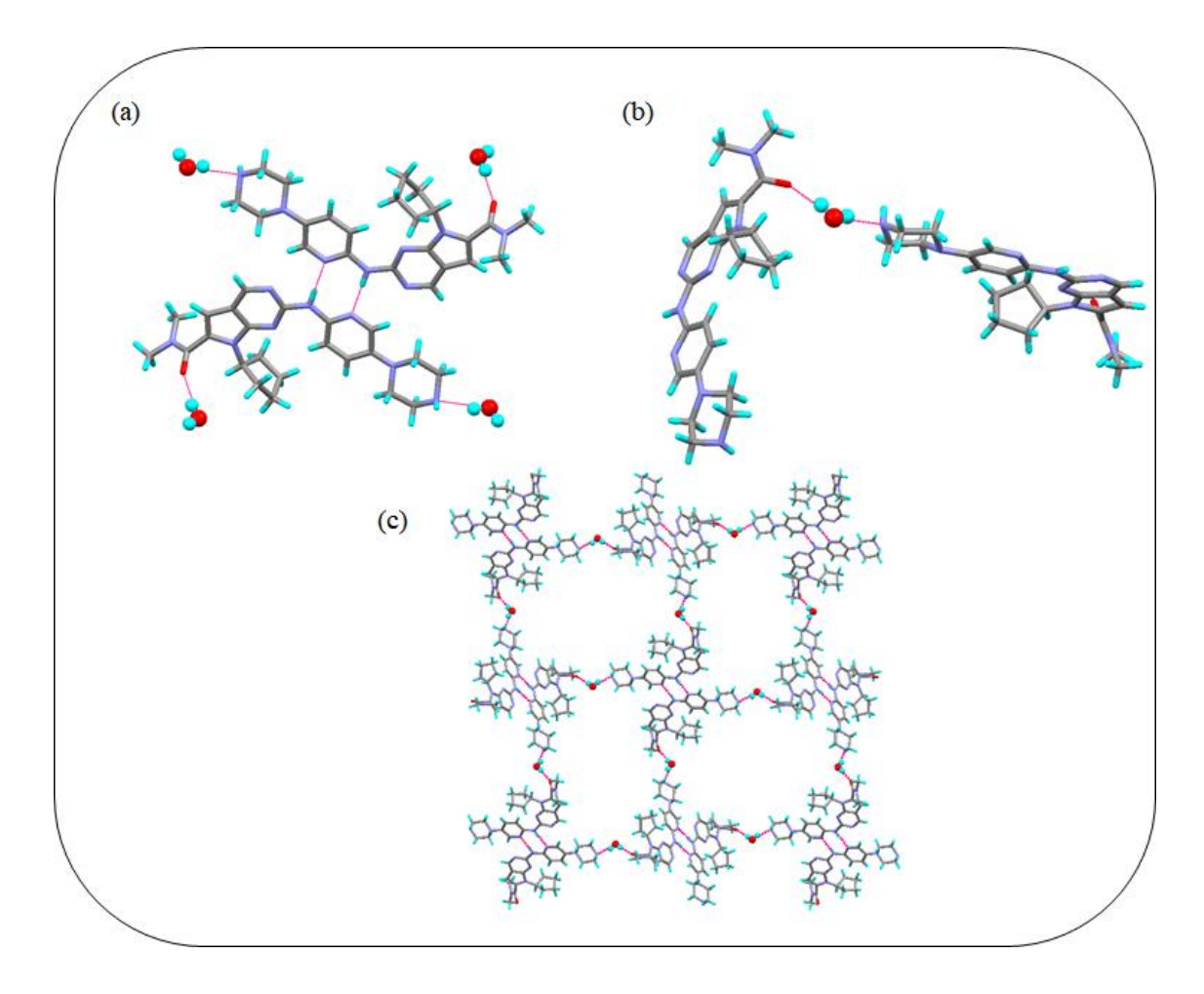


**Figure 6.1:** (a) Hydrogen bonds of RBC with the surrounding water molecules and RBC (b) Hydrogen bonds of a water molecule with two RBC units. (c) Hydrogen-bonded 2D corrugated layered network.

### RBC-BA-HYD (2:2:1) salt hydrate:

This salt hydrate crystallizes in P-1 space group and its asymmetric unit consists of two units each of singly protonated RBC and singly deprotonated BA units and one water molecule. Two crystallographically independent RBC units form a dimer through N-H···N (N-H···N: 2.18 Å, 170°; 2.20 Å, 158°) hydrogen bonds and further these dimers are self-assembled via N<sup>+</sup>-H···O (N-H···O: 2.28 Å, 135°) hydrogen bond which leads to the formation of a cyclic ring structure (Figure 6.2a). Coformer and water molecules are found to construct a hydrogen-bonded cyclic synthon and further water molecules are connected to the RBC units via N<sup>+</sup>-H···O (N···O: 2.797 Å) hydrogen bonds (Figure 6.2b). Above-mentioned hydrogen bonds are found to form a two dimensional hydrogen-bonded layered structure (Figure 6.2c).

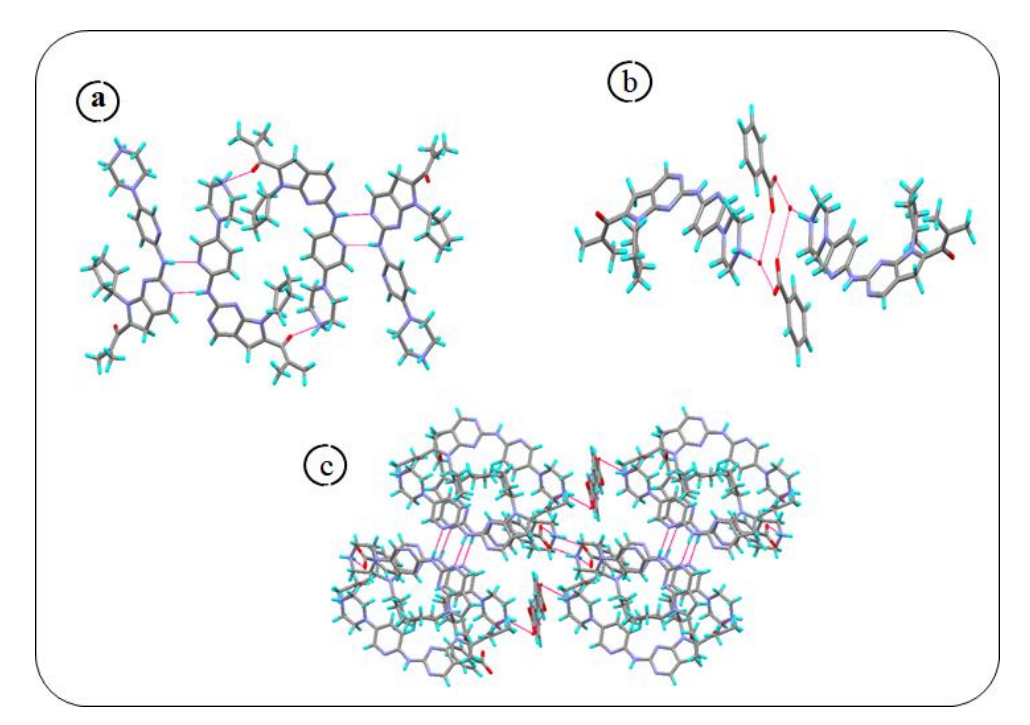


**Figure 6.2:** Crystal structure of **RBC-BA** salt (a) Self-assembled hydrogen-bonded cyclic structure of protonated RBC units (b) Hydrogen-bonded cyclic synthon formed by water molecules and coformers, and the APIs remain as pendant from this structural unit. (c) Hydrogen bonded 2D layered structure

### **RBC-3-MBA-HYD** (1:1:1) salt-hydrate:

Single crystals of hydrated **RBC-3-MBA** salt were obtained by crystallization from a equimolar mixture of acetonitrile and water. The crystal structure was solved in *P*-1 space group in which **RBC** molecule forms a salt by transferring proton from the acid coformer **3-MBA**. In this crystal structure, two molecules of **RBC** are connected by N<sup>+</sup>-H<sup>--</sup>O hydrogen bonds (N-H<sup>--</sup>O, 1.90 Å, 170°) in a centrosymmetric synthon. **RBC-3-MBA** salt is stabilized between piperazine (-NH<sup>+</sup>) of **RBC** and acid (-COO<sup>-</sup>) of **3-MBA** by N<sup>+</sup>-H<sup>--</sup>O hydrogen bonds (N-H<sup>--</sup>O, 1.79 Å, 160°). **RBC-3-MBA** salt is connected by hydrogen bonds of water (O-H) with the (-COO<sup>-</sup>) of **3-MBA** via O-H<sup>--</sup>O (O<sup>--</sup>O, 2.927 Å) interactions. Further **RBC-3-MBA** salt extends with water molecules in a layered packing of one-dimensional (1D) tapes (Figure 6.3).

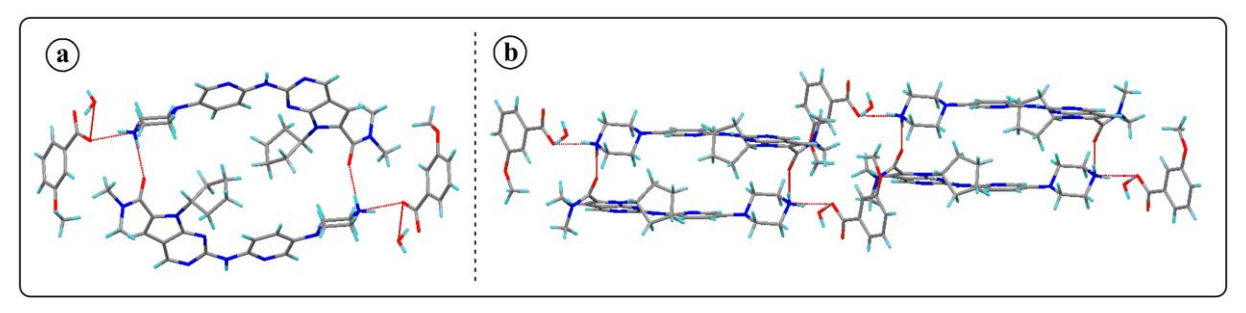


**Figure 6.3:** Crystal structure of **RBC-3-MBA** salt (a) **RBC** connected with **3-MBA** and H<sub>2</sub>O via N<sup>+</sup>-H<sup>...</sup>O, N<sup>+</sup>-H<sup>...</sup>O<sup>-</sup> and O-H<sup>...</sup>O<sup>-</sup> synthons (b) layered packing of **RBC-3-MBA** with water.

### **RBC-4-HBA** (1:1) salt:

Good quality single crystals of **RBC-4-HBA** salt were obtained by crystallization from an equimolar mixture of acetonitrile and water. The crystal structure was solved in P 2<sub>1</sub>/n space group in which **RBC** molecule forms a salt by transferring a proton from the acid coformer 4-**HBA**. In this crystal structure, **RBC-4-HBA** salt is stabilized between piperazine (-NH<sup>+</sup>) of **RBC** and acid (-COO<sup>-</sup>) of **4-HBA** by N-H<sup>+</sup>···O<sup>-</sup>hydrogen bonds (N-H···O: 1.92 Å, 171°; 1.87 Å, 156°). **RBC-4-HBA** salt is connected by hydrogen bonds with (-COO<sup>-</sup>) of **4-HBA** via O-H···O<sup>-</sup> (O-H···O, 1.90 Å, 161°). **RBC-4-HBA** salt extends in a layered packing (Figure 6.4).

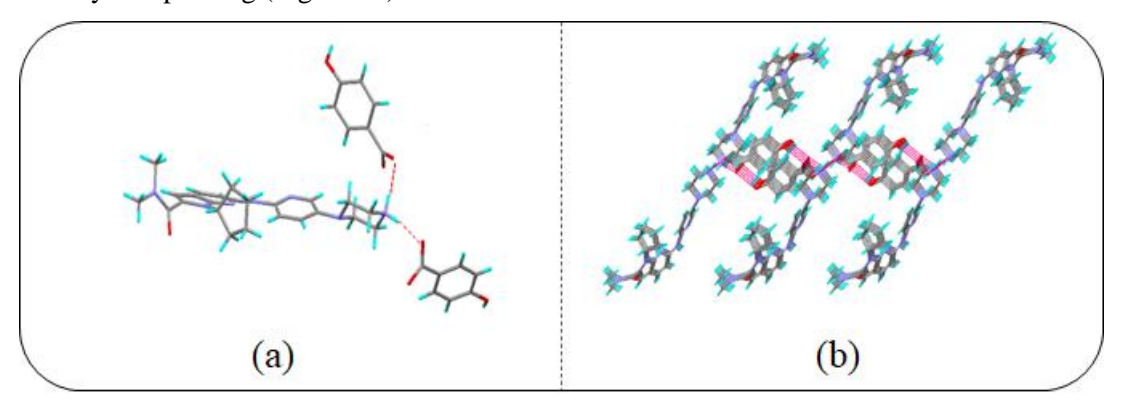


**Figure 6.4:** Crystal structure of **RBC-4-HBA** salt (a) **RBC** connected with **4-HBA** via N-H<sup>+...</sup>O<sup>-</sup> synthon (b) layered packing of **RBC-4-HBA** extended via O-H<sup>...</sup>O<sup>-</sup> interactions.

### RBC-345-THBA (1:4) salt-cocrystal:

This complex crystallizes in P-1 space group and its asymmetric unit is composed of one unit each of protonated RBC unit and deprotonated 345THBA and three neutral 345THBA units. Due to the presence of both neutral and ionic coformer, this complex can be considered as a salt-cocrystal. Each protonated RBC unit is hydrogen bonded to two crystallographically independent neutral 345THBA coformers and two crystallographically singly deprotonated acid coformers. Between two neutral 345THBA coformers, one is connected with pyrimidine moiety of RBC via O-H...N (O18-H18O...N4: 1.92 Å, 168°) hydrogen bond and the other one is connected with aminopyridine moiety of RBC through O-H...N (O8-H8O...N6: 1.81 Å, 167°) and N-H...O (N5-H5N...O7: 2.14 Å, 162°) hydrogen bonds with R<sup>2</sup><sub>2</sub>(8) ring motif. Remaining two crystallographically identical ionic coformers are linked with piperazinium moiety of the RBC unit via charge-assisted N<sup>+</sup>-H...<sup>-</sup>OOC (N8-H00A...O12: 1.94 Å, 155°; N8-H00B...O13: 1.97 Å, 162°) hydrogen bonds (Figure 6.5a). Four crystallographically independent coformer units (three neutral and one ionic) are assembled to form a discrete unit via charge-assisted O-H...<sup>-</sup>O (O3-H3O...O13: 1.72 Å, 169°) hydrogen bond between –COOH and –COO<sup>-</sup>, and O-H...O (O15-H150...O21: 1.98 Å, 161°; O19-H19O...O11: 1.94 Å, 173°) hydrogen bonds between hydroxyl groups (Figure 6.5b). Each of the discrete units of the coformers are connected to three protonated RBC units leading to the formation of 1D-chain of molecules/ions (Figure 6.5c).

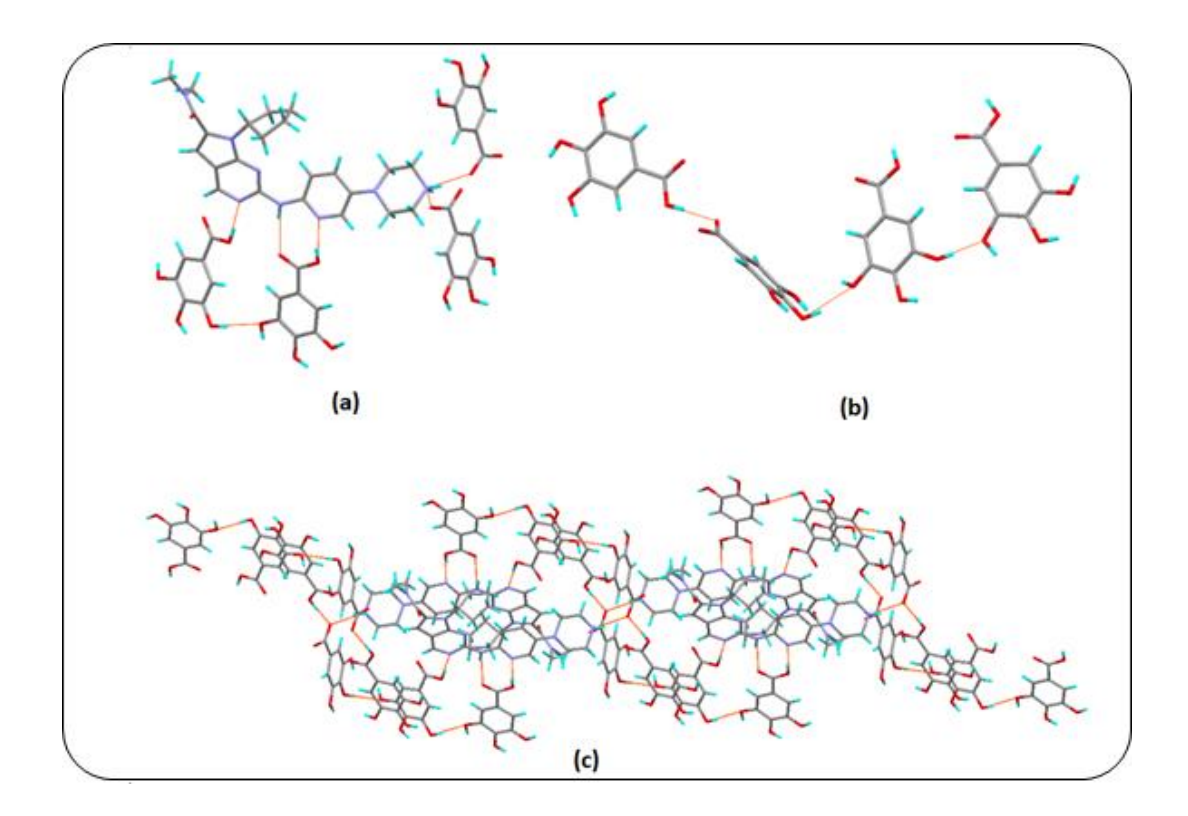


**Figure 6.5:** Crystal structure of **RBC-345-THBA** salt. (a) hydrogen bonding of a RBC unit, (b) hydrogen bonding among the coformers, (c) hydrogen-bonded 1D chain.

RBC-BA = 
$$-N \odot N + O \odot N + O$$

Figure 6.6: Synthons in RBC salts crystal structures.

### **6.4 FT-IR Spectroscopy**

Infrared spectroscopy provides information about the vibration modes of a molecule due to changes in molecular conformations and hydrogen bonding. The tertiary amide carbonyl (C=O) stretching vibrations of RBC appears at 1630 cm<sup>-1</sup> and NH stretching band is at 3388 cm<sup>-1</sup>. All these functional groups showed significant changes in their vibration peaks upon salts formation (Table 6.3 and Figure 6.7-6.10). all the salts were characterized by single crystal structures and their unique powder X-ray diffraction pattern and molecular level interactions in FT-IR spectra. The stretching bands of C=O, O-H and N-H are significantly shifted compared to RBC to indicate hydrogen bonding. These differences support the presence of O-H····N, C=O···H, and NH···O bonding between RBC and coformer. (Figure 6.7-6.10)

**Table 6.3:** IR stretching frequencies of RBC/coformer functional groups in the crystalline forms (Figure 6.7-6.10 spectra).

Compounds	$v_{C=O}$ (cm <sup>-1</sup> ) for -COOH/ -COO-/ -CONMe <sub>2</sub>	ν <sub>N-H/O-H</sub> (cm <sup>-1</sup> )	v <sub>C-H</sub> (cm <sup>-1</sup> ) for aliphatic and aromatic CH
RBC	1630, 1604	3388, 3225	3094, 3038, 2942, 2863
RBC-BA	1696, 1618	3432, 3071, 3006	2883, 2835, 2725
BA	1611	3035,2960	2847
RBC-4HBA	1605,1536	3648,2962,2866	2687,2463
4HBA	3382	2969	2667,2549
RBC- 345THBA	1609, 1535	3391,3226	
345-THBA	1662,1627		
RBC-3MBA	1669,1606	3016	2949,2843,2638
3MBA	1632,1606	3674,3326,3220	3002,2961

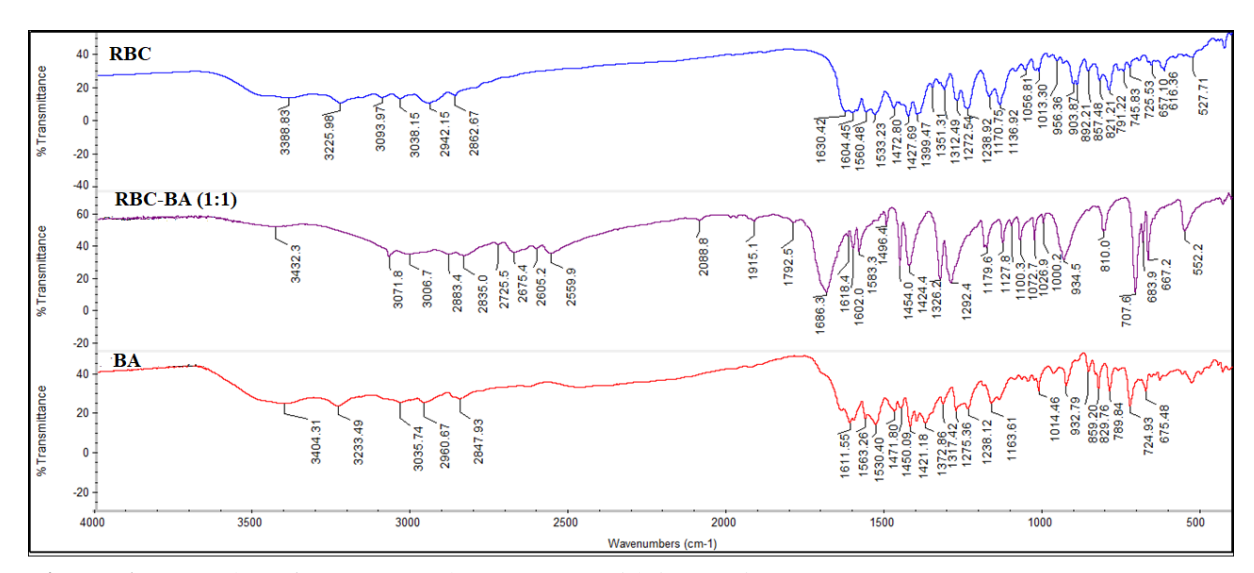


**Figure 6.7:** Overlay of RBC-BA salt IR spectra with its starting components.

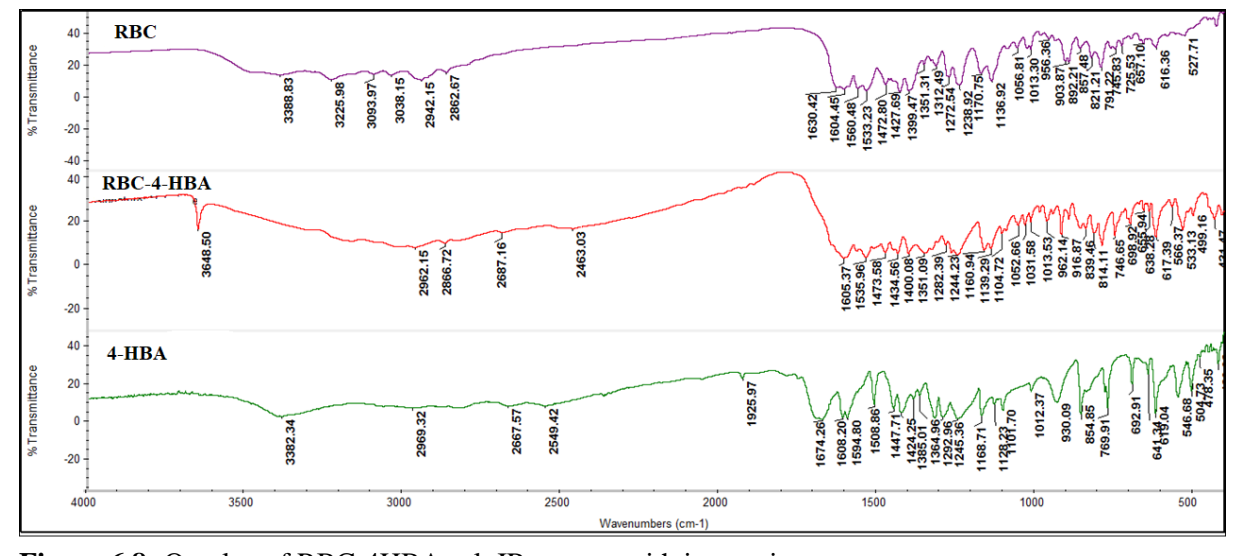


**Figure 6.8:** Overlay of RBC-4HBA salt IR spectra with its starting components.

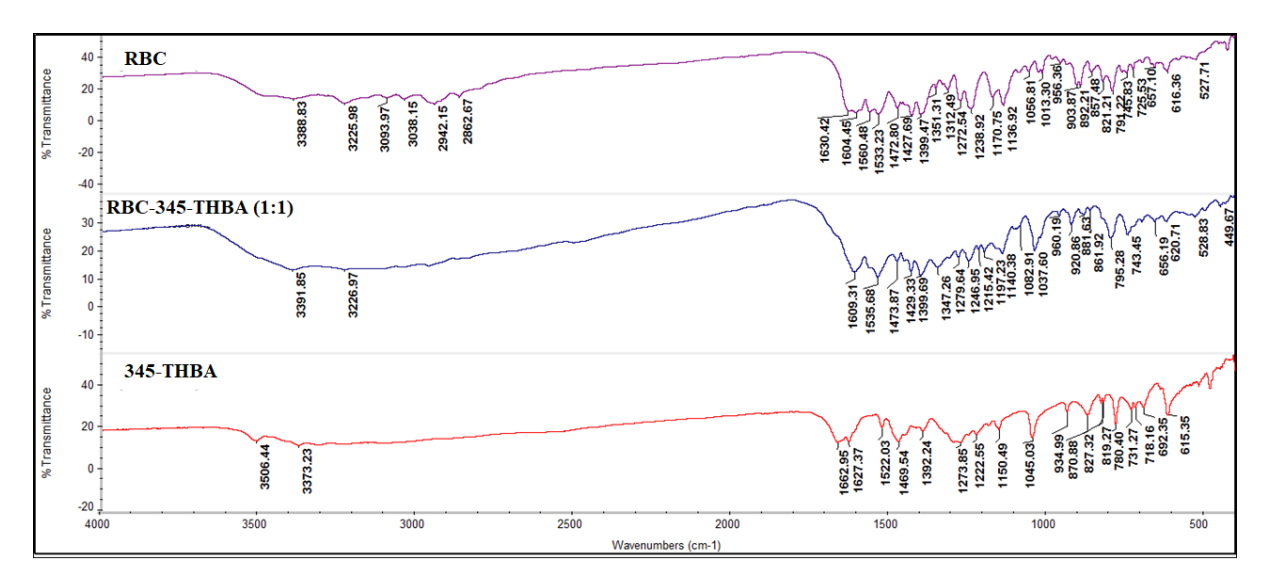
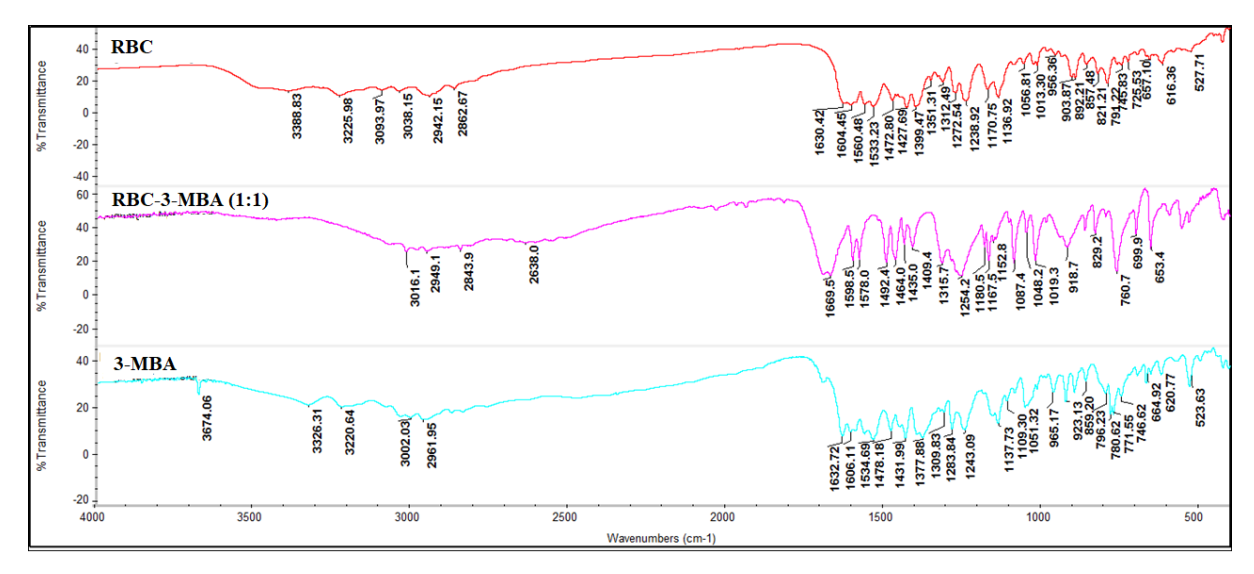


Figure 6.9: Overlay of RBC-345-THBA salt IR spectra with its starting components.



**Figure 6.10:** Overlay of RBC-3MBA salt IR spectra with its starting components.

### 6.5 Powder X-ray Diffraction

PXRD: In order to check bulk purity, PXRD patterns of the synthesized materials (through liquid-assisted grinding method) were compared with the simulated PXRD patterns generated from crystal structures of those materials. From the PXRD studies, it was observed that PXRD patterns of the ground materials matched well with simulated PXRD patterns of the respective single crystal materials. This experiment clearly shows that after liquid-assisted grinding, pure single-phase materials are produced for these four complexes.

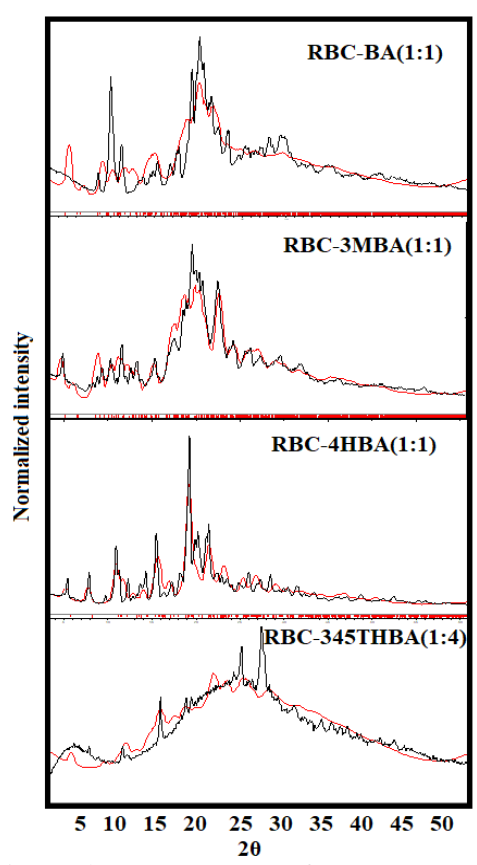


**Figure 6.11:** Overlay of experimental PXRD patterns of RBC cocrystal (black) shows excellent match with the calculated line profile from the X-ray crystal structure (red), indicating bulk purity and phase homogeneity.

### **6.6 Differential Scanning Calorimetry**

The salts were analyzed by DSC to measure accurate melting point/decomposition of the solid (Figure 6.12-6.17 and Table 6.4). RBC-BA (hydrate) exhibited a broad endotherm at 90 °C prior to the melting endotherm at 210 °C as well as RBC-345-THBA exhibited a broad endotherm at 110 °C prior to the melting endotherm at 220 °C which is due to dehydration of water molecule as observed from the weight loss of the material in TGA at the same temperature. Remain salts RBC-4HBA, RBC-3MBA, were subjected to DSC, observed each salt melted at 190 °C and 150 °C, respectively. This coformer dissociation during heating was confirmed by controlled heating experiment followed by powder X-ray diffraction analysis.

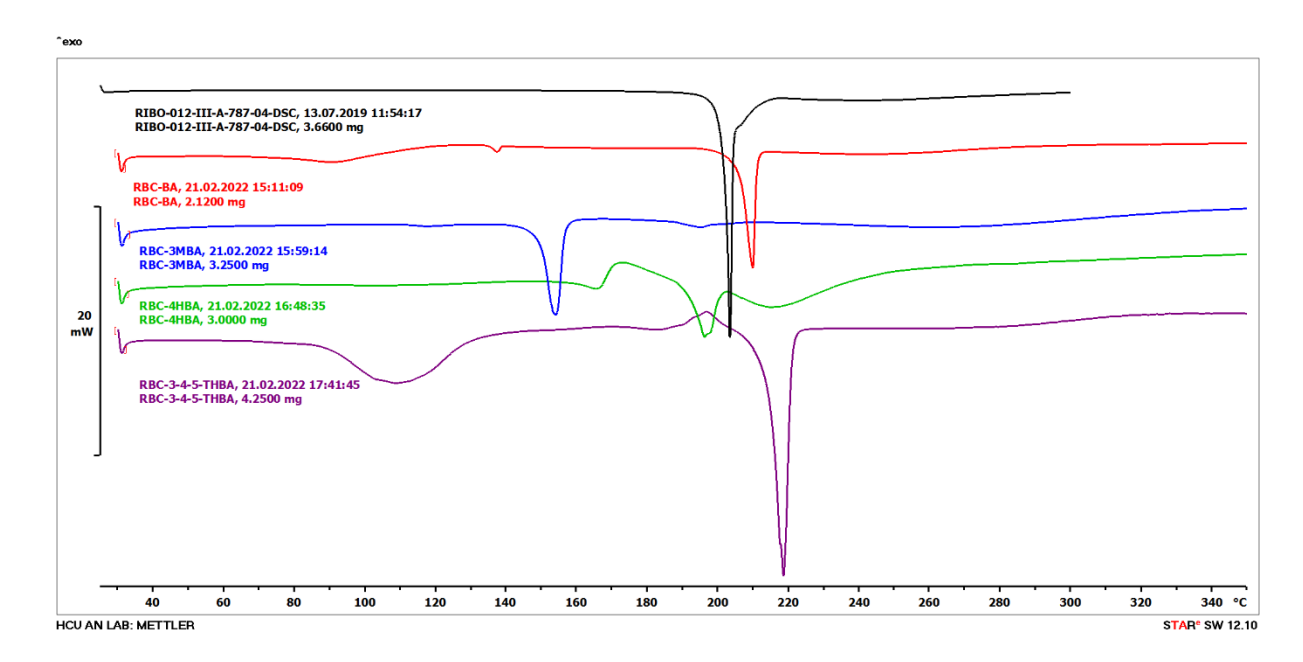


**Figure 6.12:** Overlay of DSC thermograms of RBC and salts showing their unique melting behaviour and sharp endotherms.

Table 6.4: Melting point of RBC, Salts and coformers.

	RBC/Salts	m.p. (°C)	Coformer	m.p. (°C)
1	RBC	201-204		
2	RBC-BA	135-138	BA	122.3
3	RBC-3MBA	149-156	3MBA	107
4	RBC-4HBA	155-170	4HBA	214.5
5	RBC-345THBA	213-220	345THBA	251

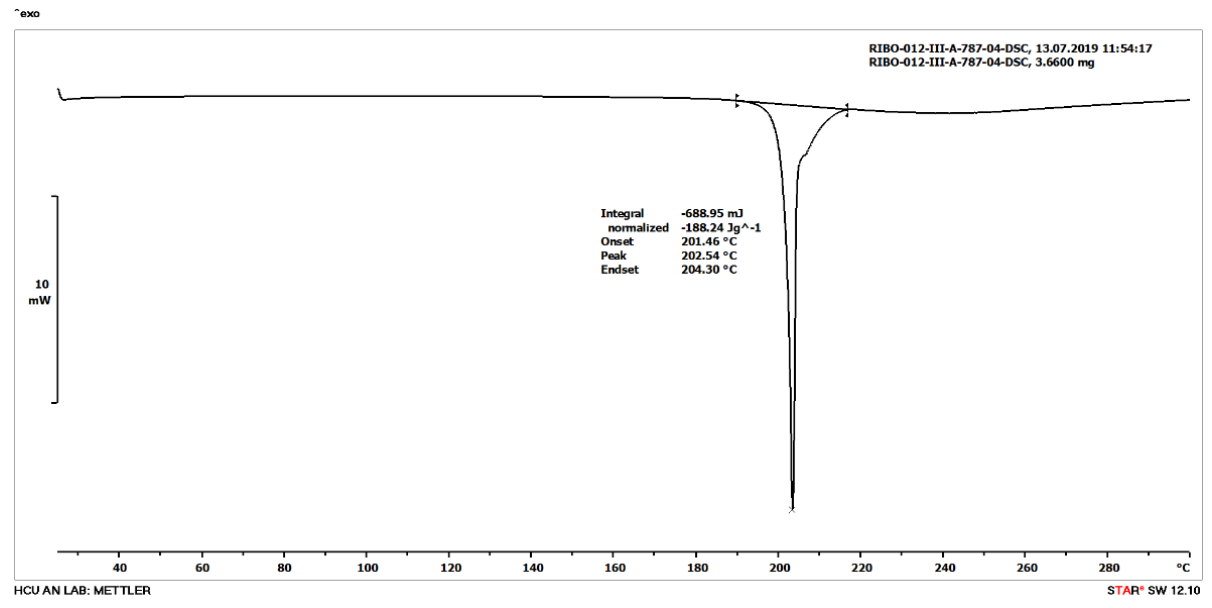


Figure 6.13: DSC thermogram of RBC

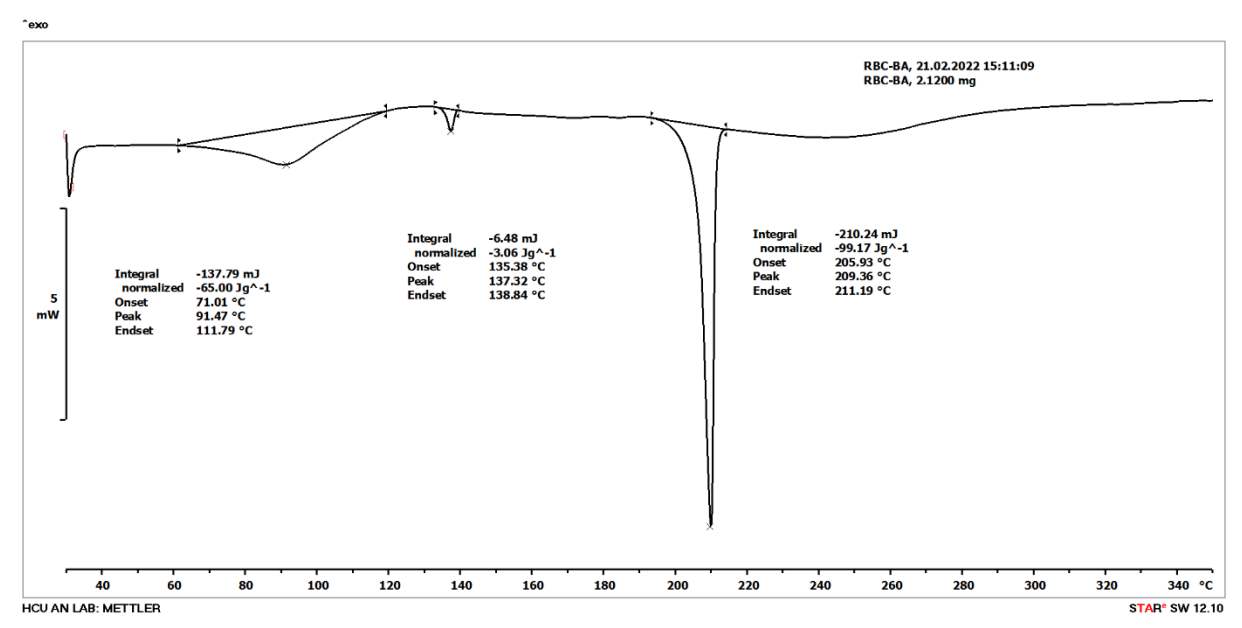


Figure 6.14: DSC thermogram of RBC-BA

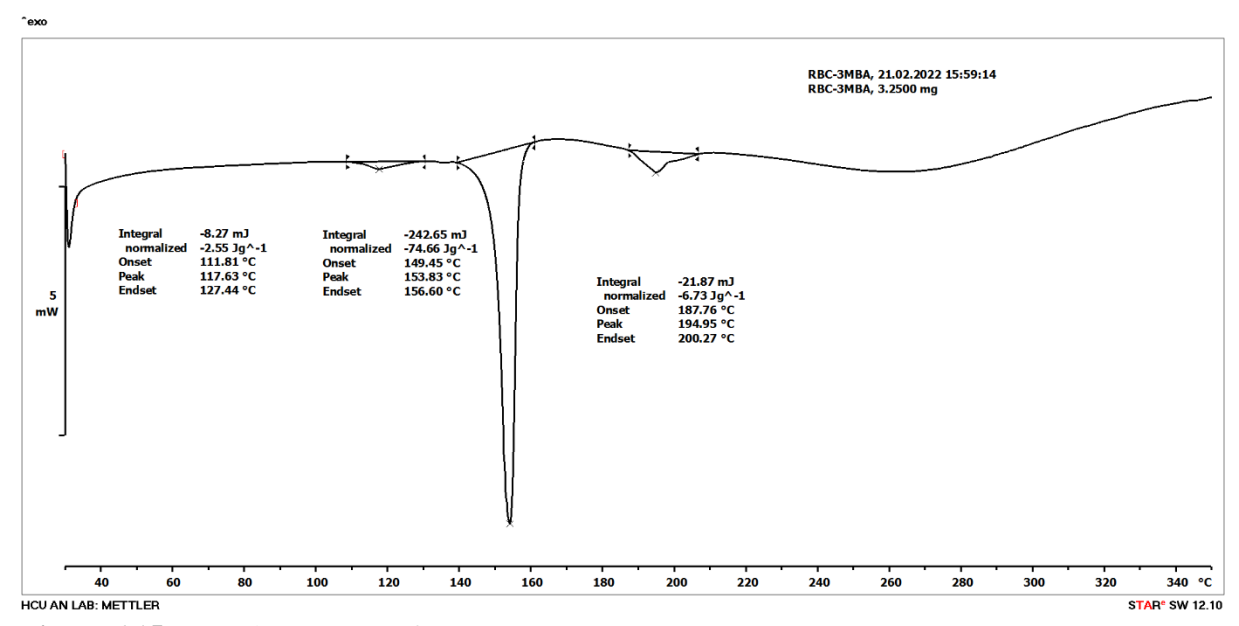


Figure 6.15: DSC thermogram of RBC - 3MBA

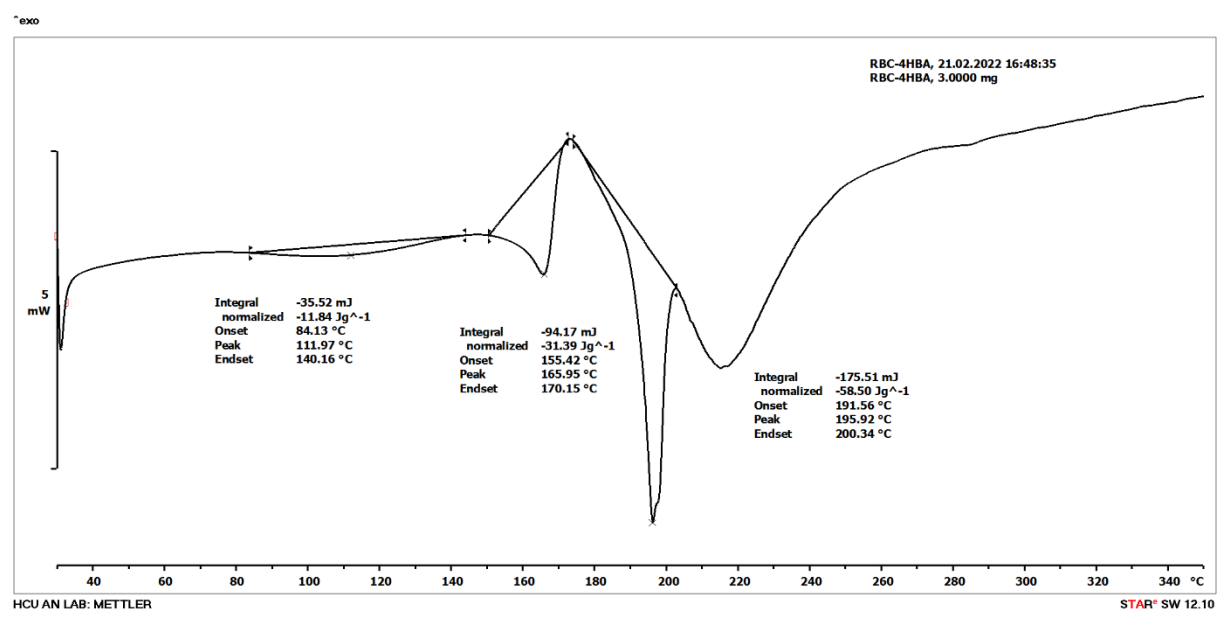
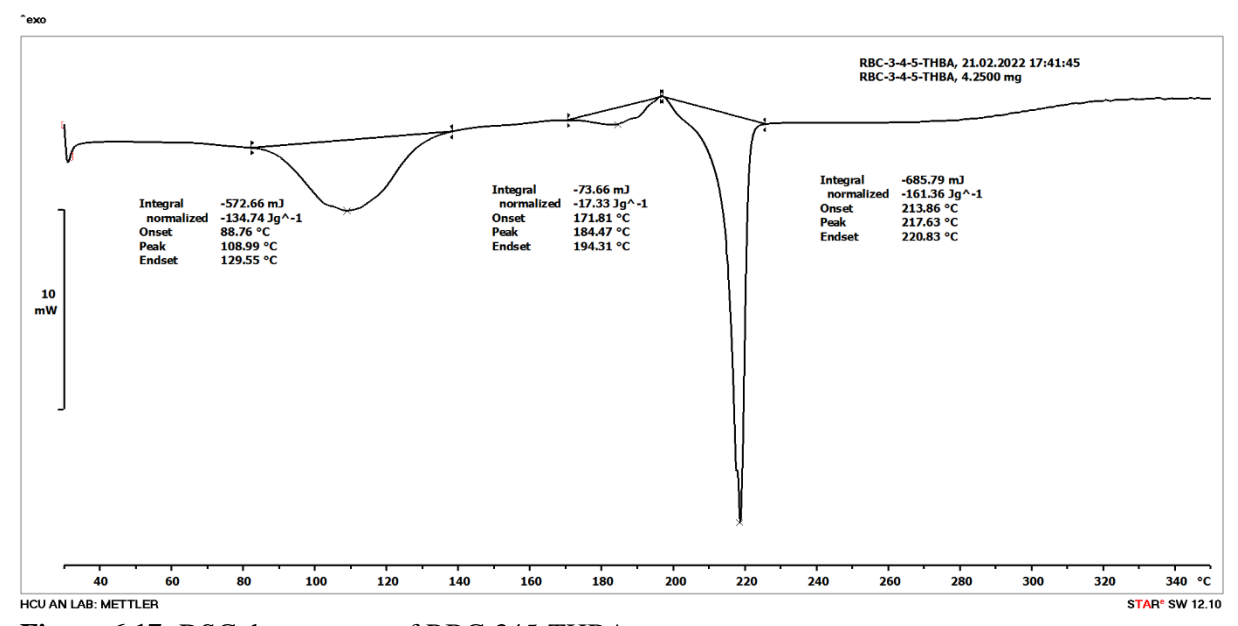


Figure 6.16: DSC thermogram of RBC -4HBA



**Figure 6.17:** DSC thermogram of RBC-345-THBA.

### **6.7 Conclusions**

In this chapter, synthesis, characterization and in-depth crystal structure analyses of four new organic salts of the anticancer drug RBC with the coformers BA, 3MBA, 4HBA and 345-THBA have been delineated thoroughly. Liquid-assisted grinding method was applied for the bulk-synthesis of these organic salts, and single crystals of these complexes were obtained by slow solvent evaporation method. Synthesized materials were characterized with IR, DSC, PXRD and single-crystal X-ray diffraction techniques. Crystal structure analyses revealed that in all the complexes, carboxylate moiety of the coformers is connected to the piperazinium moiety of RBC via charge-assisted N<sup>+</sup>-H····OOC

interactions. Due to presence of strong drug-coformer hydrogen-bonding interactions, these complexes may have the potential to improve solubility as well as permeability of this BCS class IV drug.

### **6.8 Experimental Section**

### **6.8.1** Synthesis and crystallization of salts

**RBC salt:** 25 mg of **RBC** was taken in 20 mL of solvent as a mixture of CH<sub>3</sub>OH-H<sub>2</sub>O (1:1) which was heated for clear solution and further filtered to remove undissolved particles. The obtained colourless clear solution allowed for crystallization at 60 °C in oven and pale yellow crystals (hydrated **RBC**) were obtained within 2 days by moderate evaporation. M.P. 202.50°C

**RBC-BA** (1:1) salt: A mixture of **RBC** (100.00 mg, 0.377 mmol) and **BA** (59.56 mg, 0.377 mmol) was taken in mortar and added 10 drops of acetonitrile. Subsequently, the mixture was ground vigorously by pestle for 30 minutes. The resultant mixture was obtained as off-white crystalline powder which was dried at room temperature. The obtained solid was dissolved in 20 mL of solvent as a mixture of CH<sub>3</sub>CN-H<sub>2</sub>O (1:1) which was heated for clear solution and further filtered to remove undissolved particles. The obtained colourless clear solution allowed for crystallization at 60 °C in oven and pale yellow crystals (hydrated **RBC-BA**) were obtained within 1 day by moderate evaporation. M.P. 209.36°C

**RBC-3-MBA** (1:1) salt: A mixture of **RBC** (100.00 mg, 0.377 mmol) and **3MBA** (59.56 mg, 0.377 mmol) was taken in mortar and added 10 drops of acetonitrile. Subsequently, the mixture was ground vigorously by pestle for 30 minutes. The resultant mixture was obtained as off-white crystalline powder which was dried at room temperature. The obtained solid was dissolved in 20 mL of solvent as a mixture of CH<sub>3</sub>CN-H<sub>2</sub>O (1:1) which was heated for clear solution and further filtered to remove undissolved particles. The obtained colourless clear solution allowed for crystallization at 60 °C in oven and pale yellow crystals (hydrated **RBC-3MBA**) were obtained within 1 day by moderate evaporation. M.P. 153.83°C

**RBC-4-HBA** (1:1) salt: A mixture of **RBC** (100.00 mg, 0.377 mmol) and **4HBA** (59.56 mg, 0.377 mmol) was taken in mortar and added 10 drops of acetonitrile. Subsequently, the mixture was ground vigorously by pestle for 30 minutes. The resultant mixture was obtained as off-white crystalline powder which was dried at room temperature. The obtained solid was dissolved in 20 mL of solvent as a mixture of CH<sub>3</sub>CN-H<sub>2</sub>O (1:1) which was heated for clear solution and further filtered to remove undissolved particles. The obtained colourless clear solution allowed for crystallization at 60 °C in oven and pale yellow crystals (hydrated **RBC-4HBA**) were obtained within 1 day by moderate evaporation. M.P. 195.92°C

**RBC:** 345-THBA (1:1) salt: A mixture of **RBC** (100.00 mg, 0.377 mmol) and 345-THBA (256 mg, 1.508 mmol) was taken in mortar and added 50 drops of methanol. Subsequently, the mixture was ground vigorously by pestle for 30 minutes. The resultant mixture was obtained as off-white crystalline

powder which was dried at room temperature. The obtained solid was dissolved in 20 mL of solvent as a mixture of CH<sub>3</sub>CN-H<sub>2</sub>O (1:1) which was heated for clear solution and further filtered to remove undissolved particles. The obtained colourless clear solution allowed for crystallization at 60 °C in oven and pale yellow crystals (hydrated **RBC-4HBA**) were obtained within 1 day by moderate evaporation. M.P. 217.63°C

### **6.8.2** X-ray crystallography

X-ray reflections were collected on Bruker SMART-APEX CCD diffractometer equipped with a graphite monochromator and using Mo-K $\alpha$  radiation ( $\lambda$ =0.71073 Å). Data reduction was performed using Bruker APEXII Software.<sup>13</sup> Intensities were corrected for absorption using SADABS, and the structure was solved and refined using SHELX-2014.<sup>14</sup> X-ray reflections for the RBC Salts were collected at 298 K on Oxford Xcalibur Gemini Eos CCD diffractometer using Mo-K $\alpha$  radiation ( $\lambda$  = 0.7107 Å). Data reduction was performed using CrysAlisPro (version 1.171.33.55) and OLEX2-1.0 was used to solve and refine the structures. All non-hydrogen atoms were refined as anisotropic. Hydrogen atoms on heteroatoms were located from difference electron density maps and all C-H hydrogens were fixed geometrically. Hydrogen bond geometries were determined in Platon<sup>15, 16</sup>. The packing diagrams were prepared in Mercury<sup>17, 18</sup>.

### **6.8.3 Powder X-ray diffraction**

All the solid samples were recorded by Powder X-ray diffraction on Bruker D8 Advance diffractometer (Bruker-AXS, Karlsruhe, Germany) utilizing Cu-K $\alpha$  X-radiation ( $\lambda$  = 1.5406 Å) at 40 kV and 30 mA power. X-ray diffraction patterns were collected over the 2 $\theta$  range 5-50° at a scan rate of 1°/min. Powder Cell 2.4<sup>19</sup> (Federal Institute of Materials Research and Testing, Berlin, Germany) was used for Rietveld refinement of experimental PXRD and calculated lines from the X-ray crystal structure.

### **6.8.4 Vibrational spectroscopy**

Thermo-Nicolet 6700 FT-IR-NIR spectrometer with NXR FT-Raman module (Thermo Scientific, Waltham, MA) was used to record IR spectra. IR spectra were recorded on samples dispersed in KBr pellets. Data was analyzed using the Omnic software (Thermo Scientific, Waltham, MA).

### **6.8.5 Differential Scanning Calorimetry (DSC)**

Thermal analysis was performed on a Mettler Toledo DSC 822e module. Samples were loaded in sealed pin-pricked aluminum sample pans. The typical sample size used in 3-5 mg approximately, and the heating rate at 10 °C/min in the temperature range 30-350 °C was employed. Samples were purged by a stream of dry nitrogen flowing at 80 mL/min.

### **6.9 References**

- 1. Nangia, A. K., Desiraju, G. R. Crystal engineering: an outlook for the future. *Angewandte Chemie International Edition*, **2019**, *58*(13), 4100-4107.
- 2. Mukherjee, A., Tothadi, S., Desiraju, G. R. Halogen bonds in crystal engineering: like hydrogen bonds yet different. *Accounts of Chemical Research*, **2014**, *47*(8), 2514-2524...
- 3. Bolla, G., Nangia, A. Pharmaceutical cocrystals: walking the talk. *Chemical communications*, **2016**, *52*(54), 8342-8360.
- Haleblian, J., McCrone, W. (1969). Pharmaceutical applications of polymorphism. *Journal of pharmaceutical sciences*, 58(8), 911-929. Serajuddin, A. T. M. Adv. *Drug Delivery Rev.* 2007, 59, 603–616. Steed, J.W. *Trends Pharmacol. Sci.* 2013, 34, 85-193.
- Berge, S. M.; Bighley, L. D.; Monkhouse, D. C. J. Pharm. Sci. 1977, 66, 1-19. Prohotsky, D. L.; Zhao, F. J. Pharm. Sci. 2012, 101, 1-6. Maddileti, D.; Swapna, B.; Nangia, A. Cryst. Growth Des. 2014, 14, 2557-2570.
- Generally Regarded as Safe chemicals by the U.S. FDA. http://www.fda.gov/Food/IngredientsPackagingLabeling/FoodAdditivesIngredients/ucm091048.htm.
- 7. Remenar, J. F.; Morissette, S. L.; Peterson, M. L.; Moulton, B.; MacPhee, J. M.; Guzman, H. R.; Almarsson, O. *J. Am. Chem. Soc.* **2003**, *125*, 8456-8457.
- 8. Sanphui, P.; Bolla, G.; Nangia, A. *Cryst. Growth Des.* **2012**, *12*, 2023-2036. Elder, D. P.; Holm, R.; Heidi Lopez de Diego. *Int. J. Pharm.* **2013**, *453*, 88–100.
- 9. Ribociclib, https://www.drugbank.ca/drugs/DB11730. Tanay, S. S.; Shyeilla, D.; Yasong, Lu.; Marc, L.; Shu, Yang.; Arnaud, G.; Martin, M.-Z.; Kenichi, U.; Felix, H.; Michelle, M.; Caroline, G.; Mohamed, E. *Clin. Pharmacol. Ther.* **2018**, *104*, 374-383.
- 10. FDA BCS classification system for guidance. http://www.fda.g o v / A b o u t F D A / C e n t e r s O ffi c e s /OfficeofMedicalProductsandTobacco/CDER/ucm128219.htm. Yalkowsky, S. *Techniques of Solubilisation of Drugs*, Marcel Dekker New York, **1981**. Amidon, G. L.; Lennernas, H.; Shah, V.P.; and Crison, J. R. A Theoretical Basis for a Biopharmaceutic Drug Classification: The Correlation of in vitro Drug Product Dissolution and in vivo Bioavailability. *Pharm. Res.* **1995**, *12*, 413-420.
- 11. Ribociclib-succinate salt patents, WO/2019/111160. WO 2016/166703. WO 2012/064805A1.
- 12. Bolla, G., Nangia, A. Novel pharmaceutical salts of albendazole. *CrystEngComm*, **2018**, 20(41), 6394-6405.
- 13. Bruker SMART, Version 5.625, SHELXTL, Version 6.12. Bruker AXS Inc., Madison, Wisconsin, USA. **2000**.
- 14. Sheldrick, G. M. *Program for Refinement of Crystal Structures*, University of Göttingen, Germany, **1997**.

- 15. Sheldrick, G. M. A short history of SHELX. Acta Crystallogr., Sect. A. 2008, 64, 112–122.
- 16. Sheldrick, G. M.Crystal structure refinement with SHELXL. *Acta Cryst.*, *Sect. C: Struct. Chem.* **2015**, *71*, 3–8.
- 17. Barbour, L.J. Supramol. Chem., 2001, 1, 189–191.
- 18. Barbour, L.J. *X-Seed, Graphical Interface to SHELX-97 and POV-Ray;* University of Missouri-Columbia, Columbus, MO, **1999**.
- 19. Powder Cell, A program for structure visualization, powder pattern calculation and profile fitting. www.ccp14.ac.uk/tutorial/powdercell. (Accessed 29 May 2018).

### **CHAPTER SEVEN**

# **Conclusions and Future prospects**

This thesis covers the identification, characterization and the applications of multicomponent systems of active pharmaceutical ingredients (APIs) such as new cocrystals (chapter 2), polymorphs (chapter 3), salts (chapter 4 and 6) and xenograft study of amorphous solids (chapter 5). The studies were carried out towards the controlled modification of physicochemical properties to enhance solubility, permeability and in addition extensive studies of polymorphs (chapter 3) to understand the structure-property relationship under thermal stress. Xenograft studies on co-amorphous solids showed that these materials have the potential to inhibit tumour growth (chapter 5).

Introduction of crystal engineering, pharmaceutical solid forms of APIs and few models' organic compounds are discussed in Chapter 1.

Chapter 2 deals with the cocrystals of Entacapone (ETP, an inhibitor of catechol-O-methyltransferase), a BCS class IV drug (brand name: Comtan; used for the treatment of Parkinson's disease, a chronic and degenerative disorder of the central nervous system) with the coformers- acetamide (ACT, 1:1), nicotinamide (NAM, 1:1), isonicotinamide (INAM, 1:1), pyrazinamide (PYZ, 1:1) and isoniazid (INZ, 1:1). Cocrystallization of ETP with the coformer theophylline (THP) resulted in the formation of a cocrystal hydrate (ETP-THP-HYD, 1:1:1). The synthesized materials were characterized by SC-XRD, PXRD, DSC, TGA, IR and NMR spectroscopy. Solubility and dissolution rate studies showed that there is a correlation between cocrystal stability (post-dissolution) and solubility governed by the heteromeric N-H···O, O-H···N and O-H···O hydrogen bonds and conformational changes of ETP in the cocrystal structures. ETP-THP-HYD and ETP-PYZ exhibited faster dissolution rate and higher solubility compared to the other cocrystals which were dissociated partially during solubility experiments. From diffusion studies, it was found that the stable and high soluble ETP-THP-HYD cocrystal showed enhanced permeability. Given that stability, solubility and permeability are in general inversely related, the entacapone-theophylline hydrate cocrystal is a unique example of the thermodynamically stable cocrystal exhibiting high solubility and high permeability. So, ETP-THP-HYD may be useful as a suitable formulation of the drug ETP to prevent Parkinson's disease.

In chapter 3, exploration of novel polymorphs of ETP has been highlighted. ETP form-I was first published in 2001. However, analysis of its X-ray crystal structures and stability relationship of ETP polymorphs and their dissolution and permeability profile have not yet been reported. In our studies, two new conformational polymorphs of ETP were obtained from water and acetone solvent mixture,

and further for these materials, the structural origin of polymorphism and their phase transformations, stability, equilibrium solubility, dissolution, and permeability properties were studied thoroughly. The ETP molecule adopts different conformations in the polymorphic structures with slight changes in carbonyl and nitrile group orientations. Thermal analysis suggests that form-III and form-IV are enantiotropically related to form-I, which is the thermodynamically stable form at ambient conditions. In contrast, form-II is monotropically related to form-I. Equilibrium solubility, dissolution, and permeability studies show that form-II persists in the slurry medium and dissolves faster with a high flux rate compared to the stable form-I in phosphate buffer solution at  $37 \pm 0.5$  °C. Here, form-II dissolves and diffuse faster than the form-I, form-III and form-IV due to variation in crystal packing (i.e Z'=2 for form-II and Z'=1 for form-I and form-III) which implies its relatively lower lattice energy to dissolve and diffuse. Therefore, form II is superior among the four polymorphic forms isolated so far. Thus, selection of the thermodynamically stable ETP polymorph-II is preferred in drug formulation to avoid polymorphic changes with superior solubility, dissolution and permeability. During process development, formulation and marketing, this can be used an alternative formulation of ETP in future.

Chapter 4 deals with the attempts towards improvement of solubility, dissolution and permeability of poorly water soluble drug PMZ via synthesis of binary organic salts with some dicarboxylic acid coformers (OA, SA, FA, GA and AA) using crystal engineering approach. The synthesized five binary organic salts were characterized by IR, DSC, PXRD and single crystal-XRD techniques. Crystal structure analyses unveil that in all the complexes, PMZ is connected with the coformers via charge-assisted –N+H····OOC- interactions. PMZ encapsulates the coformers with its arms acting as a molecular tweezer. In PMZ-OA complex, oxalic acid and oxalate ions form one dimensional hydrogen bonded chain through charge-assisted O-H...OOC- hydrogen bonding interactions. Bulk phase purity of the materials was confirmed by PXRD. From IDR studies, it was inferred that all the complexes improved the dissolution rate of the drug and here, PMZ-SA exhibited highest cumulative dissolved amount throughout the experiment time period. In diffusion studies, it was found that all the complexes enhanced the permeability of the drug, and like IDR result, PMZ-SA complex showed highest cumulative drug diffused amount for the entire experiment time period. From these experiments, it can be concluded that PMZ-SA salt may be suitable for the drug formulation development of PMZ.

The primary aim of chapter 5 is to increase the therapeutic effect and inhibited of tumor growth at oral dosage of curcumin-pyrogallol (CUR-PYR) cocrystal and curcumin-artemisinin (CUR-ART) coamorphous solid. Both these solid forms exhibited superior dissolution and pharmacokinetic behavior compared to pure CUR. Curcumin and artemisinin are herbal drugs of Indian and Chinese origins. The low solubility and short half-life of curcumin, and hence high dosage administered, have been a limitation to making drug formulations of curcumin. We have overcome the multiple disadvantages of curcumin in the designed CUR-ART coamorphous dispersion. This novel binary solid exhibits high

solubility and bioavailability, extended half-life and action of bioactive curcumin at normal drug dose regime of 100 mg/kg. The therapeutic activity of CUR-ART in Xenograft models of Panc-1 is comparable to commercial drug doxorubicin. Given the diverse biological action of curcumin and artemisinin, the high quantity of net drug delivered as coamorphous solid could open opportunity for an herbal formulation in cancer, malaria and several other treatments.

In Chapter 6, Synthesis, characterization and crystal structure analysis of four organic salts of Ribociclib (RBC) have been delineated thoroughly. RBC, a BCS Class IV drug is a selective cyclin-dependent kinase inhibitor containing two proteins called cyclin-dependent kinase 4 and 6 (CDK4/6), and which inhibit the progression of cancer slowly. Pharmaceutical solid-forms of RBC with improved physicochemical properties are essential but such type of materials are less explored. Few polymorphs, hydrates, solvates and one binary salt (RBC-Succinate) have been reported. So far, there is no report on crystal structures of RBC and its other binary solids. We successfully prepared salts of Ribociclib (RBC) with different coformers such as benzoic acid (BA), 3-methoxybenzoic acid (3-MBA), 4-Hydroxybenzoic acid (4-HBA) and 345-Tryhydroxy benzoic acid (345-THBA). Bulk synthesis of those organic salts was done by liquid-assisted grinding method and single crystals of these complexes were obtained by slow solvent evaporation method. Synthesized materials were characterized with IR, DSC, PXRD and single-crystal X-ray diffraction techniques. Crystal structure analyses revealed that in all the complexes, carboxylate moiety of the coformers is connected to the piperazinium moiety of RBC via charge-assisted N<sup>+</sup>-H···OOC interactions. Due to presence of strong drug-coformer hydrogen-bonding interactions, these complexes may have the potential to improve dissolution and permeability properties of the drug

# **Future prospects**

This thesis highlights and evaluates the importance and usefulness of polymorphs, cocrystals, organic salts and coamorphous materials in drug development. Role of these pharmaceutical solids towards the improvement of solubility, intrinsic dissolution rate and permeability of poorly water soluble and/or poorly permeable drugs has been delineated with plenty of instances in this thesis. Our research outcomes clearly pave the way to obtain better drug formulations. Despite several advantages of these strategies, there are some issues such as stability, dosage volume, cost, bulk-synthesis or scale-up, tabletability etc. which need to be overcome. Implementation of suitable techniques including use of functionalized common coformers (e.g. fluoro-coformers), synthesis of ternary or higher-order cocrystals or organic salts, continuous crystallization etc. may play pivotal role to wipe out those issues in future.

### **ABOUT THE AUTHOR**

Manish Kumar Bommaka, S/o Laxmaiah Bommaka and Nirmala Bommaka, was born at Godavarikhani, Karimnagar Dist, and Telangana, India. He received the primary education at Singareni School, and secondary education at Phani High School, he completed Intermediate (Bi.P.C. 2002-04) at S. V. Junior college, Karimnagar. He pursued Bachelor of Pharmacy (B. Pharmacy 2006-2010) at Pallavan Pharmacy College, Kanchipuram, Dr. M. G. R Medical University, Tamilnadu and Master of Pharmacy (M. Pharmacy pharmaceutical chemistry 2010-12) Gokaraju Rangaraju College of Pharmacy, Osmania University, and Hyderabad. He worked as Assistant Professor in Netaji college of Pharmacy (Dec 2012 - Dec 14), located at Kazipet, Warangal. He then joined (in 2015) Prof. Ashwini Nangia's Research Group, School of chemistry, University of Hyderabad, and He was awarded Rajiv Gandhi National Fellowship (RGNF) by University Grant Commission (UGC), as a Ph.D. student and was upgraded as a 'Senior Research Fellow' (SRF) in 2017.

About the author...182

### LIST OF PUBLICATIONS

- Curcumin-artemisinin coamorphous solid: Xenograft model preclinical study.
   Mannava, M. K., Suresh, K., Bommaka, M. K., Bhavani Konga, D., Nangia, A. *Pharmaceutics* 2018, 10, 7.
- 2. Entacapone: improving aqueous solubility, diffusion permeability, and cocrystal stability with theophylline.
  - **Bommaka, M. K.,** Mannava, M. C., Suresh, K., Gunnam, A., Nangia, A. *Cryst. Growth Des.* **2018**, *18*, 6061-6069.
- 3. Entacapone Polymorphs: Crystal Structures, Dissolution, Permeability, and Stability. **Bommaka, M. K.,** Chaitanya Mannava, M. K., Rai, S. K., Suresh, K., Nangia, A. K. *Cryst. Growth Des.* **2021**, *21*, 5573-5585.
- 4. Improvement of Physiochemical Properties of Pimozide through Co-crystalization with Dicarboxylic Acids.
  - **Bommaka, M. K.,** Garai, A., Sunil K. Rai, R Dandela and Ashwini K. Nangia. (Manuscript under preparation).
- 5. Synthesis and crystal structure investigation for pharmaceutical salts of Ribociclib Bommaka, M. K., Bandi, S., Garai, A., Rana, M., and Ashwini K. Nangia. (Manuscript under preparation).
- 6. Salts and Cocrystal and its hydrate forms of Ribociclib: Solubility and diffusion profile. Mannava, M. C., **Bommaka, M. K.,** Garai, A., Solomon, A, K., Ashwini K. Nangia. (**Manuscript under preparation**).
- 7. Furobenzoic acids as cofrmers to optimize the solubility and permiability by altering the crystal lattice of BCS Class 4 drug Naftopidil.
  - Mannava, M. C., **Bommaka, M. K.**, Dandela, R., Solomon, K. A., & Nangia, A. K. *Chemical Communications*, 58(37), 2022, 5582-5585.
- 8. Inhibiting protein-protein interactions of Hsp90 as a novel approach for targeting cancer.
  - Gupta, S. D., **Bommaka, M. K**., & Banerjee, A. European Journal of Medicinal Chemistry, 178, **2019**, 48-63.
- 9. Eco-sustainable synthesis and biological evaluation of 2-phenyl 1, 3-benzodioxole derivatives as anticancer, DNA binding and antibacterial agents.
  - Gupta, S. D., Rao, G. B., **Bommaka, M. K**., Raghavendra, N. M., & Aleti, S. *Arabian Journal of Chemistry*, 9, **2016**, \$1875-\$1883.

10. Molecular docking study, synthesis and biological evaluation of Mannich bases as Hsp90 inhibitors.

Gupta, S. D., Bommaka, M. K., Mazaira, G. I., Galigniana, M. D., Subrahmanyam, C. V. S., Gowrishankar, N. L., & Raghavendra, N. M. *International journal of biological macromolecules*, 80, **2015**, 253-259.

## Citation for publications till date:

Cited by		
	All	<b>Since 2017</b>
Citations	133	129
h-index	5	5
i10-index	5	5

**Source: Google Scholar** 

# PARTICIPATION IN SYMPOSIA, WORKSHOPS AND CONFERENCES

- 1. Participated at the "chemfest-2016" (13<sup>th</sup> Annual In- house Symposium) held at University of Hyderabad, Hyderabad, India, during March 18-19, 2016.
- Presented a Poster entitled "Novel Entacapone cocrystals and their physicochemical properties study" in 24<sup>th</sup> Congress and General Assembly of the International Union of Crystallography" held at HICC, Hyderabad, India, during August 21-28,2017.
- 3. Attended the work shop on "X-ray Absorption Spectroscopy for the Crystallographer" at the 24<sup>th</sup> Congress and General Assembly of the International Union of Crystallography" held at HICC, Hyderabad, India, during August 21, 2017.
- 4. Presented a Poster entitled "Novel Entacapone cocrystals and their physicochemical properties study" at "chemfest-2018" ( Chemfest beyond the challenges) held at University of Hyderabd, Hyderabd, India, during March, 2018.
- 5. Participated at the "chemfest-2020 Flyer" (Sponsored by the Royal Society of Chemistry) held at University of Hyderabad, Hyderabad, India, during Feb 21-22, 2020.
- 6. Delivered an oral presentation entitled "Entacapone Polymorphs: Crystal Structures, Dissolution, Permeability and Stability Analysis" at "chemfest-2021" (Chemfest beyond the challenges) held at University of Hyderabd, Hyderabd, India, during March 19-20, 2021.

# PERMEABILITY OF ACTIVE PHARMACEUTICAL INGREDIENTS (APIs) IN THEIR SALTS, COCRYSTALS AND POLYMORPHS

by Manish Kumar Bommaka

Submission date: 20-Jun-2022 11:04AM (UTC+0530)

Submission ID: 1859931005

File name: MANISH\_KUMAR\_BOMMAKA.pdf (12.89M)

Word count: 29225

Character count: 150109

Prof. Ashwini K. Nangia School of Chemistry University of Hyderabad Central University P.O. Hyderabad 500 046

# **ENHANCING SOLUBILITY AND PERMEABILITY OF ACTIVE** PHARMACEUTICAL INGREDIENTS (APIs) IN THEIR SALTS, COCRYSTALS AND POLYMORPHS

**ORIGINALITY REPORT** 

SIMILARITY INDEX

**27**%

**INTERNET SOURCES** 

**PUBLICATIONS** 

STUDENT PAPERS

**PRIMARY SOURCES** 

Manish Kumar Bommaka, M. K. Chaitanya Mannava, Sunil K. Rai, Kuthuru Suresh, Ashwini K. Nangia. "Entacapone Polymorphs: Crystal Structures, Dissolution, Permeability, and Stability", Crystal Growth & Design, 20

Publication

University of Hyderabad Central University P.O. Hyderabad 500 046

www.mdpi.com

Internet Source

School of Che University of Hyderabe Central University P.O. Hyderabad 500 046

Manish Kumar Bommaka, M K Chaitanya Mannava, Kuthuru Suresh, Anilkumar Gunnam, Ashwini Nangia. "Entacapone: Improving Aqueous Solubility, Diffusion Permeability, and Cocrystal Stability with Theophylline", Crystal Growth & Design, 2018 Publication

University of Hyderabad Central University P.O. Hyderabad 500 046

Submitted to University of Hyderabad, Hyderabad

Student Paper

Iniversity of Hyder Central University P.O. Hyderabad 500 046

baadalsg.inflibnet.ac.in

Prof. Ashwini K. Nangia School of Chemistry University of Hyderabad Central University P.O. Hyderabad 500 046

6	Internet Source  Internet Source  Advantagia - 1 School of Chemistry School of Hyderabad University of Hyderabad Contral University P.O.	(
7	Abhijit Garai, Kumar Biradha. "Cocrystals de and Salts of 4,4'-Dinitro-2,2',6,6'- tetracarboxybiphenyl with N-Heterocycles: Solid State Photodimerization of Criss-Cross Aligned Olefins and Photophysical Properties", Crystal Growth & Design, 2020 Publication	(
8	Internet Source  Intern	(
9	Internet Source  Central University of Hyderabad University of Hyderabad University P.O.	(
10	Manish Kumar Bommaka, M.K.Chaitanya  Mannava, Kuthuru Suresh, anilkumar gunnam, Ashwini Nangia. "Entacapone: Improving Aqueous Solubility, Diffusion Prof. Ashwini K. Nangia Permeability and Cocrystal Stability with University P.O.  Central Univer	2

Theophylline", Crystal Growth & Design, 2018

krclib.ncl.res.in Internet Source

Publication

M. K. Chaitanya Mannava, Rambabu Dandela, 12 Srinu Tothadi, K. Anand Solomon, Ashwini K.